THE CLASSICAL ANALYSIS OF STRUCTURAL INTEGRITY AND FATIGUE SAFE-LIFE OF PRELOADED BOLTED JOINTS

by

Michael Adrian Welch

MSc CEng MIMechE

Thesis submitted to Nottingham Trent University

For the degree of Doctor of Philosophy

July 2024

Abstract

The purpose of the published works presented was to contribute to the understanding of preloaded bolted joints. Emphasis was on considering bolted joints as systems. Areas of interest included both static and fatigue analysis of preloaded bolted joints.

Classical methods of analysis were applied throughout each of the papers being presented. Each paper develops new methods of detail analysis and provides guidance on how the methods can be applied to bolted joint designs.

In-plane loads on the joint produce bending stresses in the bolts that have an effect on the fatigue life. Existing methods of calculating these bending stresses are not satisfactory. They are based on an oversimplified, and unrealistic, model which assumes bolt bearing at the holes in the flanges. This would only occur if there were slip at the faying surface or the joint had been assembled with misalignment. The work presented here proposes an improved method for calculating bolt shear and bending stresses.

It was found that the shear strain produced by in-plane external loads and moments results in a transverse displacement of the bolt head/nut which generates shear, bending and axial loads on the bolt. Under high flange shear stress conditions, the individual bolt tensile loads produced by the in-plane external loads can be of a similar order of magnitude to the bolt tensile load component produced by the out-of-plane external loads and moments.

A new damage-equivalent stress function, suited to high mean stress situations, has also been developed. It is suitable for a wide range of stress concentrations and tensile strengths, typical of those found in preloaded bolts. This new function has an accuracy to within 16% with a root mean square error of 8%, a significant improvement on existing methods.

A series of S-N curve specific to high strength bolts and screws, property-class 8.8 to 12.9 have also been produced.

A holistic approach to the analysis of preloaded bolted joints has been adopted throughout the presented works. This has been achieved by considering multi-bolt preloaded bolted joints and as consisting of multiple elements that interact with each other

to produce a complex system. The purpose of conducting an analysis is to show a bolted joint has structural integrity and is durable. Structural integrity can be demonstrated by static stress analysis of each element of the joint. Durability is demonstrated by assessment against appropriate safety factors or by a detailed fatigue analysis.

The presented published works have made a contribution to the understanding of preloaded bolted joints. The first two of the published works being presented identified a knowledge gap in the understanding of how in-plane loads are supported within a bolted joint. It was understood that friction at the faying surface would transmit in-plane loads between the flanges. However, the effect that the in-plane loads would have on individual bolts within a multi-bolt joint was an unknown. This lack of knowledge was the research challenge for the subsequent published works. Each making its own contribution, while combining to make a whole body of work.

Copyright statement

Statement on Thesis Referencing Style

This thesis is being submitted for a PhD by Published Works and contains Author Accepted Manuscripts (AAM) of each published work embedded within the main body of text. Each AAM has its own systems for numbering section headings, figures, tables and references.

The thesis uses the Harvard system of referencing for the main body of text. Each of the embedded AAM's has its own list of Vancouver style references. The benefit of using the Harvard referencing for the main body of text is that the list of references for each of the embedded publications automatically, and almost seamlessly, cross-references with the Harvard style references of the thesis body.

List of Outputs

Publications

1. "*Classical Analysis of Preloaded Bolted Joint Load Distributions*". International Journal of Structural Integrity. Vol. 9 (2018)
2. "*Analysis of Bolt Bending in Preloaded Bolted Joints*". Journal of Mechanical Engineering – Strojnicky časopis. Vol. 68 (2018), Issue 3
3. "*A Paradigm for the Analysis of Preloaded Bolted Joints*". Journal of Mechanical Engineering – Strojnicky časopis, Volume 69 (2019), Issue 1
4. "*Bolted Joint Preload Distribution From Torque Tightening*". Journal of Mechanical Engineering – Strojnicky časopis, Volume 71 (2021), Issue 2
5. "*An Analytical Study of Asymmetrical Preloaded Bolted Joints*". International Journal of Modern Research in Engineering and Technology, Volume 7 (2022), Issue 3
6. "*An Empirical Approach to a Comprehensive Damage-Equivalent Stress for Fatigue*". FME Transactions. 2022
7. "*Fatigue Analysis of Preloaded Bolted Joints*". FME Transactions. 2022
8. "*Supplementary Material to: An Empirical Approach to a Comprehensive Damage-Equivalent Stress for Fatigue"*. ResearchGate publication, 2023

Conference and Seminar Presentations

9. Michael Welch. "Analysis of Bolt Bending in Preloaded Bolted Joints". 26th July 2019, Prifysgol Glyndŵr Wrecsam/Wrexham Glyndŵr University
10. Michael Welch. "Analysis of Bolt Bending in Preloaded Bolted Joints". 1st November 2019, Prifysgol Glyndŵr Wrecsam/Wrexham Glyndŵr University
11. Michael Welch. "An Empirical Damage-Equivalent Stress Function for Fatigue". 3rd November 2022, Prifysgol Glyndŵr Wrecsam/Wrexham Glyndŵr University
12. Michael Welch. "Relaxation of Bolt Preload Resulting from Bolt Bending Arising from In-Plane Loads"**.** *Bolted Joints: Insights, Failures & Solutions*. Engineering Integrity Society. 8 February 2024, AMP Technology Centre, Rotherham

CONTENTS

List of Figures

Bolted Joint Preload Distribution From Torque Tightening

An Empirical Approach to a Comprehensive Damage-Equivalent Stress for Fatigue

Fatigue Analysis of Preloaded Bolted Joints

Appendix A: Analysis of Bending Induced Bolt Tension

Appendix B: Supplementary Material to: An Empirical Approach to a Comprehensive Damage-Equivalent Stress for Fatigue

List of Tables

Glossary of Abbreviations

AAM	Author Accepted Manuscript
AISC	American Institute of Steel Construction
AISI	American Iron and Steel Institute
BSI	British Standards Institution
CAD	Computer Aided Design
EN	Europäische Norm (European Standard)
FAA	Federal Aviation Administration
FEA	Finite Element Analysis
FEM	Finite Element Methods
ISO	International Organization for Standardization
MMPDS	Metallic Materials Properties Development and Standardization
NASA	National Aeronautics and Space Administration
RMS	Root Mean Square
RCSC	Research Council on Structural Connections (Formerly: Research Council on Riveted and Bolted Structural Joints)
SCI	The Steel Construction Institute
VDI	Verein Deutscher Ingenieure (Association of German Engineers)

CHAPTER 1

INTRODUCTION

1.1 General Background

Bolted joints are such a common feature in all types of structures and components that are employed within commercial, industrial, and domestic surroundings that quite often their importance and significance are overlooked. Bolts and screws have a variety of uses which range from simple non-structural applications, holding two parts together while supporting minimal force or load, through to highly loaded structural joints, such as connections within the steel frame of a building or retaining the engine of a transatlantic airliner to the aircraft. They are also used to maintain sealing within pipework, wellhead assemblies and similar connections used within the Oil and Gas industry, the Petro-chemical industry. They are frequently used throughout all industries where safety critical structural connections are required.

Far from being simple structural elements, bolted joints comprise of multiple components that interact with each other to produce a complex system. During the design phase these systems require load and engineering stress analysis to ensure they meet structural integrity requirements.

Engineering stress analyses can be broadly considered as having three objectives. They are intended to show a component, system or structure is fit-for-purpose, has structural integrity and is durable. Structural integrity can be demonstrated by detailed analysis to determine induced stresses as accurately as possible and be assessed against appropriate failure criteria or by a design analysis that uses assumptions that produce a conservative assessment of the joint. Durability is usually demonstrated by a fatigue assessment or, if required, a detailed fatigue analysis to show that components are capable of achieving the required operating life. Fitness-for-purpose assessment requires not only structural integrity and durability, it also requires the ability to function continuously without undue deflection, wear or corrosion or other impediment that could interfere with performance.

Each of the papers being presented here arose from work carried out as part of the same, broad, project and share common nomenclature and terminology. Each paper is unique and stand alone, by which it is meant that each paper can be read and the results applied without cause to refer to the other works. However, all the papers have a consistent approach, use a common notation and terminology, leading to an overall contribution to knowledge.

1.2 Bolt Materials

For bolted joints to be able to achieve a wide and varying range of tasks in an economic manner there is a wide range of bolt sizes, materials, and material grades available. The two most common materials are carbon steel and stainless steel, each of which are available in a range of material grades.

1.2.1 Carbon Steel

Referring to BS EN ISO 898:2009 "*Mechanical properties of fasteners made of carbon steel and alloy steel Code*", BSI (2009a), and BS EN 20898-1:1992 "*Mechanical properties of fasteners – Part 1: Bolts, Screws and Studs*", BSI (1992), it can be seen that the types of carbon steel bolts and screws used in mechanical engineering can be categorised into three broad material types:

> Carbon steel without heat treatment, used in the manufacture of property-class 3.6, 4.6, 4.8, 5.6, 5.8 and 6.8 bolts and screws. These bolt grades are used in general purpose, non-structural, applications.
>
> Carbon steel quenched and tempered, used in the manufacture of property-class 8.8, 9.8 and 10.9 bolts and screws. These bolt grades are commonly classed as high strength and used in load bearing structural applications.

Alloy steel quenched and tempered, used in the manufacture of property-class 10.9 and 12.9 bolts and screws. Again, these bolt grades are classed as high strength and used in load bearing applications.

It is a requirement of BS EN ISO 898:2009, BSI (2009a), that both the manufacturer and the bolt property class are marked on the bolt head, as illustrated by the examples shown in Figure 1.

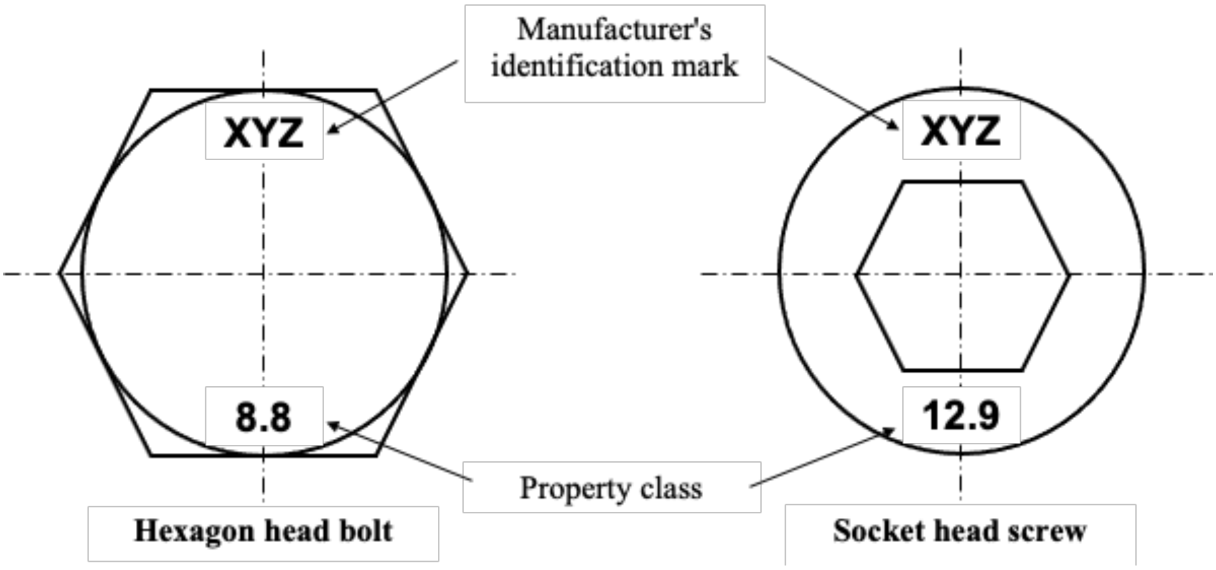

Figure 1: Carbon steel bolt identification markings

1.2.2 Stainless Steels

Stainless steel bolt grades are covered within BS EN ISO 3506-1:2009 "*Mechanical properties of corrosion-resistant stainless steel fasteners Part 1: Bolts, screws and studs*", BSI (2009b), and BS EN ISO 3506-3:2009 "*Mechanical properties of corrosion-resistant stainless steel fasteners Part 3: Set screws and similar fasteners not under tensile stress*", BSI (2009d). Stainless steel nuts are covered within BS EN ISO 3506-2:2009 "*Mechanical properties of corrosion-resistant stainless steel fasteners Part 2: Nuts*", BSI (2009c).

The difference between stainless steel bolts to BS EN ISO 3506-1:2009, BSI (2009b), and those to BS EN ISO 3506-3:2009, BSI (2009d), can be regarded as being a difference in quality assurance rather than a difference in physical properties.

Referring to BS EN ISO 3506-1:2009, BSI (2009b), it can be seen that structural stainless steel bolts and screws are categorised into three broad material groups, Austenitic, Martensitic and Ferritic stainless steels. Each of these material groups are further sub-divided into steel grades and property class:

> Austenitic stainless steel grades A1, A2, A3, A4 and A5, used in the manufacture of property-classes 50, 70 and 80 bolts and screws. These grades of Austenitic stainless steel are strengthened by cold working, not heat treated like carbon and alloy steel fasteners. The common stainless steel types and specifications associated with each of the above steel grades are identified in Table 1.
>
> Martensitic stainless steel grade C1, used in the manufacture of property-classes 50, 70 and 110 bolts and screws, grade C3 property-class 80 bolts and screws, and grade C4 property-classes 50 and 70 bolts and screws. These stainless steel grades are also included in Table 1.
>
> Ferritic stainless steel grade F1, used in the manufacture of property-classes 45 and 60 bolts and screws. This stainless steel grade is also included in Table 1.

Material Group	**Bolt Grade**	**Stainless Steel Type**	**Specification**	**Werkstoff Number**
Austenitic	A1	303	BS 303S31 EN 58M UNS S30300	1.4305
	A2	304	BS 3111	1.4301
	A3	321 347		1.4541 1.4550
	A4	316		1.4401
	A5	316Ti 316Cb		1.4571 1.4580
Martensitic	C1	410		1.4006
	C3	431		1.4057
	C4	416		1.4005
Ferritic	F1	430 430Ti 430Cb		1.4016 1.4520 1.4511

Table 1: Stainless steel types

Again, it is a requirement of BS EN ISO 3506-1:2009, BSI (2009b), that the manufacturer, material grade and the bolt property class are marked on the bolt head, as illustrated by the examples shown in Figure 2.

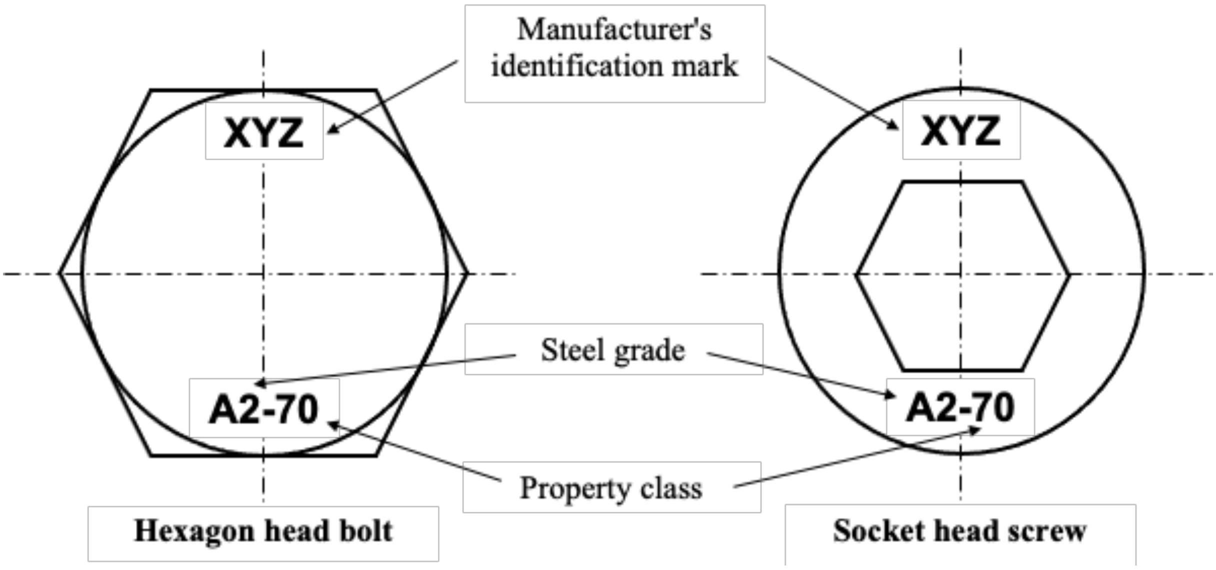

Figure 2: Stainless steel bolt identification markings

Only property-classes 70 or greater would be regarded as 'high strength' bolts. In practical terms, a property-class 70 stainless steel bolt has a minimum tensile strength that falls between property-class 6.8 and property-class 8.8 carbon steel bolts, property-class 8.8 being the lowest grade of carbon steel that is classified as high strength.

1.3 Types of Bolted Joints

Structural bolted joints generally fall into two main types, snug tightened and preloaded, although preloaded bolted joints are occasionally sub-divided into various categories. These sub-divisions are usually based on quality assurance considerations rather than the way the joint is preloaded or the way the joint actually behaves under external loads.

Both snug tightened and preloaded bolted joints are defined by the loading condition on the bolts in the final joint assembly, before being subjected to external loads.

1.3.1 Snug Tightened Bolted Joints

Snug tightened joints, sometimes referred to as wrench tightened, can be defined as when the bolts are tightened sufficient to close up the joint face, or faying surface, but without introducing any significant load in the bolts, or contact pressure at the joint faying surface. The faying surface of a joint member is the prepared surface that is in contact with the faying surface of another member of the joint. The term ‘wrench tightened’ is a reference to a spud wrench or podger spanner. A spud wrench is illustrated in Figure 3.

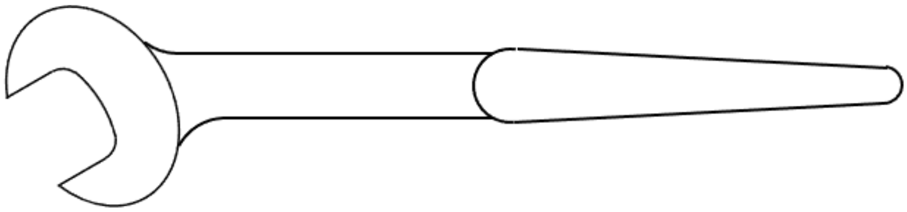

Figure 3: Spud wrench/Podger spanner

This type of joint is commonly used in civil engineering. Snug tightened joints work well where the joint is always under a heavy, static, loads that predominantly act on the joint to put it under compression and/or shear. Snug tightened joints are generally poor under fatigue conditions although they can be used under cyclic conditions provided the joint does not become unloaded, or near unloaded, during its life. They are not suitable for applications or situations where there are full load reversals on the joint or where the joint becomes unloaded.

1.3.2 Preloaded bolted joints

Preloaded bolted joints can be defined as when the bolts are tightened with the intention of producing a significant amount of preload, or pre-tension, in each bolt. When creating the pretension it is usual for the bolts to be first tightened just sufficient to close up the joint and maintain joint alignment prior to further tightening. Once alignment has been established the bolts are further tightened to produce the required preload in each bolt. Importantly, inducing this preload creates a significant contact pressure at the faying surface, which is critical to the performance of the joint. Various methods of preloading the bolts can be adopted. The most common is probably the use of a torque wrench, ‘torque-controlled tightening’. Other common methods include ‘direct tension indicators’ or load indicating washers, ‘angle-controlled tightening’, sometimes referred to as turn-of-nut or part-turn method, and the ‘yield-controlled tightening’ method.

1.3.3 Torque controlled tightening

Torque controlled tightening is quite often carried out using a torque wrench, which makes it a convenient method for use in the field or for maintenance purposes, but it can also be carried out on production lines using multi-head nut driving machines.

1.3.4 Direct tension indicators

The specification for load indication washers is given by BS 7644-1:1993 “*Direct tension indicators Part 1: Specification for compressible washers*”, BSI (1993b). A typical load indication washer is illustrated in Figure 4.

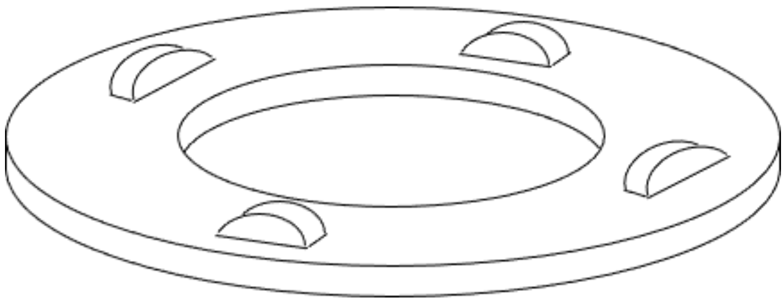

Figure 4: Load indication washer

These load indicating washers should be used in conjunction with plane washers manufacture to BS 7644-2:1993 “*Direct tension indicators Part 1: Specification for nut face and bolt face washers*”, BSI (1993c).

1.3.5 Angle-controlled tightening

The ‘angle-control tightening’ method, sometime called ‘turn-of-nut’ is becoming much more common. Initially the bolts are tightened just sufficient to close up the joint. This should be done producing the minimum amount of preload, the bolts being little more than ‘finger-tight’. The nut and protruding thread are then marked, usually with paint or permanent marker. Each nut and bolt assembly is then tightened, rotating the nut through a set angle relative to the bolt shank. In the case where the internal thread is tapped into the mating part the bolt head is rotated through the set angle.

The angle-control tightening method is often used when maintenance or repair work requires joints, originally assembled using the yield-controlled tightening method, to be re-made using hand tools.

1.3.6 Yield-controlled tightening

Yield-controlled tightening requires all the bolts to be tightened simultaneously up to the point each bolt has begun to yield. This requires an automated system that monitors both applied torque and relative nut rotation. Hence, yield-controlled is usually limited to operations being carried out on production lines.

1.3.7 Preloaded Joints in Operation

When external tensile forces are applied to preloaded joints the contact pressure at the faying surface, which is in effect a compressive residual stress in the joint, will change. Providing the contact pressure does not reduce to zero the joint will act as if it were a single, continuous, member. In-plane loads are supported by friction at the faying surface, which allows for in-plane load reversals to occur without movement within the joint that would lead to bolt loosening. Maintaining a positive contact pressure at the faying surface results in a low working alternating stress range within the bolts. This in turn results in good fatigue performance for the joint.

Preloaded joints are occasionally used in civil and structural engineering applications but are universally used in mechanical engineering load bearing bolted joints. The important benefits of preloaded joints are in producing a stiff joint, without slippage, and with good fatigue resistance.

The way that preloaded bolted joints work is often misunderstood. Contrary to intuition, external tensile loads on a preloaded bolted joint do not generate any significant additional tensile loads on the bolts. When external loads are applied to the joint most of tensile load component is supported by a reduction in contact pressure at the joint faying surface. Only a small proportion of the tensile load component is supported by an increase in bolt tension.

This thesis discusses a number of published works produced by the author that concentrate on the performance of joints made using preloaded bolts. The presented published works generally considers bolts to BS EN ISO 898:2009, BSI (2009a), bolt property-class 8.8, 9.8, 10.9 and 12.9. The works can also be applied to bolts that comply with BS EN ISO 3506-1:2009, BSI (2009b), property-class 70 or greater.

1.4 Brief history of development of bolted joint technology

Research into bolted joints appears to have been carried out from around the early 1920's through to the present day. Much of this early work relates to snug tightened bolted joints and is mainly applicable to civil/structural engineering works (ref. AISC (2004b), AISC (2005) and Tamboli (2017)), and not really relevant to mechanical engineering. In mechanical engineering load carrying bolted joints are predominantly preloaded. One significant impetus for the early research work into bolted joints was the desire to replace the more expensive hot driven rivets being used in the construction of high-rise steel framed buildings (skyscrapers) that were starting to become much more common at that time. Additionally, during the construction of high-rise steel framed buildings, it was not always possible/practical to heat the hot driven rivets local to where the joint was being made. Hence, the rivets often had to be heated at a remote location and then transported to the point of installation. Since the rivets had to be installed and driven whilst still at red heat, the use of bolts in high-rise steel framed building not only had economic advantages, it was also significantly safer.

An early method of analysis snug tightened joints was to consider each bolt as a structural element and assumed moments were reacted at a 'hard' pivot along one edge of the flange, as illustrated in Figure 5. A hard point is defined as a point, or small region, of a structure that lies on the load path.

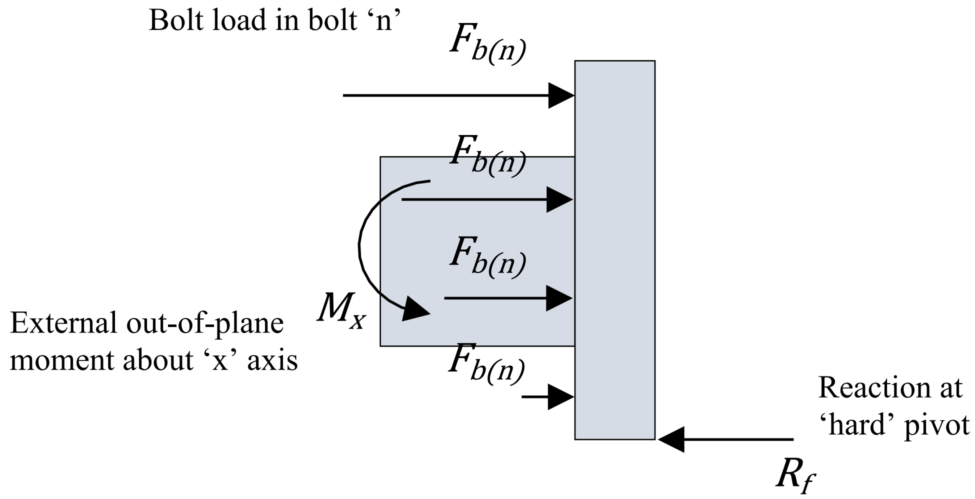

Figure 5: Snug tightened joint: 'Hard' pivot point

It is not clear when this method of analysis was first introduce however, it will almost certainly have been in use at the time bolted joints were first used in load bearing civil structural constructions. These early civil structures would have used mild steel bolts, approximately equivalent to modern property-class 3.6, 4.6 or 4.8 and possibly slightly higher grades equivalent to property-class 5.6, 5.8 and 6.8 and the bolts would be acting in shear, reference Batho and Bateman (1934). Any tensile loads would be secondary, arising from load offset.

By 1927 the idea of applying significant bolt preload had formed when Rotscher (1927) described how a preloaded bolt does not produce a uniform pressure at the faying surface. Instead, he suggested that the bolt would form a pressure cone resulting in a circular region of high pressure. A further significant step in the development of bolted joints occurred in 1934 when Batho and Bateman (1934) suggested that bolts with a yield strength of 54ksi (372MPa), which approximately equates to modern a property-class 5.8 bolt, could be tightened sufficient to prevent slip. This appears to be the first time that it was suggested that what were then considered high strength bolts could be used as direct replacements for hot driven rivets in civil structural steelwork.

In 1947 the Research Council on Riveted and Bolted Structural Joints was formed (now renamed the Research Council on Structural Connections), located in the United States of America. In January 1951 the Research Council introduced the "*Specifications for Assembly of Structural Joints Using High Tensile Steel Bolts*", RCSC (1951), endorsed and published by the American Institute of Steel Construction (AISC). This new specification permitted high strength bolts to be used as direct, one-to-one, replacements/alternative to rivets of the same nominal dimensions.

This specification, RCSC (1951), required all high strength bolts to be preloaded. This would have led to complexity in the building process, the type of bolt in each joint would have to be monitored and recorded. This requirement no longer exists and now it is common practice to use high strength bolts, usually property-class 8.8, throughout and only preload those bolts in joints that require it.

Since its inception, the Research Council has been a catalyst for research into bolted joints. A major revision of the earlier method analysis of snug tightened joints came out of this research activity. This new method assumed moments were reacted through a linearly distributed compression zone, rather than the 'hard' pivot about an edge. This, then, new method is illustrated in Figure 6.

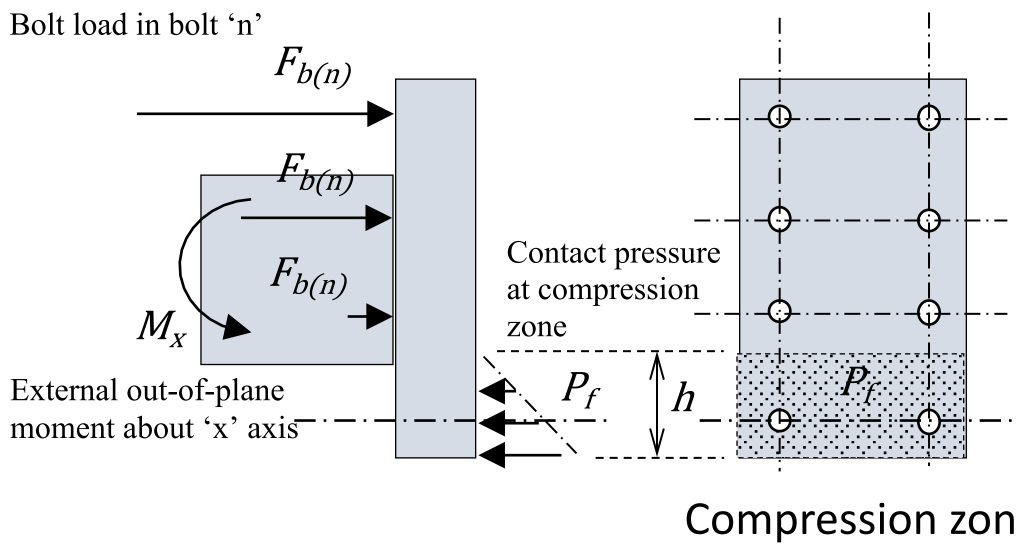

Figure 6: Snug tightened joint: Linearly distributed compression zone

Again, it is not clear when this method of analysis was introduced but it would have been well established by the 1970's and forms the basis of bolted joint analysis of current civil engineering design codes. The "*Steel Constructors Manual*", AISC (2005), published by the American Institute of Steel Construction used this method for the analysis of 'eccentric loading normal to the faying surface', that is, the analysis of out-of-plane moment on snug tightened joints.

1.5 Brief history of analysis methods

The foundation for the research work being presented in this thesis probably has its origins dating back some 30 years, or more. During these earlier years it was common practice in stress analysis to calculate the minimum sizes that a structure would require to ensure the design stress was not exceeded. It was the author's usual practice to size bolts for preloaded joints by first considering the joint as a solid structure, that is, treating the flanges of the joint as a single member. The stresses that would be produced in this 'solid connection' by the external loads and moments applied to the joint were calculated. These tensile stresses would have to be less than or equal to the flange surface contact stresses created by the preloaded bolts for the joint flanges to remain in contact. Hence, the clamping force required to maintain closure of the joint could then be calculated by multiplying the maximum tensile stress in the 'solid connection' by the surface area of the joint. Any shear stresses on the joint would have to be supported by friction at the joint face. This would require an additional component of clamping force that would need to be equivalent to the maximum shear stress divided by the friction coefficient for the faying surface. An appropriate size of bolt would be chosen and the number of bolts required to provide the total clamping force would be calculated. This method of analysis is based on the requirement to maintain contact at the faying surface but does not analyse the bolt loads or faying surface contact pressure distribution for individual load cases. It simply indicates the size and number of the bolts required for the joint design to maintain a contact stress.

From the early 1970's and onwards, computers started to be more routinely used in engineering analysis and Finite Element Analysis (FEA) packages started to be developed. The use of computers became much more common after about 1980 when desktop computers became available. At the same time, main-frame computers became physically smaller and significantly cheaper. As a result, Finite Element Analysis packages to run on these smaller main-frame computers became commercially available. At this point there was a fundamental shift in the way engineering stress analyses were carried out. Instead of starting with an allowable stress and then calculating the minimum ruling section requirements, which Finite Element Analysis cannot readily achieve, it became usual practice to specify the geometry and then calculate the stresses that would occur. At the same time, Computer Aided Design (CAD) packages also became available.

Classical analysis and finite element methods (FEM) are both still relevant to modern calculations. Classical methods have two main strengths. Firstly, they can be used to provide ‘scantlings’ for a design. That is, they can be used to provide a guide to the minimum section properties required for the design. Secondly, when classical methods are used in computer-based applications such as spreadsheets, MathCAD© or SMath© Studio they ‘program’ the calculations into a ‘model’. If parametric geometry is also created within this model then, in effect, it becomes what could be described as a ‘Digital Twin’. With this type of model/’Digital Twin’ it is relatively easy, and fast, to answer ‘what-if’ questions. ‘What-if’ the number of bolts in the joint in reduced/increased? ‘What-if’ the flange thickness is change? These types of ‘what-if’ questions, that can be answered in a matter of minutes with a computer application-based model utilising classical analysis methods, could take hours to answer using FEA/FEM models. While FEA/FEM has the potential to produce more accurate analysis results than classical methods and are able to address design details their output should not be accepted without verification and validation checks. Classical analysis application-based models can provide data that can be employed as part of the validation process.

1.6 Aims and Objectives

Welch (2018a) had observed that it was not unusual for preloaded to be treated as structural members when analysing the load distribution. The "Fastener Design Manual" by Barrett (1990) recommends analysing preloads bolted joints in this manner. However, Welch (2018a) observes that this results in an under estimate of bolt loads, typically around 30% or more. Welch's concern, that inappropriate methods of analysing preloaded bolted joints were being promoted, and used, was the driver for the work being presented. An additional driver was that existing works on preloaded bolted joints for mechanical engineering applications, where external loads are axial to the bolts, was limited to single bolts and did not consider multi-bolt preloaded joints.

When the work started, the initial aim was to promote the 'best practice' in the analysis of preloaded bolted joints. Best practice includes understanding the background of methodology and its limitations. The objective was to produce a single, citeable, paper that could be used by mechanical engineering stress analysts as a guide to the analysis of preloaded bolted joints. Focus on this initial objective led to the realisation that there were gaps in the knowledge and understanding of how multi-bolted joints function. As a result, the aim of the work was extended to include the development of understanding and contribute to knowledge of preloaded bolted joints by conducting further original research work. Each of the presented papers had their own aims and objectives

Established works on preloaded bolts consider a single bolt within a cylinder, reference ESDU (2005), Budynas and Nesbett (2006) and VDI (2003). This cylinder can be thought of as a region of the flanges surrounding the bolt. This 'model' is then used to calculate the effective spring stiffness for one bolt assembly. Two of the papers being presented, "*Classical Analysis of Preloaded Bolted Joint Load Distributions*", Welch (2018a), and "*A paradigm for the Analysis of Preloaded Bolted Joints*", Welch (2019), consider all of the bolts within the joint as acting together and part of a single system. One of the objectives of these published works was to consider the interaction between the bolts in multi-bolted preloaded joints. In these papers, both the 'detailed analysis' and the 'design analysis' of a preloaded bolt were considered. The detailed analysis of preloaded bolted joints uses classical theory of elasticity methods to gives an understanding of how preloaded joints work and the interaction of the various components of the joint. Using this understanding, a less detailed, more pragmatic, method of design analysis was developed.

The second of the two papers, Welch (2019), introduces the concept of including dowels in the analysis, ‘pegging’ the joint to prevent slip and discusses how they should be analysed. Maintaining the objective of considering the whole joint, the understanding of flange bending and thread shear in threaded holes are also developed. These are presented as a practical design analysis process that is applicable for many cases of preloaded bolted joints and are adequate to demonstrate the structural integrity of each element of the joint.

The initial papers Welch (2018a) and Welch (2019), highlighted areas where there appeared to be a need for more work to improve and expand on the understanding of how preloaded bolted joint support in-plane external loads. This led to the papers “*Analysis of Bolt Bending in Preloaded Bolted Joints”*, Welch (2018b), and “*Bolted Joint Preload Distribution from Torque Tightening*”, Welch (2021). The objective of the first of these papers, Welch (2018b), was to consider what actually happens to preloaded bolts under in-plane loading conditions. The objective was to determine the true bolt shear stress. Classical analysis methods were used, to show how flexural deflections of the bolts due to shear strain in the flange pack produce bending moments and additional tensile loads on the preloaded bolts. The paper by Welch (2018b), considers shear strain through the flange pack and the transverse flexibility of the bolt. This approach is less conservative than other methods that have been considered in the past. Using this approach it was possible to show that in-plane loads can produce a tensile load component on the bolt which is additive to the bolt preload and the component of axial load due to out-of-plane external loads. These additional tensile loads arise from the shear strain in the flanges and the high through flange stiffness of the joint.

The ability for the joint to transmit shear loads across the faying surface relies on the effectiveness of the bolt tightening procedure used to makeup the joint. Bolt tightening procedures are intended to achieve an optimum preload condition. Usually bolt tightening starts with the bolt nearest the centre of the bolt group. The tightening sequence then spreads outwards, crossing from one side of the joint to the other to avoid tightening adjacent bolts, ASME PCC-1 (2010). This tightening procedure is carried out in increment over several passes. The paper on torque tightening, Welch (2021), was a theoretical study of what occurred within a joint during the tightening sequence and the final preloaded condition of each individual bolt in the joint. The objective was to determine how well the bolt tightening procedure achieved the intended final preload condition. The method of analysis used in the paper would not be required for the majority of preloaded bolted joint analyses. However, it could be used in establishing the optimum bolt tightening sequence for some critical joints or for investigating joint failures.

The paper on bolt bending, Welch (2018b), concluded that the method of bolt bending analysis presented was suitable for calculating stresses for use in a fatigue analysis. Fatigue analyses usually take one of two forms, they can be based on either 'Safe-Life' or 'Damage Tolerance'. A safe-life fatigue analysis uses Wöhler plots, or S-N curves, to determine a component's total life to failure as a number of cycles to failure based on the mean and alternating stresses to which the component is subjected. The damage tolerance procedure uses fracture mechanics to determine the number of load cycles that would cause an 'existing' small defect, acting as the nucleus, to first form a crack and then to propagate the crack to a size that is unstable and would cause the component to fracture. The damage tolerance method of analysis is applied to situations where any cracks in the structure or component can be detected during routine planned maintenance and then monitored until the time the structure is rectified or replaced.

A characteristic of preloaded bolted joints is that it is not feasible to carry out visual inspection of the bolts. Removing the bolts for inspection purposes and then reinstalling the bolt would introduce a large fatigue load cycle which would induce a significant amount of fatigue damage hence, they are usually analysed using safe-life methods. The two papers, "*An Empirical Approach to a Comprehensive Damage-Equivalent Stress for Fatigue*", Welch (2022b), and "*Fatigue Analysis of Preloaded Bolted Joints*", Welch (2022c), represent a significant piece of research work in the area of safe-life fatigue analysis. The work carried out in producing first of the two papers, Welch (2022b), was originally intended to form just one section of the second of the two papers, Welch (2022c). The original objective for this one section was to determine which of the existing methods of calculating a damage-equivalent stress was the more accurate and most applicable to preloaded bolts. However, this piece of work showed that none of the methods considered were entirely suitable hence, the scope of the work was revised. The revised aim and objectives were to produce a Damage-Equivalent stress function suitable for use on preloaded bolted joints. However, the complexity and significance of this new piece of work meant that it was more appropriate to publish it in its own right.

The complexity of producing S-N curves means that there are not any readily available S-N curves for preloaded bolts. The objective of the work presented in the paper, Welch (2022c), was to develop and present a series of S-N curve specific to high strength bolts and screws, property-class 8.8 to 12.9. Methods based on notch sensitivity, Chapter 4 of Pilkey (1997), were used to modify several existing S-N curves to the elastic stress concentrations, Pilkey (1997), applicable to a range of ISO metric screw thread sizes. Curve fitting techniques were then used to present these S-N curves as a function of the damage-equivalent stress, calculated using the function presented in the previous paper, Welch (2022b).

CHAPTER 2

THE PRELOADED BOLTED JOINT AS A SYSTEM

2.1 The Preloaded Bolted Joint as a System

Many studies into the effects of bolt preload are based on a single bolt, ESDU (2005), Budynas and Nesbett (2006) and VDI (2003). Typically they concentrate on how a single bolt interacts with the cylindrical region of the flanges surrounding it. Chapter 8 of "*Shigley's Mechanical Engineering Design*" Budynas and Nisbett (2006), and VDI 2230 Part 1, *"Systematic calculation of high duty bolted joints with one cylindrical bolt"*, VDI (2003), both consider only single bolt assemblies. One of the objectives of the published works being presented herein was to consider the interaction between the bolts in multi-bolted preloaded joints.

The work being presented in this section was initially part of a much larger package of work. However, the original work was far too large and too wide ranging for presentation as a single paper but, at the same time, too small to be published as a monograph. As a result, this larger work was split into two separate, sensibly sized papers, Welch (2018a) and Welch (2019).

The objectives of the first of these two papers were to demonstrate how preloaded bolted joints perform their task and to show that the bolts cannot be considered as a single entity, they have to be considered as part of a bolt group and working as part of the total joint assembly.

In the first of these papers, both the 'detailed analysis' and the 'design analysis' of a preloaded bolt are both considered. Initially the detailed analysis of preloaded bolted joints using classical theory of elasticity methods is discussed. This gives an understanding of how preloaded joints work and the interaction of the various components of the joint. Using this understanding, a less detailed, pragmatic, method of design analysis is developed. This 'design analysis' method is an adaption of an early method of analysing snug tightened joints, Barrett (1990), as illustrated in Figure 5, replacing the concept of pivoting about a ‘hard’ point with the introduction of beam theory and pivoting about the neutral axis. The method of analysing snug tightened joints considers each bolt as a structural element to calculate individual bolt loads however, the pragmatic ‘design analysis’ method introduces the concept of a ‘bolt-related’ load. This bolt-related load is defined within Welch (2018a) (AAM P1 Section 3) as: “The loads on each region of the joint that is under the influence of a bolt”. It is not the actual bolt load. It is the component of external load reacted through the bolt assembly, comprising a bolt and its surrounding region of flange.

2.2 Classical Analysis of Preloaded Bolted Joint Load Distributions

Over the years, the author made several attempts to find a citable reference to the analysis of multi-bolt preloaded bolted joints. During these attempts several papers that are applicable to snug tightened joints, as used in civil engineering structures, were found, AISC (2005) and Barrett (1990). This first article was prompted to be written because it was not possible to find references to any papers that used classical methods to consider how multi-bolt preloaded bolted joints behave under both in-plane and out-of-plane loads.

This first paper, Welch (2018a), develops an understanding of how external loads are reacted through preloaded bolted joints. The objective was to consider the whole joint. This is quite different to what had already been published, which generally concentrated on the stiffness of a single bolt and the region of flange surrounding it, usually represented as a cylindrical region, ESDU (2005), Budynas and Nesbett (2006), and VDI (2003). The paper being discussed develops a detail analysis method, based on the theory of beams, and a simplified design analysis method based on loads. The article then presents a practical design analysis process for preloaded bolted joints. Interpretation of results, within the context of design standards, is provided.

2.2.1 P1 - Author Accepted Manuscript (International Journal of Structural Integrity. Vol. 9 (2018), No. 4, pages 455 – 456.)

Classical Analysis of Preloaded Bolted Joint Load Distributions

Michael Welch

Michael A Welch (Consulting Engineers) Limited, West Lancashire, UK.

Abstract

Purpose – This paper develops the understanding of how external loads are reacted through preloaded bolted joints and the interaction of the joint elements. The article develops ideas from how to do an analysis to understanding the implications of the results

Design/Methodology/Approach - Classical methods of analysis are applied to preloaded bolted joints, made with multiple bolts. The article considers both the detailed analysis of bolts stresses, for use in fatigue analysis, and load based design analysis, to demonstrate the structural integrity of preloaded bolted joints.

Findings – In preloaded joints the external tensile axial load and moments are mainly supported by changes in contact pressure at the faying surface. Only a small proportion of the external loads produce changes in bolt tensile stress. The bolts have a significant mean stress but experience a low working stress range. This low stress range is a factor explaining in why preloaded bolted have good fatigue performance.

Practical implications – In many cases the methods presented are adequate to demonstrate the structural integrity of joints. In some cases finite element methods may be more appropriate, and the methods discussed can be used in the validation process.

Originality/Value – The article brings together a number of concepts and links them into a practical design analysis process for preloaded bolted joints. Interpretation of results, within the context of design standards, is provided.

Keywords: bolted joint, preloaded bolt, bolt preload, bolt tension, multiple bolt, multi bolt

Article type: General Review

Nomenclature

A_b	Tensile area of each bolt
A_f	Area of faying surface
A_j	Total area of joint (Faying surface plus bolts)
$A_{s.b(n)}$	Shear area of bolt 'n'
$F_{b(n)}$	Bolt load in bolt 'n'
$F_{br(n)}$	Bolt-related load for bolt 'n'
F_{dp}	Design preload
F_p	Preload in each bolt
$F_{p.0}$	Minimum required preload
$F_{s.b(n)}$	Shear load on bolt 'n'
$F_{s.br(n)}$	Resultant bolt-related shear load for bolt 'n'
F_x	External In-plane force acting in x-direction
$F_{x.br(n)}$	Bolt-related shear load in x-direction for bolt 'n'
F_y	External In-plane force acting in y-direction
$F_{y.br(n)}$	Bolt-related shear load in y-direction for bolt 'n'
F_z	External axial load in direction of 'z' axis
$I_{xx.j}$	Second Moment of Area of joint about 'x' axis
$I'_{xx.j}$	Second Moment of Area transposed about x'-axis
$I_{xy.j}$	Product Moment of Area of joint
$I_{yy.j}$	Second Moment of Area of joint about 'y' axis
$J_{zz.j}$	Polar Second Moment of Area of joint
L_g	Bolt grip length (including washers)
$M_{b(n)}$	Bending moment on bolt 'n'
M_x	External moment acting about 'x' axis
M'_x	Resultant moment
M_y	External moment acting about 'y' axis
M_z	External torsional moment acting on joint

N_b	Number of bolts in joint
P_f	Contact pressure at faying surface
P_p	Pressure at faying surface, preload pressure
x	Coordinate in plane of joint face
$x_{(n)}$	Coordinate of bolt 'n'
y	Coordinate in plane of joint face
$y_{(n)}$	Coordinate of bolt 'n'
y'	Transposed coordinate
μ_f	Friction coefficient at faying surface
$\sigma_{a.b(n)}$	Axial stress in bolt 'n'
τ_x	Shear stress from loads in x direction
τ_y	Shear stress from loads in y direction
τ_{xy}	Resultant shear stress
$\tau_{xy(n)}$	Shear stress in bolt 'n'
θ	Angle of resultant moment

1 Introduction

Threaded connections, in particular bolted joints, are a common engineering feature found in most manufactured equipment and structures.

In preloaded joints the bolts are first tightened sufficient to establish closure of the joint with alignment of the mating components, then further tightened to produce the required bolt preload and (more importantly) a compressive load at the faying surface. The faying surface is the joints prepared contact face. Preloading is intended to maintain closure of the joint and make it perform as a single continuous member.

Whilst there is a clear understanding of a tensile load acting upon a single/individual preloaded bolt there is often some misunderstanding about the way loads are distributed within multiple bolt joints. It is not unusual for preloaded bolts to be treated as structural members when analysing the load distribution. This results in an under estimate of bolt loads, typically around 30% or more.

This article considers the analysis of out-of-plane moments acting on joints made using preloaded bolts. Attention is paid to the load distributed among the bolts.

In many cases the methods presented are adequate to demonstrate the structural integrity of joints. In some cases finite element methods may be more appropriate, and the methods discussed can be used in the validation process. Guidance on the application of finite element techniques is available in reference [1].

Where equipment is being designed to meet specific standards, any safety factors, partial safety factors and design factors required by the standard should be incorporated into the analysis and should take precedence over any equivalent factors suggested here.

2 Preloaded Bolt Joint Theory

Ideally, preloading the joint’s bolts induces a near uniform compressive stress at the faying surface. When external loads are applied any resulting tensile stress components act to reduce this compressive stress. While the faying surface retains some compressive stress the joint will continue to perform as a continuous member. If a resulting tensile stress component attempts to exceed the pre-compression at the faying surface separation of the joint occurs. At this point the joint is deemed to have failed, even though none of the joint components have failed.

The way a preloaded joint performs is illustrated in Figures 1 to 3.

Figure 1(a) shows a typical bolted joint. Figure 1(b) is the free body diagram for one mating component, with the bolt preloads considered as point loads. Equation 1 gives the resulting pressure at the faying surface.

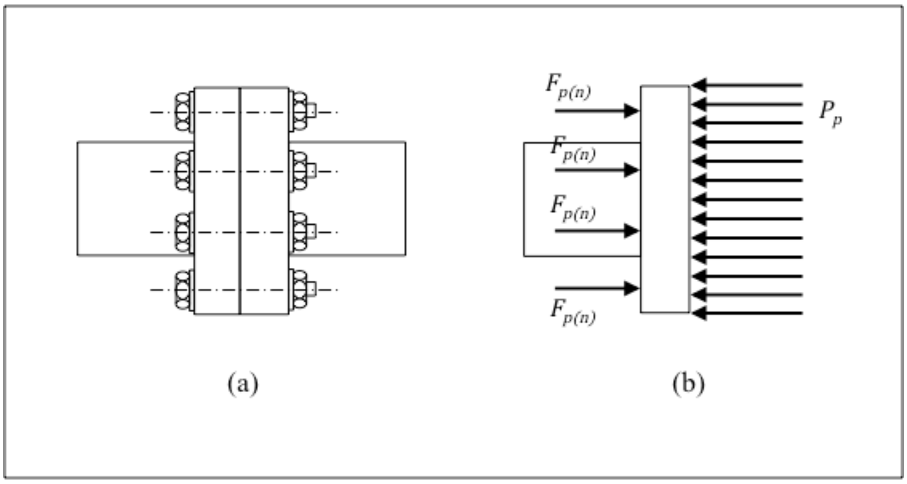

Figure 1. Preloaded Joint.

Pressure at faying surface $$P_p = \frac{-N_b \cdot F_p}{A_f} \tag{1}$$

The negative sign in equation 1 indicates that the tensile preload in the bolts produces a compressive stress at the faying surface.

Figure 2(a) shows the joint with an external axial (tensile) load applied and Figure 2(b) shows the free body diagram of one mating component. Similarly, Figure 3(a) shows the joint with an external moment applied and Figure 3(b) shows the free body diagram of one mating component.

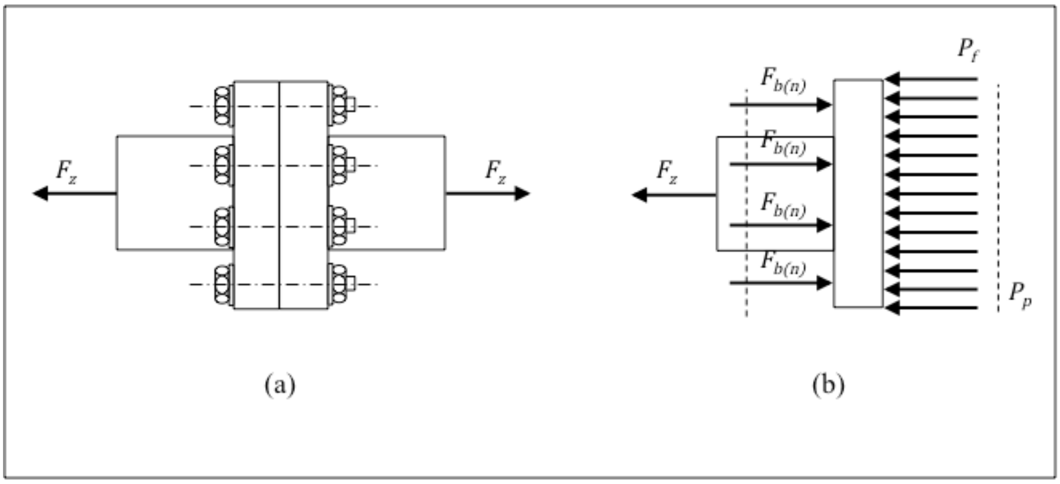

Figure 2. External Axial load Applied.

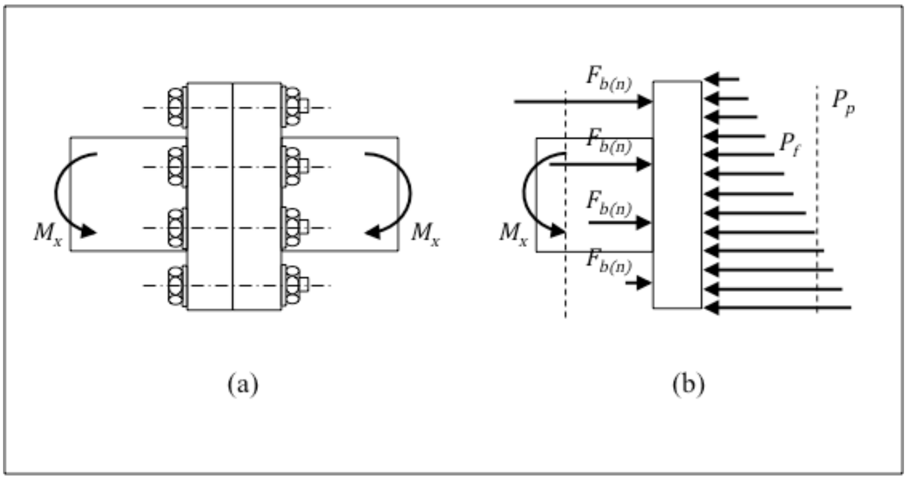

Figure 3. External Moment Applied.

The bolt axial stresses resulting from the combined loading of the preload, external axial load and external moment are given by equation 2a.

Axial stress in bolt 'n' $$\sigma_{a.b(n)} = \frac{F_p}{A_b} + \frac{F_z}{A_j} + \frac{M_x}{I_{xx.j}} \cdot y_{(n)} \tag{2a}$$

The total area of the joint A_j is given by $A_j = A_f + N_b \cdot A_b$

In deriving equation 2a it is assumed that superposition of stresses resulting from F_z and M_x is valid. The y-coordinates are defined with respect to the neutral axes of the joint.

In equation 2a the moment M_x acts about the x-axis of the joint, as illustrated in Figure 4(a). When there is a second moment, M_y, acting about the joint y-axis the assumption of superposition of stresses is not always applicable. To maintain a general method of analysis an alternative coordinate system, aligned to the resultant moment, is considered. This alternative coordinate system is illustrated in Figure 4(b).

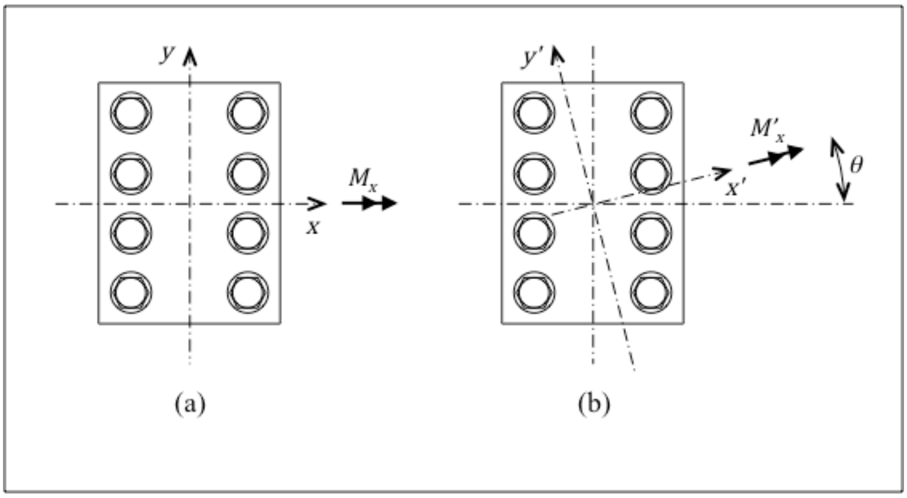

Figure 4. Joint coordinate systems.

The resultant moment is given by $M'_x = \sqrt{M_x^2 + M_y^2}$

The angle between the transposed coordinate system and the joint coordinate system is given by $\theta = arctan\left(M_y/M_x\right)$

The transposed coordinates are given by $y' = y \cdot \cos(\theta) - x \cdot \sin(\theta)$

The second moment of area about the *x*-axis transposed to the *x'*-axis is given by

$$I'_{xx.j} = I_{xx.j} \cdot cos^2(\theta) + I_{yy.j} \cdot sin^2(\theta) - I_{xy.j} \cdot \sin(2\theta)$$

Using the resultant moment, the transposed coordinates and the transposed second moment of area in equation 2a and then simplifying the resulting equation leads to equation 2b.

$$\sigma_{a.b(n)} = \frac{F_p}{A_b} + \frac{F_z}{A_j} + \frac{\left(M_x^2+M_y^2\right)\left(M_x \cdot y_{(n)} - M_y \cdot x_{(n)}\right)}{I_{xx.j} \cdot M_x^2 + I_{yy.j} \cdot M_y^2 - 2 \cdot I_{xy.j} \cdot M_x \cdot M_y} \qquad \text{(2b)}$$

where $x_{(n)}$ and $y_{(n)}$ are the coordinates of bolt 'n' about the joint centroid.

Equations 2a and 2b both follow the "right hand" rule. A positive axial load produces a positive (tensile) stress component in all bolts. A positive moment about the *x*-axis produces positive (tensile) stress components in bolts with positive *y*-axis coordinates and negative (compressive) stress components in bolts with negative *y*-axis coordinates. In equation 2b, a positive moment about the *y*-axis produces positive (tensile) stress components in the bolts with negative x-axis coordinates and negative (compressive) stress components in the bolts with positive x-axis coordinates.

The total bolt load is given by equation 3.

Bolt load $$F_{b(n)} = \sigma_{a.b(n)} \cdot A_b \tag{3}$$

The resulting pressure at the faying surface, as a function of the joint coordinates, is given by equation 4a or equation 4b.

Pressure at faying surface $$P_f = P_p + \frac{F_z}{A_j} + \frac{M_x}{I_{xx.j}} \cdot y \tag{4a}$$

or $$P_f = P_p + \frac{F_z}{A_j} + \frac{(M_x^2+M_y^2)(M_x \cdot y - M_y \cdot x)}{I_{xx.j} \cdot M_x^2 + I_{yy.j} \cdot M_y^2 - 2 \cdot I_{xy.j} \cdot M_x \cdot M_y} \tag{4b}$$

where x and y are coordinates about the centroid of the joint.

Again, equations 4a and 4b follow the "right hand" rule. Equations 4a and 4b are based on the same assumptions and transforms used in deriving equations 2a and 2b.

Equations 2b and 4b show that the magnitude of the change in tensile stress of any particular bolt is the same as the magnitude of the change in pressure at the surrounding faying surface. Studying the first two terms on the right hand side of equations 2b and 4b it is concluded that the external tensile axial load is mainly supported by a reduction in the faying surface contact pressure/stress, with only a small proportion of the external load acting to increase the bolt tensile stress.

Similarly, the external moments are also mainly carried by changes in the faying surface contact pressure distribution. Again, the external moments produce only a small increase/decrease in bolt stresses.

Hence, the preloaded bolts have a significant mean stress but experience a low working stress range. This low stress range is a major factor in why preloaded joints have good fatigue performance.

The detail analysis discussed here is suitable for calculating stresses for use in a fatigue analysis. Safety factors, partial safety factors and design factors would not be incorporated into a fatigue analysis (although stress concentration factors may be applied). The analysis would use the bolt preload intended to be applied during assembly. Any safety factors, partial safety factors and design factors required by standards would be incorporated into the static analysis. The static analysis would be carried out for the design bolt preload, which should be specified within the standards. The design bolt preload can be expected to be in accordance with section 3.8 of BS 7608:1990 [2] which says that;

> 'If reliance is to be placed on this pre-load, it should be at least 1.5 times the design tension'

Or in other words, the design bolt preload (F_{dp}) = 2/3 the applied bolt preload (F_p). The design bolt preload takes account of a number of factors, including tolerances on the bolt preload applied during assembly.

The allowable faying surface contact pressure for the joint, limited by the design bolt preload, is defined by equation 5.

Faying surface contact pressure limit $$P_f \leq \left(1 - \frac{F_{dp}}{F_p}\right) \cdot P_p \quad (5)$$

And the contact pressure P_p is calculated for the applied bolt preload.

2.1 In-Plane Loads on the Joint

External in-plane loads and torsional moments are supported by two mechanisms, friction at the faying surface and bolt shear. In some joints, dowels, or other positive method of location of the joint, can assist these two mechanisms.

Assume that there is little or no rotation of the bolt head or nut. Figure 5 illustrates the way external in-plane loads are reacted into the bolts. The shear loads on the bolts are transmitted by friction under the bolt head and nut.

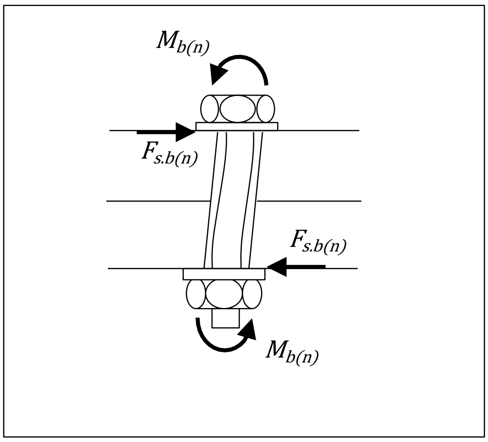

Figure 5. Joint In-Plane loads reacted into a bolt.

Assuming there is no slip at the faying surface, the shear stress in the plane of the faying surface, is given by equations 6 to 8.

Shear stress from loads in x direction $\tau_x = \frac{F_x}{A_j} - \frac{M_z}{J_{zz.j}} \cdot y$ (6)

Shear stress from loads in y direction $\tau_y = \frac{F_y}{A_j} + \frac{M_z}{J_{zz.j}} \cdot x$ (7)

Resultant shear stress $\tau_{xy} = \sqrt{\tau_x^2 + \tau_y^2}$ (8)

Equation 6 gives the shear stress component acting in the x-direction. Similarly, equation 7 gives the shear stress component acting in the y-direction. Equation 8 gives the resultant shear stress at any point on the faying surface defined by the x and y coordinates. This shear stress is carried across the faying surface by friction.

The allowable shear stress for the joint is limited by friction at the faying surface as defined by equation 9.

Shear stress limit $\tau_{xy} \leq P_f \cdot \mu_f$ (9)

where μ_f is the friction coefficient at the faying surface.

Equation 9 uses the faying surface contact pressure based on the applied bolt preload F_p. Some standards may instead require the design bolt preload, or the minimum preload, to be used for calculating the contact pressure.

If the joint does not incorporate dowels the shear stress limit should be determined using a dynamic friction coefficient for μ_f. By using dynamic friction in calculating the shear stress limit, any potential movement or slip, resulting from an impact or dynamic load overcoming static friction, will be arrested.

The incorporation of a positive means of location, such as dowels, prevents movement or slip of the joint face. Hence, the shear stress limit can be determined using a static friction coefficient for μ_f.

2.2 Bolt Shear and Bending

The friction loads under the bolt head and nut, normal to the axis of the bolt, produce bending moments at the bolt head and nut and a shear load on each bolt within the joint. This shear load exists even though the bolts do not bear on the holes in the flanges. The shear stress in the bolts can be calculated from equations 6 to 8 using the appropriate *x* and *y* coordinates for the bolts.

The loads on the bolt head/nut acting perpendicular to the bolt shank are given by equation 10.

Shear load on bolt 'n'
$$F_{s.b(n)} = \tau_{xy(n)} \cdot A_{s.b} \tag{10}$$

The bending moments at the bolt head and nut are given by equation 11.

Bending moment on bolt 'n'
$$M_{b(n)} = \frac{F_{s.b(n)} \cdot L_g}{2} \tag{11}$$

where L_g is the bolt grip length (including washers)

It can be seen from equations 6 and 7 that the torsional stiffness of the joint is dominated by friction at the faying surface, which arises from the bolt preload. The bolt shear stress has only a small influence on torsional stiffness.

2.3 Dowels

The dowels assist in carrying the in-plane loads by "pegging" the joint, preventing slip and the associated reduction in friction. The shear stress in location dowels can be calculated from equations 6 to 8 using the *x* and *y* coordinates for the dowels.

It is common practice to size dowels to be capable of supporting all of the shear loads without considering friction at the faying surface

3 Design Analysis

A simplified method of design analysis can be developed which can be used for static analysis, based on loads, to demonstrate the structural integrity of the joint.

Consider only the changes in bolt load and faying surface pressure when external loads are applied. These changes are illustrated in Figure 6. Figure 6(a) shows only the changes to the free body diagram when the external loads are applied.

In practice, the contact pressure at the faying surface will not be uniform across the surface. Each preloaded bolt influences an approximately circular region of the faying surface that surrounds it. A method of calculating the area of faying surface influenced by a bolt is presented in part 3, section 8.5 of Shigley's Mechanical Engineering Design [3]. Assume each bolt influences the same amount of faying surface, and that the regions influenced by the bolts can be considered as springs of similar stiffness. In this case, an external moment is distributed onto the effective springs proportional to the distance of the bolt/spring from the neutral axis of the bolt group. Figure 6(b) illustrates the bolt-related loads resulting from the combined loading of the external axial load and external moment.

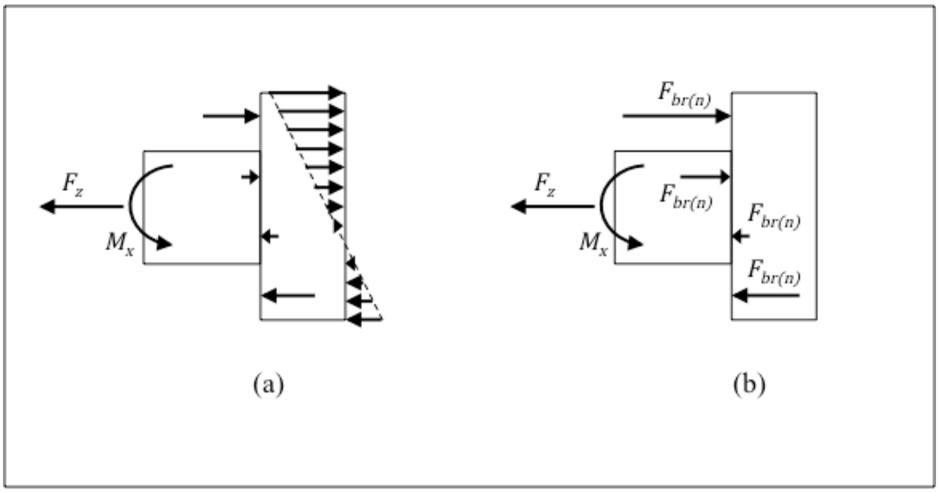

Figure 6. Internal load changes when external loads applied.

These bolt-related loads are given by equation 12a.

Bolt-related load for bolt '*n*' $$F_{br(n)} = \frac{F_z}{N_b} + \frac{M_x \cdot y_{(n)}}{\sum_n y_{(n)}^2} \quad (12a)$$

In deriving equation 12a the *y*-coordinates are defined with respect to the neutral axes of the bolt group.

In equation 12a the moment M_x acts about the *x*-axis of the bolt group. When there is also a moment M_y acting about the *y*-axis of the bolt group an alternative coordinate system, aligned to the resultant moment, is considered. This alternative coordinate system has already been illustrated in Figure 4. Appling the previously discussed transforms to equation 12a results in equation 12b

$$F_{br(n)} = \frac{F_z}{N_b} + \frac{(M_x^2+M_y^2)(M_x \cdot y_{(n)} - M_y \cdot x_{(n)})}{\sum_n (M_x \cdot y_{(n)} - M_y \cdot x_{(n)})^2} \quad (12b)$$

where $x_{(n)}$ and $y_{(n)}$ are the coordinates of bolt '*n*' defined with respect to the neutral axes of the bolt group.

The bolt-related loads are the loads on each region of the joint that is under the influence of a bolt, they do not represent the bolt loads. They are also independent of the joint geometry, other than for the bolt locations.

Equation 12a and 12b both follow the "right hand" rule. A positive axial load produces positive (tensile) bolt-related loads for all bolts. A positive moment about the *x*-axis produces positive (tensile) bolt-related loads for bolts with positive *y*-axis coordinates and negative (compressive) bolt-related loads for bolts with negative *y*-axis coordinates. In equation 12b a positive moment about the *y*-axis produces positive (tensile) bolt-related loads for bolts with negative *x*-axis coordinates and negative (compressive) bolt-related loads for bolts with positive *x*-axis coordinates.

The detailed analysis discussed earlier showed that the application of the external loads produced only small load changes in the preloaded bolts. The major effect of the external loads was to induce significant changes in the faying surface contact pressures. It follows that joint separation does not occur until the tensile bolt-related load exceeds the bolt preload. Hence, the minimum bolt preload required for the joint bolts can be assumed to be equal to the maximum value of tensile bolt-related loads, as expressed by equation 13.

Minimum required preload $$F_{p.0} = max\left(F_{br(n)}\right) \tag{13}$$

When discussing the faying surface contact pressure calculated by either equation 4a or equation 4b, the limiting factor, when the contact pressure reduced to zero, was based on the design bolt preload (F_{dp}). Following the same reasoning here, the limit on the minimum required preload is defined by equation 14.

Minimum preload limit $$F_{p.0} \leq F_{dp} \tag{14}$$

3.1 In-Plane Bolt-Related Loads

Again, assume that the preload in each bolt influences the region of the faying surface that surrounds the bolt. Also assume each region influenced by a bolt can be considered as a spring. Then the bolt-related loads resulting from the combined loading of the external in-plane loads and torsional moments are given by equations 15 to 17.

Bolt-related shear load in *x*-direction for bolt 'n'

$$F_{x.br(n)} = \frac{F_x}{N_b} - \frac{M_z \cdot y_{(n)}}{\sum_n\left(x_{(n)}^2 - y_{(n)}^2\right)} \tag{15}$$

Bolt-related shear load in *y*-direction for bolt 'n'

$$F_{y.br(n)} = \frac{F_y}{N_b} + \frac{M_z \cdot x_{(n)}}{\sum_n\left(x_{(n)}^2 - y_{(n)}^2\right)} \tag{16}$$

Resultant bolt-related shear load for bolt 'n'

$$F_{s.br(n)} = \sqrt{F_{x.br(n)}^2 + F_{y.br(n)}^2} \tag{17}$$

The allowable bolt-related shear load is limited by friction at the joint face as defined by equation 18.

Bolt-related Shear load limit $$F_{s.br(n)} < \left(F_p - F_{br(n)}\right) \cdot \mu_f \tag{18}$$

Equation 18 uses the applied bolt preload F_p. Some standards may require the design bolt preload or the minimum bolt preload to be used.

The choice of appropriate friction coefficient at the joint face is the same as for the detailed analysis described previously.

The bolt-related shear load limit should be determined using a dynamic friction coefficient for μ_f. If the joint incorporates a positive means of location a static friction coefficient can be used for μ_f.

Any safety factors, partial safety factors and design factors required by any standards being followed should be incorporated into the static analysis.

Because the load analysis is “disconnected” from the geometry it is not possible to separate out the in-plane loads on the bolts and dowels. Generally, bolt shear will not be an issue provided equation 18 shows that the bolt preload can support the bolt-related shear load along with the bolt-related tensile load. Dowels can be sized to be capable of supporting all shear loads without considering friction at the faying surface.

4 Summary

Preloading the joint bolts induces a compressive stress at the faying surface. When external loads are applied any resulting tensile stress components act to reduce this compressive stress. As long as the joint remains closed it will continue to perform as if it were a continuous member.

External tensile axial load and moments are supported mainly by a reduction in the contact pressure at the faying surface, with only a small proportion of the external loads producing changes in the bolt tensile stresses. This low working stress range is a major factor in the fatigue performance of preloaded joints.

External in-plane loads and torsional moments on the joint are supported mainly by friction at the faying surface. In some joints dowels, or other positive method of location of the joint, can assist in supporting the shear loads by preventing slip at the joint face.

References

[1] Verein Deutscher Ingenieure (Association of German Engineers) VDI 2230 Part 2. 2014, *Systematic calculation of highly stressed bolted joints Multi bolted joints*

[2] British Standards Institution. BS 7608:1990, *Code of practice for Fatigue design and assessment of steel structures.*

[3] Budynas R, Nisbett J K. (2006) *Shigley's Mechanical Engineering Design.* 8th edition. McGraw Hill, Primis Online, ISBN 0-390-76487-6

2.2.2 Further Discussion

As discussed in the paper, Welch (2018a), in reality, the contact pressure at the faying surface of a preloaded joint is not uniform across the surface. Each preloaded bolt influences an approximately circular region of the flanges and faying surface that surrounds it, Rotscher (1927). As a result, the total active area and the effective second moment of area of the joint are less than the faying surface area and its second moment of area. Hence, the surface contact pressure around the bolt installation is higher than the mean contact pressure predicted by using the total faying surface area. Similarly, the change in bolt stress and the change in contact pressure due to the applied loads are also higher. These two effects act to cancel each other out when considering the external loads that could cause joint separation.

The paper draws attention to the fact that the design analysis method does not apply to joints made with a single row of fasteners or a joint made with a single bolt. This illustrates the difference between a detailed analysis, which attempts to describe as closely as possible how a structure or component actually behaves, and a design analysis, which is intended to simply show the structure or component is fit for purpose.

The design analysis method is independent of flange geometry. The second moment of area of the flange is not calculated but is, in effect, approximated by the sum of the squares of the bolt coordinates, measured from the neutral axis of the bolt group, multiplied by an unspecified area. This unspecified area can be considered as being equivalent to an area surrounding a bolt, and the resulting bolt related load is the component of external load carried by this area and the bolt. This method of analysis reduces the amount of calculation required but results in a conservative solution, high value, for loads. This is due to the slightly low value for the effective second moment of area that is implicit with the method of analysis. This low value of the second moment of area for the joint stems from omitting the summation of the individual second moment of area for each of the unspecified areas. The design method is particularly useful if the flange has a complex shape and if the design is evolving.

The aspects of seal glands and pressure seals within structural members were not discussed in the paper. It is common practice in many industries, such as the Oil and Gas industry, and the Petro-chemical industry, to incorporate seals within bolted joints. Some typical bolted joint arrangements that incorporate seals are illustrated in Figure 7.

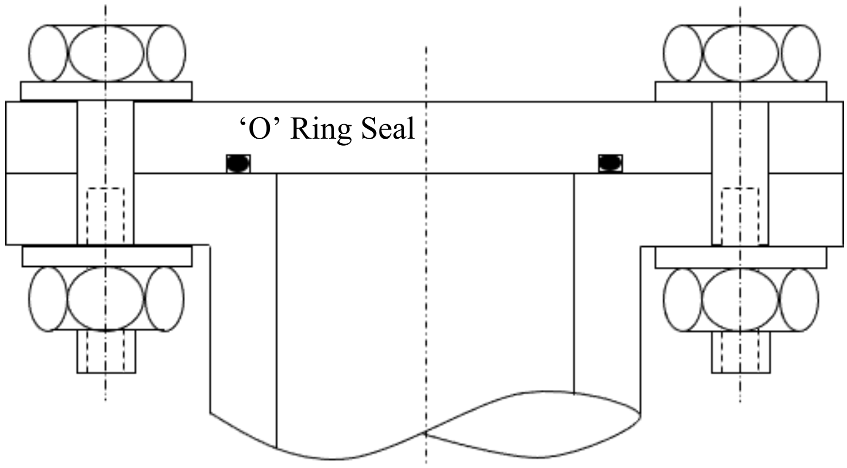

Figure 7a

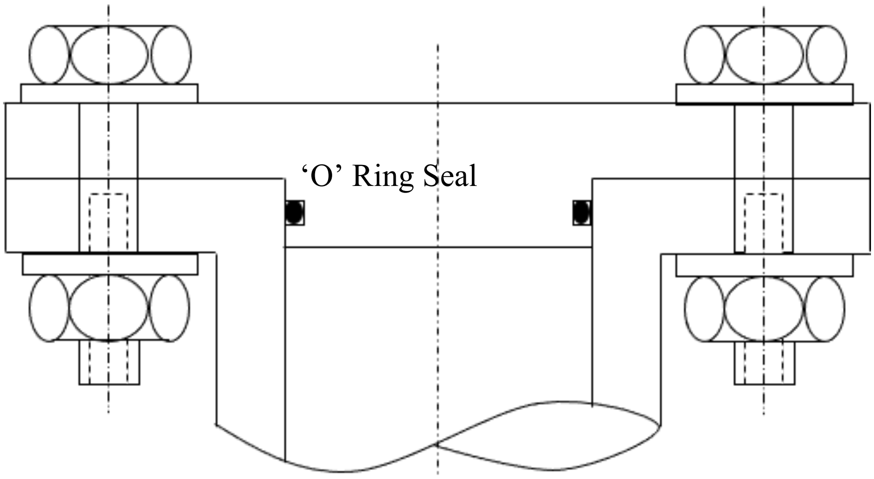

Figure 7b

Figure 7. Bolted joints incorporating seals

In seal arrangements that require the joint bolts to provide the initial seal compression for the installation, as in Figure 7a for example, the joint compression load has to be provided by the bolt preload. This means that slightly less than the full preload is available to produce the contact pressure at the joint face. When incorporating seals into structural bolted connections it is essential to ensure that installation procedures do not result in contamination of joint faces with grease or, other mediums used in the installation of the seal, that can change/reduce the friction at the joint face. Particularly where friction is being relied upon to transmit in-plane shear loads.

2.3 A Paradigm for the Analysis of Preloaded Bolted Joints

As stated previously, this paper, Welch (2019), was initially part of a much larger work that also included the basis for the paper Welch (2018a).

This paper, Welch (2019), recaps on the design analysis method presented in the first paper, Welch (2018a). It then introduces the concept of including dowels in the analysis, 'pegging' the joint to prevent slip. Maintaining the objective of considering the whole joint, the understanding of flange bending and thread shear in threaded holes are also developed. These are presented as a practical design analysis process that is applicable for many cases of preloaded bolted joints and are adequate to demonstrate the structural integrity of each element of the joint.

2.3.1 P2 - Author Accepted Manuscript (Journal of Mechanical Engineering – Strojnicky časopis, Volume 69 (2019), Issue 1, pages 143 to 152.)

A PARADIGM FOR THE ANALYSIS OF PRELOADED BOLTED JOINTS

WELCH Michael

Michael A Welch (Consulting Engineers) Limited, West Lancashire, UK,

email: mike.welch@mail.co.uk

Abstract: The purpose of this paper is to present a paradigm, or guide, to the analysis of preloaded bolted joints made using multiple bolts. Classical analysis methods are applied to the interaction of the joint elements subjected to combinations of both in-plane and out-of-plane loads and moments. The distribution of the external loads and moments within the preloaded joint is determined in relationship to individual bolts. An analysis of loads and stresses in individual bolts and dowels along with flange bending and thread shear in tapped or threaded holes is developed. The article brings together a number of concepts and links them into a practical design analysis process that is applicable for many cases of preloaded bolted joints and are adequate to demonstrate the structural integrity of each element of the joint. Interpretation of results, within the context of design standards, is provided. In some cases finite element methods may be more appropriate, and the methods discussed can be used in the validation process.

KEYWORDS: bolted joint, preloaded bolt, bolt preload, bolt tension, multiple bolt, multi bolt

1 Introduction

Threaded connections, in particular bolted joints, are a common engineering feature found in most manufactured equipment and in many structures.

In preloaded (or pretensioned) joints the bolts are first tightened sufficient to establish closure of the joint with alignment of the mating components, and then further tightened to produce the required bolt preload and (more importantly) a compressive load at the faying surface. The faying surface of a joint member is the prepared surface (i.e. machined or ground) that is in contact with the faying surface of another member of the joint.

The important benefits of preloaded joints are in producing a stiff joint, without slippage. The bolts have a significant mean stress but experience a low working stress range. This low stress range is a major factor in why preloaded joints have good fatigue performance.

In many cases the method of analysis presented here will be adequate to demonstrate the structural integrity of the joint and compliance with design standards. When equipment is being designed to meet specific standards, any safety factors, partial safety factors and design factors or allowable design stresses and loads required by the standard should be incorporated into the analysis and should take precedence over any equivalent factors suggested here.

2 Nomenclature

A_s	Tensile area of each bolt thread
AS_n	Shear area of the internal thread
$D_{s.min}$	Minimum major diameter of the external thread
$E_{n.max}$	Maximum effective (pitch) diameter of the internal thread
$F_{B(n)}$	Minimum bolt preload required to prevent slip at bolt 'n'
$F_{b.max(n)}$	Maximum bolt load on bolt 'n'
$F_{br(n)}$	Bolt-related external load for bolt 'n'
F_{dp}	Design preload
$F_{dwl(r)}$	Resultant shear load for dowel 'r'
$F_{f(n)}$	Faying surface contact force local to bolt 'n'
F_p	Preload in each bolt
$F_{p.max}$	Maximum possible preload in any bolt
$F_{p.min}$	Minimum possible preload in any bolt
$F_{s.br(n)}$	Resultant bolt-related shear load for bolt 'n'
F_x	External In-plane force acting in x-direction
$F_{x.br(n)}$	Bolt-related shear load in x-direction for bolt 'n'

$F_{x.dwl_{(r)}}$ Dowel shear load in x-direction for dowel 'r'

F_y External In-plane force acting in y-direction

$F_{y.br_{(n)}}$ Bolt-related shear load in y-direction for bolt 'n'

$F_{y.dwl_{(r)}}$ Dowel shear load in y-direction for dowel 'r'

F_z External axial load in direction of 'z' axis

$I_{xx.j}$ Second moment of area of joint about 'x' axis

L_e Bolt edge distance (distance from bolt centre to flange edge)

L_{eng} Length of thread engagement

$L_{eng.min}$ Minimum length of thread engagement required

M_x External moment acting about 'x' axis

M_x' Resultant moment

M_y External moment acting about 'y' axis

M_z External torsional moment acting on joint

N_b Number of bolts in joint

N_d Number of dowels in joint

$P_{f_{(n)}}$ Contact pressure at faying surface local to bolt 'n'

p_{thrd} Thread pitch

QS_n Yield, or proof, shear strength of the internal thread material

UTS_s Ultimate tensile strength of the bolt or external thread

$x_{(n)}$ Coordinate of bolt 'n'

$x_{(r)}$ Coordinate of dowel 'r'

Y_s Tensile yield/proof stress of internal thread material

$y_{(n)}$ Coordinate of bolt 'n'

$y_{(r)}$ Coordinate of dowel 'r'

y' Transposed coordinate

μ_f Friction coefficient at faying surface

$\sigma_{b.f}$	Flange bending stress
τ_n	Internal thread shear stress
θ	Angle of resultant moment
θ_{thrd}	Thread flank angle (included angle between thread flanks)

3 Preloaded Bolt Joint Theory

Ideally, preloading the joint's bolts induces a uniform (or near uniform) compressive stress at the faying surface. When external loads are applied to the joint any resulting tensile stress components act to reduce this compressive stress. As long as the faying surface retains some compressive stress the joint will continue to perform as if it were a continuous member. It is only when a resulting tensile stress component attempts to exceed the pre-compression at the faying surface that separation of the joint occurs. At this point the joint can be deemed to have failed, even though none of the constituent parts of the joint have failed.

A detailed analysis of preloaded bolted joint load distributions has been discussed by Welch (2018) [1]. A less detailed method of design analysis was developed for use in a static analysis to demonstrate the structural integrity of the joint. This method of design analysis assumes each preloaded bolt influences an approximately circular region of the faying surface that surrounds it. From this, it also assumes that the regions influenced by the bolts can be considered as springs.

Figure 1 illustrates the bolt-related loads on one half of the joint resulting from the combined loading of the external axial load and external out-of-plane moment.

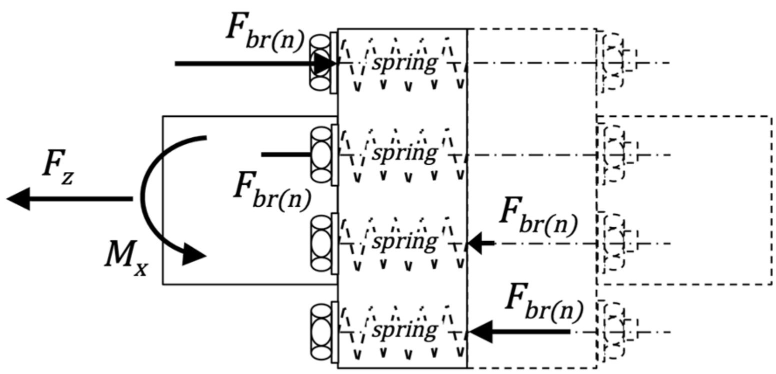

Fig. 1 Bolt Related Loads.

An external moment applied to the joint results in loads on each of the effective springs. These loads are proportional to the distance of the bolt/spring from the neutral axes of the bolt group. These bolt-related loads are given by the following equation.

$$F_{br\,(n)} = \frac{F_z}{N_b} + \frac{M_x \cdot y_{(n)}}{\sum_n y_{(n)}^2} \tag{1}$$

where the neutral axes, or centroid, of the bolt group are defined by $\frac{1}{N_b} \cdot \sum_n x_{(n)} = 0$ and $\frac{1}{N_b} \cdot \sum_n y_{(n)} = 0$

Equation (1) uses an implied second moment of area of $I_{xx.j} = A_s \cdot \sum_n y_{(n)}^2$ which is less than the actual second moment of area of the joint. The bolt-related loads are not the loads on the bolts; they are the external load components on each bolt assembly, comprising a bolt and its surrounding region of flange.

It is common for the out-of-plane moment on a joint to be described by a pair of moments, M_x and M_y, acting about the principle axes of the joint, or another convenient pair of perpendicular axes. These moments and their resultant, M_x', are illustrated in Figure 2.

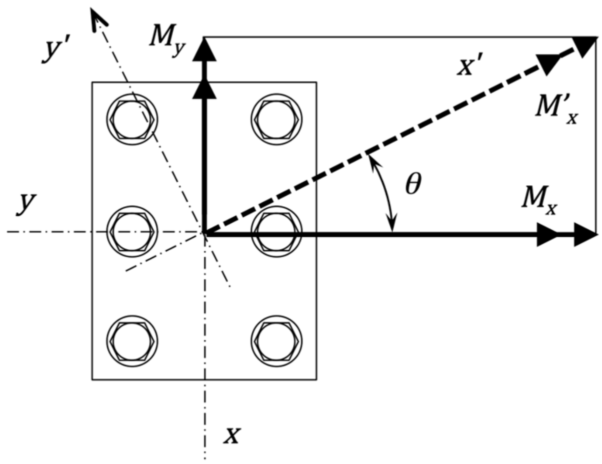

Fig. 2 Orientation of resultant moment.

Since the resultant moment acts about a different axis to those used to define the joint, an alternative coordinate system, aligned to the resultant moment, needs to be considered.

The angle between the transposed coordinate system and the joint coordinate system is given by:

$$\theta = arctan\left(M_y/M_x\right) \quad (2)$$

If M_x is negative then 180 degrees (π radians) needs to be added to the angle θ to ensure the direction of the resultant moment is in the correct 'quadrant'.

The transposed bolt coordinates are given by:

$$y'_{(n)} = y_{(n)} \cdot \cos(\theta) - x_{(n)} \cdot \sin(\theta) \quad (3)$$

where $x_{(n)}$ and $y_{(n)}$ are the coordinates of bolt 'n' defined with respect to the centroid of the bolt group.

The resultant moment, M'_x, is given by:

$$M'_x = M_x \cdot \cos(\theta) + M_y \cdot \sin(\theta) \quad (4)$$

When considering an out-of-plane moment that is not aligned with the joint x-axis the terms for y' and M'_x given by equations (3) and (4) should be used in equation (1).

Equations (1) to (4) follow the "right hand" rule. Loads are positive in the direction of the axes and positive moments act clockwise about the axes when viewed from the origin.

The external loads and moments produce only small load changes in the preloaded bolts. The major effect of the external loads is to induce significant changes in the faying surface contact pressures. Joint separation does not occur until the tensile bolt-related load exceeds the bolt preload. Hence, the tensile (positive) bolt related loads given by equation (1) should not exceed the minimum bolt preload.

$$F_{br\,(n)} \leq F_{p.min} \quad (5a)$$

The maximum and minimum bolt preloads, $F_{p.max}$ and $F_{p.min}$, reflect the tolerance on the nominal preload, F_p. Table A8 of VDI 2230 Part 1, "Systematic calculation of high duty bolted joints with one cylindrical bolt" [2] suggests a tolerance of $\pm 17\%$ for angle controlled bolt tightening (turn of nut). The suggested tolerances for bolts tightened by a torque wrench are $\pm 23\%$ if the torque is determined by experiment or $\pm 33\%$ if the torque is determined by calculation based on friction.

Section 3.8 of British Standard BS 7608:1990, "*Code of practice for Fatigue design and assessment of steel structures*" [3] says that;

> 'If reliance is to be placed on this pre-load, it should be at least 1.5 times the design tension'

Hence, when designing against fatigue the following equation can be used in place of equation (5a):

$$F_{br_{(n)}} \leq F_{dp} \tag{5b}$$

where the design preload, F_{dp}, is given by:

$$F_{dp} = \frac{2}{3} \cdot F_p \tag{6}$$

The use of a design bolt preload takes account of a number of factors, which includes a tolerance on the bolt preload applied during assembly. Applying equations (5b) and (6) produces a "design against fatigue", but should not be regarded as a fatigue assessment.

Any safety factors, partial safety factors and design factors required by any standards being followed should be incorporated into equations (5a) and/or (5b).

It has been shown that external out-of-plane loads are carried mainly by changes in the faying surface contact pressure distribution and produce only a small change in bolt loads [1]. Section 3.8 of British Standard BS 7608:1990 [3] suggests that the working stress range of a bolt is up to a maximum of 20% of the applied external load. Hence, the maximum possible tensile load on a bolt can be estimated as:

$$F_{b.max_{(n)}} = F_{p.max} + 20\% \cdot F_{br_{(n)}} \tag{7}$$

This maximum load should not exceed the proof load for the bolt.

3.1 In-Plane Loads on the Joint

Bolted joints for mechanical engineering purposes are usually designed to support external in-plane loads and torsional moments by friction at the faying surface. In some joints dowels, or other positive method of location of the joint, can assist in supporting these loads.

Again, assume that the preload in each bolt influences the region of the faying surface that surrounds the bolt. Also assume each region influenced by a bolt can be considered as a spring. Then the bolt-related loads resulting from the combined loading of the external in-plane loads and torsional moments are given by the following equations.

$$F_{x.br_{(n)}} = \frac{F_x}{N_b} - \frac{M_z \cdot y_{(n)}}{\sum_n \left(x_{(n)}^2 + y_{(n)}^2\right)} \tag{8}$$

$$F_{y.br_{(n)}} = \frac{F_y}{N_b} + \frac{M_z \cdot x_{(n)}}{\sum_n \left(x_{(n)}^2 + y_{(n)}^2\right)} \tag{9}$$

$$F_{s.br_{(n)}} = \sqrt{F_{x.br_{(n)}}^{2} + F_{y.br_{(n)}}^{2}} \tag{10}$$

Equation (8) gives the bolt-related shear load component acting in the *x*-direction. Similarly, equation (9) gives the bolt-related shear load component acting in the *y*-direction. Equation (10) gives the resultant bolt-related shear load at each bolt. These shear loads are carried across the faying surface by friction.

The minimum bolt preload required to both maintain closure of the joint and prevent slip is given by:

$$F_{B_{(n)}} = F_{br_{(n)}} + \frac{F_{s.br_{(n)}}}{\mu_f} \tag{11}$$

where μ_f is the friction coefficient at the faying surface.

If the joint does not incorporate dowels or other means of positive location then equation (11) should use a dynamic friction coefficient for μ_f. Dynamic friction will be less than static friction. Hence, any potential movement or slip, resulting from impact or dynamic loads overcoming static friction, will be arrested.

If dowels are incorporated into the joint face, they act to prevent movement or slip that would otherwise occur if the load overcame static friction. Hence, the minimum preload can be determined using a static friction coefficient for μ_f.

Joint slip, particularly on load reversals, could induce self-loosening of the bolts. Slip at macroscopic levels could produce fretting at the faying surface, which in turn could lead to a loss of preload and bolt loosening. Hence, the tensile (positive) bolt related loads given by equation (11) should not exceed the bolt preload, as expressed by the following equation.

$$F_{B_{(n)}} \leq F_p \tag{12}$$

Equations (11) and (12) can be combined to give the alternative equation:

$$F_{s.br_{(n)}} = \left(F_p - F_{br_{(n)}}\right) \cdot \mu_f \tag{13}$$

Equations (12) and (13) use the nominal bolt preload F_p. Some standards may instead require the design bolt preload, or the minimum preload, to be used for calculating the contact pressure.

Again, any safety factors, partial safety factors and design factors required by any standards being followed should be incorporated into the static analysis.

3.2 Bolt shear and Bending

Because the load analysis is "disconnected" from the geometry it is not possible to separate out the in-plane loads on the bolts and dowels, or other positive means of location. Generally, for typical flange thicknesses of 1.5 to 2 times the bolt diameter, bolt shear and bolt bending will not be an issue provided equations (10) and (11) or equation (12) show that the bolt preload can support the bolt-related shear load along with the bolt-related tensile load.

A detailed theoretical study of bolt bending [4] shows that in-plane loads and moments produce both bending stresses and additional tensile stresses in the bolts. Section 3.2.4 of VDI 2230 Part 1 [2] says;

> 'In highly preloaded bolted joints there is generally no risk of self-loosening by rotation. In the case of bolts with low bending resistance, additional locking may be necessary in order to avoid an inadmissible loss of preload. Locking means to prevent loosening by rotation ensure that at least 80% of the assembly preload remains as residual preload.'

Long bolts can be considered as having low bending resistance. Hence, bolts with a grip length of say 4 or more times the nominal bolt diameter are likely experience relaxation of preload. A preload of 80% of that which would be produced by the bolt assembly, or make up, torque should be used in equations (5a), (5b), (6) and equations (12) or (13) when calculating load limits.

4 Dowels

The dowels assist in carrying the out-of-plane loads by "pegging" the joint, preventing slip and the associated reduction in friction. The stiffness of each dowel in shear will be less than the stiffness of the region of the flange that is under the influence of a bolt. Hence a conservative estimate of the in-plane load carried by each dowel can be made using the following equation:

$$F_{x.dwl_{(r)}} = \frac{F_x}{N_b + N_d} - \frac{M_z \cdot y_{(r)}}{\sum_n \left(x_{(n)}^2 + y_{(n)}^2\right) + \sum_r \left(x_{(r)}^2 + y_{(r)}^2\right)} \tag{14}$$

$$F_{y.dwl_{(r)}} = \frac{F_y}{N_b + N_d} + \frac{M_z \cdot x_{(r)}}{\sum_n \left(x_{(n)}^2 + y_{(n)}^2\right) + \sum_r \left(x_{(r)}^2 + y_{(r)}^2\right)} \tag{15}$$

$$F_{dwl_{(r)}} = \sqrt{F_{x.dwl_{(r)}}^{\,2} + F_{y.dwl_{(r)}}^{\,2}} \tag{16}$$

Equations (14) and (15) uses coordinates about the centroid of the combined bolt and dowel locations, and may be different to that used for equations (8) and (9).

The centroid used in equations (14) and (15) is at the position where: $\frac{\sum_n x_{(n)}+\sum_r x_{(r)}}{N_b+N_d} = 0$ and $\frac{\sum_n y_{(n)}+\sum_r y_{(r)}}{N_b+N_d} = 0$

Often equations (14) to (16) are not used to size dowels. Instead dowels are sized to support all of the shear loads, without considering friction at the faying surface. This is not a condition that would occur in normal operation but it does provide the joint with the ability to maintain some structural integrity in the event of bolts loosening in service.

5 Flange Bending

The joint flange(s) will experience bending due to pressure at the faying surface acting at the edge of the flange, as illustrated in Figure 3.

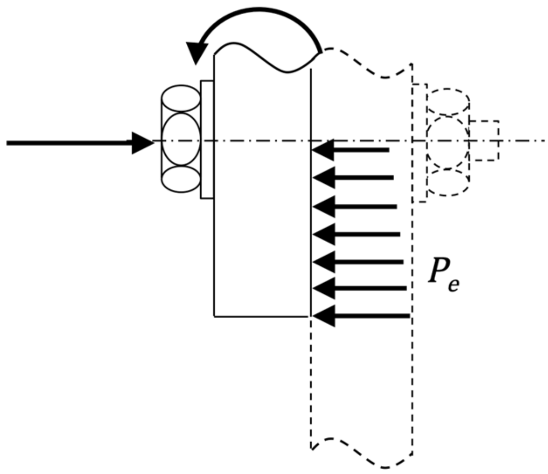

Fig. 3 Pressure Load on Flange Face.

The compressive (negative) bolt related loads given by equation (1) act to increase the contact pressure on the region of faying surface surrounding the bolt.

The contact forces acting at the faying surface local to each bolt are given by:

$$F_{f\,(n)} = F_{br\,(n)} - F_{p.max} \tag{17}$$

The negative sign in equation (17) indicates that the tensile preload in the bolts produce a compressive stress at the faying surface. Assuming that the circular region of faying surface influenced by the bolts closest to the edge of the flange extends to the edge, then the contact pressure is given by:

$$P_{f_{(n)}} = \frac{F_{f_{(n)}}}{\pi \cdot L_e^2} \tag{18}$$

The flange bending stress is calculated using the most compressive value of contact pressure, $P_{f_{(n)}}$, as the flange edge pressure. The bending stress in the flange is given by:

$$\sigma_{b.f} = \frac{-3 \cdot L_e^2 \cdot P_e}{t_f^2} \tag{19}$$

where the contact pressure at the edge of the faying surface, P_e, is taken to be the most compressive (negative) value of contact pressure $P_{f_{(n)}}$.

6 Thread Shear

In the preceding sections it was assumed that the bolted connections were made using appropriate grade nuts. However, it is not unusual for bolts to be tightened into threaded, or tapped, holes within one of the mating components. In these cases the thread shear stresses will need to be calculated.

It is usual for bolted connections to be designed so that the bolt will fail in tension at the threaded portion of the shank before failure by thread shearing. This type of failure gives an early indication that failure has occurred during assembly, due to over-tightening, or due to overloading during service.

If the internal thread material has a tensile strength the same as or greater than the bolt, then the thread engagement needs to be at least that of a standard nut (plus an allowance for the chamfered lead of the bolt if required). However, if the internal thread is formed within a material having a lower ultimate strength than the bolt then the shear stress in the internal thread and the minimum length of thread engagement required has to be considered.

The shear area of the internal thread at the minimum major diameter of the external thread is given by:

$$AS_n = \frac{\pi \cdot L_{eng} \cdot D_{s.min}}{p_{thrd}} \left(\frac{p_{thrd}}{2} + tan\left(\frac{\theta_{thrd}}{2}\right) \cdot (D_{s.min} - E_{n.max}) \right) \tag{20}$$

Equation (20) is based on that given in Appendix A of British Standard BS 3580:1964 "*Guide to the design considerations on: The strength of screw threads*" [5]. However, the equation presented here has been put into a format that can be applied to any thread form commonly used for bolts.

It has been shown that the first full internal thread supports a large proportion of the load and is subject to yielding [6]. When determining the length of thread engagement, L_{eng}, it can be assumed that one half of each of the end threads in the thread engagement does not contribute to carrying load in shear. Hence, the active length of thread engagement is the nominal length of engagement less one thread pitch. If the end of the bolt is within the tapped hole then the length of thread engagement should account for the bolt's chamfered lead.

British Standard BS 3692:2001 "*metric precision hexagon bolts, screws and nuts – specification*" [7] calls for a tolerance of 6H/6g on nuts and bolts. This is the usual tolerance for precision high strength fasteners, where the use of a standard nut results in short lengths of thread engagement, typically 0.8d (where d is the nominal thread size). Internal threads in materials with lower shear strength than nuts require a longer thread engagement and tolerances of 6H/6g can lead to interference between the internal and external threads. It is common practice to change the tolerance of the internal thread to accommodate the pitch and flank angle errors of long thread engagements. Often the true tolerance on the internal thread is not recorded within the design data but should be reflected in the analysis.

The internal thread shear stress is given by:

$$\tau_n = \frac{F_b}{AS_n} \tag{21}$$

where F_b is the maximum bolt load, which can be taken to be the bolt preload F_p.

The minimum length of thread engagement required is given by:

$$L_{eng.min} = \frac{p_{thrd} \cdot A_s \cdot UTS_s}{\pi \cdot D_{s.min}\left(\frac{p_{thrd}}{2} + tan\left(\frac{\theta_{thrd}}{2}\right) \cdot (D_{s.min} - E_{n.max})\right) \cdot QS_n} \tag{22}$$

Again, this equation is based on those given in British Standard BS 3580:1964 Appendix A [5]. The effect of the internal thread material having a lower ultimate strength than the bolt has been incorporated into equation 27.

Equation (22) uses the yield/proof based shear strength instead of an ultimate shear strength, based on half the ultimate strength, as suggested in BS 3580:1964 [5]. Using the yield/proof yield strength protects the (more expensive) internally threaded component from permanent deformation of its thread. For steel $QS_n = Y_s/\sqrt{3}$ where Y_s is the yield/proof stress.

CONCLUSION

In many cases the method of analysis presented here will be adequate to demonstrate the structural integrity of the joint and compliance with design standards.

Preloading the bolts of the joint induces a compressive stress at the faying surface. The bolt preload keeps the joint closed when external loads are applied to the joint, producing tensile stress components that act to reduce this compressive stress. As long as the faying surface retains some compressive stress the joint will continue to perform as if it were a continuous member.

External out-of-plane moments and tensile loads are supported mainly by a reduction in the contact pressure at the faying surface, with only a small proportion of the external loads acting to increase the bolt tensile stress. This results in a low working stress range, which is a major factor in why preloaded joints have good fatigue performance and high stiffness.

External in-plane loads and torsional moments on the joint are supported mainly by friction at the faying surface. In some joints dowels, or other positive method of location of the joint, can assist in supporting the shear loads by preventing movement or slip at the joint face.

The joint flange(s) experience bending due to the pressure at the faying surface acting at the edge of the flange.

The approach presented here cannot be applied to all bolted joint configurations. In some cases a detailed analysis has to be considered. In particular, joints with single bolts, or a single line of bolts, are usually special cases and have to be considered from first principles.

REFERENCES

[1] Welch, M. *Classical Analysis of Preloaded Bolted Joint Load Distributions*. International Journal of Structural Integrity, Volume 9 (2018), Issue 4, pages 455 to 464.

[2] Verein Deutscher Ingenieure (Association of German Engineers). VDI 2230 Part 1. 2003, *"Systematic calculation of high duty bolted joints with one cylindrical bolt"*, Verein Deutscher Ingenieure, Dusseldorf.

[3] British Standards Institution. BS 7608:1990, *Code of practice for Fatigue design and assessment of steel structures*, British Standards Institution, London.

[4] Welch, M. *Analysis of Bolt Bending in Preloaded Joints*. Journal of Mechanical Engineering – Strojnicky časopis, Volume 68 (2018), Issue 3, pages 183 to 194.

[5] British Standards Institution. BS 3580:1964, *Guide to the design considerations on: The strength of screw threads*, British Standards Institution, London.

[6] Pástor, M. et al. *The use of Optical Methods in the Analysis of Areas With Stress Concentration*. Journal of Mechanical Engineering – Strojnicky časopis, Volume 68 (2018), Issue 2, pages 61 to 76.

[7] British Standards Institution. BS 3692:2001, *ISO metric precision hexagon bolts, screws and nuts – specification*, British Standards Institution, London.

2.3.2 Further Discussion

What was not discussed within the paper, Welch (2019), was that the flanges are also subjected to high contact stresses under the bolt head. An experimental study of contact pressures under the bolt head and nut, Archer (2010), shows that a peak pressure occurs around the edge of the bolt hole. This peak pressure can be 40% greater than the nominal average pressure. This study also indicated that a standard washer is not stiff enough to distribute the load effectively beyond the bolt head.

The main purpose of the washer is not to distribute the bolt load into the flange but rather to provide a consistent, hard, surface for the nut to react against. This results in more consistent and reliable friction coefficients across all joint types, irrespective of the joint flange material or surface finish. A secondary purpose of the washer is to protect the surface, and surface finish, of the component/flange in the region directly under the nut or bolt head from mechanical damage and galling that could occur from turning the nut/bolt head during tightening.

The papers, Welch (2018a) and Welch (2019), both highlighted that the method of design analysis is not applicable to joints made with a single threaded fastener or, in certain instances, made with a single row of fasteners. This is because the second moment of area of the faying surface is not considered in the analysis. Trying to use the design analysis method would result in the prediction of infinite bolt related loads. To be able to analyse these types of joints a detailed analysis based on first principles as described in the first paper, Welch (2018a), needs to be carried out.

An implicit assumption within the paper Welch (2018a) is that the flanges of the joint are both thick enough and stiff enough to be able to consider the flanges as rigid. The paper Welch (2019) addresses this issue by considering flange bending. Provided the flanges have sufficient thickness to prevent failure due to flange bending under the contact pressure the assumption of rigid, or near rigid, flanges can be considered reasonable. It is worth noting that section 3.4 of BS 4604-1:1970, BSI (1970), specifies :

> "In connections using high strength friction grip bolts, no outer ply shall be smaller in thickness than half the bolt diameter or 10 mm whichever is less."

The ‘outer plies’, in the context of BS 4604-1:1970, BSI (1970), are the two flanges of the joint. ‘Inner plies’ refer to any spacers or intermediate flanges within the joint.

Section 4 of the paper “*A paradigm for the Analysis of Preloaded Bolted Joints*”, Welch (2019), suggests treating dowels as if they have the same stiffness as the area of the flange surrounding the bolts. The paper by Welch (2019) acknowledges that this overestimates the stiffness of the dowels and would result in an over estimate of the load on the dowels support. However, the purpose of this type of analysis was to demonstrate the design had sufficient ‘engineering integrity’ for the dowels, not to provide an accurate analysis of the shear stress. The actual shear stress within a dowel would be equivalent to the shear stress at the faying surface local to the dowel’s position.

Section 6 of the paper by Welch (2019) discusses thread shear. The method of analysis is based on Appendix A of the British Standard BS 3580:1964, BSI (1964). This analysis assumes a uniform distribution of the shear load along the length of the engaged thread. In reality the first of the engaged threads will carry a larger proportion of the shear load. The thread shear load will then reduce with each subsequent thread.

2.4 Analysis of Asymmetrical Preloaded Bolted Joints

It was realised that the two previous published works, Welch (2018a) and Welch (2019), did not present adequate methods for dealing with asymmetrical joints. The third paper being presented, "*An Analytical Study of Asymmetrical Preloaded Bolted Joints*", Welch (2022a), was a short technical note that addressed the practice of treating the bolts in asymmetrical joints as structural elements. Welch (2022a) showed that it is more appropriate to consider asymmetrical joints as 'continuous' structures by applying beam theory. The note discusses how joints with asymmetrical geometry influence the way external loads are reacted through the joint. It also discusses how asymmetrical bolt groups can influence joints that are nominally symmetrical, causing them to act in an asymmetrical way. By rethinking of preloaded bolted joints as an extension to the theory of beams, the bolts simply maintaining continuity by introducing a residual compressive stress, the classical theories surrounding asymmetry could be applied. The detail analysis method also considered the effects of Rotscher's pressure cone. This allowed a relatively simple adaption to develop the design analysis method to make it suitable for the application to asymmetrical joints.

2.4.1 P3 - Author Accepted Manuscript (International Journal of Modern Research in Engineering and Technology, Volume 7 (2022), Issue 3, March 2022, Pages 6 to 11.)

Analytical Study of Asymmetrical Preloaded Bolted Joints

Michael Welch

Michael A Welch (Consulting Engineers) Limited, West Lancashire, UK.

Abstract

The purpose of this paper is to develop an understanding of the influence of asymmetrical geometry within preloaded bolted joints. Classical analysis methods are applied to the analysis of preloaded bolted joints that use asymmetrical bolt group patterns. Both a detailed analysis of asymmetrical joints, using classical beam theory, and a less detailed design analysis are considered. The detailed analysis method is extended, using Rotscher's pressure cone, and is suitable to produce calculated bolt loads that can be used in a fatigue analysis. The design analysis provides a quick method of establishing the structural integrity of the asymmetrical joint. The detailed analysis method can be applied to the structure being connected by the bolted joint and the welds connecting the structure to the joint flanges. The design method is also appropriate for application to sprung suspension systems. The methods presented are suitable for use in automated procedures of calculation, such as spread sheets, MathCAD ©, SMath Sutdio ©, etc.

Keywords: asymmetric bolted joint, preloaded bolted, bolt preload, bolt tension, multi bolt, spring suspension.

1 Introduction

Bolted joints are an extremely useful feature in mechanical engineering. They allow disassembly for maintenance and end of life disposal purposes. Bolted joints also allow complex assemblies to be made on site without the need for specialist processes such as welding, stress relieving, heat treatment or other post process activities. Preloading the bolts also produces a stiff joint, suitable for load bearing structures subjected to load reversals and also offer good fatigue resistance.

There are basically two, related, methods of analysing preloaded bolted joints. Firstly, a detailed analysis that is based on the theory of beams. Secondly, a design analysis method that considers each bolt, and a region of flange surrounding it, as acting together and performing as a stiff spring.

Preloading the bolts of the joint is intended to produce a uniform, or near uniform, contact pressure at the faying surface. This in turn makes the two flanges of the joint perform as if they were a single, solid, structure. The detailed analysis of a preloaded bolted joint assumes that the classical theory of bending of beams can be applied to an, effectively, single continuous member. The stresses that would be produced in this ‘solid member’ by the application of external loads act to change the contact pressure at the faying surface and to change the tensile stresses in the preloaded bolts. Any external out of plane bending will also introduce a bending stress component in each of the bolts

The design analysis treats each bolt, and a region of the flanges surrounding the bolt, as a spring. This type of design analysis is a simplification of the detailed, classical, analysis but does not require the calculation of section properties. However, this simplification of the analysis does not reflect the flexural stiffness of the joint and results in an over estimate of the axial loads acting at the area of the joint flange being controlled by each bolt, and hence, an overestimate of the minimum bolt preload required to maintain closure of the joint.

Both the detailed and the design methods of analysis consider that shear stresses on the joint are supported by friction at the joint face. This requires the bolt preload to include an additional component of clamping force to support the in-plane loads. This additional clamping force has to be equivalent to the maximum shear stress divided by the friction coefficient for the faying surface. Some joints use dowels, or other positive means of restraint, to assist in supporting shear loads. These should be considered as providing alignment and preventing slip, but not as the primary method of supporting in-plane, shear, loads.

2 Nomenclature

A_b Tensile area of each bolt

A_j Total area of joint (Faying surface plus bolts)

d_b Nominal bolt diameter

$D_{f.e}$ Projected diameter of Rotscher's pressure cone at faying surface

$F_{b(n)}$ Bolt load in bolt 'n'

$F_{br(n)}$ Bolt-related load for bolt 'n'

F_{dp} Design preload

F_p Preload in each bolt

F_z External axial load in direction of 'z' axis

$I'_{p.max}$ Maximum second moment of area about a principal axis

$I'_{p.min}$ Minimum second moment of area about a principal axis

$I_{xx.j}$ Second moment of area of joint about 'x' axis

$I'_{xx.j}$ Second moment of area transposed about x'-axis

$I_{xy.j}$ Product moment of area of joint

$I'_{xy.j}$ Transposed product moment of area of joint

$I_{yy.j}$ Second moment of area of joint about 'y' axis

$I'_{yy.j}$ Second moment of area transposed about y'-axis

M_x External moment acting about 'x' axis

M'_x Transposed moment

M_y External moment acting about 'y' axis

M'_y Transposed moment

N_b Number of bolts in joint

P_p Pressure at faying surface, preload pressure

P_f Pressure at faying surface when external loads are applied

$t_{f.min}$ Flange thickness, minimum of the two flanges

x	Coordinate in plane of joint face
x'	Transposed coordinate
$x_{(n)}$	Coordinate of bolt 'n'
$x'_{(n)}$	Transposed coordinate of bolt 'n'
y	Coordinate in plane of joint face
y'	Transposed coordinate
$y_{(n)}$	Coordinate of bolt 'n'
$y'_{(n)}$	Transposed coordinate of bolt 'n'
φ	Rotscher's pressure cone angle, half cone angle
θ	Angle of principal axis

3 Detail Analysis of Asymmetrical Joints

It is quite common for asymmetrical joints to be defined in terms of a geometrical coordinate system that are not the principal axes. This is illustrated in Figure 1.

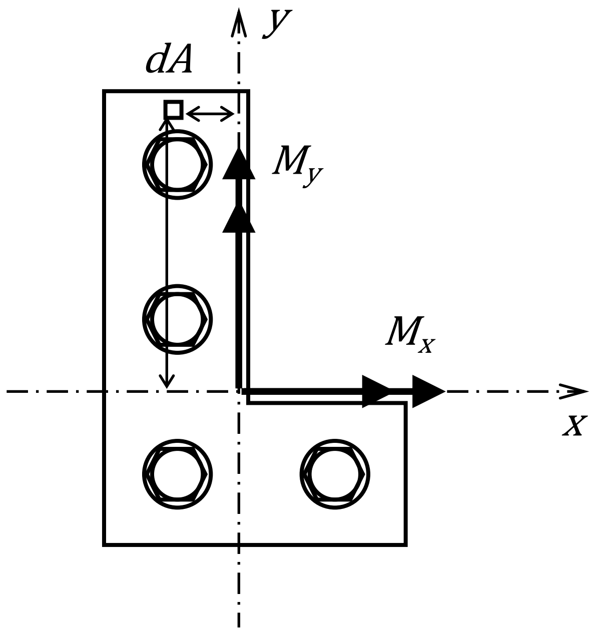

Figure 1. Asymmetrical Joint

The centroid of the joint lies at the point where $0 = \frac{1}{A_j}\int x \cdot dA$ and $0 = \frac{1}{A_j}\int y \cdot dA$

In Figure (1) the joints geometry and the moments M_x and M_y are defined with respect to the joint's coordinate system, which may not aligned with the principal axes of the joint. When dealing with an asymmetric joint it is necessary to determine the direction of the principal axes of the joint's cross-section. Then, in order to be able to carry out an analysis of the joint, the coordinate system and section properties have to be transposed to align with the joints principal axes, as illustrated in Figure (2). Also, the moments M_x and M_y have to be resolved to act about the principal axes.

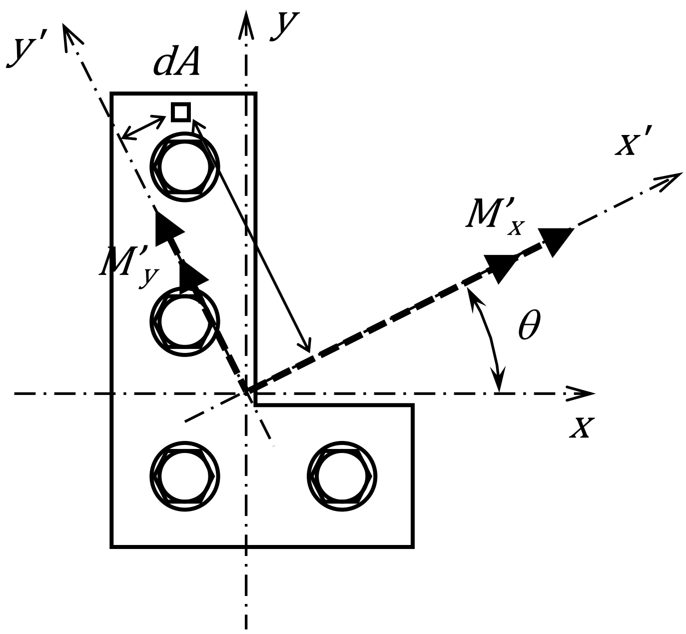

Figure 2. Transposed Coordinate System and Moments

If the principal axes are assumed to be at an angle θ to the axes defining the joint the transposed coordinate system is given by the following equations:

$$x' = x \cdot cos(\theta) + y \cdot sin(\theta) \tag{1}$$

$$y' = y \cdot cos(\theta) - x \cdot sin(\theta) \tag{2}$$

The second moments of area for the joint are described by the two equations:

$$I'_{xx.j} = \int y'^2 \cdot dA \tag{3}$$

$$I'_{yy.j} = \int x'^2 \cdot dA \tag{4}$$

Similarly, the product moment of area is described by the equation:

$$I'_{xy.j} = \int x' \cdot y' \cdot dA \tag{5}$$

The principal axes are defined by when the product moment area, $I'_{xy.j}$, is zero. Hence, using equations (1) and (2) in equation (5):

$$I'_{xy.j} = \int \big(x \cdot cos(\theta) + y \cdot sin(\theta)\big) \cdot \big(y \cdot cos(\theta) - x \cdot sin(\theta)\big) \cdot dA$$

Working with this term:

$$I'_{xy.j} = \int x \cdot y \cdot \big(cos^2(\theta) - sin^2(\theta)\big) \cdot dA + \int (y^2 - x^2) \cdot \sin(\theta) \cdot \cos(\theta) \cdot dA$$

$$I'_{xy.j} = I_{xy.j} \cdot \big(cos^2(\theta) - sin^2(\theta)\big) + \big(I_{xx.j} - I_{yy}.j\big) \cdot \sin(\theta) \cdot \cos(\theta)$$

Resulting in the equation:

$$I'_{xy.j} = I_{xy.j} \cdot \cos(2 \cdot \theta) + \frac{1}{2} \cdot \big(I_{xx.j} - I_{yy.j}\big) \cdot \sin(2 \cdot \theta) \tag{6}$$

Equating the product moment of area, $I'_{xy.j}$, to zero and rearranging the resulting equation shows that the angle of principal axis from the joints x-axis (positive anticlockwise) is given by the equation:

$$\theta = \frac{1}{2} \cdot arctan\left(\frac{2 \cdot I_{xy.j}}{I_{yy.j} - I_{xx.j}}\right) \tag{7}$$

A term for the second moment of area about the x'-axis can be found by substituting equation (2) into equation (3):

$$I'_{xx.j} = \int \big(y \cdot cos(\theta) - x \cdot sin(\theta)\big)^2 \cdot dA$$

Working with this term:

$$I'_{xx.j} = \int \big(y^2 \cdot cos^2(\theta) + x^2 \cdot sin^2(\theta) - 2 \cdot x \cdot y \cdot sin(\theta) \cdot cos(\theta)\big) \cdot dA$$

Resulting in the equation

$$I'_{xx.j} = I_{xx.j} \cdot cos^2(\theta) + I_{yy.j} \cdot sin^2(\theta) - 2 \cdot I_{xy.j} \cdot sin(\theta) \cdot cos(\theta) \tag{8}$$

Similarly, a term for the second moment of area about the y'-axis can be found by substituting equation (1) into equation (4):

$$I'_{yy.j} = I_{yy.j} \cdot cos^2(\theta) + I_{xx.j} \cdot sin^2(\theta) + 2 \cdot I_{xy.j} \cdot sin(\theta) \cdot cos(\theta) \qquad (9)$$

It is possible to use equations (6), (8) and (9) to show that the maximum and minimum second moments of area about the principal axes are given by the following equations.

$$I'_{p.max} = \frac{1}{2} \cdot \left(\left(I_{xx.j} + I_{yy.j}\right) + \sqrt{\left(I_{yy.j} - I_{xx.j}\right)^2 + 4 \cdot I_{xy.j}^2} \right) \qquad (10)$$

$$I'_{p.min} = \frac{1}{2} \cdot \left(\left(I_{xx.j} + I_{yy.j}\right) - \sqrt{\left(I_{yy.j} - I_{xx.j}\right)^2 + 4 \cdot I_{xy.j}^2} \right) \qquad (11)$$

It should be noted that the connection between which of the second moment of area given by equations (10) and (11) is parallel to the principal axis defined by the angle θ, obtained from equation (7) has been lost. This is usually relatively easy to establish by observation, although not by computation. There is an advantage in using equations (8) and (9) in preference to equations (10) and (11) when 'automatic' calculation methods, such as spreadsheets, MathCAD © and SMath Studio © are used since the relationships between second moments of area and direction of axes are maintained.

Besides transposing the joint coordinates and section properties, the analysis of the joint also requires the external out-of-plane moments to be transposed. The transposed moments are given by the following equations:

$$M'_x = M_x \cdot cos(\theta) + M_y \cdot sin(\theta) \qquad (12)$$

$$M'_y = M_y \cdot cos(\theta) - M_x \cdot sin(\theta) \qquad (13)$$

If it is assumed that the bolts are distributed in a regular manner across the faying surface and the centroid and principal axes of the bolt group coincide with those of the faying surface then the contact pressure at the faying surface under preload and the pressure distribution under the external loads can be given by the following two equations.

$$P_p = \frac{-1}{A_f} \cdot \sum_n F_b \qquad (14)$$

$$P_f = P_p + \frac{F_z}{A_j} + \frac{M'_x}{I'_{xx.j}} \cdot y' - \frac{M'_y}{I'_{yy.j}} \cdot y' \tag{15}$$

Similarly, the total load on individual bolts in the joint can be given by the equation:

$$F_{b(n)} = F_p + \left(\frac{F_z}{A_j} + \frac{M'_x}{I'_{xx.j}} \cdot y'_{(n)} - \frac{M'_y}{I'_{yy.j}} \cdot x'_{(n)}\right) \cdot A_b \tag{16}$$

The negative sign in equation (14) indicates that the contact pressure at the faying surface is compressive. For the joint to be able to function correctly it is required that the contact pressure calculated by equation (15) remains compressive (i.e. negative) under all cases of external loading. This has to be true for all points on the faying surface. If in-plane external loads are applied, it is a requirement that the resultant shear stress at the joint does not overcome the friction between the joint's flanges. The analysis of shear loads on the joint is outside the scope of this paper but it has been discussed in detail by Welch (2018) in reference [1]. It is also a requirement that the total bolt load given by equation (16) does not exceed the proof load for the bolt. If the bolt load does exceed the proof load there could be some relaxation of the bolt preload, which in turn could lead to joint failure.

4 Rotscher's Pressure Cone

The preceding work assumes a uniform, or near uniform, pressure distribution at the faying surface. In practice, the contact pressure of a preloaded joint will not be uniform across the faying surface. It has been shown by Rotscher (1927), reference [2], that each preloaded bolt influences an approximately circular region of the faying surface that surrounds it. As a result, the total effective area and the effective second moment of area of the joint are less than those of the nominal faying surface area and the nominal second moment of area. Hence, the surface contact pressure produced when the bolts are installed is higher than that predicted using the full, or nominal, faying surface area. Similarly, the change in bolt stress and the change in contact pressure due to applied loads are also higher. These two effects tend act to act cancel each other out when considering the external loads that could cause joint separation.

When considering a joint similar to that illustrated in Figure 3, where the bolts are not regularly distributed and the principal axes of the faying surface and bolt group are not coincident, the effects of Rotscher's pressure cone need to be taken into account.

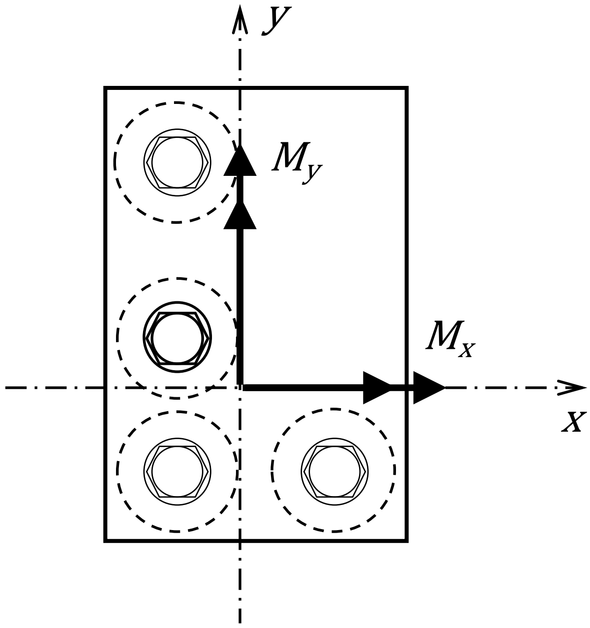

Figure 3. Joint with Non-regularly Distributed Bolts

Figure 4 illustrates how Rotscher's pressure cone is formed and equation (17) provides an estimate of the resulting contact area diameter.

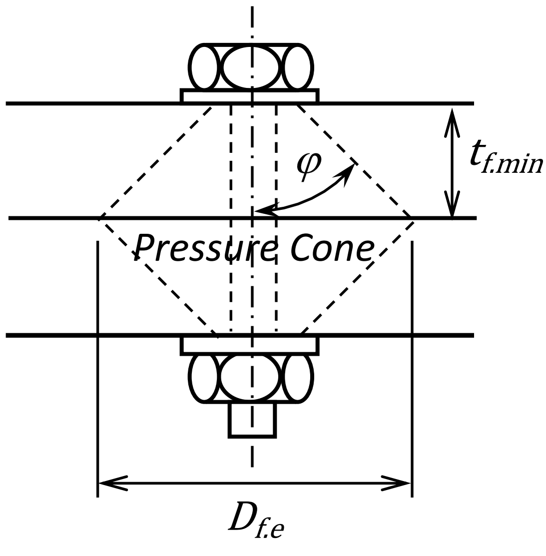

Figure 4. Rotscher's Pressure Cone.

$$D_{f.e} = 1.5 \cdot d_b + 2 \cdot t_{f.min} \cdot tan(\varphi) \qquad (17)$$

Rotscher proposed a half cone angle of $\varphi = 45^o$. However, later researchers have found that this is an overestimate and the half cone angle, or pressure angle, can depend on a number of factors including flange thickness and the stiffening effects of surrounding structure attached to the flanges. A more realistic, or accurate, suggestion would be to use a pressure angle of $\varphi = 30^o$. Rotscher's pressure cone is discussed in more detail in section 8-5 *"Joints – Member Stiffness"* of reference [3] *"Shigley's Mechanical Engineering Design"* (2006). The application of a compression cone, based on Rotscher's pressure cone, is also discussed in detail in section 3 "*Load and deformation conditions*", and section 5 "*Calculation quantities*", of reference [4] *"Systematic calculation of highly stressed bolted joints Multi bolted joints"* (2014).

5 Design Analysis

The method of detailed analysis that has been described is particularly relevant as part of a full fatigue assessment or when investigating specific aspects of a bolted joint such as an in-service failure. In most instances a method of design analysis is adequate to provide evidence of structural integrity for a bolted joint. This design analysis is based on the assumption that each bolt assembly, comprising the nut, bolt washers and a region of the flanges defined by Rotscher's pressure cone, can be considered as a spring. Section 3.2 *"Principles for calculating single-bolted joints; analysis of forces and deformation*" of reference [4] *"Systematic calculation of highly stressed bolted joints Multi bolted joints"* (2014) presents a theoretical study of a single bolt assembly which shows the principle that forms the basis for this assumption.

In a design analysis, when only the location of the bolt centres is being considered, not the joints section properties, the centroid of the bolt group is defined as the point where $0 = \frac{1}{N_b} \cdot \sum_n x_{(n)}$ and $0 = \frac{1}{N_b} \cdot \sum_n y_{(n)}$

It is worth noting that the design analysis does not require the diameter of Rotscher's pressure cone or the effective spring stiffness to be calculated. The design analysis method is simply based on an understanding of how the effective spring stiffness influences the joint.

The direction of the principal axes of the bolt group can then be given by the following modified version of equation (7):

$$\theta = \frac{1}{2} \cdot arctan\left(\frac{2 \cdot \sum_n x_{(n)} \cdot y_{(n)}}{\sum_n x_{(n)}^2 - \sum_n y_{(n)}^2}\right) \tag{18}$$

The design analysis method also requires that the bolt centre coordinates are transposed into the coordinate system defined by the principal axes of the bolt group. This can be achieved by applying equation (1) and (2) to the bolt geometry. Re-writing these two equations in terms of the bolt location geometry:

$$x'_{(n)} = x_{(n)} \cdot cos(\theta) + y_{(n)} \cdot sin(\theta) \tag{19}$$

$$y'_{(n)} = y_{(n)} \cdot cos(\theta) - x_{(n)} \cdot sin(\theta) \tag{20}$$

The design analysis also requires the external out-of-plane moments to be transposed. The transposed moments are again given by equations (12) and (13), using the angle of direction of the principal axes as given by equation (18).

The bolt related load is then given by the following equation

$$F_{br(n)} = \frac{F_z}{N_b} + \frac{M'_x}{\sum_n {y'}^2_{(n)}} \cdot y'_{(n)} - \frac{M'_y}{\sum_n {x'}^2_{(n)}} \cdot x'_{(n)} \tag{21}$$

The bolt related load given by equation (21) is not the load on an individual bolt; it is the component of external load that is passing through the region of the joint that is controlled by the bolt. In effect, the bolt related load represents an approximation to the minimum bolt preload required to ensure contact pressure is maintained across the faying surface.

This minimum bolt preload requirement represents a design preload. Section 3.8 of British Standard BS 7608:1990, "*Code of practice for Fatigue design and assessment of steel structures*" (1990), reference [5], says that the target or nominal bolt preload, F_p, should be at least 1.5 times the design preload, F_{dp}. Hence, the design requirement for the joint is;

$$F_{br(n)} \leq F_{dp} \tag{22}$$

where the design preload, F_{dp}, is given by:

$$F_{dp} = \frac{2}{3} \cdot F_p \tag{23}$$

The target preload, F_p, is usually based on a percentage of the bolt's proof load. Typically, calculations would assume a bolt preload of between 60% and 80% of the bolt proof load. When bolts are preloaded by tightening with a torque wrench, they are tightened to a specify bolt/nut 'make up' torque, which has been calculated or experimentally shown to achieve the required preload.

CONCLUSIONS

The method of detailed analysis for an asymmetrical bolted joint is based on the theory of beams. Hence, the equations that are derived for this method of analysis can also be applied to the bending analysis of any asymmetrical structures that are being connected by the bolted joint.

Similarly, any welds attaching structures to the joint flanges can be analysed using the same principles.

The joint design should, ideally, produce the situation where the centroid and principle axes of the bolt group, load bearing structures being connected and any welds attaching the structures to the joint flanges are all aligned.

The design analysis method is a simplification of the detailed analysis and does not require the calculation of section properties. This simplification of the analysis does not account for the flexural stiffness of the joint and results in an over estimate of the axial loads acting at the area of the joint flange being controlled by each bolt.

The method of design analysis is based on the assumption that each bolt in the joint and a surrounding region of the flanges can be considered as acting as a spring. Therefore, this method of analysis can be applied to calculate load the distributions of sprung suspension systems, and hence calculate the spring deflections.

The analysis methods presented are suitable for use in 'automated' calculation procedures.

References

[1] Welch, M. *Analysis of Bolt Bending in Preloaded Joints*. Journal of Mechanical Engineering – Strojnicky časopis, Volume 68 (2018), Issue 3, pages 183 to 194.

[2] Rotscher, F. *Die Maschinenelements*. Julius Springer, Berlin, Germany (1927).

[3] Richard Budynas, J Keith Nisbett. *Shigley's Mechanical Engineering Design.* 8th edition. McGraw Hill, 2006, ISBN 0-390-76487-6

[4] Verein Deutscher Ingenieure (Association of German Engineers) VDI 2230 Part 2. 2014, *Systematic calculation of highly stressed bolted joints Multi bolted joints*

[5] British Standards Institution. BS 7608:1990, *Code of practice for Fatigue design and assessment of steel structures*, British Standards Institution, London.

2.5 Basis of a Design Standard for Preloaded Bolted Joints

At present there are a number of standards, codes and guides that are either specific to, or contain sections/chapters that are specific to, bolted joints within civil engineering structures. For example, BS EN 1993-1-8:2005 "*Eurocode 3: Design of steel structures - Part 1-8: Design of joints*", BSI (2005), and Section 5 Connection Design, Chapter 23 Bolts, of the "*Steel Designers' Manual*" edited by Davidson and Owen (2012) are commonly used within the United Kingdom. Similarly, AISI "*Steel Construction Manual*" AISC (2005), AISI "*Specification for structural steel buildings – Allowable Stress Design and Plastic Design*" AISC (1989) and the "*Guide to design criteria for bolted and riveted joints*" by Kulak, Fisher and Struik (2001), are commonly used within the USA. These codes and guides cover the use of both snug tightened and preloaded joints within civil structures. The analysis of preloaded bolted joints subjected to in-plane loads and moments, i.e. friction grip, slip resistant, slip critical joints, are generally covered in some detail with partial safety factors and friction coefficients being specified. However, the analysis of out-of-plane moments and tensile loads are not considered. The approach to designing joints subjected to direct out-of-plane tension or combined tension and shear is to ensure that the out-of-plane tensile load component acts through the centroid of the joint's bolt group. This eliminates the need to consider out-of-plane moments within the analysis and, as far as practically possible, ensuring each bolt is subjected to the same out-of-plane tensile load.

At present there are not any mechanical engineering standards or codes dedicated specifically for the design and analysis of preloaded bolted joints. The design of cranes could be considered mechanical engineering and BS EN 13001-3-1: 2013 "*Cranes - General Design - Part 3-1: Limit States and proof competence of steel structure*", BSI (2013), does contain sections related to preloaded bolted joints. However, the type of structures covered by BS EN 13001-3-1, BSI (2013), are more akin to civil engineering structures, bridges, than mechanical engineering. This standard covers the use of both snug tightened and preloaded joints within crane structures but predominance is given the analysis of preloaded joints. The analysis methods for preloaded bolted joints subjected to in-plane loads are similar to those presented in the standards and codes relating to civil engineering steel structures but using partial safety factors specific to crane structures.

The effects of out-of-plane moments and loads are considered within BS EN 13001-3-1, BSI (2013). Section 5.2.3.3 “Connections loaded in tension” states:

> “The proof calculation shall be done for the bolt under maximum external force in a connection, with due consideration to the force distribution in a multi-bolt connection and the prying effects (i.e. leverage).”

However, analysis methods for determining the force distribution are not discussed. Section 5.2.3.3 also says:

> “Proof of competence calculations of a preloaded connection shall take into account the stiffness of the bolt and the connected parts.”

Procedures to calculate connection stiffnesses are presented in Annex G “Calculation of stiffnesses for connections loaded in tension” but these are based on a single bolt, not multi-bolt connections.

Other authors have also noted that methods for analysing load distributions within multi-bolted preloaded joints are absent from the available standards, codes, and guides. This is reflected in the article “*The road to a code*” by Natarajan Krishnamurthy (1999). This article was not published in a journal and hence, has not been peer reviewed. The article is a review of published works caried out by Krishnamurthy over a number of years which includes “*Correlation Between 2- and 3-Dimensional Finite Element Analysis of Steel Bolted End Plate Connections*” Krishnamurthy and Graddy (1976) and “*A Fresh Look at Bolted End- Plate Behavior and Design*” Krishnamurthy (1978). These works played a significant role in the development of AISC “*Steel Design Guide: Extended End-Plate Moment Connections*” AISC (2004a), first published in the 1990’s and now at its 39th revision.

In general, civil engineering steel structures tend to have thinner flange/steel-work thickness in relation to the bolt diameter than mechanical engineering components. These thinner sections can allow the flanges/mating surfaces of snug tightened joints to have some degree of separation under tensile load conditions. This separation can in turn produce ‘prying’ forces within the joint, as illustrated in Figure 8.

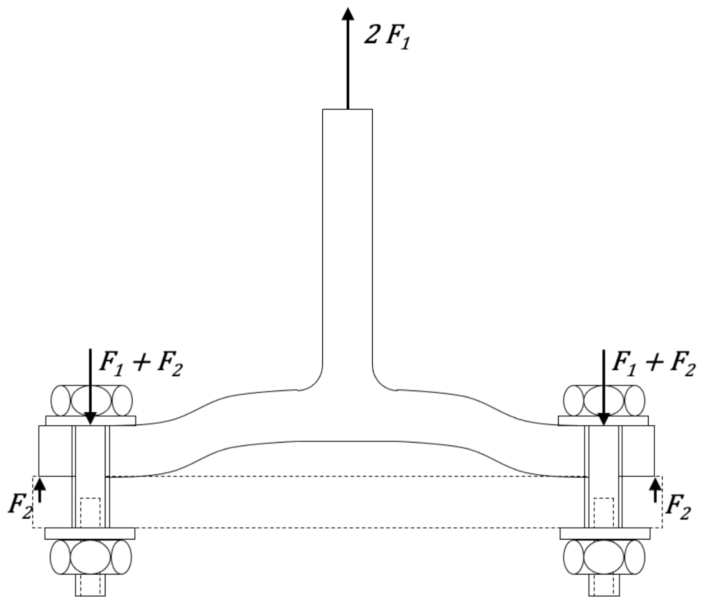

Figure 8: Prying forces within a "Tee" connection.

However, Krishnamurthy (1999) concludes that:

> "Prying force is not a significant factor in end-plate failure, because the pre-tensioning eliminates or postpones the development of the reactive force, and hence may be omitted from design consideration in most cases."

This observation by Krishnamurthy is consistent with the assumption made previously by the author when discussing "*A paradigm for the Analysis of Preloaded Bolted Joints*" Welch (2019) that:

> "Provided the flanges have sufficient thickness to prevent failure due to flange bending under the contact pressure the assumption of rigid, or near rigid, flanges can be considered reasonable".

The Verein Deutscher Ingenieure (Association of German Engineers) have also noted an absence of procedures for the analysis of multi-bolted preloaded joints and have introduced their own guide, VDI 2230 Part 2, VDI (2014). This document gives useful advice and guidance on analysing multi-bolted preloaded joints using Finite Elements Methods (FEM) and should encourage uniformity procedures, resulting in consistency, across industries. However, the guide does not provide a basis for design standards and codes.

The author believes that the analysis methods presented in the three papers presented previously, Welch (2018a), (2019) and Welch (2022a), could be used as the basis for a design guide for preloaded bolted joints, and possibly a national design code or standard. Such a guide, code or standard would need to include the engineering data required to allow the application of quality assurance of the design. For example, appropriate factors of safety, friction coefficients, bolt installation procedures and bolt make-up torques would need to be specified.

CHAPTER 3

DEVELOPMENTS IN STATIC ANALYSIS

3.1 Developments in Static Analysis

During his industrial career, the author had noticed over a number of years that when bolt shear and bolt bending due to in-plane loads were considered, stress engineers often assumed joint slip, resulting in the assumption of bolts bearing on the flange, to calculate bolt shear and bolt bending stresses. Occasionally, they would assume the shear stress at the faying surface was transmitted to the bolt via friction under the bolt head. The methods that assume joint slip and bolt bearing are really only applicable to snug tightened bolted joints, not preloaded joints. Methods that assume the bolt experiences the same shear stress as the faying surface are suitable for preloaded joints but are also very conservative.

Bolts are usually installed with clearance holes in the flange. In-plane shear loads on a preloaded bolted joint are carried mainly by friction at the contact surface and not a direct shear load on the bolts. When considering in-plane shear loads the joint design often includes dowels, and occasionally fitted bolts, or other means of positively locating the joint. Even dowels or 'fitted' bolts are unlikely to have a positive interference fit within their holes and will have a small clearance. Whether or not positive location is used, if the joint is going to be subjected to cyclic in-plane loading and possible load reversals, the bolts have to be tightened sufficient to avoid joint slippage. In some cases, when positive location cannot be used and where any joint slippage could cause a serious detrimental change in the joint's geometry, the joint may be classified as a 'slip critical' type of connection (or some similar name). In all cases, whether classed as slip critical or not, the joint performs in the same way and can be analysed using the same methods. The differences in the analyses are in the safety factors, partial safety factors and friction coefficients used for the analysis. In effect, this is applying quality assurance criteria based on the risk of joint slippage and its results. In some instances, design standards may require the use of bolts that are themselves also subject to specific quality assurance driven tests as part of their specification. Examples of this are BS 4395-1:1969, BSI (1969a) and BS 4395-2:1969, BSI (1969b).

3.2 Analysis of Bolt Bending in Preloaded Bolted Joints

The objectives of the early papers being presented, Welch (2018a) and (2019), included the aim of promoting good practices in the static analysis of preloaded bolted joints. Good practice also includes understanding the background to the methods being employed and their limitations. These papers highlighted areas where there appeared to be a need for more work to improve and expand on the understanding of how preloaded bolted joint support in-plane external loads. The current method of calculating bolt bending by assuming bolt bearing is inappropriate since this situation would only occur as a result of joint failure resulting in slippage. This led to the paper, "*Analysis of Bolt Bending in Preloaded Bolted Joints"*, Welch (2018b), which also arose from thoughts and observations that the author had accrued over a number of years. These thoughts were in considering what actually happens to preloaded bolts under in-plane loading conditions, and asking the question; what was the true bolt shear stress? Again, classical analysis methods were used, but this time to show how flexural deflections of the bolts due to shear strain in the flange pack produce bending moments and additional tensile loads on the preloaded bolts. These tensile loads and bending moments can cause yielding of the bolt, reducing bolt preload. The phenomena of loss of preload in bolts with a low bending resistance is well known. Indeed, VDI 2230 Part 1, VDI (2003), suggests that there could be up to 20% reduction in preload, and possibly more.

The paper on bolt bending by Welch (2018b), considers shear strain through the flange pack and the transverse flexibility of the bolt. This approach is less conservative than other methods that have been considered in the past. Using this approach it is possible to show that in-plane loads can produce a tensile load component on the bolt which is additive to the bolt preload and the component of axial load due to out-of-plane external loads. These additional tensile loads arise from the shear strain in the flanges and the high through flange stiffness of the joint. These additive loads could contribute to causing the bolt tensile load to exceed the bolt proof load and limit of proportionality, thus producing permanent deformation and bolt extension. This in turn can result in a reduction of the bolt preload. The predicted increase in bolt tensile stress, and hence possible reduction in preload, is particularly noticeable in joints using long bolts, say a grip length of greater than four times the nominal bolt diameter.

3.2.1 P4 - Author Accepted Manuscript (Journal of Mechanical Engineering – Strojnicky časopis. Vol. 68 (2018), Issue 3, pages 183-194.)

ANALYSIS OF BOLT BENDING IN PRELOADED BOLTED JOINTS

WELCH Michael

Michael A Welch (Consulting Engineers) Limited, West Lancashire, UK,
email: mike.welch@mail.co.uk

Abstract: Classical analysis methods are applied to show how flexural deflections due to shear strain in the flange pack produce bending moments and tensile loads on bolts within preloaded bolted joints. It was found that in joints made with long bolts these loads can be significant. The loads can cause yielding of the bolt, reducing bolt preload. The methods presented are adequate to demonstrate the structural integrity of joints made with long bolts or with a small footprint.

KEYWORDS: bolted joint, preloaded bolt, bolt preload, bolt bending, long bolt

Nomenclature

A_b	Tensile area of each bolt
A_j	Total area of joint
$A_{s.b}$	Shear area of each bolt
d_b	Nominal bolt diameter
d_h	Bolt hole diameter
D_b	Effective diameter of bolt tensile area
D_n	Basic effective diameter of bolt thread (pitch diameter)
D_s	Minor diameter of bolt thread (root diameter)
E_b	Young's Modulus of elasticity for bolt material
$F_{b(n)}$	Total axial bolt load on bolt 'n'

F_p Preload in each bolt

$F_{s.b_{(n)}}$ Shear load on bolt 'n'

$F_{s.b.lim_{(n)}}$ Limiting shear load on bolt 'n'

$F_{t.b_{(n)}}$ Tensile load on bolt 'n'

F_x External In-plane force acting in x-direction

F_y External In-plane force acting in y-direction

F_z External axial load in direction of 'z' axis

G_f Shear Modulus for flange material

I_b Second Moment of Area of the tensile area of each bolt

I'_b Second Moment of Area of the tensile area of a bolt

$I_{xx.j}$ Second Moment of Area of joint about 'x' axis

$I'_{xx.j}$ Second Moment of Area transposed about x'-axis

$I_{xy.j}$ Product Moment of Area of joint

$I_{yy.j}$ Second Moment of Area of joint about 'y' axis

$J_{zz.j}$ Polar Second Moment of Area of joint

k_{jp} Joint pack stiffness

L_f Through flange thickness

L_g Bolt grip length (including washers)

M_x External moment acting about the 'x' axis

M'_x Resultant moment

M_y External moment acting about the 'y' axis

M_z External torsional moment acting on joint

T_p Residual torque in each bolt

$x_{(n)}, x_{s_{(n)}}$ Coordinate of bolt 'n'

$y_{(n)}, y_{s_{(n)}}$ Coordinate of bolt 'n'

$y'_{(n)}$ Transposed coordinate of bolt 'n'

$\propto$	Flank angle of thread (half the included angle)
$\delta_{b(n)}$	Displacement of bolt 'n' bolt head normal to bolt axis
$\delta_{z(n)}$	Bolt Extension
θ	Angle of resultant moment
μ_b	Friction coefficient under bolt head
μ_t	Friction coefficient at thread flank
$\sigma_{a.b(n)}$	Axial stress in bolt 'n'
$\sigma_{b(n)}$	Total tensile stress in bolt 'n'
$\sigma_{b.b}$	Bending stress component in each bolt
$\sigma_{mb(n)}$	Total bending stress in bolt 'n'
$\sigma_{mx(n)}$	Bending stress in bolt 'n' from moments about x-axis
$\sigma_{my(n)}$	Bending stress in bolt 'n' from moments about y-axis
$\sigma_{s.b(n)}$	Bending stress component in bolt 'n'
$\sigma_{VM.c(n)}$	Equivalent (Von Mises) stress at core of bolt 'n'
$\sigma_{VM.r(n)}$	Equivalent (Von Mises) stress at thread root of bolt 'n'
$\tau_{b(n)}$	Shear stress in bolt 'n'
τ_p	Residual shear stress in each bolt
$\tau_{x(n)}$	Shear stress at faying surface surrounding bolt 'n' from loads in x direction
$\tau_{xy(n)}$	Shear stress at faying surface surrounding bolt 'n'
$\tau_{y(n)}$	Shear stress at faying surface surrounding bolt 'n' from loads in y direction

1 Introduction

The detailed analysis of preloaded joints using classical theory of elasticity methods has been discussed in the paper "Classical Analysis of Preloaded Bolted Joint Load Distributions" [1]. This provided an understanding of how preloaded joints work and the interaction of the various components of the joint. Reference [1] considered the distribution of tensile loads on the bolts but did not go into depth on bolt bending.

Bolts with a low bending resistance, such as long bolts with a grip length several times greater than the nominal bolt diameter, can be prone to self loosening under transverse load reversals. Even with nut locking there can be a relaxation in bolt preload. Section 3.2.4 of VDI 2230 Part 1, "Systematic calculation of high duty bolted joints with one cylindrical bolt" [2] suggests that there could be up to 20% reduction in bolt preload.

The paper being presented here considers the classical analysis of bolt bending within preloaded bolted joints loaded with out-of-plane moments, in-plane loads and torsional moments. The effects these external loads have on bolt tensile stresses and their influence on bolt preload is discussed.

2 Out-of-Plane Loads on the Joint

Any external out-of-plane moments on the joint produces a stress gradient across the faying surface. The faying surface is the joints prepared contact face. This stress gradient produces a bending moment and bending stress component common to each of the bolts. The resulting bending stress component is given by:

$$\sigma_{b.b} = \pm \frac{M_x}{I_{xx.j}} \cdot \frac{D_b}{2} \tag{1}$$

It is common for the out-of-plane moment on a joint to be described by a pair of moments, M_x and M_y, acting about the principle axes of the joint, or another convenient pair of perpendicular axes. These moments and their resultant, M'_x, are illustrated in Figure (1).

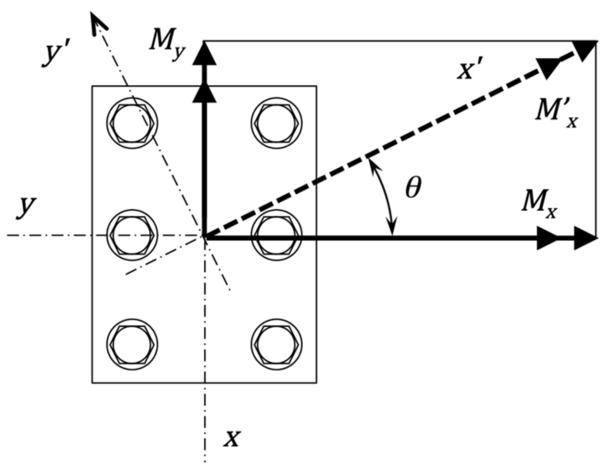

Fig. 1 Orientation of resultant moment.

Since the resultant moment acts about a different axis to those used to define the joint, an alternative coordinate system, aligned to the resultant moment, needs to be considered. The angle between the transposed coordinate system and the joint coordinate system is given by:

$$\theta = arctan\left(M_y/M_x\right) \tag{2}$$

If M_x is negative then 180 degrees (π radians) needs to be added to the angle θ to ensure the direction of the resultant moment is in the correct 'quadrant'.

The resultant moment, M'_x, is given by:

$$M'_x = M_x \cdot \cos(\theta) + M_y \cdot \sin(\theta) \tag{3}$$

The Second Moment of Area about the *x*-axis transposed to the *x'*-axis is given by:

$$I'_{xx.j} = I_{xx.j} \cdot cos^2(\theta) + I_{yy.j} \cdot sin^2(\theta) - I_{xy.j} \cdot \sin(2\theta) \tag{4}$$

Equations (2) to (4) follow the "right hand" rule, as illustrated in Figure (2). Loads are positive in the direction of the axes and positive moments act clockwise about the axes when viewed from the origin.

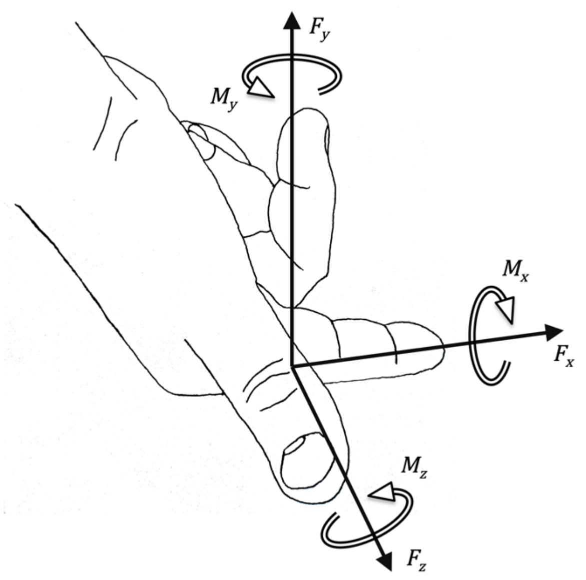

Fig. 2 Right hand rule coordinates.

When considering an out-of-plane moment that is not aligned with the joint x-axis the terms for M'_x and $I'_{xx.j}$ given by equations (3) and (4) should be used in equation (1).

In most joints the bolt diameter is small compared to the overall size of the joint hence, the bending stress given by equation (1) is usually small compared to the bolt's axial stress. However, for joints with a narrow footprint, such as a single bolt or a single line of bolts, the bolt diameter may be almost the same as the width/length of the faying surface and this bolt bending stress can be significant.

3 In-Plane Loads on the Joint

External in-plane loads and torsional moments on the joint are supported by two mechanisms, friction at the faying surface and bolt shear. In some joints dowels, or other positive method of locating the joint, can assist these mechanisms.

Figure (3a) illustrates the way external in-plane loads are reacted into the bolts. The shear stresses in the flanges produced by the external in-plane loads and moment result in deflections at the bolt head, relative to the nut, perpendicular to the bolt axis. The shear loads producing these deflections are transmitted by friction under the bolt head/nut. The through thickness stiffness of the flanges is significantly greater than the flexural stiffness of the bolts. Hence, it is assumed that there is no flexural rotation of the bolt head or nut.

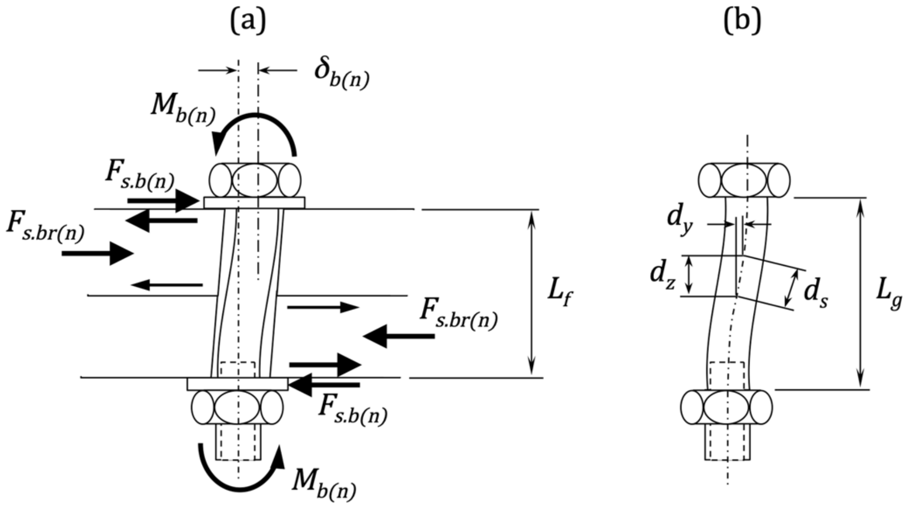

Fig. 3 Joint In-Plane loads reacted into a bolt.

The friction loads under the bolt head/nut, $F_{s.b_{(n)}}$, are normal to the axis of the bolt and produce bending moments on the bolt at the head and nut and a shear load on the shanks of each bolt within the joint. These shear loads exist even though the bolts do not bear on the sides of the holes in the flanges.

It was shown in reference [1] that, assuming there is no joint slip at the faying surface, the mean shear stress at the region of faying surface surrounding each bolt is given by the following three equations.

$$\tau_{x_{(n)}} = \frac{F_x}{A_j} - \frac{M_z}{J_{zz.j}} \cdot y_{s_{(n)}} \tag{5}$$

$$\tau_{y_{(n)}} = \frac{F_y}{A_j} + \frac{M_z}{J_{zz.j}} \cdot x_{s_{(n)}} \tag{6}$$

$$\tau_{xy_{(n)}} = \sqrt{\tau_{x_{(n)}}^2 + \tau_{y_{(n)}}^2} \tag{7}$$

where $x_{s_{(n)}}$ and $y_{s_{(n)}}$ are the coordinates of the bolt holes, relative to the centroid of the joint.

Again, Equations (5) to (7) follow the “right hand” rule, as illustrated in Figure (2).

Equation (5) gives the shear stress component from loads acting in the x-direction. Similarly, equation (6) gives the shear stress component from loads acting in the y-direction. Equation (7) gives the resultant mean shear stress at the region/area of faying surface that surrounds the location of bolt ‘n’. This shear stress is carried across the faying surface by friction.

In an Ideal joint, preloading the joint’s bolts induces a uniform compressive stress at the faying surface. In practice, the contact pressure will not be uniform across the surface. Each preloaded bolt influences an approximately circular region of the faying surface that surrounds it.

The bolt bending stresses calculated from equations (1) to (4) are influenced by the section properties $I_{xx.j}$, $I_{yy.j}$ and $I_{xy.j}$. These section properties can be calculated assuming the contact surface consists of the circular regions described above. However, the shear loads on the bolts calculated by equations (5) to (7) are determined by the shear strains in the joint pack. These shear strains are influenced by the whole of the joint pack. Hence, the section properties A_j and $J_{zz.j}$ should be calculated from the geometry of the full flange section.

A method of calculating the area of the faying surface influenced by a bolt is presented in part 3, section 8.5 of Shigley’s Mechanical Engineering Design [3] and in section 5.1.2 of VDI 2230 Part 1 [2].

Assume the transverse, normal to the bolt axis, flexural displacement of the bolt head arises from the shear strain across the thickness of the flanges. Then the displacement of bolt ‘n’ is approximated by:

$$\delta_{b\,(n)} = \frac{\tau_{xy\,(n)} \cdot L_f}{G_f} \tag{8}$$

The bolt head displacement calculated by equation (8) is relative to the nut, not absolute.

The through flange thickness L_f is the total flange thickness that carries the shear load. It does not include washers or packers under the bolt head or nut that do not directly react the external loads that produce in-plane shear in the flanges.

The bolt, as illustrated in figure (3a), is treated as a beam. Assuming the effective beam is fixed at the nut and there is no rotation at the bolt head then the shear load on the bolt, acting perpendicular to the bolt shank, is given by:

$$F_{s.b(n)} = \frac{12 \cdot E_b \cdot I_b}{{L_g}^3} \cdot \frac{\tau_{xy(n)} \cdot L_f}{G_f} \tag{9}$$

The grip length L_g is the total length of bolt between the contact faces of the bolt head and nut, including washers. It has been shown that the first internal thread supports a large proportion of the load and is subject to yielding [4]. Hence, an additional allowance of one bolt thread pitch can be added to the grip length to account for flexibility of the thread within the nut.

The Second Moment of Area for the bolt thread tensile section has been used in equation (9). This is the case for bolts threaded for their full length. When the bolts have two or more cross-sectional elements, such as a plain shank and threaded section then a mean effective Second Moment of Area could be used. The mean effective Second Moment of Area is given by:

$$I_b' = \frac{L_g}{\sum_i \frac{L_{(i)}}{I_{(i)}}}$$

where, $I_{(i)}$ and $L_{(i)}$ are the Second Moment of Area and Length respectively of each cross-sectional element of the bolt.

The resulting shear stress in the bolt is given by:

$$\tau_{b(n)} = \frac{F_{s.b(n)}}{A_{s.b}} \tag{10}$$

The flexural stiffness of the bolts is considerably less than the torsional stiffness of the joint. Hence, shear stresses in the bolts are significantly less than the shear stress at the faying surface.

The bending stress at each bolt's thread root, at a location just under the nut, is given by:

$$\sigma_{s.b_{(n)}} = \pm \frac{F_{s.b_{(n)}} \cdot L_g}{2 \cdot I_b} \cdot \frac{D_b}{2} \tag{11}$$

3.1 Bending Induced Bolt Tension

Figure (3b) illustrates how the flexural deflection of the bolt and the high through flange stiffness results in some axial extension of the bolt. The extended length of an element is:

$$ds = \sqrt{dz^2 + dy^2}$$

which can be approximated as:

$$ds = dz + \frac{1}{2} \cdot \left(\frac{dy}{dz}\right)^2 dz$$

The extended bolt length is given by:

$$Extended\ length = L + \delta_z = \int_0^L ds$$

Hence:

$$\delta_z = \frac{1}{2} \cdot \int_0^L \left(\frac{dy}{dz}\right)^2 dz$$

Solving this leads to:

$$\delta_{z_{(n)}} = \frac{F_{s.b_{(n)}}^{2} \cdot L_g^{5}}{240 \cdot (E_b \cdot I_b)^2} \tag{12}$$

where the transverse force, $F_{s.b_{(n)}}$, is the shear force given by equation (9).

This axial extension results in an axial load in addition to the bolt preload. This additional tensile bolt load component is given by:

$$F_{t.b\,(n)} = \frac{{F_{s.b}}_{(n)}^{2} \cdot {L_g}^{4} \cdot A_b}{240 \cdot E_b \cdot {I_b}^{2}} \tag{13a}$$

The additional tensile load given by equation (13a) is based on an infinitely stiff joint pack. Allowing for the stiffness of the joint pack the equation is rewritten as:

$$F_{t.b\,(n)} = \frac{{F_{s.b}}_{(n)}^{2} \cdot {L_g}^{4} \cdot A_b}{240 \cdot E_b \cdot {I_b}^{2} \cdot \left(1 + \frac{A_b \cdot E_b}{k_{jp} \cdot L_g}\right)} \tag{13b}$$

where k_{jp} is the through thickness stiffness of the joint pack under the bolt head.

The joint pack contained within the grip length of a bolt can be considered as consisting of a number of elements. A typical joint would consist of four elements, a washer under the bolt head, two flanges and a washer under the nut. A joint made with a tapped, or threaded, component would typically consist of two elements, a washer under the bolt head and a single flange. These two examples are of the most common joint configurations but other joints could include additional flanges, packers and spacers. The overall stiffness of the joint pack is found by combining the stiffness's of each element and can be estimated from:

$$k_{jp} = \frac{1}{\sum_i \frac{t_{(i)}}{A_{(i)} \cdot E_{(i)}}}$$

where, $t_{(i)}$, $A_{(i)}$ and $E_{(i)}$ are the thickness, Area and Young's Modulus of Elasticity respectively of each element of the joint pack.

More refined methods of calculating the joint pack stiffness are suggested in both section 5.1.2 of reference [2] and part 3, section 8.5 of reference [3].

Neglecting the effects of the joint pack stiffness will results in a slightly conservative (high) tensile load component.

4 Combined Bending

The bending stresses $\sigma_{b.b\,(n)}$ and $\sigma_{s.b\,(n)}$ are from moments acting about different axes. The vector addition of the two stress components is performed by the following equations:

$$\sigma_{mx\,(n)} = \sigma_{b.b} \cdot \sin(\theta) - \sigma_{s.b\,(n)} \cdot \frac{\tau_{y\,(n)}}{\tau_{xy\,(n)}} \tag{14}$$

$$\sigma_{my\,(n)} = \sigma_{b.b} \cdot cos(\theta) + \sigma_{s.b\,(n)} \cdot \frac{\tau_{x\,(n)}}{\tau_{xy\,(n)}} \tag{15}$$

$$\sigma_{mb\,(n)} = \sqrt{\sigma_{mx\,(n)}^{2} + \sigma_{my\,(n)}^{2}} \tag{16}$$

Equation (14) gives the bending stress component about the *x*-axis. Equation (15) gives the bending stress component about the *y*-axis. Equation (16) gives the resultant bending stress component in the bolt.

4.1 Total Bolt Load

Reference [1] shows that the bolt axial stresses resulting from the combined loading of the preload, external axial load and external out-of-plane moment are given by:

$$\sigma_{a.b\,(n)} = \frac{F_p}{A_b} + \frac{F_z}{A_j} + \frac{M_x}{I_{xx.j}} \cdot y_{(n)} \tag{17}$$

When considering an out-of-plane moment that is not aligned with the joint x-axis the terms for M_x and $I_{xx.j}$ in equation (17) should be replaced with M_x' and $I_{xx.j}'$ as given by equations (3) and (4) and the term for $y_{(n)}$ should be replaced by:

$$y_{(n)}' = y_{(n)} \cdot \cos(\theta) - x_{(n)} \cdot \sin(\theta) \tag{18}$$

where $x_{(n)}$ and $y_{(n)}$ are the coordinates of bolt '*n*' defined with respect to the centroid of the bolt group.

The total axial load on each bolt is given by:

$$F_{b(n)} = \sigma_{a.b(n)} \cdot A_b + F_{t.b(n)} \tag{19}$$

The total bolt stress, including the bending stresses, is given by:

$$\sigma_{b(n)} = \frac{F_{b(n)}}{A_b} \pm \sigma_{mb(n)} \tag{20}$$

The localised increase in bolt stress, above the preload stress, may cause plastic deformation in the bolt thread that could result in some relaxation of the bolt preload.

4.2 Bolt Limit of Proportionality

The increase in bolt tension and bending stresses due to the external loads could produce some plastic deformation that could lead to relaxation of the bolt preload. The Von Mises yield criterion can be applied to both the core and thread root of the bolt.

In addition to the stresses produced by the external loads each bolt will also have residual stresses from the axial preload and from some residual bolt tightening torque being locked in the bolt shank. Appendix B of BS 3580:1964 “Guide to the design considerations on: The strength of screw threads” [5] describes the bolt torque-tension relationships. From these relationships it is concluded that the residual torque in each bolt is:

$$T_p = F_p \cdot \frac{D_n}{2} \cdot \frac{\mu_t}{\cos{(\alpha)}} \tag{21}$$

The residual shear stress is given by:

$$\tau_p = \frac{16 \cdot T_p}{\pi \cdot {D_s}^3} \tag{22}$$

The Von Mises, or equivalent, stress in the bolt is given by the following two equations.

$$\sigma_{VM.c_{(n)}} = \sqrt{\left(\frac{F_{b_{(n)}}}{A_b}\right)^2 + 3 \cdot \left(1.5 \cdot \tau_{b_{(n)}} + \tau_p\right)^2} \tag{23a}$$

$$\sigma_{VM.r_{(n)}} = \sqrt{\sigma_{b_{(n)}}^2 + 3 \cdot \left(\tau_{b_{(n)}}^2 + \tau_p{}^2\right)} \tag{23b}$$

Equation (23a) gives the Von Mises stress at the core of bolt ‘n’. The peak shear stress, at the centre of the bolt section, will be 1.5 times the mean shear stress.

Equation (23b) gives the Von Mises stress at the thread root. For this equation it has been assumed that some bolt shear stress will exist in the bolt thread root local to the nut, along with the residual shear stress.

5 Joint Slippage

In the previous sections it has been assumed that there is no joint slippage. This will be the case if dowels have been used to assist in carrying the in-plane loads by “pegging” the joint. However, if joint is not doweled then dynamic or impact loads may induce some joint slip.

Joint slippage is most likely to occur at the bolts where external out-of-plane loads and moments reduce the contact pressure at the faying surface. In doweled joints any slippage would take the form of localised slip as the shear stress at the faying surface is relaxed. In none doweled joints the slip could be more significant.

5.1 Slip Limited by Displacement

If the joint is not dowelled, the maximum flexural deflection of the bolt head relative to the nut is limited by the bolt and hole diameters. The bolt shear load due to transverse deflection of the bolt head is given by:

$$F_{s.b.lim} = \frac{12 \cdot E_b \cdot I_b}{L_g{}^3} \cdot \left(\frac{d_h - d_b}{2}\right) \tag{24a}$$

In deriving equation (24a) it is assumed that the bolt and hole axes are aligned prior to slip occurring. Under extreme geometric tolerance stack up of the joint assembly the bolt shear load, $F_{s.b.lim}$, could potentially be doubled.

The limiting shear load, $F_{s.b.lim(n)}$, calculated by equation (24a) can be used in equations (10) and (11) in place of the shear load, $F_{s.b_{(n)}}$, given by equation (9).

5.2 Slip Limited by Friction

In an extreme case slippage may occur between the bolt head or nut and the washer/flange. In this instance the load perpendicular to the bolt shank will be limited by friction under the bolt head or nut. It was shown in reference [1] that external loads and moments are supported mainly by a reduction in contact pressure at the faying surface, with only a small proportion of the external loads producing changes in the bolt tensile stresses. Hence, it is assumed that the limiting bolt shear load for an extreme case is given by:

$$F_{s.b.lim} = \mu_b \cdot F_p \tag{24b}$$

where μ_b is the friction coefficient under the bolt head or nut.

Soon after the installation of the bolt the friction coefficient μ_b will be that produced by any lubricant used during assembly. However, the value of the friction coefficient may change with the age, environment and history of the joint.

Again, the limiting shear load, $F_{s.b.lim_{(n)}}$, calculated by (24b) can be used in equations (10) and (11) in place of the shear load, $F_{s.b_{(n)}}$, given by equation (9).

CONCLUSION

External out-of-plane moments produce a stress gradient across the faying surface. This results in a bending stress component on each of the bolts, common to all of the joint's bolts. In joints with narrow footprints, such as a single bolt or a single line of bolts, the stress gradient and resulting bending stress can become significant.

The transverse flexural displacement of the bolt head produces a tensile load component in the bolt in addition to the existing preload. The total tensile load in the bolt may cause the limit of proportionality for the bolt material to be exceeded. This could lead to permanent set in the bolt, causing a relaxation of the bolt preload. This is a significant problem in joint assemblies incorporating long bolts.

The low flexural stiffness of a long bolt assembly means that, if the joint is not dowelled, the joint is more prone to slippage than one made using short bolts.

The bolt bending analysis discussed is suitable for calculating stresses for use in a fatigue analysis. In which case, stress concentration factors may also need to be applied to the calculated bolt stresses.

REFERENCES

[1] Welch, M. (2018) *Classical Analysis of Preloaded Bolted Joint Load Distributions*. International Journal of Structural Integrity, Volume 9, Issue 4, pages 455 to 464.

[2] Verein Deutscher Ingenieure (Association of German Engineers). VDI 2230 Part 1. 2003, *"Systematic calculation of high duty bolted joints with one cylindrical bolt"*, Verein Deutscher Ingenieure, Dusseldorf.

[3] Budynas, R. and Nisbett, J.K. (2006) *Shigley's Mechanical Engineering Design.* 8th edition. McGraw Hill, Primis Online. 2006, ISBN 0-390-76487-6

[4] Pástor, M. et al. (2018) *The use of Optical Methods in the Analysis of Areas With Stress Concentration*. Journal of Mechanical Engineering – Strojnicky časopis, Volume 68, Issue 2, pages 61 to 76.

[5] British Standards Institution. BS 3580:1964, *Guide to the design considerations on: The strength of screw threads*, British Standards Institution, London.

3.2.2 Further Discussion

The analysis of "Bending Induced Bolt Tension" presented by Welch (2018b) is given in more detail in Appendix A.

It can be seen from Welch (2018b) that the torsional stiffness of the joint depends on the second polar moment of area of the flange cross-section. Similarly, the bending stiffness of the bolts, and their influence on the torsional stiffness of the joint, depends on the much smaller second moment of area of the bolt shanks. Hence, the torsional stiffness of the joint is dominated by friction at the faying surface, which arises from the bolt preload. The bolt shear and bending stresses have only a small influence on the torsional stiffness of the joint.

The analysis presented in the paper is based on a number of assumptions. It is assumed that the in-plane loads are introduced into the flanges across the entire flange surface in the plane directly under the bolt heads/nuts. It is also assumed the shear stress component produced by the torsional loads are determined by the second polar moment of area of the joint, based on the properties of the faying surface, and the radial distance from the centroid of the joint. Side, or shear, loads acting directly in-plane of the flange are assumed to produce a uniform shear stress component which is again assumed to be introduced into the flange across the entire flange surface. Therefore, the assumed shear stress distribution represents an 'average shear stress'.

In reality, the in-plane loads will be introduced across the interface between the flanges and the structural elements to which they are attached. This will result in a much higher, localised, shear stress at this interface. The 'intensity' of this shear stress will begin to be dispersed through the thickness of the flange, tending towards the value of the assumed average shear stress. This dispersion of the shear stress is illustrated in Figure 9.

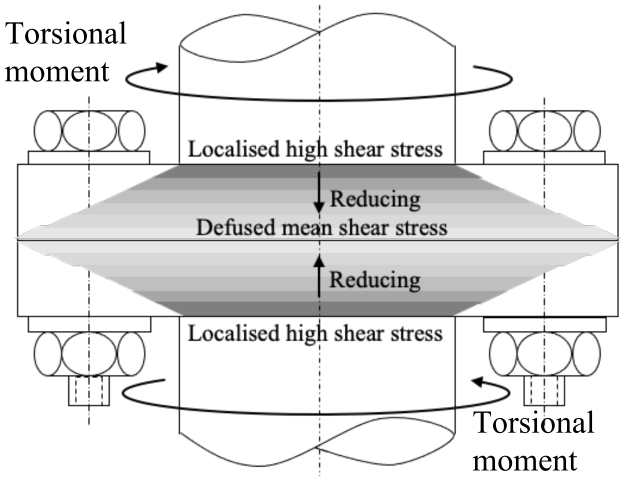

Figure 9: Shear stress dispersion

Hence, it can be argued that the bolts closest to the interface of the flange and attached structural elements will experience flexural displacement of the bolt head greater than the displacement predicted by using the mean shear stress. This will result in greater additions tensile stresses than those predicted by the analysis. Similarly, it is possible to argue that the bolts furthest from the interface of the flange and structural elements will experience smaller bolt head flexural displacements than predicted.

The foregoing discussion is based on using the second polar moment of area of the joint and the radial distance from the centroid of the joint to calculate the shear stresses produced by in-plane torsional loads. However, it is known that for non-circular sections the ‘torsional constant’ is always less than the second polar moment of area and that the maximum shear stress is not necessarily at the maximum distance from the centroid. For example, for a rectangular cross-section the maximum shear stress is at the mid-positions of the longest sides, as illustrated in Figure 10.

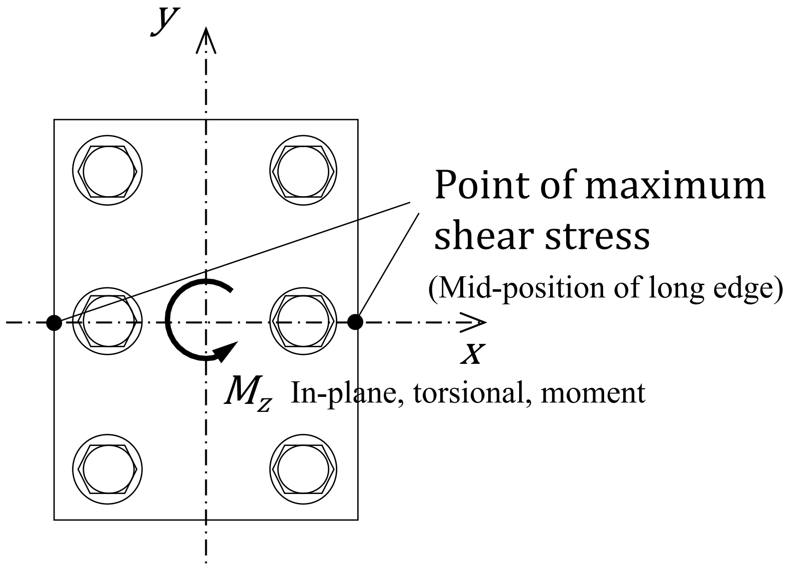

Figure 10: Position of maximum shear stress from torsion of a rectangular section

Also, for non-circular sections, the true shear stress is always greater than that predicted by using the second polar moment of area. Given this, it is recommended that, wherever possible, the calculation of the bolt head flexural displacement, the resulting bending moment and additional tensile stress in the bolt should be calculated using an appropriate torsional constant for the flange geometry. The previous discussion of the way the shear stress is introduced into the flanges and the shear stress intensity is dispersed through the thickness of the flange will still hold true. The bolts closest to the attached structural elements will experience bolt head flexural displacement, in the plane of the faying surface, greater than the predicted displacement. Again, this will result in greater additions tensile stresses than those predicted by the analysis. Similarly, the bolts furthest from the attached structural elements will experience smaller bolt head flexural displacements than predicted.

The total shear stress in the joint flanges will be given by the summation of the torsional shear stress and the shear stress components from the direct in-plane loads.

If the bolt total maximum tensile stress, including the calculated additional tensile stress from the sideways flexural deflection of the bolt head, exceeds the bolt material yield stress then there will be some loss of the initial preload. An estimate of this loss of preload can be made by following the procedure illustrated by Figure 11.

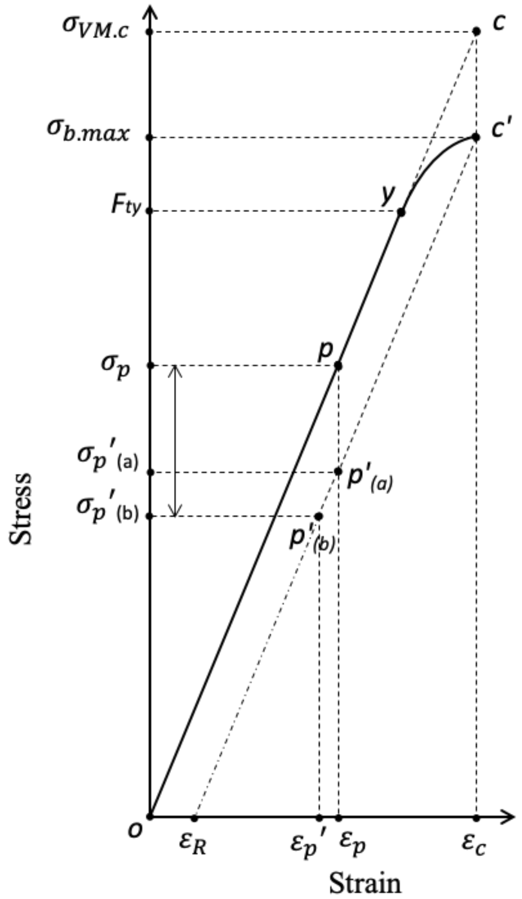

Figure 11a

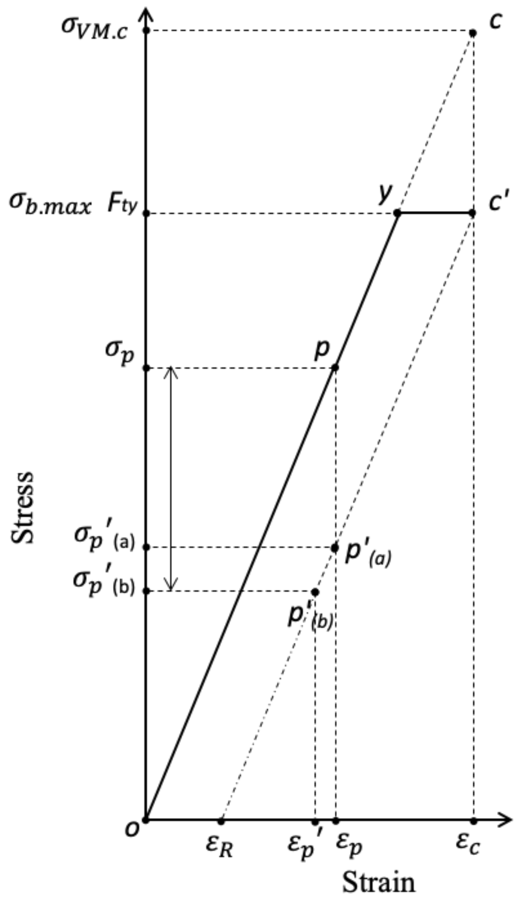

Figure 11b

Figure 11: Graphical assessment of loss of bolt preload

The solid curve, line oc', which also passes though points p and y, as shown in Figure 11a, is part of the stress-strain curve of the bolt material. The point p represents the initial preload condition of the bolt, prior to any external loads being applied, where σ_p is the bolt stress due to the preload and ε_p is the corresponding strain. Similarly, the point y describes the position on the stress-strain curve where, as the external loads on the joint are applied, the bolt stress reaches the yield stress F_{ty} of the bolt material and the bolt begins to behave in a non-linear, plastic manner.

When external loads are applied the method of analysis presented in the paper "*Analysis of Bolt Bending in Preloaded Bolted Joints"*, Welch (2018b), assumes a linear solution for the total bolt load, including the additional bolt load produced by the flexural displacement at the bolt head, and predicts a total elastic axial load for the bolt and the nominal shear stress. The total elastic axial load, along with the bolt's tensile area, and the nominal shear stress are then used to calculate the maximum, elastic, stress $\sigma_{VM.c}$ based on the Von Mises yield criteria. This theoretical condition is described/indicated by point c of Figure 11a. It should be noted that the true shear stress at the core of the bolt shank under the preload conditions is zero hence, the bolt preload stress σ_p is also equivalent to the Von Mises stress for the preload condition. If, as in this example, the maximum Von Mises stress $\sigma_{VM.c}$ exceeds the bolt material yield stress F_{ty} the bolt material will no longer act elastically but instead will enter the plastic range and behave non-linearly. Hence, the bolt material will follow the stress-strain curve until it reaches the condition described/indicated by point c' of Figure 11a. Since the joint flanges, which are in compression due to the bolt preload, will remain within the elastic range of the flange material, then the bolt displacement, under plastic deformation, will be controlled by the thickness of the flange pack. Therefore, the points c and c' will both be described by ε_c the maximum total strain at the core of the bolt. If the external loads are then removed the bolt material will behave elastically and the bolt load condition will follow the line $c\ p'_{(b)}$ passing through the point $p'_{(a)}$. The line $c'\ p'_{(b)}$ is parallel to the line oy, the slope of which represents Young's Modulus of Elasticity E_b for the bolt material. Again, the strain of the bolt will be controlled by the flange pack. The point $p'_{(a)}$ is described by ε_p which is the flange pack through thickness strain associated with the bolt's initial preload condition. The bolt stress $\sigma'_{p(a)}$ associated with the point $p'_{(a)}$ will be less than the bolt stress σ_p from the initial preload. If the through flange stiffness were infinite then the point $p'_{(a)}$ would be the new, reduced, bolt preload condition and the stress $\sigma'_{p(a)}$ would be the corresponding bolt preload stress. However, if the effect of flange pack stiffness is taken into consideration the actual reduced preload condition would be described by point $p'_{(b)}$ and $\sigma'_{p(b)}$ would be the actual bolt reduced preload stress.

It is worth noting that, if the bolt were now fully unloaded and removed from the joint the bolt material would follow the line $p'_{(b)}\ \varepsilon_R$ where ε_R is the strain describing the permanent set in the bolt.

If a stress-strain curve for the bolt material is not available an idealised curve, as illustrated in Figure 11b, can be assumed. This idealised curve neglects the effects of work hardening and hence will result in a conservative estimate of the loss of preload, that is, it will predict a greater loss of preload than would actually occur. This is illustrated by the greater value for ε_R indicated in Figure 11b compared with that of Figure 11a.

3.3 Bolted Joint Preload Distribution from Torque Tightening

The paper "*Bolted Joint Preload Distribution From Torque Tightening*", Welch (2021), was a theoretical study of what occurred within a joint during the tightening sequence and the final preloaded condition of the joint. The objective of bolt tightening procedures is to try and achieve an optimum preload condition. Generally, bolt tightening should start with the bolt nearest the centre of the bolt group. The tightening sequence would then spread outwards, crossing from one side of the joint to the other, trying to avoid tightening adjacent bolts. Bolt tightening should also be in increments, several passes, to help minimise variations in joint contact pressure. The objective being to avoid any locked in bending stresses in the flanges. This article showed that with incremental tightening the bolt preloads could, assuming good friction control, be within 95% to 101% of the target preload. With single pass tightening, still maintaining good friction control, the preload could be as low as 83% of the target load and unlikely to exceed 100%. Interestingly, sequencing the bolt tightening from the centre of the bolt group, finishing at the outer bolts, resulted in the bolts with the lowest preload being located near the centre of the bolt group. This means that bolts with the lower preloads would be subjected to the lower shear loads arising from the external in-plane torsional shear loads, the ideal or preferable condition. The method of analysis described in the paper is not required for the majority of preloaded bolted joint analyses but would be useful if establishing the required bolt tightening sequence was considered important. Similarly, the method may be of use when investigating joint failures where bolt preload, or lack of preload, could have been a contributing factor.

3.3.1 P5 - Author Accepted Manuscript (Journal of Mechanical Engineering – Strojnicky časopis, Volume 71 (2021), Issue 2, pages 329 to 342.)

BOLTED JOINT PRELOAD DISTRIBUTION FROM TORQUE TIGHTENING

WELCH Michael

Michael A Welch (Consulting Engineers) Limited, West Lancashire, UK,

email: mike.welch@mail.co.uk

Abstract: The purpose of this paper is to develop an understanding of how bolt preloads are distributed within a joint as each bolt is tightened in turn by the use of a calibrated torque wrench. It discusses how the order that the joints nuts/bolts are tightened can affect the final bolt preload. It also investigates the effect on incrementally increasing the bolt preload through a series of applications of the controlled torque tightening sequence.

Classical analysis methods are used to develop a method of analysis that can be applied to most preloaded bolted joints. It is assumed that the static friction coefficient is approximately 15% less than the dynamic friction.

It is found that the bolt preload distribution across the joint can range from slightly above the target preload to significantly less than the target preload. The bolts with a preload greater than the target preload are found to be those tightened towards the end of the tightening sequence, usually located close to the outer edges of the joint's bolt array. The bolts with a preload less than the target preload are those tightened early in the tightening sequence, located centrally within the joints bolt array.

The methods presented can be used to optimise bolted joint design and assembly procedures. Optimising the design of preloaded bolted joints leads to more efficient use of the joints.

Keywords: bolted joint, preloaded bolt, bolt preload, bolt tension, multiple bolt, multi bolt

1 Introduction

Preloaded bolted joints are a common feature in mechanical engineering. Preloading the bolts produces a stiff joint with good resistance to fatigue. However, accurate and consistent bolt preloading is required to provide optimum joint performance. A common method of producing a preload in bolted joints during assembly is by the use of a calibrated torque wrench. The use of a torque wrench is also the most popular way of remaking joints during maintenance and repair. When bolt torque is used as an indicator to bolt preload the variations in friction between the nut/bolt head and washer and between the nut and bolt threads result in potential errors in the bolt preload. In addition to this, variations in bolt preload can arise from the elastic redistribution of load as each bolt is tightened in turn.

This article considers the elastic distribution of bolt loads and contact pressure within a joint as the individual bolts are preloaded using a calibrated torque wrench. The analysis shows how variations of bolt preload within a joint can occur. The paper also considers procedures to minimise variations in bolt preload and contact pressure at the faying surface under the preload condition and optimizing the joint's performance.

The method of analysis presented assumes that as each bolt is tightened in turn the bolt preload is introduced as a load on the joint. This preload remains on the bolt being tightened and also influences the preloads on other bolts within the joint by elastic redistribution. The detail method of analysis used in this paper is an adaption of the method presented in reference [1]. The method presented here considers the preload induced in each bolt as similar to an external load on the joint.

2 Nomenclature

A_b	Tensile area of each bolt
A_f	Area of faying surface
A_j	Total area of joint (Faying surface plus bolts)
F_{dp}	Design preload
F_p	Preload in each bolt
$F_{p_{(n,i)}}$	Preload in bolt 'n' at step 'i'
$F_{p.nom}$	Nominal bolt preload resulting from make up torque
F_{zp}	Bolt load induced by torque tightening
F'_{zp}	Change in bolt preload induced by torque tightening
$I_{xx.j}$	Second Moment of Area of joint about 'x' axis
$I'_{xx.j}$	Second Moment of Area transposed about x'-axis
$I_{xy.j}$	Product Moment of Area of joint
$I_{yy.j}$	Second Moment of Area of joint about 'y' axis
$I'_{yy.j}$	Second Moment of Area transposed about y'-axis
$K_{b_{(n,i)}}$	Bolt 'resistance'
$K_{j_{(n,i)}}$	Joint 'resistance'
M_x	External moment acting about 'x' axis
M'_x	Transposed moment
M_y	External moment acting about 'y' axis
M'_y	Transposed moment
P_p	Pressure at faying surface, preload pressure
$P_{p_{(n,i)}}$	Pressure at faying surface local to bolt 'n' at step 'i'
x	Coordinate in plane of joint face
$x_{(n)}$	Coordinate of bolt 'n'
$x'_{(n)}$	Transposed coordinate of bolt 'n'

y	Coordinate in plane of joint face
$y_{(n)}$	Coordinate of bolt 'n'
$y'_{(n)}$	Transposed coordinate of bolt 'n'
$\delta P_{f\,(n)}$	Change in contact pressure local to bolt 'n'
θ	Angle of principal axis

2.1 Suffices

i	Step in bolt tightening sequence. Incrementally increases when a bolt is tightened.
n	Bolt number. Identifies each bolt within the joint or bolt group.
s	Bolt number in the bolt tightening sequence.

3 Tightening Sequence

Bolt-tightening procedures are used to try to achieve optimum preload conditions of the joint. Procedures often prescribe a sequence, or order, in which the bolts are tightened. The bolt tightening sequence usually starts with the bolt nearest the centre of the joint. The tightening sequence for the bolts then spreads outwards, with the intention of avoiding any locked in bending stresses in the flanges. Circular flanges, with circular bolt arrays, typical of piping joints, are usually tightened in a cross-pattern sequence. The bolts are also tightened in increments to help minimise the variations in contact pressure across the joint throughout the tightening procedure. The objective is to produce an as near uniform distribution of bolt preload and spread of contact pressure across the joint as possible. Locked in bending stresses can be considered as analogues to bubbles trapped under a bonded laminate sheet. They can result in deformation of the flanges resulting in an uneven contact pressure and partial lack of contact at the faying surface.

The tightening procedure usually aims to tighten the bolts by incremental steps, the final increment being the target or nominal bolt preload required for the joint. The target preload would be based on a percentage of the bolt's proof load but the tightening procedure would specify a bolt/nut 'make up' torque, which has been calculated or experimentally shown to achieve the required preload.

A typical bolt tightening procedure can be described as follows:

1. Establish joint alignment and "nip up" the bolts to prevent reintroduction of misalignment.

2. Snug tighten the bolts, following the prescribed tightening sequence for the bolts, closing up the joint.

3. Torque tightens the bolts to 25% of final make up torque, following the tightening sequence for the bolts.

4. Torque tightens the bolts to 75% of final make up torque, following the tightening sequence for the bolts.

5. Torque tightens the bolts to 100% of make up torque, following the tightening sequence.

6. Repeat step 5 until no further nut/bolt rotation occurs during the tightening operation.

When tightening a bolt that already has some preload the breakaway torque, the torque at which the nut/bolt starts to turn, is influenced by both the current level of preload and the static friction between the nut or bolt and it’s washer and the static friction between the threads of the nut and bolt. When the nut/bolt starts to turn the friction influence changes to that of dynamic friction. Since dynamic friction is always less than static friction the torque required for maintaining movement of the nut/bolt is less than the breakaway torque. The significance of this is that, during step 6 of the tightening procedure, it is possible for a bolt to have a preload that is less than the target preload and yet the target preload cannot be achieved because the breakaway torque is greater than the makeup torque, which is based on dynamic friction.

3.1 Snug Tightening

It can be assumed that during the tightening procedure each of the bolts is snug tightened to the same load. This will leave the bolts with minimal preload. Under this condition the contact pressure at the faying surface would also be near zero. The initial bolt load after snug tightening can be described by the following condition:

$$F_{p_{(n,i)}} = snug\ load \tag{1}$$

The suffix (n, i) indicates the preload applies to bolt number n when the tightening sequence is at step i. At this point i represents the first step in the tightening sequence.

The snug load could be taken as zero or a small percentage of the final make up load, typically 1% or 2% say.

The faying surface contact pressure local to each bolt is given by:

$$P_{p_{(n,i)}} = \frac{-1}{A_f} \cdot \sum_n F_{p_{(n,i)}} - F_{p_{(n,i)}} \cdot \sum_n \left(\frac{x_{(n)}^2}{I_{yy.j}} - \frac{y_{(n)}^2}{I_{xx.j}} \right) \tag{2}$$

The negative signs in equation (2) indicate the contact pressure is a compressive stress at the faying surface. The second term represents the internal moment on the joint produced by the bolt preloads and follows the ‘right-hand rule’. Hence, a positive moment about the joints y-axis will produce an increase in magnitude of contact pressure local to bolts with positive x-axis coordinates. Similarly, a negative moment about the joints x-axis will also produce an increase in magnitude of contact pressure local to bolts with positive y-axis coordinates.

3.2 First Pass of Torque Tightening

During the first pass of the torque tightening sequence each bolt is tightened in turn to the prescribed percentage of the make up torque, typically 25% of the full make up torque for the first pass. The load induced can be defined as:

$$F_{zp} = 25\% \cdot F_{p.nom} \tag{3}$$

where $F_{p.nom}$ is the target, or required, final bot preload.

The force F_{zp} is positive when closing the joint. Hence, following the ‘right-hand rule’, a positive F_{zp} combined with a positive bolt coordinate $y_{(n)}$ will lead to a negative moment about the x-axis of the joint. Similarly, a positive F_{zp} combined with a positive bolt coordinate $x_{(n)}$ will lead to a positive moment about the y-axis of the joint. In effect, a positive F_{zp} is considered as representing what would normally be regarded as a negative axial load F_z on the joint.

The loads and moments applied to the joint during torque tightening the first bolt of the tightening sequence are based on the change in bolt load required to reach the required intermediate torque tightened load F_{zp} (in this case, 25% of the target torque).

The change in load, or additional load, applied to the first bolt in the tightening sequence by the intermediate torque tightening is given by the equation:

$$F'_{zp} = F_{zp} - F_{p_{(s,i)}} \tag{4}$$

The subscript (s, i) indicates the bolt being tightened and the step in the tightening sequence respectively. Hence, $F_{p_{(s,i)}}$ is the preload in bolt s at step i in the tightening sequence. The preload at the current step in the tightening sequence is the snug tightened load on the bolt.

Hence, the moments applied to the joint by torque tightening the first bolt are given by the equations presented below.

$$M_x = -F'_{zp} \cdot y_{(s)} \tag{5a}$$

$$M_y = F'_{zp} \cdot x_{(s)} \tag{5b}$$

The moments M_x and M_y are defined with respect to the joints coordinate system, usually the principal axes of the joint. If the joint is asymmetrical the moments M_x and M_y are resolved to act about the principal axes that are aligned at an angle to the joint coordinate system, as illustrated in Figure (1). The angle of principal axis from the joints x-axis (positive anticlockwise) is given by:

$$\theta = \frac{1}{2} \cdot arctan\left(\frac{2 \cdot I_{xy.j}}{I_{yy.j} - I_{xx.j}}\right) \tag{6}$$

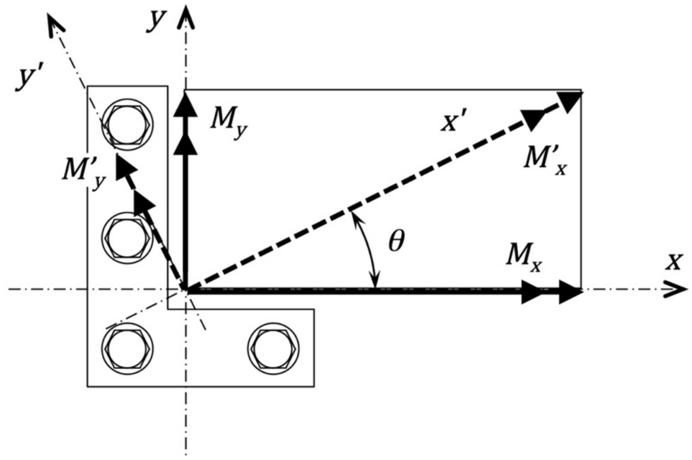

Figure 1. Moments defined in the joint coordinate system.

Hence, the resultant moments, the transposed coordinates and the transposed second moment of area of the joint are given by the following equations:

$$M'_x = M_x \cdot cos(\theta) + M_y \cdot sin(\theta) \tag{7}$$

$$M'_y = M_y \cdot cos(\theta) - M_x \cdot sin(\theta) \tag{8}$$

$$x'_{(n)} = x_{(n)} \cdot cos(\theta) + y_{(n)} \cdot sin(\theta) \tag{9}$$

$$y'_{(n)} = y_{(n)} \cdot cos(\theta) - x_{(n)} \cdot sin(\theta) \tag{10}$$

$$I'_{xx.j} = I_{xx.j} \cdot cos^2(\theta) + I_{yy.j} \cdot sin^2(\theta) - I_{xy.j} \cdot sin(2 \cdot \theta) \tag{11}$$

$$I'_{yy.j} = I_{xx.j} \cdot sin^2(\theta) + I_{yy.j} \cdot cos^2(\theta) + I_{xy.j} \cdot sin(2 \cdot \theta) \tag{12}$$

The bolt axial load component of F'_{zp} on the first bolt to be tightened (bolt s) will act to produce a compressive contact pressure at the faying surface local to the bolt. The torque tightening of bolt s will also influence the contact pressure local to the other bolts in the joint.

The change in faying surface contact pressure local to each of the bolts is given by:

$$\delta P_{f\,(n)} = \frac{-F'_{zp}}{A_j} + \frac{M'_x}{I'_{xx.j}} \cdot y'_{(n)} - \frac{M'_y}{I'_{yy.j}} \cdot x'_{(n)} \tag{13}$$

Equation (13) shows that a positive moment M'_x will act to reduce the contact pressure local to bolts with a positive y' coordinate. That is, the contact pressure will become less compressive. Therefore, the faying surface contact pressure local to bolt n after bolt s has been tightened is given by:

$$P_{p_{(n,i+1)}} = P_{p_{(n,i)}} - \frac{F'_{zp}}{A_j} + \frac{M'_x}{I'_{xx.j}} \cdot y'_{(n)} - \frac{M'_y}{I'_{yy.j}} \cdot x'_{(n)} \tag{14}$$

In equation (14) the term $P_{p_{(n,i)}}$ represents the contact pressure local to bolt n at step i, prior to tightening bolt s and the term $P_{p_{(n,i+1)}}$ represent the contact pressure after tightening bolt s. Hence, $P_{p_{(n,i+1)}}$ is the contact pressure at the end of step i and the start of step $i+1$.

A positive contact pressure cannot exist at the faying surface. A load that attempted to produce a positive contact pressure would result in an additional axial load on the bolt.

The corresponding change in load on each of the bolts is given by:

$$F_{p_{(n,i+1)}} = F_{p_{(n,i)}} - \frac{F'_{zp}}{A_j} \cdot A_b + \left(\frac{M'_x}{I'_{xx.j}} \cdot y'_{(n)} - \frac{M'_y}{I'_{yy.j}} \cdot x'_{(n)} \right) \cdot A_b \tag{15}$$

Equation (15) applies to all bolts other than bolt s, the bolt being tightened. Bolt s is loaded to the intermediate torque-tightening load, as defined by the condition presented in equation (16).

$$F_{p_{(s,i+1)}} = F_{zp} \tag{16}$$

Only positive bolt loads can exist. A loading situation that attempted to produce a negative bolt load would result in a compressive contact pressure on the faying surface.

3.3 Second and subsequent bolt tightening

The torque tightening of the second, and subsequent, bolts can be analysed by applying equations (3) to (16) with the appropriate values for subscripts (s, i) and (n, i).

The second bolt to be tightened in the tightening sequence could already have a preload $F_{p_{(s,i)}}$, induced from the snug tightening process and from tightening the first bolt in the tightening sequence. This preload is that which has already been calculated by equation (12). The suffix s now denotes the bolt number of the second bolt in the tightening sequence. In this instance, the tightening sequence, step i, has been incrementally increased by 1 from the previous, snug tightened, state and indicates the second bolt in the sequence is about to be tightened.

The effective load being applied to each bolt in the joint during the first pass of torque tightening continues to be F_{zp}. The moments applied to the joint by torque tightening the second bolt in the sequence are again based on the change in bolt load required to reach the required intermediate preload F_{zp}.

If, after the first bolt of the sequence has been tightened, the load at any other bolt is found to be negative then there is no tensile load on that bolt and the load is being reacted as a contact load at the faying surface local to the bolt.

The effects of torque tightening the second bolt in the tightening sequence can be analysed by applying equations (3) to (16). These equations can be resolved as simultaneous equations and combined/reduced into two equations, one for the contact pressure $P_{p_{(n,i)}}$ and one for the intermediate bolt preloads $F_{p_{(n,i)}}$.

When applying these equations the subscript (s, i) would relate to the bolt being tightened, in this instance the second bolt in the bolt tightening sequence, and the step in the tightening sequence respectively. Hence, $F_{p_{(s,i)}}$ is the preload in bolt s at step i in the tightening sequence. The preload at the incremented step i is the load calculated from equation (15) when considering the first, or previous, bolt in the tightening sequence.

Equations (5a) and (5b) can be substituted into equation (15) to give an equation for the bolt preload after tightening the bolt:

$$F_{p_{(n,i+1)}} = F_{p_{(n,i)}} - \frac{F'_{zp}}{A_j} \cdot A_b - F'_{zp} \cdot \left(\frac{y'_{(n)} \cdot y'_{(s)}}{I'_{xx.j}} + \frac{x'_{(n)} \cdot x'_{(s)}}{I'_{yy.j}} \right) \cdot A_b$$

Equation (4) can then be used to eliminate the terms of F'_{zp}

$$F_{p_{(n,i+1)}} = F_{p_{(n,i)}} - \left(F_{zp} - F_{p_{(s,i)}}\right) \cdot \left(\frac{1}{A_j} + \frac{y'_{(n)} \cdot y'_{(s)}}{I'_{xx.j}} + \frac{x'_{(n)} \cdot x'_{(s)}}{I'_{yy.j}}\right) \cdot A_b \qquad (17)$$

If a dimensionless 'stiffness' array is written for the bolts where:

$$K_{b_{(n,i)}} = \left(\frac{1}{A_j} + \frac{y'_{(n)} \cdot y'_{(s)}}{I'_{xx.j}} + \frac{x'_{(n)} \cdot x'_{(s)}}{I'_{yy.j}}\right) \cdot A_b \qquad (18)$$

Then equation (17) can be written as:

$$F_{p_{(n,i+1)}} = F_{p_{(n,i)}} - \left(F_{zp} - F_{p_{(s,i)}}\right) \cdot K_{b_{(n,s)}} \qquad (19)$$

As before, when considering equation (15), the bolt being tightened, bolt s, is loaded to the intermediate torque tightening load, as defined by the condition presented in equation (16). Hence;

$$F_{p_{(s,i+1)}} = F_{zp}$$

Applying this load condition for the bolt being tightened to equation (19) allows equation (19) to be written as:

$$F_{zp} = F_{p_{(n,i)}} - \left(F_{zp} - F_{p_{(s,i)}}\right) \cdot K_{b_{(n,s)}}$$

The resulting equation can then be rearranged to give:

$$K_{b_{(n,s)}} = \left(\frac{F_{p_{(n,i)}} - F_{zp}}{F_{zp} - F_{p_{(s,i)}}}\right)$$

This term can then finally be simplified to give:

$$K_{b_{(n,n)}} = -1 \qquad (20)$$

The equations for the contact pressure, $P_{p_{(n,i)}}$, can be treated in a similar manner to those for the bolt load, $F_{p_{(n,i)}}$. Equations (5a) and (5b) can be substituted into equation (14) and equation (4) used to eliminate terms of M_x, M_y and F'_{zp} in a similar manner as previous, which would lead to the equation:

$$P_{p_{(n,i+1)}} = P_{p_{(n,i)}} - \left(F_{zp} - F_{p_{(s,i)}}\right) \cdot \left(\frac{1}{A_j} + \frac{y'_{(n)} \cdot y'_{(s)}}{I'_{xx.j}} + \frac{x'_{(n)} \cdot x'_{(s)}}{I'_{yy.j}}\right) \tag{21}$$

Equation (21) can be written as:

$$P_{p_{(n,i+1)}} = P_{p_{(n,i)}} - \frac{\left(F_{zp} - F_{p_{(s,i)}}\right)}{A_j} \cdot K_{j_{(n,s)}} \tag{22}$$

Where $K_{j_{(n,s)}}$ is a dimensionless 'stiffness' array for the joint.

$$K_{j_{(n,i)}} = \left(1 + \left(\frac{y'_{(n)} \cdot y'_{(s)}}{I'_{xx.j}} + \frac{x'_{(n)} \cdot x'_{(s)}}{I'_{yy.j}}\right) \cdot A_j\right) \tag{23}$$

For analysis purposes, equations (18), (20) and (23) can be used to calculate stiffness's for the bolts and joint using the joint geometry. Equation (19) can then be used for each bolt in turn, following the bolt tightening sequence, to calculate the intermediate bolt preloads. Finally, equation (22) can be used to calculate the faying surface contact pressures local to each bolt, again following the bolt tightening sequence. This procedure needs to be followed for each pass of the torque tightening sequence. That is, it needs to be applied for each step in the torque tightening procedure.

4 Analysis Results

Figures 2 to 9 illustrate the bolt preload distribution on a range of typical bolted joints.

Figures 2 to 7 illustrate joints that have bolt patterns symmetrical about both primary axes of the joint. Figures 8 and 9 illustrate joints that are asymmetrical about one primary axis of the joint.

Each of the joints considered in the analyses are based on M16 grade 8.8 bolts with a target preload of 60% of the bolt proof load. The bolt numbering used in each of the figures follows the bolt tightening sequence considered in the analyses. The calculated final bolt preloads are given as percentages of the target preload following a 2%, 25%, 75%, 100% makeup torque tightening procedure. It was also assumed that the breakaway torque for a bolt with a preload of 85% or more of the target would be greater than the makeup torque.

4.1 Resultant Bolt Preloads from an Iterative Bolting Procedure

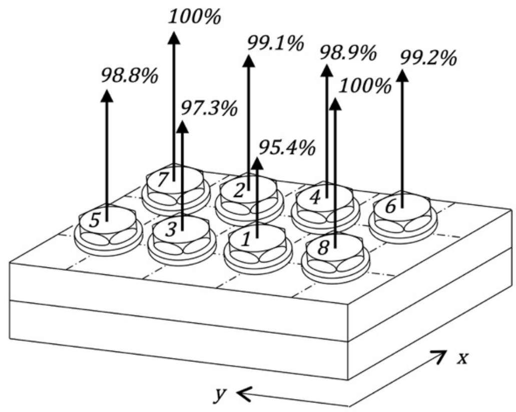

Figure 2. Compact symmetrical 8 bolt joint

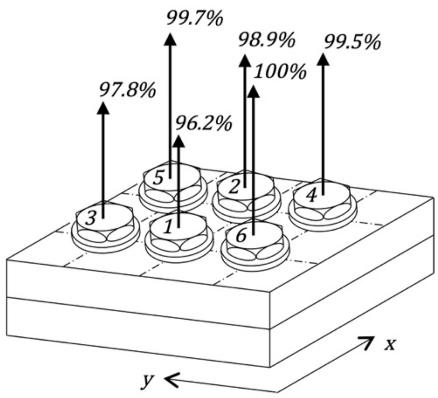

Figure 3. Compact symmetrical 6 bolt joint

Figures 2 and 3 illustrate joints with an edge distance of 24mm (1.5 times the bolt diameter) from the hole centre and the hole centres are on a pitch of 32mm (2 time the bolt diameter) in the directions of both axes.

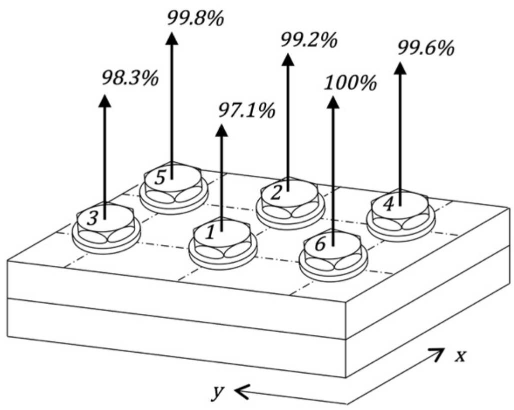

Figure 4. Symmetrical 6 bolt joint

Figure 4 illustrates a joint with an edge distance of 24mm (1.5 times the bolt diameter) from the hole centre and the hole centres are on a pitch of 32mm (2 times the bolt diameter) in the direction of the x-axis and 48mm (3 times the bolt diameter) in the direction of the y-axis.

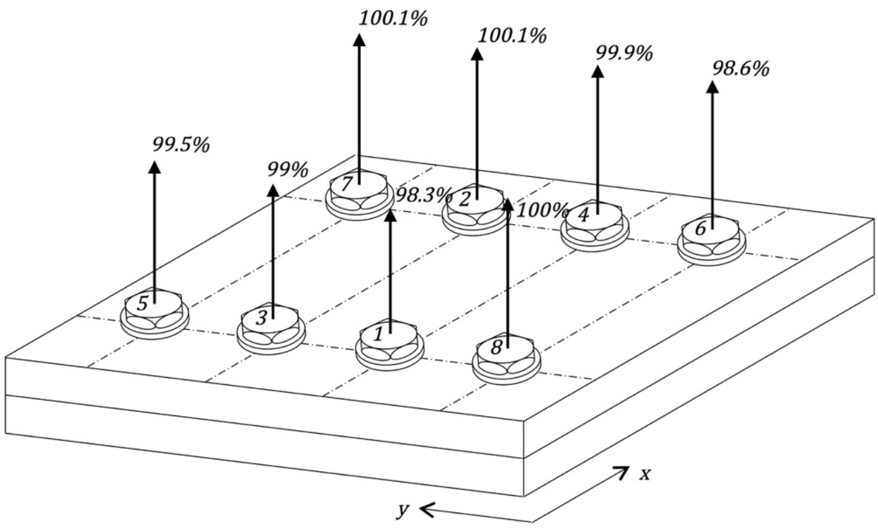

Figure 5. Symmetrical 8 bolt joint

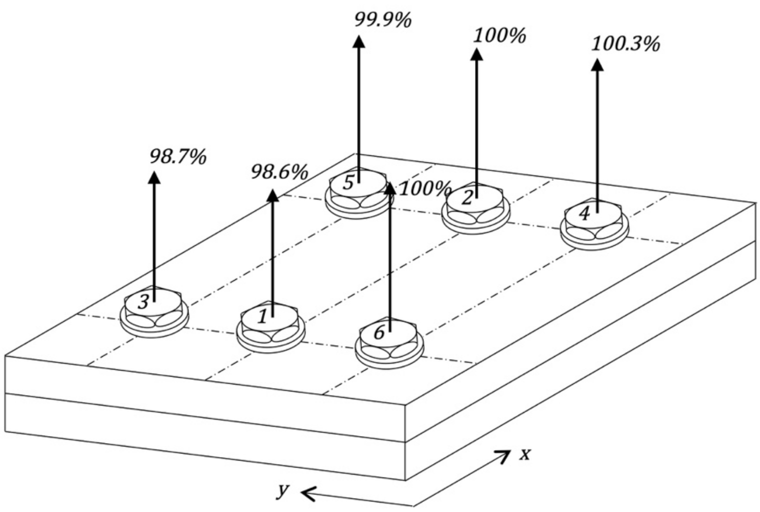

Figure 6. Symmetrical 6 bolt joint

Figures 5 and 6 illustrate joints with an edge distance of 35mm (approximately 2 times the bolt diameter) from the hole centre and the hole centres are on a pitch of 100mm (approximately 6 times the bolt diameter) in the direction of the x-axis and 50mm (approximately 3 times the bolt diameter) in the direction of the y-axis.

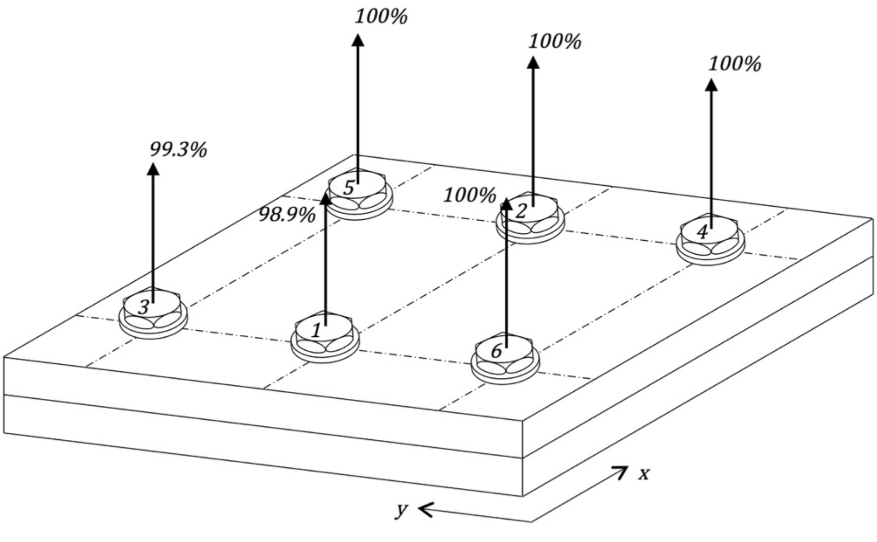

Figure 7. Symmetrical 6 bolt joint

Figure 7 illustrates a joint with an edge distance of 35mm (approximately 2 times the bolt diameter) from the hole centre and the hole centres are on a pitch of 100mm (approximately 6 times the bolt diameter) in the x-direction and 75mm (approximately 4 times the bolt diameter) in the y-direction.

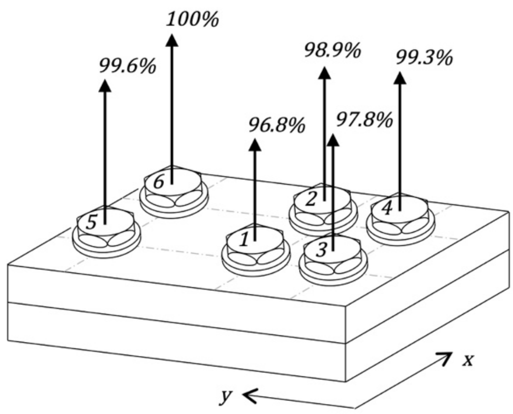

Figure 8. Compact asymmetrical 6 bolt joint

Figure 8 illustrates a joint with an edge distance of 24mm (1.5 times the bolt diameter) from the hole centre and the hole centres are on a pitch of 32mm (2 times the bolt diameter) in the direction of the x-axis and hole centres of 32mm and 64mm (3 and 6 times the bolt diameter respectively) in the direction of the y-axis.

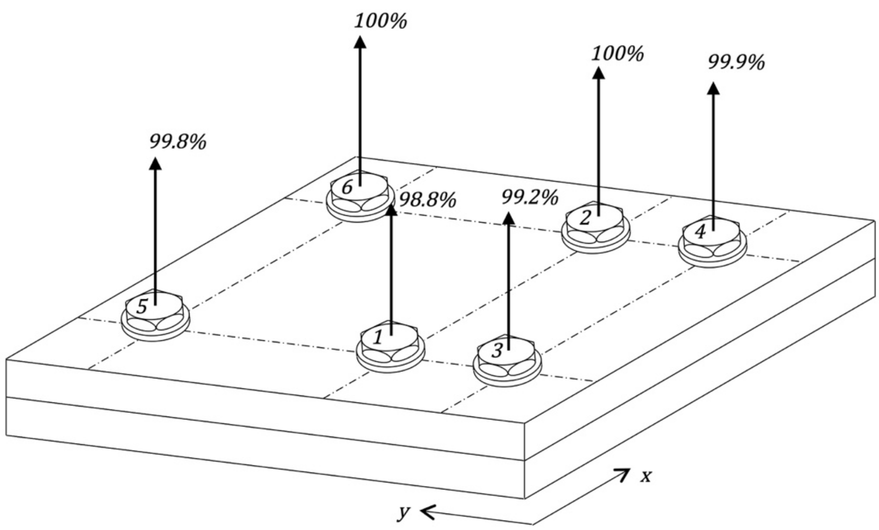

Figure 9. Asymmetrical 6 bolt joint

Figure 9 illustrates a joint with an edge distance of 35mm (approximately 2 times the bolt diameter) from the hole centre and the hole centres are on a pitch of 100mm (approximately 6 times the bolt diameter) in the direction of the x-axis and hole centres of 50mm and 100mm (approximately 3 and 6 times the bolt diameter respectively) in the direction of the y-axis.

4.2 Resultant Bolt Preloads from a Single Pass Tightening Sequence

Figures 10 to 12 illustrate the same joints as illustrated in figures 2 to 4 respectively. In these cases the calculated final bolt preloads are given as percentages of the target preload following a single pass tightening procedure of 100% of the makeup torque.

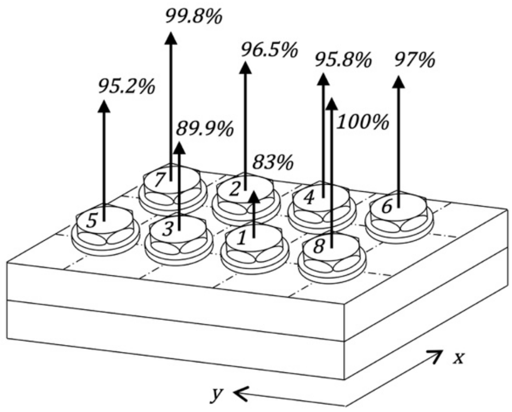

Figure 10. Compact symmetrical 8 bolt joint

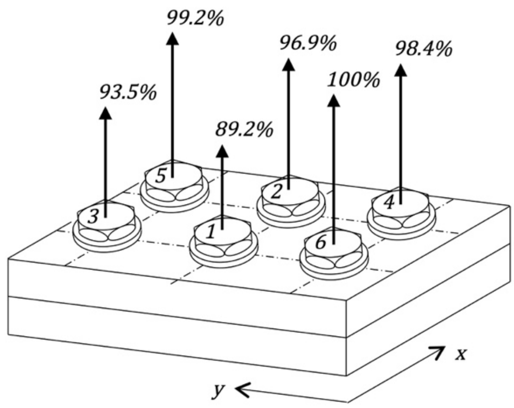

Figure 11. Symmetrical 6 bolt joint

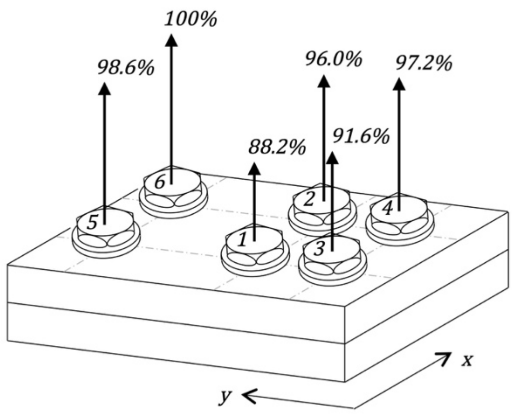

Figure 12. Compact asymmetrical 6 bolt joint

4.3 Resultant Faying Surface Pressure from a Single Pass Tightening Sequence

Figures 13 to 15 illustrate the faying surface contact pressures for the same joints as illustrated in figures 2 to 4 respectively. The contact pressures are calculated for a single pass tightening procedure of 100% of the makeup torque. The pressure results are given as percentages of the nominal pressure, calculated by using the target preload in equation (2).

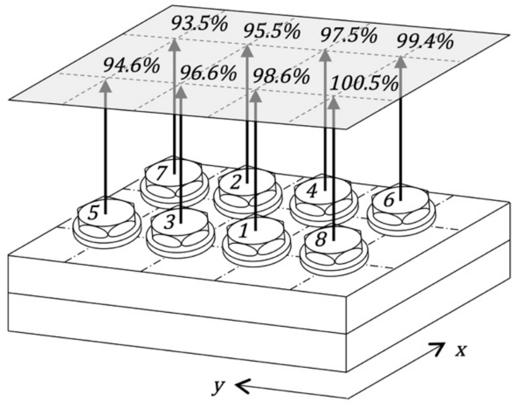

Figure 13. Compact symmetrical 8 bolt joint

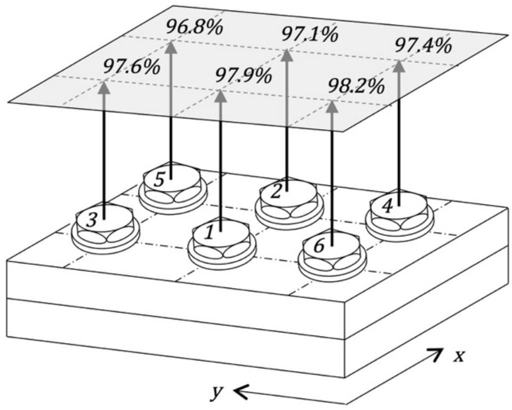

Figure 14. Symmetrical 6 bolt joint

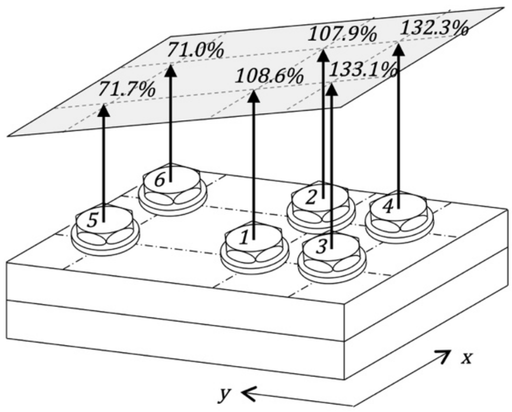

Figure 15. Compact asymmetrical 6 bolt joint

5 Discussion

Figures 2 to 9 show that, following the incremental torque tightening procedure as outlined, the preload in bolts located around the central area of the joint (i.e. those at the beginning of the tightening sequence) tended to have a preload slightly less than the target, or nominal, preload. Typically up to 5% less than the target preload. Whereas, some bolts at the outer edges of the joint area were slightly more than the target, typically 1%. Overall, the sum, or total, preload on the joint was slightly less than the total target load.

These variations in preload are as a result of elastic redistribution of loads during torque tightening. They do not include the effect of variations in friction at the sliding interfaces of the bolt, nut and washers.

The analyses presented in Figures 10 to 12 also showed that if incremental torque tightening was not used and the bolts were tightened to 100% of the makeup torque during a single pass tightening sequence, the preload in bolts located around the central area of the joint could have a preload up to 17% less than the target preload.

This characteristic of the distribution for the bolt preload acts to the benefit of the bolted joint. A study of bolt bending under the influence of shear loads [2] shows that the higher shear loads caused by in-plane loads, particularly torsional moments, will be acting at the outer edges of the joint and in the region occupied by the bolts with the slightly higher preload. This higher preload should give these bolts a marginal advantage in supporting the shear loads through friction at the faying surface.

Overall, the sum, or total, preload on the joint could be up to 5% less than the total target load.

The significant shortfall in achieving the target preload illustrated in Figures (10) and (12) shows why a design bolt preload, which is significantly less than the target preload, should be used when analysing joint designs. Section 3.8 of BS 7608:1990 "*Code of practice for Fatigue design and assessment of steel structures*" [3] recommends that the design preload should be taken as two thirds the target preload, i.e. $F_{dp} = \frac{2}{3} \cdot F_p$.

The design preload accounts for a number of factors that includes both elastic redistribution of loads during tightening and variation in friction at the bolt and nut. In addition the design preload also includes an allowance for bolt preload relaxation during service. An estimation of in-service bolt preload relaxation could be made using the methods presented in reference [2].

Figures (13) to (15) show that the contact pressure at the faying surface can be represented as an inclined plane. However, figures (10) to (12), which are for the same load cases, clearly show that the bolt preloads do not lie on a similar, or corresponding, plane. These differences reflect the effects of the elastic redistribution on the bolt preloads during torque tightening.

The method of used in this paper analysis assumes there is no out-of-plane deflection at the faying surface. This is, in effect, an assumption that there is symmetry of the joint at the faying surface. The variation in bolt preloads would result in a similar variation in through flange stresses local to each bolt and some variation in contact pressure that is not reflected in the analysis. The variation in through flange stresses would also result in some local bending in the flanges.

The contact pressure at the faying surface extends to the edge of the flange. Figure (15) shows that in joints with asymmetrical bolt patterns the maximum contact pressure local to a bolt could be up to 34% greater than the nominal pressure calculated by using only the target preload, and slightly larger at the edge of the flange. This maximum contact pressure occurs at an edge of the flange and would produce bending stresses in the flange. Reference [4] discusses flange bending in more detail and presents a method of calculating these bending stresses.

CONCLUSION

The analysis methods presented will not be required for the majority of bolted joints. However, they may be of benefit when analysing compact, highly loaded joints.

The design preload accounts for a number of factors that includes both elastic redistribution of loads due to elastic redistribution of loads during torque tightening and variation in friction at the bolt and nut. An understanding of the bolt preload variation due to the elastic redistribution of loads would allow the effects of sequential torque tightening to be removed from the factors considered when determining the design preload. This could lead to higher design preloads for used in the analyses. It could also lead to the specification of design preloads for each bolt in the joint. This would allow for a more efficient use of the joint.

Alternatively, an analysis showing that the likely bolt preloads would be below the target could allow a higher target preload, and hence higher makeup torque to be used. This would also lead to a safe and more efficient use of the joint.

The analysis methods may also be applicable to checking that a joint, originally assembled using multi-spindle nut tightening equipment, can be remade using a calibrated torque wrench, following a sequential torque tightening procedure, to produce a joint with suitable structural integrity following a repair.

REFERENCES

[1] Welch, M. *Classical Analysis of Preloaded Bolted Joint Load Distributions*. International Journal of Structural Integrity, Volume 9 (2018), Issue 4, pages 455 to 464
https://www.emeraldinsight.com/doi/abs/10.1108/IJSI-07-2017-0045

[2] Welch, M. *Analysis of Bolt Bending in Preloaded Joints*. Journal of Mechanical Engineering – Strojnicky časopis, Volume 68 (2018), Issue 3, pages 183 to 194.
https://doi.org/10.2478/scjme-2018-0034

[3] British Standards Institution. BS 7608:1990, *Code of practice for Fatigue design and assessment of steel structures*, British Standards Institution, London.

[4] Welch, M. *A Paradigm for the Analysis of Preloaded Bolted Joints*. Journal of Mechanical Engineering – Strojnicky časopis, Volume 69, (2019) Issue 1, pages 143 to 152.
https://doi.org/10.2478/scjme-2019-0012

3.3.2 Further Discussion

Again, there is an implicit assumption that the flanges of the joint are thick enough, stiff enough, to be able to consider the flanges as rigid. If the flanges of a joint are made of similar materials and are of the same thickness it is reasonable to assume that the joint will have a plane of geometrical symmetry laying on the plane of the flange faces. Similarly, if the joint flanges are of different thickness it is also reasonable to assume there is a plane of symmetry at the mid-position of the flange pack laying parallel to the plane of the flange faces. It is then reasonable to assume that out-of-plane loads on the joint will be antisymmetric, or mirror-imaged, across the plane of geometrical symmetry. Hence, it can be assumed that the plane of geometrical symmetry will cause each of the flanges to behave as if it were attached to an infinitely solid structure.

Provided the flanges have sufficient thickness to prevent failure due to flange bending under the contact pressure the assumption of rigid, or near rigid, flanges can be considered reasonable.

Another assumption within the paper "*Bolted Joint Preload Distribution From Torque Tightening*", Welch (2021), is that there is "good friction control". The purpose of using washers in preloaded bolted joints is to provide a consistent, hard, surface for the nut to react against. This results in more consistent and reliable friction coefficients across all joint types, irrespective of the joint flange material or surface finish. A secondary purpose of the washer is to protect the surface, and surface finish, of the component/flange in the region directly under the nut or bolt head. Although it could be argued that a damaged surface finish on the component flange would lead to increased, undefined, friction under the nut.

The method of analysis used in the paper would not be required for the majority of joints however, it can be applied to determine the tightening sequence for critical joints. Particularly where the joints has a liquid or gas containment requirement.

CHAPTER 4

DEVELOPMENTS IN SAFE-LIFE FATIGUE ANALYSIS

4.1 Developments in Safe-Life Fatigue Analysis

Fatigue analyses usually take one of two forms, they can be based on either ‘Safe-Life’ or ‘Damage Tolerance’. A safe-life fatigue analysis uses Wöhler plots, or S-N curves, to determine a component’s total life to failure as a number of cycles to failure based on the mean and alternating stresses to which the component is subjected. The total fatigue life represents three phases of fatigue, crack initiation, crack propagation and the final rupture. The damage tolerance procedure uses fracture mechanics to determine the number of load cycles that would cause an ‘existing’ small defect, acting as the nucleus, to first form a crack and then to propagate the crack to a size that is unstable and would cause the component to fracture.

The damage tolerance method of analysis is usually applied to critical situations where any cracks in the structure or component can be detected during routine planned maintenance and then monitored until the time the structure is restored, rectified or the component replaced.

A characteristic of preloaded bolted joints is that it is not feasible to carry out visual inspection of the bolts. Removing the bolts for inspection purposes and then reinstalling the bolt would introduce a large fatigue load cycle which would induce a significant amount of fatigue damage. The two papers being presented in this section represent a significant piece of work in the area of safe-life fatigue analysis.

The work carried out in producing first of the two papers being presented, “*An Empirical Approach to a Comprehensive Damage-Equivalent Stress for Fatigue*”, Welch (2022b), was originally intended to form just one section of the second of the two papers, “*Fatigue Analysis of Preloaded Bolted Joints*”, Welch (2022c). The original objective was to determine which of the existing methods of calculating a damage-equivalent stress was the more accurate and most applicable to preloaded bolts. However, this piece of work showed that none of the methods considered were entirely suitable hence, the scope of the work was revised.

4.2 An Empirical Approach to a Comprehensive Damage-Equivalent Stress for Fatigue

The paper, "*An Empirical Approach to a Comprehensive Damage-Equivalent Stress for Fatigue*", Welch (2022b), presents the development of a new damage-equivalent stress function. In the previous papers that have been presented in this thesis it has been emphasised that detailed analysis methods, not the simplified design method, should be used if conducting a fatigue analysis. Fatigue life is very sensitive to small variation in applied stress hence, it is critical to determine stresses as accurately as possible. Conservative design analysis methods lead to excessively conservative life predictions and gross 'over engineering'. Often S-N curves that represent suitable combinations of mean and alternating stresses are not available and it is necessary to 'correct' for mean stress by using a damage-equivalent Stress function. Frequently used methods of calculating a damage-equivalent stress are the modified Goodman Diagram, also known as the Haig Diagram, and other method proposed by Gerber, Soderberg and Smith-Watson-Topper, reference ESDU 0600 (2006). Each have their own limitations and are not necessarily accurate for high mean stresses combined with low alternating stresses, typical of preloaded bolts. It was found that the best of these methods was Smith-Watson-Topper. However, it was shown in the paper being presented that this can be up to 40% in error on stress. This error is based on comparison with the S-N Curve for fully reversed alternating stress, i.e. zero mean stress ($R = -1$), with the same number of cycles to failure.

The empirical, damage-equivalent stress function that is presented in this paper is particularly suited to high mean stress situations, where there is a high degree/increment of 'correction'. It is also suitable for a wide range of elastic stress concentrations, unnotched to an elastic stress concentration factor of Kt = 5.0, and for a wide range of tensile strengths, 800MPa to 1900MPa. These conditions are typical of preloaded bolts. This new method appears to be more consistent than the existing methods of calculating a damage-equivalent stresses and has an accuracy to within 16%, a significant improvement on existing methods.

4.2.1 P6 - Author Accepted Manuscript (FME Transactions. 2022;50(3):535-457.)

An Empirical Approach to a Comprehensive Damage-Equivalent Stress for Fatigue

Michael Welch

Michael A Welch (Consulting Engineers) Limited, West Lancashire, UK.

Abstract

This paper develops an empirical damage-equivalent stress function for fatigue. Classical methods of analysis are used to 'fit' an equation to a number of S-N curves for various grades of carbon steel. The resulting equivalent-damage stress function is applicable to steels subjected to a wide range of heat treatments, from normalised up to hardened and tempered to 1900MPa. It is also applicable to a wide range of stress concentrations, unnotched up to *Kt = 5.0* and typical of screw threads. A range of stress ratios and mean stresses are also considered. The function overcomes some of the limitations of existing methods of 'correcting' for mean stress. Existing method are limited in that, while they may give good results over a range of conditions there are some circumstances where the results are highly inaccurate. The damage-equivalent stress function is suitable for use in automated calculation procedures such as spreadsheets, MathCAD © and SMathStudio ©

Keywords: fatigue, damage-equivalent stress, bolt fatigue, mean stress correction

1 Introduction

Central to any fatigue analysis is the S-N curve, a plot of a characteristic stress (S) against the number of life cycles (N). Ideally a stress engineer would like a multitude of S-N curves applicable to a range of geometries and local configurations for each material. However, the experimental procedures to produce S-N curves are complex, requires specialist tensile test equipment capable of applying cyclic loading at controlled strain rates and are time consuming. Hence, in real life there is a limited amount of fatigue data for materials readily available.

Typically, available data will comprise of one S-N curve for an alternating stress with zero mean stress, produced using unnotched, polished, specimens. This may be supplemented by S-N curves for a small selection of stress concentration factors, obtained from notched specimens and/or S-N curves for an alternating stress with a given mean stress or stress ratio R = minimum stress/maximum stress. In some instances, curve fitting techniques are applied to the data for each S-N curve, or a group of S-N curves, enabling them to be expressed as an equation.

Fatigue is predominantly dominated by the alternating stress range but is also influenced by other factors such as the mean stress, surface finish, porosity and the geometry of the mechanical components that can result in an elastic stress concentration. It is known that a positive mean stress acts to reduce the number of life cycles a component can achieve whereas a negative mean stress acts to increase its life. However, it is not practical, or economical, to obtain S-N curves for a wide range of mean stresses or stress ratios. Hence, several methods of 'correcting' for mean stress by determining a 'damage-equivalent stress' for fatigue have been developed. The damage-equivalent stress is the alternating stress under fully reversal load conditions that would produce an amount of damage equivalent to that caused by the combination of both an alternating and a non-zero mean stress. In essence, the known or calculated alternating stress is factored prior to using it with the S-N curve produced using zero mean stress.

Several methods have been developed to determine a damage-equivalent stress, most notably the modified Goodman, or Goodman-Haig diagram and other methods proposed by Gerber, Soderberg and Smith-Watson-Topper. However, each of these methods have limitations in their application to fatigue analyses. The modified goodman diagram is conservative for ductile materials and optimistic for compressive mean stresses [1]. Gerber is better than Goodman for high mean stress levels but is not applicable to compressive mean stresses [1]. Soderberg is more conservative than the modified Goodman method [1]. Smith-Watson-Topper is better than Goodman for low mean stress levels [1].

The objective of the work being presented here is to define a method of determining the "damage-equivalent stress" for fatigue suitable for use in the fatigue analysis of preloaded bolted assemblies. A characteristic of preloaded bolts is that they have a high mean stress, typically 60% to 80% of proof stress, and a relatively small alternating stress range.

The log-linear nature of S-N curves means that the calculated fatigue life is very sensitive to stress. Hence, it is important to determine applied stresses with a high of accuracy. Some of the detail analysis techniques described in references [2 to 5] are particularly suited to this purpose. Similarly, the method of calculating the fatigue damage-equivalent stress also needs to introduce the minimum of error. The high mean stresses associated with preloaded bolts results in 'corrections' for mean stress having to be made over a large increment. The method of determining the damage-equivalent stress has to be able to deal with these large increments. This requirement virtually rules out the use of both the Goodman and Soderberg methods.

2 Materials

The S-N curves referenced by this analysis were obtained from '*Metallic Materials Properties Development and Standardization (MMPDS)*', reference [6]. The materials and the elastic stress concentration for the curves used in the analysis are presented in Table 1.

Table 1. Materials considered in the analyses.

Material	**Condition: Tensile Strength**	**Stress Concentration**	**Product form**
AISI 4130	Normalised (*Ftu* 117ksi) (807MPa)	Unnotched $K_t = 1.5$ $K_t = 2.0$ $K_t = 4.0$ $K_t = 5.0$	Sheet 0.075 inch (1.905mm) thick
	Ftu 180ksi (1241MPa)	Unnotched $K_t = 2.0$ $K_t = 4.0$	Sheet 0.075 inch (1.905mm) thick
AISI 4340	*Ftu* 200ksi (1379MPa)	Unnotched $K_t = 3.3$	Rolled bar 1.125 inch (28.575mm) diameter
300M	*Ftu* 280ksi (1931MPa)	Unnotched $K_t = 2.0$ $K_t = 3.0$ $K_t = 5.0$	Die forged
Note: 300M can be regarded as a modified AISI 4340			

The tensile strength and yield/proof stress of normalised AISI 4130 are assumed to be the tensile strength *TUS* and the yield/proof stress *TYS* quoted in MMPDS-03 Figure 2.3.1.2.8(a) for unnotched specimens. It should be noted that the tensile test used to produce these values would have been carried out at the strain rate used for the fatigue tests. Hence they could be slightly higher than those produced under a quasi-static tensile test, as would usually be performed to determine material properties.

Additional data, used to test the final damage-equivalent stress equation, is presented in Table 2. This data was not used in the analysis because there were insufficient number of S-N curves for each material condition to provide ‘points’ for equation fitting.

Table 2. Materials used as test cases for the procedure.

Material	Condition: Tensile Strength	Stress Concentration	Product form
AISI 4340	*Ftu* 125ksi (862MPa)	Unnotched $K_t = 3.3$	Rolled bar 1.125 inch (28.575mm) diameter
	Ftu 150ksi (1034MPa)	Unnotched $K_t = 3.3$	Rolled bar 1.12 inch (28.448mm) diameter

3 Methodology

It was assumed that an equation for the damage-equivalent stress for fatigue would take the form:

$$\sigma_{equ} = \sigma_{alt} \cdot f_{n1} \quad (1)$$

where f_{n1} is a function of the material properties, particularly the tensile strength *Ftu* and/or the yield or proof stress *Fty*, the stress ratio *R*, mean stress s_{mean} and the stress concentration K_t.

Equation (1) would be used to calculate the damage-equivalent stress for fatigue applicable to a curve with a specific elastic stress concentration factor. It would not be appropriate to use equation (1) to calculate the damage equivalent stress for a curve with a different elastic stress concentration factor. Hence, the part of the function involving K_t would be a scaling factor, constant for the curve being used.

The part of the function involving the tensile strength, or proof strength, of the bolt material, *Ftu* and *Fty* respectively, would ideally need to be a dimensionless function of stress. The modified Goodman or Haig equation and the Gerber equation use a dimensionless ratio:

$$\frac{\sigma_{mean}}{Ftu}$$

The stress ratio *R* is the ratio of minimum and maximum cyclic stresses:

$$R = \frac{\sigma_{min}}{\sigma_{max}}$$

Hence, by definition, the part of the function involving the stress ratio *R* is also a function of stresses due to loading.

The part of the function involving the mean stress s_{mean} has to result in $s_{equ} = s_{alt}$ when $s_{mean} = 0$ hence $f_{n1} = 1$ when $s_{mean} = 0$. Therefore, two possible shapes for the function f_{n1} were considered:

$$f_{n1} = 1 + f_{n2} \tag{2a}$$

And

$$f_{n1} = \frac{1}{1 - f_{n2}} \tag{2b}$$

The function f_{n2} in equation (2a) is not necessarily of the same farm as the function f_{n2} in equation (2b) and would not have the same numerical value.

Equation (2b) takes a similar form to those for the modified Goodman/Haig or the Gerber equations for damage-equivalent stress for fatigue.

Both equation (2a) and equation (2b) were considered during the analysis. It was found that equation (2a) provided the more accurate prediction of damage-equivalent stress for fatigue. Hence, only the work involving equation (2a) is presented in this paper.

4 Effect of Stress Ratio on the Damage-equivalent stress for fatigue Equation

The first step in studying the effect of the stress ratio was to identify groups of S-N curves for each of the material specifications being considered in the analysis. An equation relating stress ratio R to the damage-equivalent stress for fatigue s_{equ} was assumed and each group of S-N curves were then used to find constants used in defining the assumed equation.

4.1 S-N Curves for AISI 4340 Carbon Steel

The first group of S-N curves were for AISI 4340 carbon steel, heat treated to give a tensile strength of 1379MPa (200ksi). Three different S-N curves were each defined as a set of data points. The criteria for selecting the S-N curves was that they were for the same material, had the same stress concentration of $K_t = 3.3$ and shared a common range of mean stresses s_{mean}.-The variables between each of the curves were the stress ratios R. The stress ratios of the chosen curves were $R = 0.43$, $R = 0.60$ and $R = 0.74$, reference Figure 2.3.1.3.8(l) of MMPDS-03 [6]. Figure 1 shows plots of the alternating stress against life for each of the data sets and the data points used in the analysis.

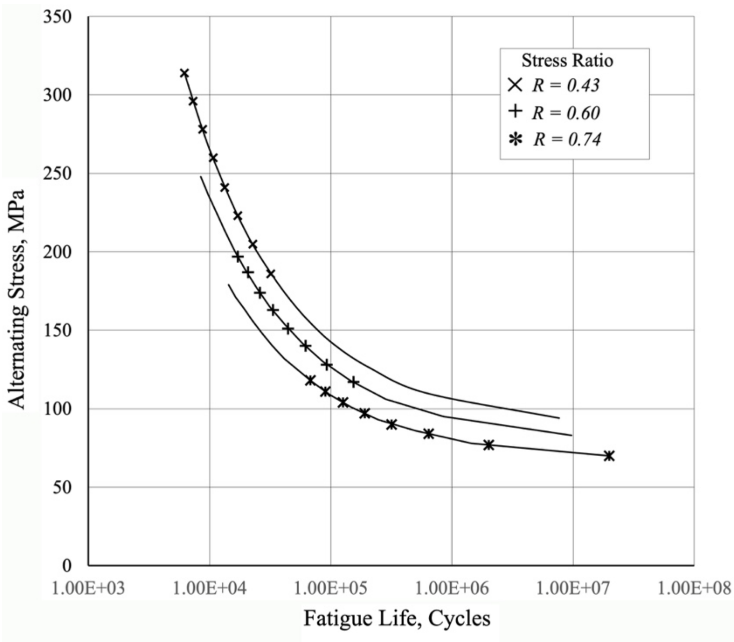

Figure 1 AISI 4340 $Ftu = 1397MPa$, $K_t = 3.3$

The first step in the analysis was to determine numerical values for function f_{n2}. Hence, from equations (1) and (2a) ;

$$\sigma_{equ} = \sigma_{alt} \cdot (1 + f_{n2}) \tag{3}$$

Rearranging;

$$f_{n2} = \frac{\sigma_{equ}}{\sigma_{alt}} - 1 \tag{4}$$

Equation (4) was then used to calculate values of f_{n2} for each of the three sets of data considered. Data sets 1, 2 and 3 related to stress ratios of $R = 0.43$, $R = 0.60$ and $R = 0.74$ respectively. The values of function f_{n2} for data set 1 were calculated to be within the range of 0.551 to 0.555, representing a variation of 0.4% from the mean value. Similarly, the values function f_{n2} for data set 2 were calculated to be within the range of 0.757 to 0.765, representing a variation of 0.5% from the mean value. Finally, the values function f_{n2} for data set 3 were calculated to be within the range of 1.067 to 1.105, representing a variation of 1.2% from the mean value.

It was concluded that the mean stress s_{mean} had negligible effect on the value of the function f_{n2}. Hence, since data sets 1, 2 and 3 were for the same material and stress concentration K_t it was also concluded that the numerical values for f_{n2} were a function of the material tensile strength or yield/proof stress, the stress ratios R and the stress concentration K_t.

Assuming the form of an equation to describe the function f_{n2} in term of the stress ratio R that also meets the criteria $f_{n1} = 1$ when $s_{mean} = 0$;

$$f_{n2} = f_{n3} \cdot (1 + R)^{a_1} \tag{5}$$

The terms for f_{n3} and a_1 will be functions of the material properties and stress concentration K_t. Rearranging equation (5);

$$f_{n3} = \frac{f_{n2}}{(1+R)^{a_1}} \tag{6}$$

Since data sets 1, 2 and 3 were all for the same material, having the same tensile strength, and for the same stress concentration K_t and shared a common range of mean stresses it was possible to assume that the numerical value of function f_{n3} would be the same for each of the data sets being considered. That is;

f_{n3} for data set 1 = f_{n3} for data set 2 = f_{n3} for data set 3

Using this assumption it was possible to adopt an iterative approach to calculate an optimum value for the constant a_1 that gave the minimum amount of variation in the values of the function f_{n3} for any of the data points of data sets 1, 2 and 3.

This iterative solution showed that a value of $a_1 = 3.349$ gave the optimum condition. The values of function f_{n3} were calculated to be within the range of 0.157 to 0.167 hence, the overall variation for the values of function f_{n3} was 3.3%. Individually, the values of function f_{n3} were within the range of 0.166 to 0.167 for data set 1, 0.157 to 0.158 for data set 2 and 0.163 to 0.167 for data set 3. The individual variations in the values of the functions f_{n3} were the same as those for the values of f_{n2}, namely 0.2%, 0.3% and 2.8% for data sets 1, 2 and 3 respectively.

The overall variation in the values of f_{n2} across data sets 1, 2 and 3 was 33.5%, which is significantly larger than the variation in the values of f_{n3}. Hence, the variation in f_{n3} could be taken to imply the methodology had an accuracy of around 3.3%

4.2 S-N Curves for 300M Carbon Steel

The second group of S-N curves were for 300M carbon steel, heat treated to give a tensile strength of 1931MPa (280ksi). Two different S-N curves were defined as sets of data points. The same criteria for selecting the first group of S-N curves were used, although in this instance the S-N curves were for unnotched ($K_t = 1.0$) 300M. Again, each set of data shared a common range of mean stresses s_{mean}. The variables between each of the curves were the stress ratios R. In this case, the stress ratios of the chosen curves were R = 0.1 and R = 0.2, reference Figure 2.3.1.4.8(a) of MMPDS-03 [6]. Figure 2 shows plots of the alternating stress against life for each of the data sets and the data points used in the analysis.

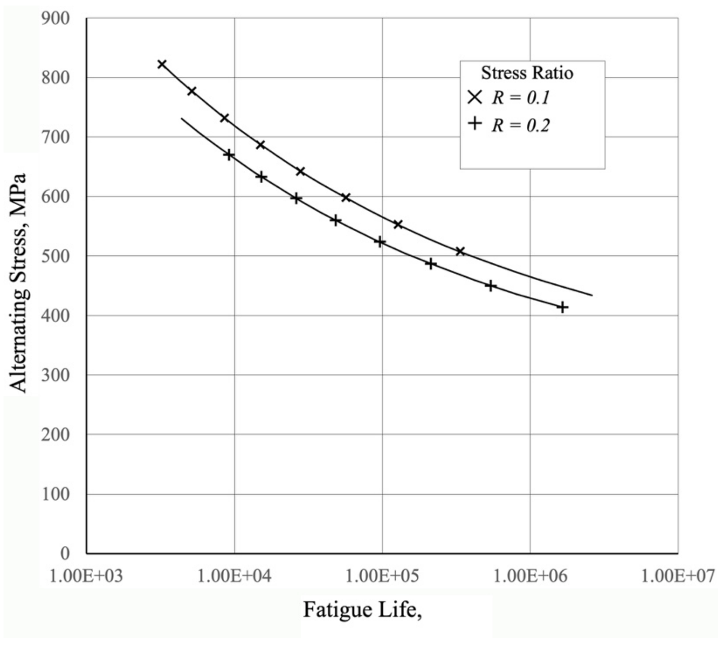

Figure 2. 300M $Ftu = 1931MPa$, unnotched ($K_t = 1.0$)

Equation (4) was again used to calculate values of f_{n2} for each of the data sets. Data sets 4 and 5 related to stress ratios of R = 0.1 and R = 0.2 respectively. The values of function f_{n2} for data set 4 were calculated to be within the range 0.587 to 0.588 for each of the data points considered, representing a variation of 0.1% from the mean value. Similarly, the values of function f_{n2} for data set 5 were calculated to be within the range of 0.720 to 0.725, representing a variation of 0.3% from the mean value.

This supported the previously made conclusion that the mean stress s_{mean} had negligible effect on the value of the function f_{n2}. Again, since data sets 4 and 5 were for a common material and stress concentration K_t the previous conclusion that function f_{n2} was a function of the stress ratios R and material properties was supported.

Using equation (6) in an iterative solution, similar to that used previously, it was shown that a value of $a_1 = 2.365$ gave the optimum condition for minimum variation in the values function f_{n3}. The values of function f_{n3} for data sets 4 and 5 were calculated to be within the range of 0.468 to 0.470 hence, the variations in the values of function f_{n3} were found to be 0.2% for both data sets.

4.3 S-N Curves for Normalised AISI 4130 Carbon Steel

As previous, the selected S-N curves were for a common material, in this instance normalised AISI 4130 carbon steel, which was assumed to have a tensile strength of 807MPa (117ksi). In total, four different S-N curves were each defined as a series of data points. However, due to the available data, different criteria for selecting the S-N curves had to be used. These four sets of data were sub-divided into groups of two sets of data. The S-N curves that formed the first of these two groups were for a stress concentration of K_t = 4.0. The S-N curves that formed the second of the two groups were for a stress concentration of K_t = 5.0. The two S-N curves within each group were each for a different mean stress. One curve was for a mean stress of s_{mean} = 138MPa (20ksi) and the other for a mean stress of s_{mean} = 207MPa (30ksi), reference Figures 2.3.1.2.8(d) and 2.3.1.2.8(e) of MMPDS-03 [6]. Hence, each data set represented a range of stress ratios R.

The focus of the analysis being presented was to develop a damage-equivalent stress equation which could be applied to high positive stress ratios, such as those typical of preloaded bolted joints. Hence, the data points used for the analysis were restricted to only positive stress ratios. The positive stress ratios occurred at the low alternating stress / low maximum stress / high life cycles end of the S-N curves.

Figures 3 and 4 show plots of the alternating stress against life for each of the data sets and the data points used in the analysis.

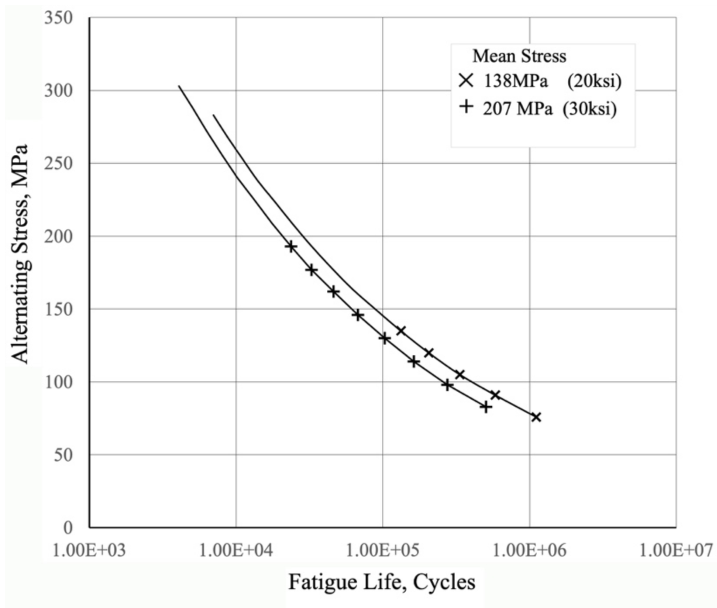

Figure 3. Normalised AISI 4130 (*Ftu = 807MPa*), $K_t = 4.0$

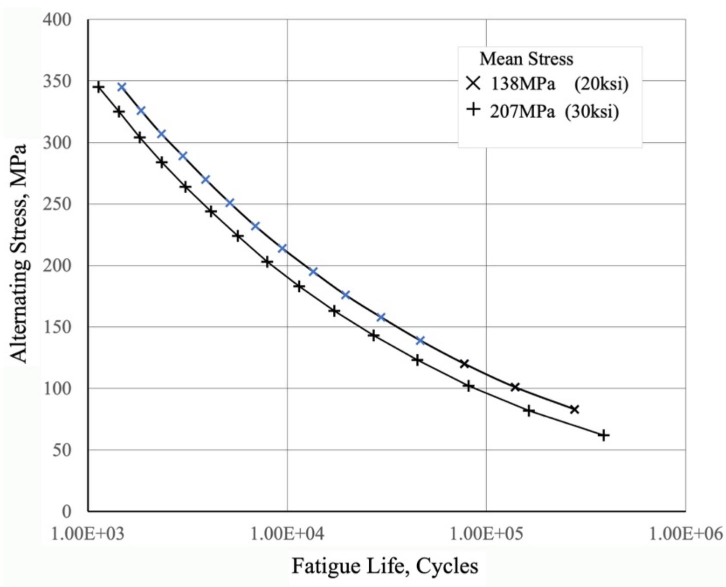

Figure 4. Normalised AISI 4130 (*Ftu = 807MPa*), $K_t = 5.0$

Equation (4) was again used to calculate values of f_{n2} for each of the four data sets. Data sets 6 and 7 were related to a stress concentration K_t = 4.0 and mean stresses of s_{mean} = 138MPa (20ksi) and s_{mean} = 207MPa (30ksi) respectively. Similarly, data sets 8 and 9 were related to a stress concentration K_t = 5.0 and mean stresses of s_{mean} = 138MPa and s_{mean} = 207MPa respectively. Since all four data sets were for constant mean stresses, and therefore over a range of stress ratios R, the resulting values for f_{n2} also covered a corresponding range. Hence, an accuracy for the calculated values of f_{n2} could not be inferred from the results.

An iterative solution for equation (6), similar to that used previously, was applied to data sets 6 and 7. This iterative solution showed that for a stress concentration of Kt = 4.0 a value of a_1 = 1.988 gave the optimum condition for minimum variation in the values function f_{n3}. Similarly, applying the iterative solution of equation (6) to data sets 8 and 9 showed that for a stress concentration of Kt = 5.0 a value of a_1 = 2.179 gave the optimum condition.

The values of function f_{n3} for data sets 6 and 7 were calculated to be within the range of 0.282 to 0.292. Similarly, the values function f_{n3} for data sets 8 and 9 were calculated to be within the range of 0.332 to 0.356. The variations in the calculated values of the functions f_{n3} were 1.8% for data sets 6 and 7, and 3.5% for data sets 8 and 9.

4.4 S-N Curves for AISI 4130 Carbon Steel

Two individual S-N curves for AISI 4130 carbon steel, heat treated to give a tensile strength of 1241MPa (180ksi) were considered. Each of the S-N curves were defined as a series of data points. The same criteria used for selecting the previous four sets of data, data sets 6, 7, 8 and 9, were used. The first of these two S-N curve was for a stress concentration of K_t = 2.0. The second S-N curve was for a stress concentration of K_t = 4.0. Both S-N curves were for a mean stress of s_{mean} = 345MPa (50ksi), reference Figures 2.3.1.2.8(g) and 2.3.1.2.8(h) of MMPDS-03 [6]. Hence, each data set represented a range of stress ratios R. Again, the data points used for the analysis were restricted to only positive stress ratios. Figures 5 show plots of the alternating stress against life for each of the data sets and the data points used in the analysis.

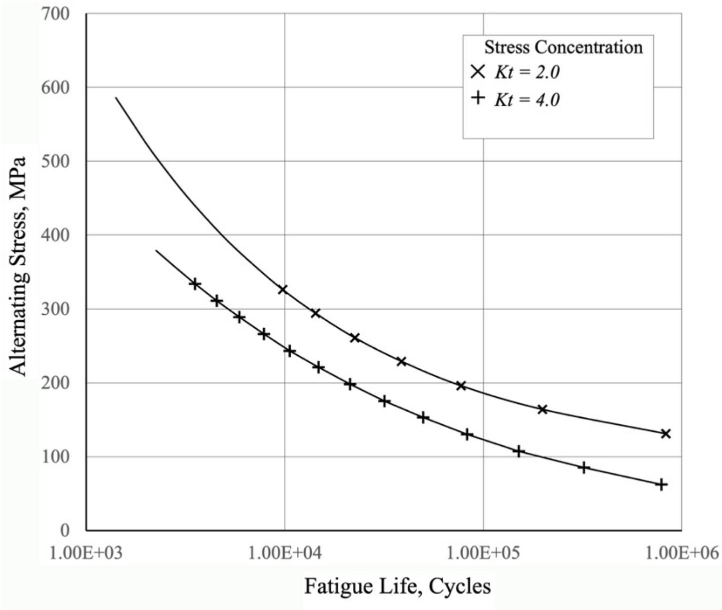

Figure 5. AISI 4130 *Ftu = 1241MPa*, s_{mean} = 345MPa

Equation (4) was used to calculate values of f_{n2} for both data sets. Data sets 10 and 11 were related to stress concentrations K_t = 2.0 and K_t = 4.0 respectively. Both data sets were for a mean stress of s_{mean} = 345MPa (50ksi). Since both sets were for constant mean stresses, and therefor over a range of stress ratios *R*, the resulting values for f_{n2} also covered a corresponding range. Hence, an accuracy for the calculated values of f_{n2} could not be inferred from the results.

Again, the iterative solution for equation (6) was applied to data sets 10 and 11. Applying the iterative solution to data set 10 showed that for a stress concentration of $K_t = 2.0$ a value of a_1 = 2.178 gave the optimum condition for minimum variation in the values function f_{n3}. Similarly, applying the iterative solution to data set 11 showed that for a stress concentration of $K_t = 4.0$ a value of a_1 = 2.417 gave the optimum condition.

This supported the conclusion that the material constant a_1 was a function of the material properties and stress concentration K_t.

The values of function f_{n3} for data set 10 were calculated to be within the range of 0.431 to 0.449. Similarly, the values function f_{n3} for data set 11 was calculated to be within the range of 0.276 to 0.316. The variations in the calculated values of the functions f_{n3} were 2.1% for data set 10, and 6.9% for data set 11.

5 Effect of Stress Concentration and Material Properties on Material Constant a_1

Values of the constant a_1 have been calculated for each material being considered. It has been observed that the value a_1 is not only dependent on the material properties but is also influenced by the stress concentration K_t of the specimens.

It was assumed that that a_1 could be best describe by a straight-line equation of the form:

$$a_1 = b_1 + b_2 \cdot \varepsilon_w \tag{7}$$

where b_1 and b_2 are constants and ε_w is a function of the material properties and the stress concentration K_t.

After trialling several plots of a_1 against various functions of the stress concentration K_t, tensile strength *Ftu* and the proof strength *Fty* it was considered the best fit for the available data would be given by:

$$\varepsilon_w = K_t \cdot \left(\frac{Fty}{E}\right)^{b_3} \tag{8}$$

The constants b_1, b_2 and b_3 were calculated using an iterative procedure. A range of initial values for b_3 were assumed, values for ε_w were calculated using equation (8) and then a linear regression was performed to determine values for b_1 and b_2 that gave the best/minimum RMS error fit for the line for each assumed value of b_3. This iterative procedure was used to optimise for the value of b_3 that gave the minimum amount of error in the fit of calculated values for a_1.

The optimum values for the constants were found to be:

$$b_1 = 1.854$$
$$b_2 = 4.224 \times 10^6$$
$$b_3 = 3.260$$

The maximum and minimum errors in the calculated value for a_1 were 17.1% and -17.1% respectively, with a RMS error of 10.8%.

The proof strain for the material is given by the term *Fty/E* hence the function for ε_w defined by equation (8) can be regarded as being related to the effect of strain, or work, hardening at the root of the notch or thread root. Work by McMillan and Jones (2020) shows that plastic deformation at the notch remains highly localised, reference [7]. Hence, it is possible to conclude that the strain at the notch, or at the thread root of a bolt, is controlled by the nett section of the notched component or the core of the thread.

6 Effect of Stress Concentration on the Damage-Equivalent Stress Equation

The approach to studying the effect of the stress concentration was again to identify groups of S-N curves for each of the materials being considered. In these cases however, the groups of S-N curves were selected to have stress concentration as the variable.

6.1 Additional S-N Curves for 300M Carbon Steel

A group of S-N curves for 300M carbon steel, heat treated to give a tensile strength of 1931MPa (280ksi) was selected. Three different S-N curves were defined as a set of data points. The criteria for selecting the S-N curves were that they were for the same material, had the same stress ratio of $R = 0.33$ and shared a common range of mean stresses σ_{mean}. The variables between each of the curves were the stress concentration K_t. The stress concentrations of the chosen curves were $K_t = 2.0$, $K_t = 3.0$ and $K_t = 5.0$, reference Figures 2.3.1.4.8(b), 2.3.1.4.8(c) and 2.3.1.4.8(d) of MMPDS-03 [6]. Figure 6 shows plots of the alternating stress against life for each of the data sets.

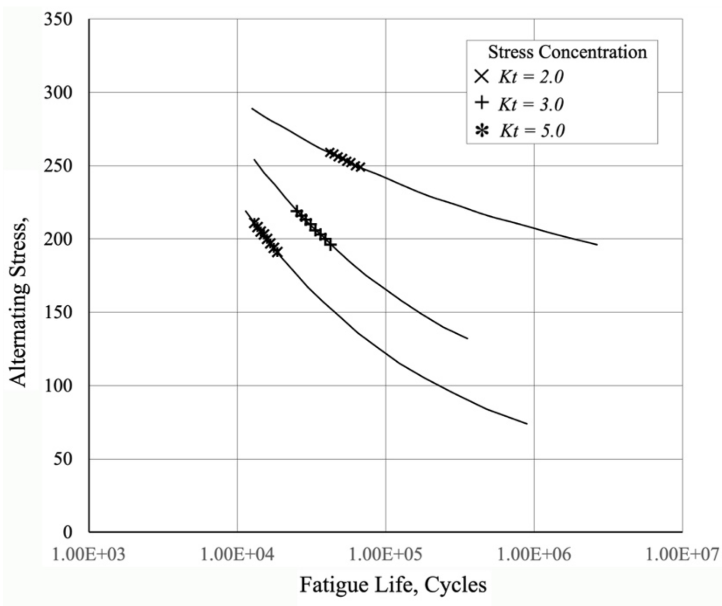

Figure 6. 300M *Ftu = 1931MPa* (280ksi), *R = 0.33*

Equation (4) was again used to calculate values of f_{n2} for each of the data sets. Data sets 12, 13 and 14 related to stress concentrations of $K_t = 2.0$, $K_t = 3.0$ and $K_t = 5.0$ respectively. The values of function f_{n2} for data set 12 were calculated to be within the range 1.013 to 1.014 for each of the data points considered, representing a variation of 0.05% from the mean value. Similarly, the values function f_{n2} for data set 13 were calculated to be within the range of 0.710 to 0.722, representing a variation of 0.8% from the mean value. Finally, the values function f_{n2} for data set 14 were calculated to be within the range of 0.690 to 0.692, representing a variation of 0.1% from the mean value. This was in line with the earlier conclusion that the mean stress s_{mean} had negligible effect on the value of the function f_{n2}.

Appling equations (7) and (8) using $K_t = 2.0$, assuming $Fty = 0.83 \ x \ Ftu$ (hence $Fty = 1602MPa$) and $E = 200MPa \ x \ 10^3$ the material constant was calculated as $a_1 = 3.094$. However, this value of the material constant a_1 is based on an estimated value for the proof stress Fty based on the mean ratio of *TYS/TUS* given in MMPDS-03 [6] and a typical value for Young's modulus of elasticity E.

An alternative, and possibly more accurate, way of estimating the material constant a_1 would be to use a value for the strain hardening factor ε_w based on the value of the more accurately known value of the material constant for unnotched 300M obtained using data sets 4 and 5. Hence, rearranging equation (7) to calculate the strain hardening factor for unnotched specimens, stress concentration $K_t = 1.0$:

$$\varepsilon_w = \frac{a_1 - b_1}{b_2} \tag{9}$$

By reference to equation (8), an estimate of the strain hardening factor can be made by ratio of stress concentration factors:

$$\varepsilon'_w = \varepsilon_w \cdot \frac{K_t}{K_{t.datum}} \tag{10}$$

where, in this instance, $K_{t.datum} = 1.0$ is the datum stress concentration applicable to data sets 4 and 5.

Using equations (9) and (10) with the material constant of $a_1 = 2.365$ found from data sets 4 and 5 and the stress concentration of $K_t = 2.0$ for data set 12, the effective strain hardening factor was calculated as $\varepsilon'_w = 2.420 \ x \ 10^{-7}$. Using this value for the effective strain hardening constant in equation (7) gave a value for the material constant of $a_1 = 2.867$ for data set 12.

Similarly, using equations (9) and (10) with a stress concentration of $K_t = 3.0$ the effective strain hardening factor was calculated as $\varepsilon'_w = 3.630 \times 10^{-7}$. Again, using this value for the effective strain hardening constant in equation (7) gave a value for the material constant of $a_1 = 3.387$ for data set 13.

Finally, using equations (9) and (10) with a stress concentration of $K_t = 5.0$ the effective strain hardening factor was calculated as $\varepsilon'_w = 6.049 \times 10^{-7}$. And, using this value for the effective strain hardening constant in equation (7) gave a value for the material constant of $a_1 = 4.409$ for data set 14.

Using equation (6) with the values for the material constant and the appropriate range of values for f_{n2} presented earlier in this section the value of function f_{n3} were calculated. The value of function f_{n3} for data set 12 were calculated to be within the range of 0.446 to 0.447. Similarly, the values function f_{n3} for data set 13 were calculated to be within the range of 0.270 to 0.275. Finally, the value function f_{n3} for data set 14 was calculated to be within the range of 0.196 to 0.197. The variations in the calculated values of the functions f_{n3} were the same as those for the calculated values of f_{n2}.

6.2 Additional S-N Curve for AISI 4340 Carbon Steel

A total of three S-N curves for AISI 4340 carbon steel, heat treated to give a tensile strength of 1379MPa (200ksi) were considered. Again, each S-N curve was defined as a set of data points.

The first of the S-N curves was for unnotched material, i.e. a stress concentration of $K_t = 1.0$, with a constant stress ratio of $R = 0.43$ and hence had a variable range of mean stresses σ_{mean}, reference Figure 2.3.1.3.8(k) of MMPDS-03 [6]. The other two S-N curves had a common stress ratio of $R = 0.0$ and also had a common range of mean stresses. One was for unnotched material, stress concentration $K_t = 1.0$, and the other was for a stress concentration of $K_t = 3.3$, reference Figures 2.3.1.3.8(k) and 2.3.1.3.8(l) of MMPDS-03 [6]. Figures 7 and 8 show plots of the alternating stress against life for each of the data sets.

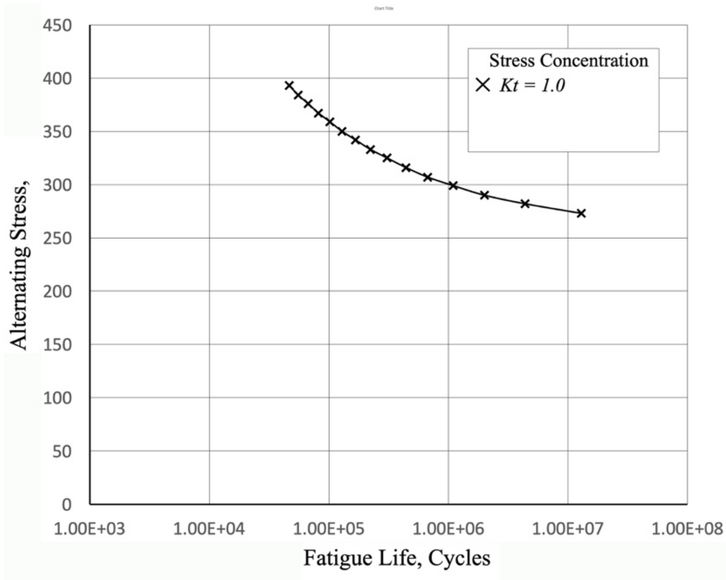

Figure 7. AISI 4340 *Ftu = 1379MPa*, *R = 0.43*

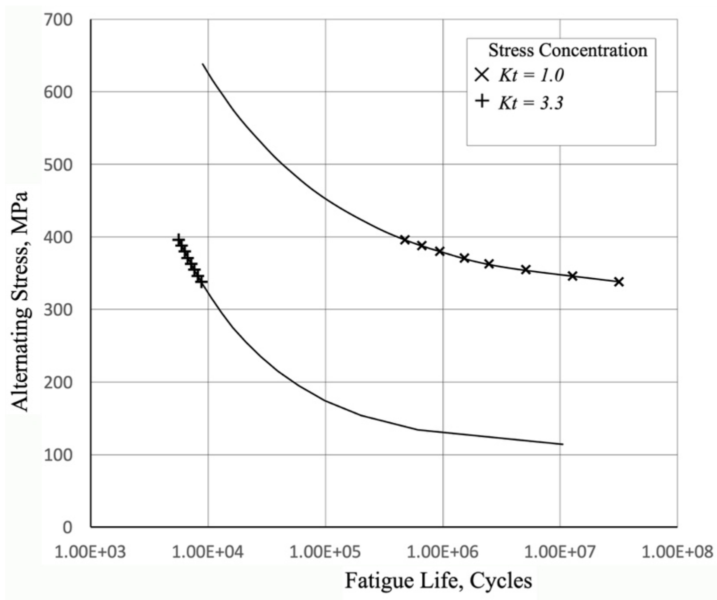

Figure 8. AISI 4340 *Ftu = 1379MPa*, *R = 0.0*

Equation (4) was used to calculate values of f_{n2} for each of the three sets of data considered. Data set 15 related to a stress ratio of $R = 0.43$ for a concentration $K_t = 1.0$. Data sets 16 and 17 related to stress ratios of $R = 0.0$ for stress concentrations of $K_t = 1.0$ and $K_t = 3.3$ respectively. The values of function f_{n2} for data set 15 were calculated to be within the range of 0.673 to 0.682, representing a variation of 0.6% from the mean value. Similarly, the values function f_{n2} for data set 16 were calculated to be within the range of

0.317 to 0.330, representing a variation of 2.2% from the mean value. Finally, the values function f_{n2} for data set 17 were calculated to be within the range of 0.274 to 0.275, representing a variation of 0.2% from the mean value.

Considering data set 15, equations (9) and (10) were used with a material constant of $a_1 = 3.349$ and a stress concentration of $K_{t.datum} = 3.3$ as the datum conditions, found from data sets 1, 2 and 3. Using the stress concentration of $K_t = 1.0$ for data set 15, the effective strain hardening factor was calculated as $\varepsilon'_w = 6.613 \ x \ 10^{-8}$. Equation (7) was then used to calculate a value of $a_1 = 2.134$ for the effective material constant.

Using equation (6) with the values for the material constant and the appropriate range of values for f_{n2} the values of function f_{n3} were calculated. The values function f_{n3} for data set 15 were found to be within the range of 0.295 to 0.299. The variations in the calculated values of the functions f_{n3} were the same as those for the calculated values of $f_{n2,}$.

When considering data sets 16 and 17, using equation (6) with a stress ratio of $R = 0.0$ the results showed that $f_{n3} = f_{n2}$ for both of these data sets. Note that any attempt to calculate a value for a_1 would result in a trivial solution.

7 Additional S-N Curves to Study the Effect of Stress Concentration

The objective of the work being presented was to derive a fatigue damage-equivalent stress function that could be applied to high, positive, stress ratios typical of those found in preloaded threaded fasteners. Hence, up until this point in the analysis only data for positive stress ratios had been considered. It was possible to continue to define a damage equivalent function with the data obtained for positive stress ratios only. However, this meant that some curve fitting had to be made through a very limited number of data points. This work was carried out and it was found that when the derived equation was applied to loading condition involving negative stress ratios the results had good correlation with actual S-N curves. This good correlation gave confidence to use fatigue data collected for negative stress ratios in the derivation of the damage-equivalent stress for fatigue function without compromising its application to high, positive stress ratios.

7.1 Additional S-N Curves for Normalised AISI 4130 Carbon Steel

Two S-N curves for normalised AISI 4130 carbon steel, which was assumed to have a tensile strength of 807MPa (117ksi), were considered. Again, each S-N curve was defined as a set of data points. Each curve was for a mean stress of s_{mean} = 207MPa (30ksi). One was for a stress concentration of K_t = 1.5 and the other was for a stress concentration of K_t = 2.0, reference Figures 2.3.1.2.8(b) and 2.3.1.2.8(c) of MMPDS-03 [6]. Figure 9 shows plots of the alternating stress against life for the two data sets.

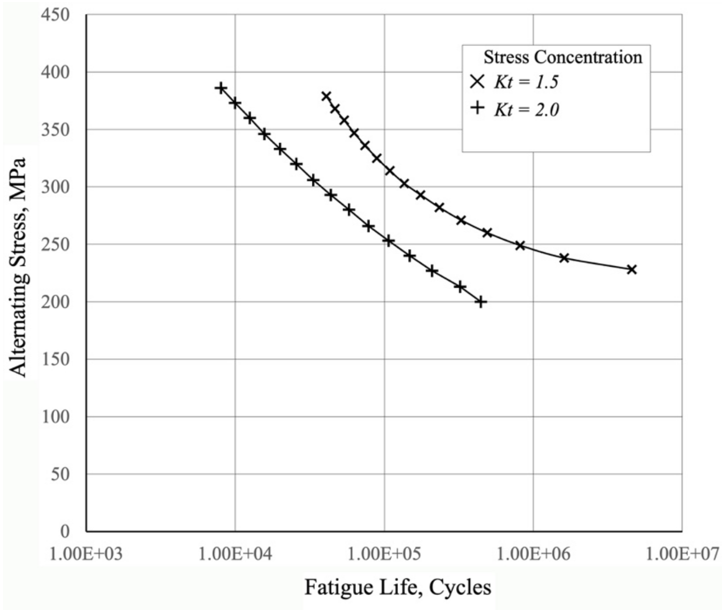

Figure 9. Normalised AISI 4130 (*Ftu = 807MPa*), s_{mean} = 207MPa

Equation (4) was used to calculate values of f_{n2} for both of the data sets. Data sets 18 and 19 related to stress concentrations of $K_t = 1.5$ and $K_t = 2.0$ respectively. Since both data sets were for constant mean stresses, and therefore over a range of stress ratios R, the resulting values for f_{n2} also covered a corresponding range.

Using equation (6) in an iterative solution, similar to that used previously, it was shown that a value of $a_1 = 1.381$ gave the optimum condition for minimum variation in the values function f_{n3}. The values of function f_{n3} for data sets 18 and 19 were calculated to be within the range of 0.083 to 0.087 hence, the variations in the values of function f_{n3} was found to be 2.6%. Similarly, applying an iterative solution of equation (6) to data set 19 showed that for a stress concentration of $K_t = 2.0$ a value of a_1 = 1.420 gave the optimum condition. The values of function f_{n3} were calculated to be within the range of 0.102 to 0.104 hence, the variations in the values of function f_{n3} was found to be 1.0%.

7.2 Additional S-N Curve for AISI 4130 Carbon Steel

A single S-N curves for AISI 4130 carbon steel, heat treated to give a tensile strength of 1241MPa (180ksi) was considered. This S-N curve was defined as a series of data points. The curve was for unnotched material, stress concentration of $K_t = 1.0$, and a mean stress of $s_{mean} = 345MPa$ (50ksi), reference Figure 2.3.1.2.8(f) of MMPDS-03 [6]. Figure 10 shows plots of the alternating stress against life.

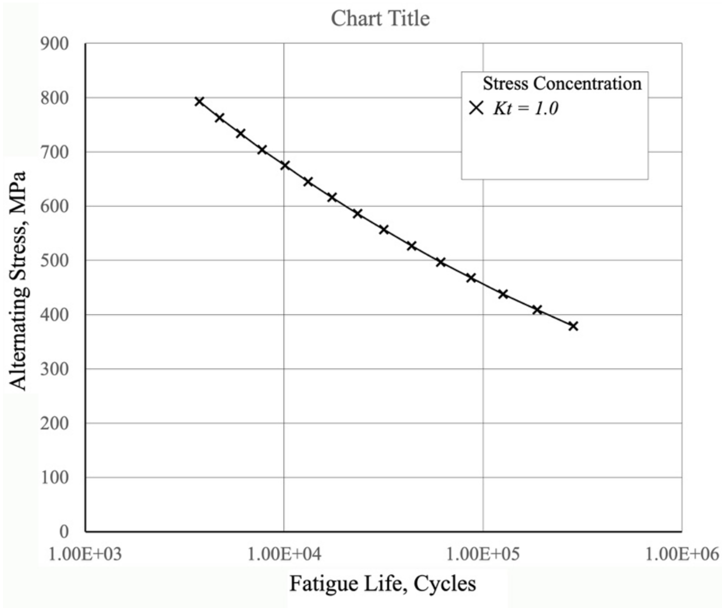

Figure 10. AISI 4130 $Ftu = 1241MPa$, s_{mean} = 345MPa

Equation (4) was used to calculate values of f_{n2} for data set 20. Since data set 20 was for constant mean stresses, and therefore over a range of stress ratios R, the resulting values for f_{n2} also covered a corresponding range.

Using equation (6) an iterative solution was applied to data set 20. This iterative solution showed that a value of a_1 = 1.461 gave the optimum condition for minimum variation in the values of function f_{n3}. The values of function f_{n3} were calculated to be within the range of 0.413 to 0.420 hence, the variation in the values of function f_{n3} was found to be 0.9%.

8 Effect of Stress Concentration and Material Properties on Function f_{n3}

From the previous workings it has been shown that f_{n3} is a function of the stress concentration K_t and the material properties, either the tensile strength Ftu or the yield/proof stress *Fty*. Numerical values of the function f_{n3} have been calculated for each data case considered.

It was now assumed that the function f_{n3} could be described by the equation for a straight line passing through the origin:

$$f_{n3} = a_2 \cdot f_{n.Kt} \tag{11}$$

where a_2 is the slope of the line and $f_{n.Kt}$ is the variable, given by a function of the stress concentration K_t.

After trialling several plots of f_{n3} for each material against various functions of the stress concentration K_t it was considered that there were two potentially good fits for the available data. These were:

$$f_{n.Kt} = \frac{1}{(K_t+1)^{a_3}} \tag{12a}$$

Or

$$f_{n.Kt} = \frac{1}{(K_t{}^2+1)^{a_3}} \tag{12b}$$

The constants a_2 and a_3 used in equations (11), (12a) and/or (12b) are both functions of the material properties.

Each of these equations for $f_{n.Kt}$ were considered and it was found that equation (12a) provided the more accurate prediction of damage-equivalent stress for fatigue. Hence, only the work involving equation (12a) is presented in this paper.

8.1 Effect of Stress Concentration for 300M Carbon Steel

The calculated values for the function f_{n3} and the associated stress concentrations K_t for data sets 8, 9, 12, 13 and 14 were used to calculate the constants a_2 and a_3 for 300M Carbon steel with a tensile strength of 1931MPa (280ksi). This group of data sets covered a range of stress concentrations, K_t equal to 1.0, 2.0, 3.0 and 5.0.

An iterative solution for the constants a_2 and a_3 was carried out, applying equations (11) and (12a) and using this data for 300M carbon steel. The constants a_2 and a_3 were calculated by first assuming a value for a_3 and then calculating values for $f_{n.Kt}$ using equation (12) before performing a linear regression to determine a value for a_2 that gave the best/minimum RMS error fit. By following this procedure it was possible to use an iterative approach to calculate an optimum value for the constant a_3 that gave the minimum amount of error in the resulting values of f_{n3}. This iterative solution showed that a value of $a_3 = 0.675$ gave the optimum condition. This led to a value of $a_2 = 0.770$ and a worst error of -17.8% in the prediction of f_{n3}.

8.2 Effect of Stress Concentration for AISI 4340 Carbon Steel

The calculated values for the function f_{n3} and the associated stress concentrations K_t for data sets 1, 2, 3, 15, 16 and 17 were used to calculate the constants a_2 and a_3 for AISI 4340 Carbon steel with a tensile strength of 1379MPa (200ksi). This group of data sets covered a range of stress concentrations, K_t equal to 1.0 and 3.3.

The previously described iterative procedure was applied using this data for AISI 4340 carbon steel. This showed that a value of $a_3 = 0.525$ gave the optimum condition. This led to a value of $a_2 = 0.430$ and a worst error of -27.2% in the prediction of f_{n3}.

8.3 Effect of Stress Concentration for AISI 4130 Carbon Steel

The calculated values for the function f_{n3} and the associated stress concentrations K_t for data sets 10, 11 and 20 were used to calculate the constants a_2 and a_3 for AISI 4130 Carbon steel with a tensile strength of 1241MPa (180ksi). This group of data sets covered a range of stress concentrations, K_t equal to 1.0, 2.0 and 4.0.

The previously described iterative procedure was applied using this data for AISI 4130 carbon steel. This showed that a value of $a_3 = 0.315$ gave the optimum condition. This led to a value of $a_2 = 0.544$ and a worst error of -12.5% in the prediction of f_{n3}.

8.4 Effect of Stress Concentration for Normalised AISI 4130 Carbon Steel

The calculated values for the function f_{n3} and the associated stress concentrations K_t for data sets 4, 5, 6 and 7 were used to calculate the constants a_2 and a_3 for Normalised AISI 4130 Carbon steel with a tensile strength of 807MPa (117ksi). This group of data sets covered a range of stress concentrations, K_t equal to 1.5, 2.0, 4.0 and 5.0.

The previously described iterative procedure was applied using this data for AISI 4340 carbon steel. This showed that a value of $a_3 = -1.705$ gave the optimum condition. This led to a value of $a_2 = 0.017$ and a worst error of -8.5% in the prediction of f_{n3}.

9. Effect of Material Properties on Material Constants a_2 and a_3

Values for the constants a_2 and a_3 had been calculated for the individual materials being considered, hence it was assumed they could be described as functions of the material properties, tensile strength *Ftu* or yield/proof stress *Fty*.

It was assumed that that a_2 could be best describe by a straight-line equation of the form:

$$a_2 = b_4 + b_5 \cdot f_{n.Fty} \tag{13}$$

where:

$$f_{n.Fty} = \left(\frac{Fty}{E}\right)^{b_6} \tag{14}$$

The constants b_4, b_5 and b_6 were calculated by assuming a value for b_6, calculating values for $f_{n.Fty}$ using equation (14) and then performing a linear regression to determine values for b_4 and b_5 that gave the best/minimum RMS error fit for the line. This procedure was used iteratively to optimise for the value of b_6 that gave the minimum amount of error in the resulting values for a_2.

The optimum values for the constants were found to be:

$$b_4 = -1.015$$
$$b_5 = 38.120$$
$$b_6 = 0.635$$

The worst error in the calculated value for a_2 was 18.2%.

A similar procedure was applied to determine the function that describes the material constant a_3. It was assumed that that a_3 could be best described by:

$$a_3 = b_7 + b_8 \cdot \left(\frac{Fty}{E}\right)^{b_9} \tag{15}$$

The optimum values for the constants were found to be:

$b_7 = 1.038$

$b_8 = -2.032 \times 10^6$

$b_9 = -2.485$

The worst error in the calculated value for a_2 was -17.3%.

10 Fatigue Damage-Equivalent Stress Function

Equations (3), (5), (11) and (12) were combined to produce the final fatigue damage-equivalent stress function:

$$\sigma_{equ} = \sigma_{alt} \cdot \left(1 + \frac{a_2 \cdot (1+R)^{a_1}}{(K_t+1)^{a_3}}\right) \tag{16}$$

where: a_1 is given by equations (7) and (8), a_2 is given by equations (13) and (14) and a_3 is given by equation (15).

The twenty S-N curves used in the derivation of equation (16) plus eighteen additional S-N curves were used to validate this function.

Two of the eighteen additional S-N curves were for AISI 4340 carbon steel, heat treated to give a tensile strength of 862MPa (125ksi) and were for stress concentrations of $K_t = 1.0$ and $K_t = 3.3$ with a stress ratio of $R = 0.0$, reference Figures 2.3.1.3.8(a) and 2.3.1.3.8(b) of MMPDS-03 [6]. Two further S-N curves were for the same grade of steel but heat treated to give a tensile strength of 1034MPa (150ksi). These second two additional S-N curves were also for stress concentrations of $K_t = 1.0$ and $K_t = 3.3$ with a stress ratio of $R = 0.0$, reference Figures 2.3.1.3.8(c) and 2.3.1.3.8(d) of MMPDS-03 [6]. The remaining fourteen additional S-N curve were for the material grades used in the analysis, although these specific curves had not been used in the analysis. Nine were for normalised AISI 4130 and five were for 300m with a tensile strength of 1931MPa.

As part of the validation process the damage-equivalent stress for fatigue calculated using equation (16) was compared with existing methods of calculating damage-equivalent stresses, reference ESDU 06009 [1]. The other methods used for comparison were:

Goodman-Haig: $$\sigma_{equ} = \frac{\sigma_{alt}}{1-\frac{\sigma_{mean}}{Ftu}} \tag{17}$$

Gerber: $$\sigma_{equ} = \frac{\sigma_{alt}}{1-\left(\frac{\sigma_{mean}}{Ftu}\right)^2} \tag{18}$$

Soderberg: $$\sigma_{equ} = \frac{\sigma_{alt}}{1-\frac{\sigma_{mean}}{Fty}} \tag{19}$$

Smith-Watson-Topper: $$\sigma_{equ} = \sigma_{alt} \cdot \left(1 + \frac{\sigma_{mean}}{\sigma_{alt}}\right)^{\frac{1}{2}} \tag{20}$$

It was found that the fatigue damage-equivalent stress function derived in this paper, equation (16), gave the most consistent results over the range of thirty-six S-N curves used for the validation process. Equation (16) provided the most accurate prediction of damage-equivalent stress for twenty-seven out of the thirty-six cases considered. In seventeen of the cases equation (16) gave very close correlation. The worst-case deviations of the fatigue damage-equivalent stress calculated by equation (16) from the datum S-N curve for the stress ratio $R = -1.0$ were +15.7% and -13.1%. Plots of results for the worst-case deviations are presented in Figures 11 and 12.

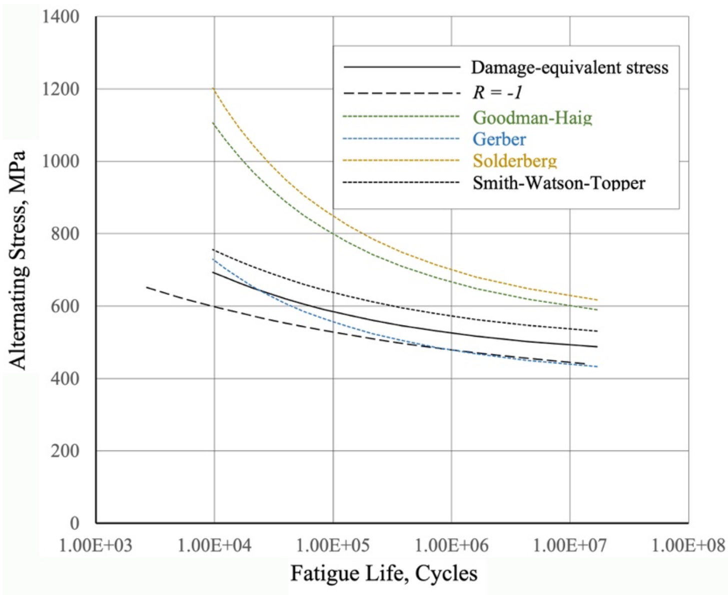

Figure 11. AISI 4340, *Ftu = 1034MPa*, $K_t = 1.0$, $R = 0.0$

Figure 11 shows the plots of results of the validation case for unnotched AISI 4340 heat treated to have a tensile strength of 1034MPa (150ksi) and with a stress ratio of

$R = 0.0$. The results from equation (16) had a worst-case deviation of +15.7%. The results using Gerber's method, equation (18), gave the best fit.

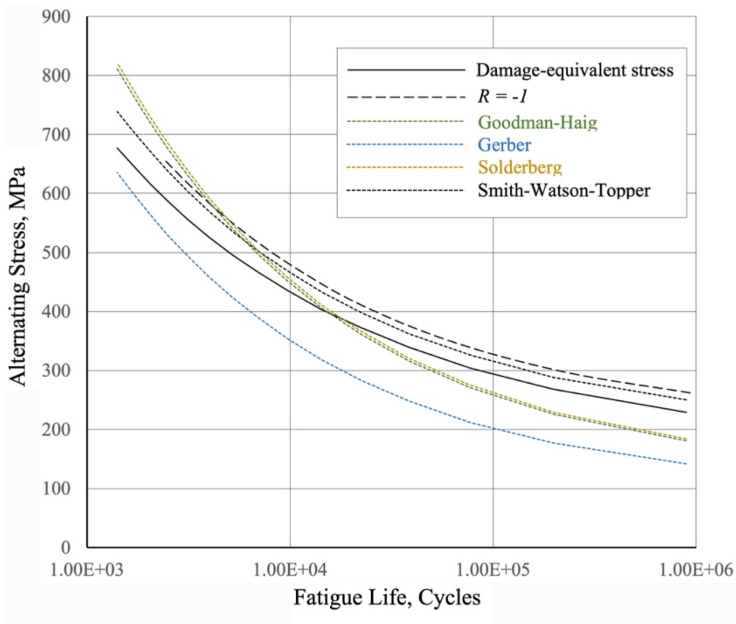

Figure 12. AISI 4130, $Ftu = 1241MPa$, $K_t = 2.0$, s_{mean} = 345MPa

Figure 12 shows the plots of results of data set 10, notched AISI 4130 heat treated to have a tensile strength of 1241MPa (180ksi) with a stress concentration of $K_t = 2.0$ and a mean stress of $s_{mean} = 345MPa$. The results from equation (16) had a deviation of -13.1%. The results using the Smith-Watson-Topper method, equation (20), gave the best fit.

The stated objective was to determine a method of calculating a damage-equivalent stress for fatigue that could be applied to preloaded bolted assemblies. The most representative validation cases, in terms of tensile strength, stress concentration and stress ratio or mean stress are presented in Figures 13 to 16

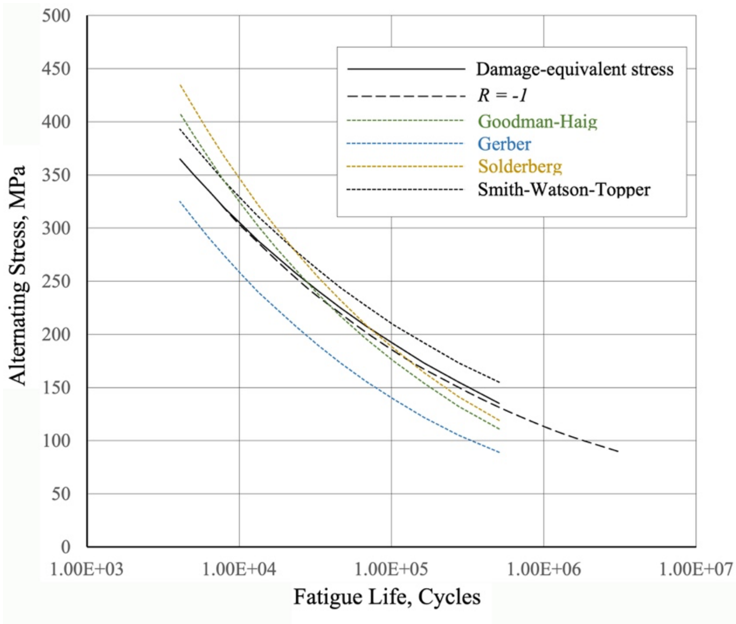

Figure 13. Normalised AISI 4130, Kt = 4.0, s_{mean} = 207MPa

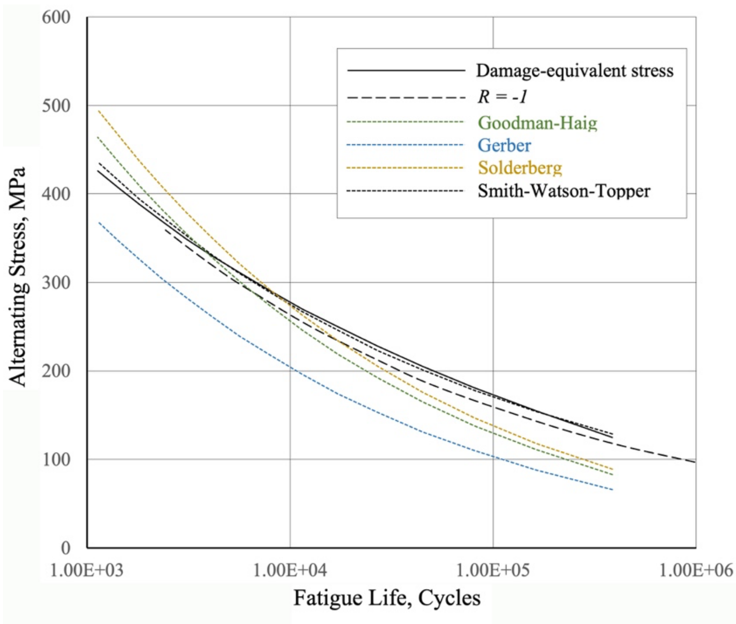

Figure 14. Normalised AISI 4130, $K_t = 5.0$, s_{mean} = 207MPa

Figures 13 and 14 show the plots of results of data sets 7 and 9 respectively. Both of these figures are for normalised AISI 4130 that had an estimated tensile strength of 807MPa. This material specification could be regarded as typical of a Grade 8.8 bolt. Figure 13 presents plots for a stress concentration of $K_t = 4.0$ with a mean stress of

s_{mean} = 207MPa (30ksi). Similarly, Figure 14 presents plots for a stress concentration of $K_t = 5.0$ with the same mean stress of s_{mean} = 207MPa.

The errors in the calculated values for the damage-equivalent stress for data set 7 were all within +3.2% with a RMS error of 2.0%. Similarly, the calculated values for the damage-equivalent stress for data set 9 were within the range +1.8% to +8.4% with an RMS error of 5.4%.

A theoretical study of bolt thread elastic stress concentration factors has been conducted by Lehnoff et. al. (2000) [8]. This work showed that M8 and M12 bolts, with maximum metal condition, had stress concentration factors of 4.33 and 4.32 respectively. Hence, Figure 13 could be considered as an approximate representation to these bolt sizes. Similarly, Figure 14 could be considered as representative of M16, M20 and M24, which Lehnoff (200) [8] shown had stress concentration factors of 4.67, 4.77 and 4,82 respectively for maximum metal conditions and stress concentration factors of 5.12, 5.17 and 5,22 respectively for minimum metal conditions.

The mean stress of s_{mean} = 207MPa could be considered as representing a bolt preload of 32% of proof stress. It is usual for high tensile bolts (Grade 8.8 and above) to be preloaded 60% to 80% of proof load, and in some circumstances even higher hence, the figure of 32% is a little low. However, the thread rolling of bolts during manufacture induces compressive residual stresses. This means that whilst a bolt may be preloaded to say 80% of proof load only the core of the thread is subjected to that level of pre-stress, the thread root would experience a lower stress. Work carried out by Furukawa and Hagiwara (2015) [9] estimated that the compressive residual stress of a thread, rolled after heat treatment, was 830MPa. Importantly, this was for a thread rolled after heat treatment however, bolt manufactures prefer to heat treat after thread rolling. This minimises the power required to roll the thread, extends die life and hence minimises production costs. It has been shown by Marcelo et. al. (2011) [10] that threads rolled after heat treatment exhibited a higher tensile strength than those rolled before being heat treated and tempered at the same temperature. Hence, it may be assumed that the mean stress of s_{mean} = 207MPa is representative of the mean stress at the thread root, where a crack would initiate, but is lower than would normally be expected in the core of the thread, which is the region the crack would grow into once initiated. Work by Leitner et. al. (2000) [11]

has shown that compressive residual stresses, in this case induced by high frequency peening, improves the fatigue strength, particularly at stress concentrations.

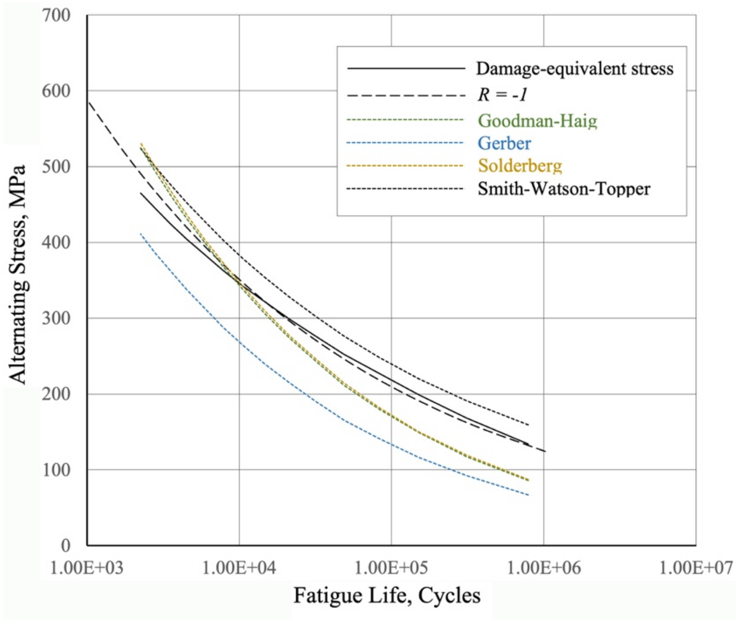

Figure 15. AISI 4130, $Ftu = 1241MPa$, $K_t = 4.0$, s_{mean} = 345MPa

Figure 15 shows the plots of results of data set 11 for notched AISI 4130 heat treated to give a tensile strength of 1241MPa. This material specification could be regarded as typical of a Grade 12.9 bolt.

The errors in the calculated values for the damage-equivalent stress for data set 11 were within the range -5.4% to +4.4% with an RMS error of 3.3%.

Again, the work by Lehnoff et. al. (2000) [8] can be taken to show that the stress concentration of $K_t = 4.0$ could be considered as an approximate representation of M8 and M12 bolts.

In this case, the mean stress of s_{mean} = 207MPa could be considered as representing a bolt preload of 19% of proof stress. However, it is not unreasonable to assume that residual stresses combined with a preload of say 60% of proof load could still be representative of the mean stress at the thread root, where a crack would initiate.

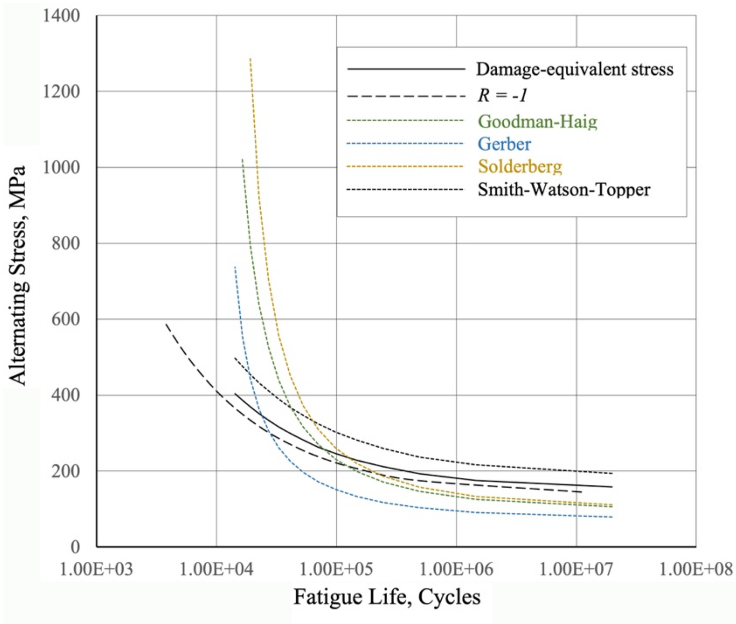

Figure 16. AISI 4340, $Ftu = 1379MPa$, $K_t = 3.3$, $R = 0.74$

Figure 16 shows the plots of results of data set 3 and relates to notched AISI 4130 heat treated to give a tensile strength of 1379MPa. This tensile strength is higher than the minimum requirement for Grade 12.9 bolts. However, statistically approximately 50% of Grade 12.9 bolts could achieve this strength. Hence, the material can still be regarded as applicable to a Grade 12.9 bolt.

The errors in the calculated values for the damage-equivalent stress for data set 3 were within the range +9.1% to +13.5% with an RMS error of 10.2%.

The work by Lehnoff et. al. (2000) [8] shows that Figure 16 could be considered as a representation of M16, M20 and M24 bolts.

When considering the results in Figure 16 as representing preloaded bolts the tensile strength of 1379MPa is not relevant since bolt preloads are based of the minimum material properties for the bolt grade. Hence, the arguments made regarding data set 11 for Figure 15 hold true.

CONCLUSIONS

A viable method of determining a damage-equivalent stress function for fatigue is presented. This empirical method was produced by developing an equation that fitted existing S-N curves.

The presented damage-equivalent stress function is applicable to carbon steels with heat treatments ranging from the normalised state to hardened and tempered for a tensile strength of 1900MPa.

This new damage-equivalent stress function is consistently more accurate than existing methods of 'correcting' for mean stress.

Validation of this damage-equivalent stress function indicates that it has a maximum/minimum accuracy of +16% to -13%, with a root-mean-square error of 8%, for fatigue stress.

The damage-equivalent stress function that has been presented can be applied to the fatigue analysis of almost any steel structure or component. It is particularly suited to high positive stress ratios, particularly preloaded bolts. However, it also has good corelation with results for negative stress ratios.

The damage-equivalent stress function could also be applied to civil engineering structural using 'snug tightened' bolted joints. Although, as the name implies, snug tightened bolts are not subject to preload during the initial assembly the joints usually carry a heavy dead load from subsequent construction work. Dynamic loading can then occur through wind loading.

The work presented is based on available S-N available for carbon steel. It is expected that the resulting damage-equivalent stress function will also be appropriate for other materials with similar hardness, for example stainless steels. Future work would be to test if this assumption is correct.

References

[1] ESDU, 2006. *Fatigue damage and life under random loading*. ESDU 06009. The Royal Aeronautical Society.

[2] Novoselac S, Kozak D, Ergić T, Damjanović D. *Fatigue of shaft flange bolted joints under preload force and dynamic response*. FME Transactions. 2014;42(4):269-76.

[3] Welch, M. *Classical Analysis of Preloaded Bolted Joint Load Distributions*. International Journal of Structural Integrity, Volume 9 (2018), Issue 4, pages 455 to 464

[4] Welch, M. *Analysis of Bolt Bending in Preloaded Joints*. Journal of Mechanical Engineering – Strojnicky časopis, Volume 68 (2018), Issue 3, pages 183 to 194.

[5] Welch, M. *An Analytical Study of Asymmetrical Preloaded Bolted Joints*. International Journal of Modern Research in Engineering and Technology, Volume 7 (2022), Issue 3, March 2022, Pages 6 to 11.

[6] Federal Aviation Administration. *Metallic Materials Properties Development and Standardization (MMPDS)*, Battelle Memorial Institute, MMPDS-03, October 2006

[7] McMillan AJ, Jones R. *Combined effect of both surface finish and sub-surface porosity on component strength under repeated load conditions*. Engineering Reports. 2020 Sep;2(9):e12248.

[8] Lehnhoff TF, Bradley A, Bunyard A. *Bolt thread and head fillet stress concentration factors*. Journal of Pressure Vessel Technology. May 2000, 122(2): Pages 180-185.

[9] Furukawa A, Hagiwara M. *Estimation of the residual stress on the thread root generated by thread rolling process*. Mechanical Engineering Journal, *2*(4), pp.14-00293.

[10] Marcelo AL, Uehara AY, Utiyama RM, Ferreira I. *Fatigue properties of high strength bolts*. Procedia Engineering. 2011 Jan 1;10:1297-302.

[11] Leitner M, Stoschka M, Schanner R, Eichlseder W. *Influence of high frequency peening on fatigue of high-strength steels*. FME transactions. 2012;40(3):99-104.

Nomenclature

a_1 to a_3	Constants, calculated from geometry and material properties
b_1 to b_9	Numerical constants
f_{n1} to f_{n3}	Function of stress and stress concentration
$f_{n.Fty}$	Function of the yield/proof stress
$f_{n.Kt}$	Function of the stress concentration
Ftu	Tensile strength of a material
Fty	Yield or proof stress of a material
K_t	Stress concentration factor
$K_{t.datum}$	A datum stress concentration factor
R	Stress ratio (s_{min} / s_{max})
TUS	Tensile strength of a material, at the fatigue test strain rate
TYS	Yield or proof stress of a material, at the fatigue test strain rate
ε_w	Function, related to work hardening
ε'_w	Function, related to work hardening
σ_{alt}	Alternating stress
σ_{equ}	Damage-equivalent stress for fatigue
σ_{max}	Maximum stress
σ_{mean}	Mean stress
σ_{min}	Minimum stress

4.2.2 Further Discussion

The application of safe-life fatigue analysis requires a suitable S-N curve, a plot of a characteristic stress (S) against the number of life cycles (N). However, the experimental procedures to produce S-N curves are complex, requires specialist tensile test equipment. Therefore, it is rare for an S-N curve that matches the duty of the bolted joint in question to be available. A common approach is to use S-N curves with a zero mean stress. The high mean stress experienced by the bolts is accounted for using a function to calculate a 'damage-equivalent' stress. Existing methods of calculating a damage-equivalent stress are not satisfactory. It was found that the best of the currently available methods, Smith-Watson-Topper, could be up to 40% in error. The work that has been presented here developed an empirical damage-equivalent stress function with an improved accuracy, reducing the potential error to 16% with a root mean square error of 8% for equivalent alternating stress. The root mean square error (RMS error) is an indication of the mean error, unaffected by negative error values. It can be taken to be the standard deviation of the predicted data.

Figures AAM P1 – Figure 13 through to P1- Figure 15 are for S-N Curves for high stress concentration factors, within the range typical of bolt threads ($K_t = 4.0$ and $K_t = 5.0$). Similarly, AAM P1 – Figure 16 are for S-N Curves with a high mean stress ($R = 0.74$), typical of pre-loaded bolted joints. They show that the new damage-equivalent stress function gives the best overall correlation with S-N Curves for fully reversed alternating stress, ($R = -1$).

Hence, it was concluded that this new function is consistently more accurate than the existing methods. It is also particularly suited to high positive stress ratios, typical of those experienced by preloaded bolts, but also has good corelation with results for negative stress ratios. Hence, it can be applied to the fatigue analysis of almost any carbon steel structure or component.

The improvement in accuracy of the new damage-equivalent function arises from curve fitting to a significant quantity of data. This has been achieved partly by the significant amount of data publicly available through MMPDS-03 (2006) and also through the availability of computers. This results in the new function being more complex than the earlier. However, the increased complexity is not an issue when using the function in computer-based analyses.

The paper by Welch (2022b) did not include any zinc plated steels. However, Zinc plated high strength steel bolts can be susceptible to Hydrogen embrittlement. This could result in a loss of tensile strength over a period of time, due to the creation of microscopic cracks at the surface caused by the inclusion of Hydrogen. The sources of hydrogen are from the acid used to degrease the steel prior to Zink plating and the water content of the platin bath. It is possible to mitigate Hydrogen embrittlement by heat treating within a few hours of the plating process. The temperatures involved in this heat treatment would not have any significant effect on the hardness of the bolt material.

The functions used in the presented analysis that are related to work hardening incorporate the elastic stress concentration factor K_t and the term (F_{ty}/E), which represents the strain at proof/yield stress. It is well understood that fatigue is influenced by plastic deformation at crack tips. Hence, using the elastic stress concentration factor K_t instead of a fatigue stress concentration factor K_f that reflects the effects of work hardening more could result in a loss of accuracy. From an analysis point of view, the elastic stress concentration factor K_t is much easier to define than the fatigue stress concentration factor K_f. Peterson charts, Pilkey (1997), can be used to determine elastic stress concentration factors for a wide range of engineering detail geometries.

4.3 Supplementary Material to: An Empirical Approach to a Comprehensive Damage-Equivalent Stress for Fatigue

The paper by Welch (2022) used twenty S-N curves to derive the damage-equivalent function and a further eighteen S-N curves for validation. All of these thirty-eight S-N curves were used to created plots of calculated results comparing the new damage-equivalent stress function with four other existing methods of calculating a damage-equivalent stress. Six of these plots were presented in the paper, Welch (2022). These six plots, P6 Figure 11 through to P6 Figure 16, represented the bounding cases that span all of the five methods used.

The journal FME Transactions, where the paper "*An Empirical Approach to a Comprehensive Damage-Equivalent Stress Function for Fatigue*", Welch (2022b), was published, does not support the inclusion of supplementary material. Therefore, the full thirty-eight validation plots were published in a separate document. The document that contains the supplementary material was not prepared until after the publication of reference Welch (2022b). Hence the document "*Supplementary Material to: An Empirical Approach to a Comprehensive Damage-Equivalent Stress for Fatigue*", Welch (2023), has not been peer reviewed. It has, however, been included as Appendix B of this thesis since it fully illustrates the consistency of the damage-equivalent stress function being presented.

4.4 Fatigue Analysis of Preloaded Bolted Joints

The complexity of producing S-N curves means that there are not any readily available S-N curves for preloaded bolts. There are some individual fatigue test results available but not enough to produce a complete curve. The work presented in this paper, "*Fatigue Analysis of Preloaded Bolted Joints*", Welch (2022c), develops and presents a series of S-N curve specific to high strength bolts and screws, property-class 8.8 to 12.9. A number of carbon steel material specifications, with chemical compositions that are encompassed within the material specification for high strength bolts, are considered. Methods based on notch sensitivity, Chapter 4 of Pilkey (1997), are used to modify several S-N curves to the elastic stress concentrations applicable to a range of ISO metric screw thread sizes. Curve fitting techniques were used to present these S-N curves as a function of the damage-equivalent stress, calculated using the function presented in the previous paper, Welch (2022b). Commercially manufactured bolts are produced using thread rolling techniques. This results in the finished thread having compressive residual stresses at the thread root. Using existing bolt fatigue data, it was possible to estimate the residual stresses produced by the thread rolling process for a range of thread sizes. All of this was combined to produce a procedure for the safe-life fatigue analysis of preloaded bolts. The functions for S-N curves for high strength bolts and screws, and the residual stress values for screw threads should be of significant benefit to anyone undertaking safe-life fatigue analysis of bolts and screws.

4.4.1 P7 - Author Accepted Manuscript (FME Transactions. 2022;50(4):607-614.)

Fatigue Analysis of Preloaded Bolted Joints

Michael Welch

Michael A Welch (Consulting Engineers) Limited, West Lancashire, UK.

Abstract

This article presents Wöhler plots, or S-N curves, for use in the analysis of bolt fatigue of preloaded bolted joints. Preloaded bolts under cyclic loading have a high mean stress with a small alternating stress. This is combined with a large stress concentration at the thread root. The method of fatigue analysis presented uses S-N curves with a zero mean stress. The high mean stress experienced by the bolts is accounted for using a function to calculate a damage-equivalent stress. Notch sensitivity was considered to modify S-N curves for materials with chemical compositions encompassed within the material specifications for high strength bolts. This produced S-N curves for stress concentrations relevant to bolt threads. Curve fitting techniques were used to express these curves as a function of the equivalent stress and stress ratio. An estimate of residual stresses in bolts produced by thread rolling was made. The work provides a practical method of calculating fatigue life.

Keywords: bolt fatigue, Wöhler plots, S-N curve, residual stress

1 Introduction

Preloaded bolted joints are a common feature in mechanical engineering. They are a convenient means by which to assemble components. There is no requirement for post assembly heat treatment to remove or reduce residual stresses, as is often the case for welded assemblies. Most importantly, they can be used to facilitate disassembly for maintenance and repair. The main disadvantage with preloaded bolted joints is that they tend to be bulky and take up a relatively large space envelope compared to the cross-sections of the structural elements or components they are used to connect. This can lead to designers keeping the joint size to an absolute minimum, particularly where the space envelope is critical. This often leads to the joint having to work at its maximum capacity. In many bolted joint applications, the main issue is the static strength of the joint. Providing the bolt preload is at least 1.5 time the design tension and the alternating load is less than 20% of the applied load fatigue should not be an issue, reference BS 7608 (1990) [1]. When bolted joints are highly loaded and/or subjected to high alternating loads the effect of fatigue of the joint needs to be considered.

The log-linear nature of Wöhler plots, or S-N curves, means that the calculated fatigue life is very sensitive to stress. It is well known that a small change in alternating stress can have a significant effect on the fatigue life of a component. Hence, it is important to determine applied stresses with a high degree of accuracy to be able to achieve a meaningful assessment of life. In order to produce an accurate prediction of actual stresses, margins of safety, safety factors, partial safety factors or reserve factors should not be applied to the loads or calculated stresses. The two most common methods of conducting stress analyses of bolted joints are Finite Element Analysis (FEA) and classical methods. A good example of an appropriate FEA can be found in the work conducted by Novoselac et. al. (2014) [2]. Classical methods of analysis need to consider a detailed analysis of stresses. The methods of detail analysis described by Welch (2018) [3] and (2022) [4] are particularly suited to this purpose. Note that the design analysis method that is also described by Welch (2018) [3] should not be used since it does not predict the true bolt stress, instead, it calculates a "bolt related load", which can be defined as "the load passing through the region of the joint controlled by the bolt".

This article considers the classical analysis of bolt fatigue within joints made using preloaded bolts.

2 Classical Analysis of Bolt Loads

Figure 1 shows a typical bolted joint and the free body diagram for one mating component, with the bolt preloads considered as point loads.

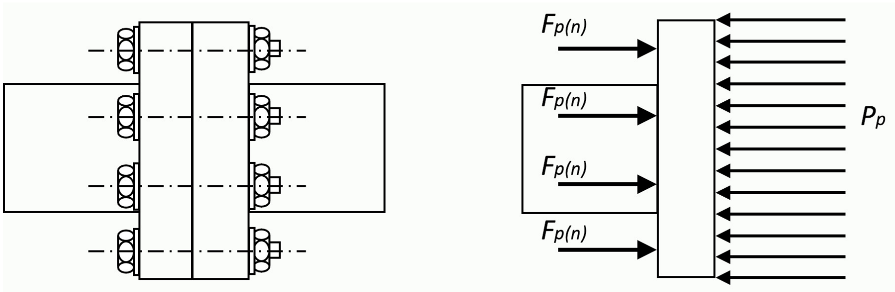

Figure 1. Preloaded Joint.

Figure 2 shows the same joint with an external axial load (tensile) and an external moment applied along with the free body diagram of one mating component.

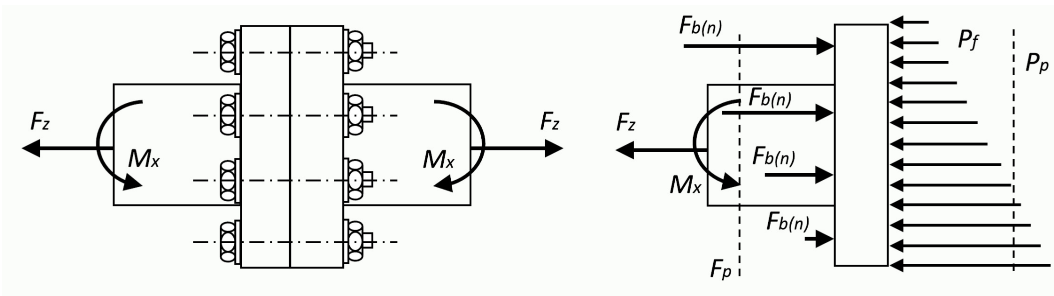

Figure 2. Bolted Joint with External loads Applied.

The axial bolt load resulting from the combined loading of the preload, external axial load and external moment are given by equation (1).

$$F_{b_{(n)}} = F_p + F_z \cdot \frac{A_b}{A_j} + \frac{M_x}{I_{xx.j}} \cdot y_{(n)} \cdot A_b \tag{1}$$

where $F_{b(n)}$ is the axial load in bolt ‘n’.

The area and second moment of area for the joint, A_j and $I_{xx.j}$ respectively, should ideally reflect the effect of Rotscher’s pressure cone on the contact area of the joint. Hence, the total area of the joint A_j is given by $A_j = A_c + N_b \cdot A_b$ where A_c is the effective, or true, contact area, A_b is the bolt tensile area and N_b is the number of bolts.

3 S-N Curves for bolts

A characteristic of preloaded bolts under cyclic loading is that they have a high mean stress, due to the bolt preload, which is typically between 60% to 80% of the bolt proof load, with a relatively small alternating stress. This is combined with a large stress concentration at the thread root, in particular at the first thread of the thread engagement where bending loads in the thread flank accentuates the stress concentration. Any fatigue failures usually occur at the root of the first engaged thread. The engaged threads experience bending which results in higher stresses at the root of the first engaged thread than in the threads that are not engaged but are still subjected to the same axial load. The engaged threads after the first thread experience reducing tensile loads, and hence a lower stress, than the first engaged thread as some of the tensile load is transferred from the bolt to the nut or internally threaded component.

Ideally, Wöhler plots, or S-N curves, produced using the same mean stress as experienced by the bolt should be used for the analysis. However, this is impractical since each load case, for each bolt, will have a different mean stress. The method of fatigue analysis being presented here is based on the use S-N curves with a zero mean stress. The high mean stress experienced by the bolts is accounted for by the use of a function that calculates a damage-equivalent stress which can be used with these S-N curves. The damage-equivalent stress is the alternating stress under fully reversal load conditions that produces the same amount of damage as the combination of both the alternating stress and the (non-zero) mean stress.

A theoretical study of stress concentration at the root of bolt threads has been carried out by Lehnoff et. al. (2000) [5]. This work used FEA to determine the thread stress concentration factors at the first engaged thread for M8, M12, M16, M20 and M24 bolts. The results of this work are summarised in Table (1).

Table 1. Summary of elastic stress concentration factors.

Thread Size	Stress Concentration Factors		Mean elastic stress concentration factor
	Maximum metal condition	Minimum metal condition	
M8	4.33	4.80	4.565
M12	4.32	4.80	4.56
M16	4.67	5.12	4.895
M20	4.77	5.17	4.97
M24	4.82	5.22	5.02

A selection of fatigue S-N curves for materials with chemical compositions that are encompassed by the material specification for high strength bolts, Grade 8.8 and higher, can be found within '*Metallic Materials Properties Development and Standardization (MMPDS)*', reference [6]. These material and available S-N curves are presented in Table 2 and the chemical compositions of the materials compared with the requirements of the bolt specification, given in BS EN ISO 868-1 (2009) [7], are presented in Table 3. Some fatigue tests have been carried out on Grade 10.9 M8 bolts by Marcelo et. al. (2011) [8]. The materials for these bolts were AISI 4135 and SCM 435H wire. The chemical compositions of the wires used by Marcelo et. al. (2011) [8] are also included in Table 3.

Table 2. Materials considered in the analyses.

Material	Condition: Tensile Strength	Stress Concentration	Product form
AISI 4130	Normalised (*Ftu* 117ksi) (807MPa)	Unnotched $K_t = 5.0$	Sheet 0.075 inch (1.905mm) thick
	Ftu 180ksi (1241MPa)	Unnotched $K_t = 4.0$	Sheet 0.075 inch (1.905mm) thick
AISI 4340	*Ftu* 125ksi (862MPa)	Unnotched $K_t = 3.3$	Rolled bar 1.125 inch (28.575mm) diameter
	Ftu 150ksi (1034MPa)	Unnotched $K_t = 3.3$	Rolled bar 1.12 inch (28.448mm) diameter
	Ftu 200ksi (1379MPa)	Unnotched $K_t = 3.3$	Rolled bar 1.125 inch (28.575mm) diameter

Table 3. Chemical composition of materials.

Bolt Grade	**Material**									
		C	P	S max	B max	Cr	Mn	Mo	Ni	Si
	AISI 4130	0.28 to 0.33	0.035 max	0.04 max		0.80 to 1.10	0.40 to 0.60	0.15 to 0.25		0.15 to 0.35
Grade 8.8	Carbon steel with additives	0.15 to 0.40	0.035 max	0.035 max	0.003					
	Carbon steel	0.25 to 0.55	0.035 max	0.035 max						
	AISI 4340	0.37 to 0.43	0.035 max	0.04 max		0.70 to 0.43	0.65 max	0.20 to 0.30	1.85 max	0.25 max
Grade 9.8	Carbon steel with additives	0.15 to 0.35	0.035 max	0.035 max	0.003					
	Carbon steel	0.25 to 0.55	0.035 max	0.035 max						
	AISI 4135	0.36	0.022	0.010		0.97	0.81	0.17		0.26
	Standard AISI 4135	0.34	0.018	0.008		0.94	0.79	0.16		0.23
	SCM 435H	0.35	0.032	0.011		0.98	0.76	0.15		0.19
	Standard SCM 435H	0.35	0.012	0.006		0.99	0.74	0.17		0.20
Grade 10.9	Carbon steel with additives	0.15 to 0.35	0.035 max	0.035 max	0.003					
	Carbon steel with additives	0.20 to 0.55	0.035 max	0.035						
	Carbon steel	0.25 to 0.55	0.035 max	0.035	0.003					
	Alloy steel	0.20 to 0.55	0.035 max	0.035						
Grade 12.9	Alloy steel	0.28 to 0.50	0.035 max	0.035	0.003					

The approximation of S-N curves for the elastic stress concentrations given in Table 1 were made by considering notch sensitivity and the ratio of fatigue stress concentrations.

A number of 'donor' S-N curves, taken from MMPDS-03 [6], were modified using the term:

$$\sigma_{alt} = S_{alt.D}\frac{K_{f.D}}{K_f} \quad (2)$$

where s_{alt} and K_f were the alternating stress and fatigue stress concentration factor of the approximated S-N curve and $S_{alt.D}$ and $K_{f.D}$ refer to the donor S-N curve used for the approximation. Considering the notch sensitivity of a material it was possible to say that:

$$q = \frac{K_f - 1}{K_t - 1} \quad (3)$$

where K_t was the elastic stress concentration factor and q was a constant for the material at a given fatigue life.

Hence it was possible to write:

$$\frac{K_f - 1}{K_t - 1} = \frac{K_{f.D} - 1}{K_{t.D} - 1}$$

Rearranging:

$$K_f = \left(\frac{K_{f.D} - 1}{K_{t.D} - 1}\right) \cdot (K_t - 1) + 1 \quad (4)$$

The fatigue stress concentration factor for the donor curve was calculated from:

$$K_{f.D} = \frac{S_{alt.0}}{S_{alt.D}} \quad (5)$$

where $S_{alt.0}$ was the alternating stress of the unnotched S-N curve for the material.

Equations (2) to (5) were applied using the materials and stress concentrations presented in Table 2. The resulting S-N curves for AISI 4340, with a tensile strength of 1379MPa showed what appeared to be an anomaly. The fatigue strengths of these curves were less than the fatigue strengths of the same material specification tempered to give the lower tensile strengths of 862MPa and 1034MPa. However, this anomaly can be explained by reference to work by de Souza et. al. (2021) [9]. This work reports that heat treated specimens of AISI 4340 exhibited high tensile residual stresses at the surface after quenching. Subsequent tempering at 300°C and 400°C showed a small reduction in the residual stresses. Tempering at 500°C and 650°C resulted in compressive residual stresses. These higher tempering temperatures, and hence compressive residual stresses at the surface, result in improved fatigue performance. A conclusion that can be drawn from the work by de Souza et. al. (2021) [9] and the S-N curves produced using equations (2) to (5) is that; in general, an increase in tensile strength results in improved fatigue properties however, if a carbon steel is at or close to its maximum achievable tensile strength its fatigue performance may be impaired. Based on this conclusion, it was decided not to consider the approximated S-N curves for AISI 4340, heat treated to give a tensile strength of 1379MPa or the S-N curves for AISI 4130, heat treated to give a tensile strength of 1241MPa as appropriate for use in the fatigue analysis of preloaded bolted joints.

The work by Marcelo et. al. (2011) [8] considered Grade 10.9 bolts manufactured from AISI 4135 and SCM 435H wire. Both of these materials are at the lower end of the carbon content range allowable under BS EN ISO 868-1 (2009) [7]. AISI 4130 is of similar carbon content to AISI 4135 and SCM 435H, just slightly higher, therefore the S-N curves for bolt Grades 8.8, 9.8 and 10.9 were approximated using the S-N curves for normalised AISI 4130. These S-N curves were factored by the ratio of minimum tensile strength for the bolt grade to the tensile strength associated with normalised AISI 4130 (807MPa).

Although the minimum tensile strength requirements for Grade 12.9 bolts is achievable with AISI 4130 the work by de Souza et. al. (2021) [9] leads to the conclusion that this would result in poor fatigue performance. It was considered that it would be more appropriate to approximate the S-N curves for Grade 12.9 bolts by factoring the S-N curves for AISI 4340, heat treated to give a tensile strength of 1034MPa.

Curve fitting techniques were applied to each of the approximated S-N curves to allow them to be expressed as a function in the form of equation (6):

$$log\left(N_{life}\right) = C_1 - C_2 \cdot log\left(\frac{\sigma_{alt}}{Ftu} - C_3\right) \tag{6}$$

The constants, C_1, C_2 and C_3, were evaluated using the minimum tensile strength, *Ft*u, for each bolt grade. The results of equation (6) were then plotted for each bolt grade. The values of constants are presented in Table 4 and the resulting plots are shown in Figures 3 to 6.

Table 4. Curve fitting constants

	AISI 4130 Normalised ($Ftu = 807MPa$)			**AISI 4340,** $Ftu = 1034MPa$		
	Grade 8.8 d ≤ 16mm, $Ftu = 800MPa$ d > 16mm, $Ftu = 860MPa$ Grade 9.8, $Ftu = 900MPa$ Grade 10.9, $Ftu = 1040MPa$			Grade 12.9, $Ftu = 1200MPa$		
K_t	C_1	C_2	C_3	C_1	C_2	C_3
4.56	1.82	4.71	0.0	3.25	1.83	0.135
4.89	1.79	4.60	0.0	3.25	1.81	0.127
4.97	1.78	4.58	0.0	3.28	1.76	0.126
5.02	1.78	4.56	0.0	3.24	1.81	0.124

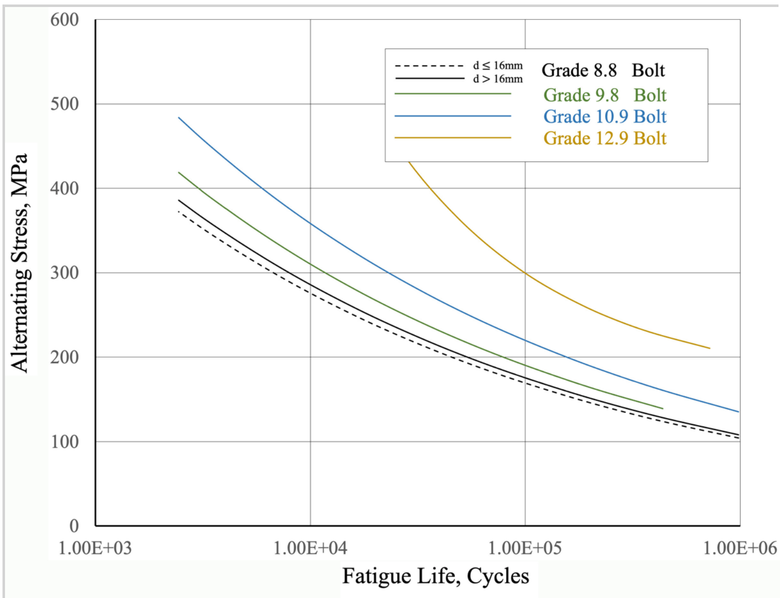

Figure 3. S-N curves for stress concentration $K_t = 4.56$

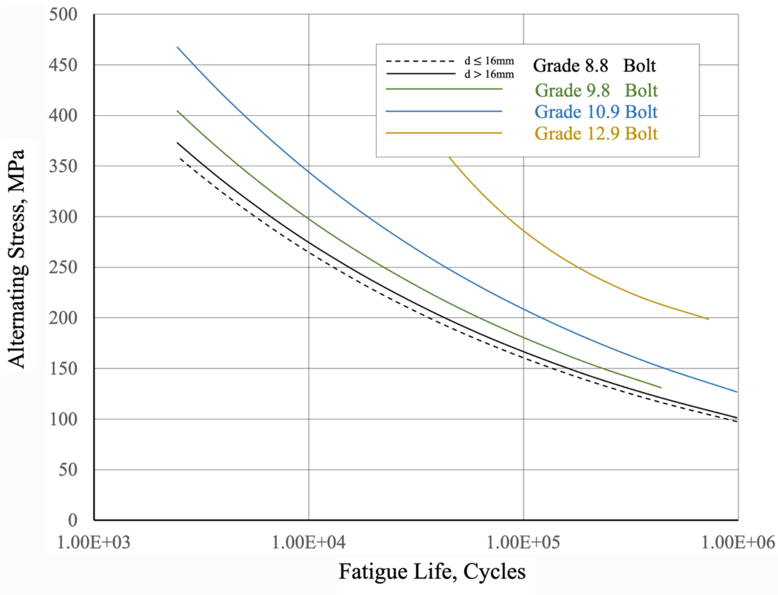

Figure 4. S-N curves for stress concentration $K_t = 4.89$

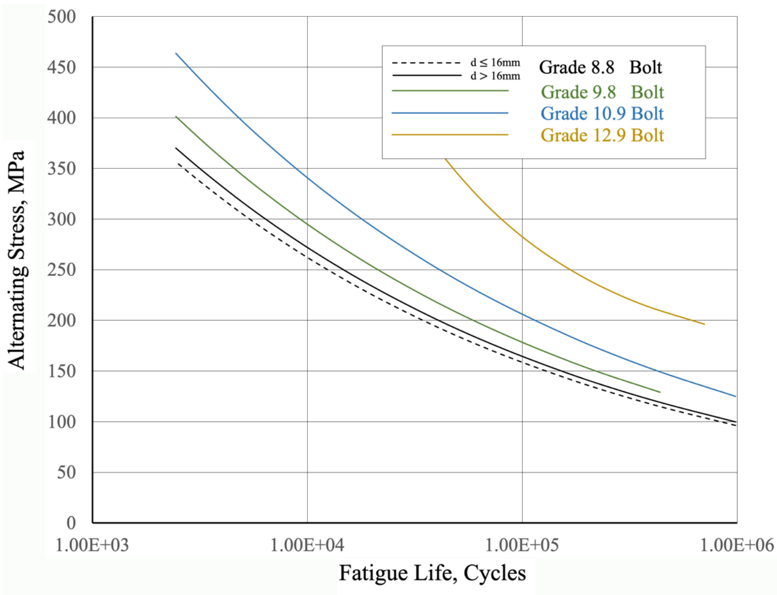

Figure 5. S-N curves for stress concentration $K_t = 4.97$

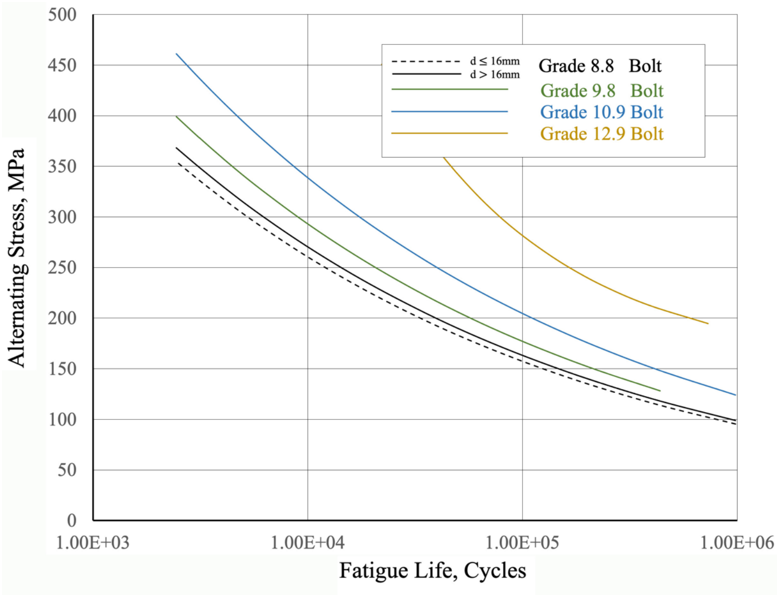

Figure 6. S-N curves for stress concentration $K_t = 5.02$

A study of bolt geometries suggests that the stress concentrations considered here could be applied to a range of bolt sizes as given in Table 5.

Table 5. Applicable thread sizes

K_t	**Coarse Thread Bolt Sizes**
4.56	Up to and including M14
4.89	M16 and M18
4.97	M20
5.02	M22 to M36

4 Damage-Equivalent Stress

Equation (6) is applicable to S-N curves with a zero mean stress hence, for the fatigue analysis of bolts with a high mean stress the value for s_{alt} used in the equation needs to represent a damage-equivalent stress. There are several methods of calculating a damage-equivalent stress, most notably, Goodman or Goodman-Haig diagram, Gerber, Soderberg and Smith-Watson-Topper. There is also a more recent damage-equivalent function proposed by Welch (2022) [10].

Again, since the calculated fatigue life is very sensitive to stress, the method of calculating the fatigue damage-equivalent stress needs to introduce the minimum of error.

The high mean stresses associated with preloaded bolts results in 'corrections' for mean stress having to be made over a large increment. The method of determining the damage-equivalent stress has to be able to deal with these large increments. This requirement virtually rules out the use of both the Goodman and Soderberg methods. Hence, Smith-Watson-Topper is probably the most reliable of the established methods of calculating a damage-equivalent stress for preloaded bolts, and can be expressed as:

$$\sigma_{equ} = \sigma_{alt} \cdot \left(1 + \frac{\sigma_{mean}}{\sigma_{alt}}\right)^{\frac{1}{2}} \tag{7}$$

However, the more recent method proposed by Welch (2022) [10] appears to provide more consistent and improved accuracy over the Smith-Watson-Topper method. This method can be expressed as:

$$\sigma_{equ} = \sigma_{alt} \cdot \left(1 + \frac{a_2 \cdot (1+R)^{a_1}}{(K_t+1)^{a_3}}\right) \tag{8}$$

Where: a_1, a_2 and a_3 are given by:

$$a_1 = b_1 + b_2 \cdot K_t \cdot \left(\frac{Fty}{E}\right)^{b_3} \tag{9}$$

$$a_2 = b_4 + b_5 \cdot \left(\frac{Fty}{E}\right)^{b_6} \tag{10}$$

$$a_3 = b_7 + b_8 \cdot \left(\frac{Fty}{E}\right)^{b_9} \tag{11}$$

With:

$b_1 = 1.854$
$b_2 = 4.224 \times 10^6$
$b_3 = 3.260$

$b_4 = -1.015$
$b_5 = 38.120$
$b_6 = 0.635$

$b_7 = 1.038$
$b_8 = -2.032 \times 10^{-6}$
$b_9 = -2.485$

The stress ratio R is given by:

$$R = \frac{\sigma_{min}}{\sigma_{max}} \tag{12}$$

5 Residual Stresses in Bolts

The method of manufacture for bolts is not prescribed in BS EN ISO 868-1 (2009) [7]. Most, if not all, bolt manufactures use thread rolling procedures to form bolt threads. These procedures result in high compressive residual stresses at the thread root, which is beneficial to fatigue performance. Thread rolling can be carried out either before or after heat treatment. Thread rolling after heat treatment requires higher operational loads than thread rolling before heat treatment. This results in higher power requirements and hence more energy consumption. Higher operational loads also lead to increased wear and hence shorter working life for the thread rolling dies. Consequently, for most manufactures, thread rolling will presumably be carried out before heat treatment in order to minimise manufacturing costs.

As an observation, BS EN ISO 868-1 (2009) [7] quotes minimum tempering temperatures of 340ºC, 380ºC and 425ºC for various bolt grades and material chemical compositions. The work by de Souza et. al. (2021) [9] would suggest that quench hardening and then tempering at these minimum temperatures would induce a tensile residual stress component. However, thread rolling before heat treatment would induce a large compressive residual stress that would not be completely removed/relaxed by the post rolling heat treatment.

Compressive residual stresses will act to reduce the maximum and minimum stresses at the thread root. This will reduce the mean stress at the thread root, hence improving the fatigue performance of the bolt, but will have no effect on the stress range. In static analyses bolt stresses are usually calculated using the bolt nominal tensile stress area. The nominal stress area for a range of bolt sizes is given in a number of standards, including BS EN ISO 868-1 (2009) [7]. The area is calculated using the mean of the pitch diameter and the minor diameter. The S-N curves presented here are applicable to stresses based on the nett section therefore, the maximum, minimum and mean stresses are given by equation (13), (14) and (15) respectively:

$$\sigma_{max} = \frac{F_{b.max(n)}}{A_{core}} + \sigma_{res} \tag{13}$$

$$\sigma_{min} = \frac{F_{b.\min(n)}}{A_{core}} + \sigma_{res} \tag{14}$$

$$\sigma_{mean} = \frac{F_{b.mean(n)}}{A_{core}} + \sigma_{res} \tag{15}$$

where $F_{b.max(n)}$, $F_{b.min(n)}$ and $F_{b.mean(n)}$ are the maximum, minimum and mean bolt loads on bolt 'n' and A_{core} is the core area of the bolt. In equations (13) to (15) the residual stress s_{res} is positive for tensile stress and negative for compressive stress. The core area is given by:

$$A_{core} = \frac{\pi \cdot D_s{}^2}{4} \tag{16}$$

where D_s is the minor diameter of the bolt thread.

An estimate of the residual stresses in the bolts used in the work by Marcelo et. al. (2011) [8] was made by iteration. Each bolt was considered in turn. A value of residual stress was assumed which was then used in equations (13) and (14), along with the maximum and minimum bolt loads given in reference [8], to calculate the maximum and minimum bolt stresses. These stresses were then used with equations (12) and (8) to calculate the damage-equivalent stress for the bolt. This stress was then used as the alternating stress s_{alt} in equation (6) to calculate a predicted life for the bolt. This calculation process was repeated, using a range assumed residual stresses, until the calculated predicted life for the bolt matched the fatigue life of 10^6 cycles, as given in reference [8].

5.1 Thread Rolling After Heat Treatment

Reference [8] considered one set of bolts manufactured from SCM 435H wire, quench hardened and then tempered at 550ºC to give a tensile strength of 1154MPa. The bolt threads were then rolled after heat treatment. The residual stress for this set of bolts was estimated to be -740MPa.

The process of thread rolling has been simulated by Furukawa and Hagiwara (2014) [11] using 3D elastic-plastic Finite Element Methods. The heat treatment process, quench hardening and tempering, was not simulated within the model hence, the results are representative of thread rolling after heat treatment. The simulation used the material properties and geometry for Grade 8.8 M10 x 1.25 bolts. A compressive residual stress at an inner layer 30mm from the thread root was calculated to be -830MPa. This is of a similar magnitude to the residual stress estimated here for the M8 x 1.25 bolts considered by Marcelo et. al. (2011) [8].

The magnitude of the residual stress in a Grade 8.8 bolt (minimum tensile stress of 800MPa) as calculated by Furukawa and Hagiwara (2014) [11] was greater than the magnitude of residual stress, as estimated in this paper, for the bolts with a tensile strength of 1154MPa as tested by Marcelo et. al. (2011) [8]. This was consistent with what had been observed in the results of the work by de Souza et. al. (2021) [9].

5.2 Thread Rolling Before Heat Treatment

Reference [8] also considered two sets of bolts that were thread rolled before heat treatment and had a final tensile strength (after heat treatment) close to the minimum requirements for Grade 10.9 bolts. One set was manufactured from AISI 4135 wire and the other from SCM 435H wire. Both sets were quench hardened and then tempered at 550ºC to give tensile strengths of 1025MPa for the bolts from AISI 4135 and 1051MPa for the bolts from SCM 435H. The residual stresses for these two set of bolts were estimated to be -679MPa for AISI 4135 and -649MPa for SCM 435H. The residual stress for a Grade 10.9 bolt with the minimum tensile stress specified in BS EN ISO 868-1 (2009) [7] (1040MPa) was then estimated to be -660MPa.

Similarly, reference [8] considered two sets of bolts that were thread rolled before heat treatment and had a final tensile strength close to the minimum requirements for Grade 12.9 bolts. Again, one set was manufactured from AISI 4135 wire and the other from SCM 435H wire. Both sets were quench hardened and then tempered at 490ºC to give tensile strengths of 1211MPa for the bolts from AISI 4135 and 1233MPa for the bolts from SCM 435H. The residual stresses were estimated to be -459MPa for AISI 4135 and -465MPa for SCM 435H. The residual stress for a Grade 12.9 bolt with the minimum tensile stress specified in BS EN ISO 868-1 (2009) [7] (1220MPa) was then estimated to be -460MPa.

Note that although the work by Marcelo et. al. (2011) [8] was primarily for Grade 10.9 bolts statistically, 33% of Grade 10.9 bolts could possibly achieve a tensile strength of 1211MPa or more. Similarly, 24% could possibly achieve a tensile strength of 1233MPa or more. Hence, the tensile strengths of 1211MPa and 1233MPa referred to above both fall within the range of Grade 10.9 bolts.

Finally, reference [8] considered two sets of bolts that were thread rolled before heat treatment and had a final tensile strength a little above the minimum requirements for Grade 10.9 bolts. Again, one set was manufactured from AISI 4135 wire and the other from SCM 435H wire. Both sets were quench hardened and then tempered at 520ºC to give tensile strengths of 1119MPa for the bolts from AISI 4135 and 1070MPa for the bolts from SCM 435H. The residual stresses were estimated to be -476MPa for AISI 4135 and -619MPa for SCM 435H.

The estimated residual stresses were plotted against tensile strength and are shown in Figure 7.

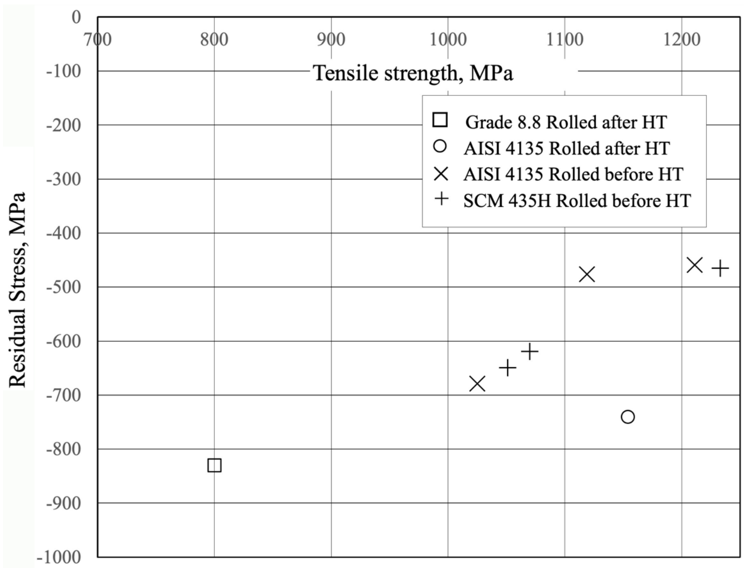

Figure 7. Residual stress vs Tensile strength

The results shown in Figure 7 indicate that extrapolating to find residual stresses outside a range of tensile strength of, say, 1000MPa to 1250MPa would produce an unreliable result and should be avoided.

Conclusions and Recommendations

In order to produce an accurate prediction of fatigue life, margins of safety, safety factors, partial safety factors or reserve factors must not be applied to the loads or calculated stresses used for the fatigue analysis.

It is more meaningful to calculate margins of safety, reserve factors or other means of expressing reliability based on predicted life rather than applied loads or stresses.

It was observed that, in general an increase in tensile strength results in improved fatigue properties. However, if a carbon steel is at or close to its maximum achievable tensile strength its fatigue performance may be impaired.

S-N curves for Grade 8.8, Grade 9.8, Grade 10.9 and Grade 12.9 have been produced for stress concentrations of 4.56, 4,89, 4.97 and 5.05 and presented in the form of an equation. The stress concentration of 4.56 is relevant for bolt sizes up to M14. The stress concentration of 4.89 is relevant to M16 and M18 bolts and the stress concentration of 4.97 is relevant to M20 bolts. Similarly, the stress concentration of 5.02 is relevant to bolt sizes within the range M22 to M36.

The residual stress in Grade 12.9 bolts can be assumed to be approximately -460MPa. This assumption is based on estimated residual stresses in bolts manufactured from AISI 4135 and SCM 435H that had tensile strengths of 1211MPa and 1233MPa respectively.

The residual stress in Grade 10.9 bolts can be assumed to be approximately -660MPa. This was the average of the results for bolts manufactured from AISI 4135 and SCM 435H that had tensile strengths of 1025MPa and 1051MPa respectively.

It was considered unreliable to extrapolate the results to determine a residual stress for Grade 8.8 and Grade 9.8 bolts. It was concluded that the residual stresses in these bolt grades would be compressive and with a higher magnitude than the residual stresses for Grade 10.9 bolts. It was recommended that the residual stresses in Grade 8.8 and Grade 9.8 should be assumed to be -680MPa. This was the residual stress associated with the bolts having lowest tensile considered, i.e. 1025MPa.

The maximum, minimum and mean stresses of the bolts should be calculated using the core area of the bolts, not the tensile area. The core area is defined by the minimum diameter of the bolt. These calculated stresses should also include the effect of the residual stresses.

The maximum and minimum stresses, which should include the effects of residual stresses, should be used to calculate the stress ratio and the damage-equivalent stress for each bolt. It is recommended that the damage-equivalent stress is calculated using the method proposed by Welch (2022) [10].

The damage-equivalent stress for each bolt can be used, along with the minimum tensile strength for the bolt grade, to calculate the bolt life. Bolt life can be calculated by means of a function that describes an appropriate S-N curve.

References

[1] British Standards Institution. BS 7608:1990, *Code of practice for Fatigue design and assessment of steel structures.* British Standards Institution, London

[2] Novoselac S, Kozak D, Ergić T, Damjanović D. *Fatigue of shaft flange bolted joints under preload force and dynamic response*. FME Transactions. 2014;42(4):269-76.

[3] Welch M. *Classical Analysis of Preloaded Bolted Joint Load Distributions*, International Journal of Structural Integrity, Volume 9 (2018), issue 4, pages 455 to 464.

[4] Welch, M. *An Analytical Study of Asymmetrical Preloaded Bolted Joints*. International Journal of Modern Research in Engineering and Technology, Volume 7 (2022), Issue 3, March 2022, Pages 6 to 11.

[5] Lehnhoff TF, Bradley A, Bunyard A. *Bolt thread and head fillet stress concentration factors*. Journal of Pressure Vessel Technology. May 2000, 122(2): Pages 180-185.

[6] Federal Aviation Administration. *Metallic Materials Properties Development and Standardization (MMPDS)*, Battelle Memorial Institute, MMPDS-03, October 2006

[7] British Standards Institution. BS EN ISO 868-1: 2009, *Mechanical properties of fasteners made of carbon and alloy steel. Part 1: Bolts, screws and studs with specified property classes – Coarse thread and fine pitch thread*. British Standards Institution, London

[8] Marcelo AL, Uehara AY, Utiyama RM, Ferreira I. *Fatigue properties of high strength bolts*. Procedia Engineering. 2011 Jan 1;10:1297-302.

[9] de Souza MF, Serrão LF, Pardal JM, Tavares SS, Fonseca MC. *Tempering influence on residual stresses and mechanical properties of AISI 4340 steel*. The International Journal of Advanced Manufacturing Technology. 2022 May;120(1):1123-34.

[10] Welch M. *An Empirical Approach to a Comprehensive Damage-Equivalent Stress for Fatigue*. FME Transactions. 2022;50(3):535-457.

[11] Furukawa A, Hagiwara M. *Estimation of the residual stress on the thread root generated by thread rolling process*. Mechanical Engineering Journal, *2*(4), pp.14-00293.

Nomenclature

A_b	Tensile area of each bolt
A_c	True contact area of the joint
A_{core}	Core area of a bolt
A_j	Total area of joint (Contact surface plus bolts)
a_1, a_2, a_3	Constants
b_1, b_2, b_3	Constants
b_4, b_5, b_6	Constants
b_7, b_8, b_9	Constants
C_1, C_2, C_3	Constants
D_s	Minor diameter of bolt thread (root diameter)
E	Young's modulus of elasticity

$F_{b(n)}$ Bolt load in bolt 'n'

$F_{b.max(n)}$ Maximum bolt load on bolt 'n'

$F_{b.mean(n)}$ Mean bolt load on bolt 'n'

$F_{b.min(n)}$ Minimum bolt load on bolt 'n'

F_p Preload in each bolt

Ftu Material ultimate tensile strength

Fty Material yield/proof stress

F_z External axial load in direction of 'z' axis

$I_{xx.j}$ Second Moment of Area of joint about 'x' axis

K_f Fatigue stress concentration factor

$K_{f.D}$ Fatigue stress concentration factor of a 'donor' S-N curve

K_t Elastic stress concentration factor

$K_{t.D}$ Elastic stress concentration factor of a 'donor' S-N curve

M_x External moment acting about 'x' axis

N_b Number of bolts in joint

N_{life} Fatigue life – Number of cycles

P_f Contact pressure at faying surface

P_p Pressure at faying surface, preload pressure

q Material notch sensitivity factor

R Stress ratio

$S_{alt.D}$ Alternating stress of a 'donor' S-N curve

$S_{alt.0}$ Alternating stress of an unnotched S-N curve

$y_{(n)}$ Coordinate of bolt 'n' (from neutral axis of joint)

σ_{alt} Alternating stress

σ_{equ} Damage-Equivalent stress

σ_{max} Maximum stress

σ_{mean} Mean stress

σ_{min} Minimum stress

σ_{res} Residual stress

4.4.2 Further Discussion

For analysis purposes, BS 7608: 1993, BSI (1993a), recommends that a design preload of two thirds the target preload should be used. In many cases it may not be necessary to carry out a full fatigue analysis if this design preload is used. When preloaded bolts are tightened using a calibrated torque wrench, friction within the bolt assembly results in a wide tolerance on the bolt preload. Using a design preload of based on two third the target makeup torque would allow for the tolerances resulting from friction and potential preload relaxation in service due to embedding of the mating surfaces.

The paper "*Fatigue Analysis of Preloaded Bolted Joints*", Welch (2022c), highlighted an anomaly in the S-N curves for AISI 4340, with a tensile strength of 1379MPa. The fatigue strengths indicated by the curves for 1379MPa AISI 4340 were less than the fatigue strengths indicated by similar curves for the same material specification but tempered to give lower tensile strengths of 862MPa and 1034MPa. This anomaly was explained by reference to work by de Souza et. al. (2022). This work showed that heat treated specimens of AISI 4340 had high tensile residual tests at the surface after quenching. The work also showed that tempering at 500°C or above resulted in compressive residual stresses. These compressive residual stresses at the surface would result in an improved fatigue performance.

The paper, Welch (2022c), concluded that;

> "in general, an increase in tensile strength results in improved fatigue properties however, if a carbon steel is at or close to its maximum achievable tensile strength its fatigue performance may be impaired."

This impairment of the fatigue performance resulting from tensile residual stresses at the surface.

As has been made clear in the paper Welch (2022c), commercially produced screws and bolts manufactured by the thread rolling process have compressive residual stresses at the thread roots. These residual stresses have a positive effect on the fatigue performance of the bolt. Machine cut threads do not benefit from residual stresses (unless they are heat treated and hardened by quenching and tempering). However, although all of the work presented has been produced with commercially produced screws and bolts in mind, the methods of analysis presented are still valid for machine cut threads.

Figures AAM P7 – Figure 3 through to P7- Figure 6 are for S-N Curves for carbon steel bolt grade materials (grade 8.8 to grade 12.9) with typical elastic stress concentration factors for ISO metric screw threads. It can be seen form hese figures show that the fatigue life of bolts is sensitive to small variations in the damage-equivalent stress. It is estimated that a deviation of 8% in stress could result in a variation of -30% to +50% in predicted life. An 8% deviation in stress is comparable to the root mean square error, or the standard deviation of the prediction made using the damage-equivalent stress function presented by Welch (2022b).

There is an inconsistency within the work presented. The statistical basis for the bolt material properties is significantly different to statistical basis of the S-N curves used for the fatigue analysis. Fortunately, these inconsistences will introduce some conservatism into any analyses. However, overall accuracy of analysis results will be indeterminate.

BS EN ISO 898:1999, BSI (2009a), does not specify the basis for determining the minimum tensile strength for bolt materials. Appendix A.3 Definitions, of MMPDS-03, (2006), defines the term *S-Basis* as:

> *"S-Basis*.—The S-value is the minimum property value specified by the governing industry specification (as issued by standardization groups such as SAE Aerospace Materials Division, ASTM, etc.) or federal or mil-itary standards for the material. (See MIL-STD-970 for order of preference for specifications.) For certain products heat treated by the user (for example, steels hardened and tempered to a designated *Ftu*), the S-value may reflect a specified quality-control requirement. Statistical assurance associated with this value is not known."

Similarly, MMPDS-03, (2006), also defines the term *A-Basis* as:

> *"A-Basis*.—The lower of either a statistically calculated number, or the specification minimum (S-basis). The statistically calculated number indicates that at least 99 percent of the population of values is

expected to equal or exceed the A-basis mechanical design property, with a confidence of 95 percent."

And MMPDS-03, (2006), also defines the term *B-Basis* as:

> "*B-Basis*.—At least 90 percent of the population of values is expected to equal or exceed the B-basis mechanical property allowable, with a confidence of 95 percent."

Hence, it is reasonable to assume that within BS EN ISO 898:1999, BSI (2009a), the term "minimum tensile strength" can be taken to indicate that at least 99% of bolts are expected to equal or exceed the material minimum mechanical properties, with a 95% confidence.

It must be assumed that the statistical basis for the best fit S-N Curves is that at least 50% are expected to equal or exceed the predicted fatigue life, with a 50% confidence.

CHAPTER 5

CONCLUSIONS AND RECOMMENDATIONS

5.1 Conclusions

The body of published works presented here have made a contribution to the understanding of preloaded bolted joints. They have highlighted the two basic types of structural bolted joints, snug tightened and preloaded, and the reasons why they have been adopted. Preloaded bolted joints are occasionally sub-divided into various categories. These sub-divisions are based on quality assurance considerations, not the way the joint is preloaded or the way the joint behaves under external loads.

The initial aim was to promote the 'best practice' in the analysis of preloaded bolted joints. Best practice includes understanding the background of methodology and its limitations.

Both snug tightened and preloaded bolted joints are defined by the loading condition on the bolts in the final joint assembly, before being subjected to external loads. Preloading bolts creates a significant contact pressure at the faying surface, which is critical to the performance of the joint. Various methods of preloading the bolts can be adopted.

The contact pressure at the faying surface of a preloaded joint is not uniform across the surface. The bolt tightening sequence combined with the elastic interaction between bolts results in differences in bolt preload among the and a non-uniform contact pressure distribution. Variations in friction coefficients of the bolts also have an influence on the variations in bolt preload and the contact pressure.

It is important to specify the appropriate type of bolted joint. In mechanical engineering, preloaded bolted joints are almost always the most appropriate. The most common likely exception is where the mechanical equipment is being attached to a civil engineering structure. In that instance the connection will be required to meet the civil structure's design standards and snug tightened joints may be the most appropriate.

It is important to use an appropriate method of analysis, applying the correct safety factors, or partial safety factors, to ensure a suitable level of quality assurance is met. Applying methods that are appropriate for snug tightened bolts to preloaded bolted joints results in the calculated minimum preload requirement being less than the actual required preload.

Many studies into the effects of bolt preload are based on a single bolt. The works presented here studied the whole joint and considered the interaction between the bolts in multi-bolted preloaded joints. They demonstrate how preloaded bolted joints perform their task and show that the bolts cannot be considered as a single entity, they have to be considered as part of a bolt group and working as part of the total joint assembly.

Engineering stress analyses have three objectives. They are intended to show a component, system or structure is fit for purpose, has structural integrity and is durable. Structural integrity can be demonstrated by analysis to determine induced stresses and producing an assessment of the joint. Durability is usually demonstrated by a fatigue assessment or, if required, a detailed fatigue analysis to show that components are capable of achieving the required operating life. Fitness for purpose requires not only structural integrity and durability, it also requires the ability to function continuously without undue deflection, wear or corrosion or other impediment that could interfere with performance.

In mechanical engineering, preloaded bolted joints quite often require a relatively large space envelope compared to the cross-section of the elements or components they connect. This can lead to joint sizes being kept to a minimum and the joint having to work at its maximum capacity.

When external tensile forces are applied to preloaded joints the contact pressure at the faying surface, which is in effect a compressive residual stress in the joint, will change. Providing the contact pressure does not reduce to zero the joint will act as if it were a single, continuous, member.

Bolts are usually installed with clearance holes in the flange. In-plane loads are supported by friction at the faying surface, not a direct, bolt bearing, shear load on the bolts. If the joint is subjected to cyclic in-plane loading and possible load reversals, the bolts have to be tightened sufficient to avoid joint slippage. This allows for in-plane load reversals to occur without movement within the joint that would lead to bolt loosening.

Maintaining a positive contact pressure at the faying surface results in a low working alternating stress range within the bolts. This in turn results in good fatigue performance for the joint.

Even when a positive means of location is employed, such as dowels, friction at the faying surface is required to prevent movement within the joint that could produce 'fretting', which again could lead to bolt loosening.

The use of computers, and the availability of specialist software such as Computer Aided Design packages and Finite Element Analysis packages, has resulted in a fundamental shift in the way engineering stress analyses are carried out. Instead of starting with an allowable stress and then calculating the minimum ruling section requirements, it has become usual practice to specify the geometry and then calculate the stresses that would occur.

5.1.1 The Preloaded Bolted Joint as a System

Each preloaded bolt influences an approximately circular region of the flanges and faying surface that surrounds it. The total active area and the effective second moment of area of the joint are less than the faying surface area and its second moment of area. Hence, the surface contact pressure around the bolt installation is higher than the mean contact pressure predicted by using the total faying surface area. Similarly, the change in bolt stress and the change in contact pressure due to the applied loads are also higher. These two effects act to cancel each other out when considering the external loads that could cause joint separation.

Shear stresses induced by in-plane loads are limited by friction at the faying surface. Bolt shear is not usually an issue provided the bolt preload can support the shear load along with the tensile load.

Provided the flanges have sufficient thickness to prevent failure due to flange bending under the contact pressure the assumption of rigid, or near rigid, flanges can be considered reasonable.

The purpose of the washer is to provide a consistent, hard, surface for the nut to react against. This results in more consistent and reliable friction coefficients irrespective of the joint flange material or surface finish.

5.1.2 Developments in Static Analysis

Prior to the work presented, there was a significant gap in the understanding of the influence external in-plain loads have on the bolts. Previous, analyses only considered bolt bending and bolt shear stress after the joint had failed and slip at the faying surface allowed the flanges to bear on the bolts. Two objectives achieved by the research was to determine the bolt shear stress and bending moment under normal working conditions, without joint failure. It was also found that bolt bending under external in-plane loads would also generate an additional tensile load.

In-plane loads induce flexural deflections of the bolts due to shear strain in the flange pack produce bending moments and additional tensile loads on the preloaded bolts. These tensile loads and bending moments can contribute to the yielding of the bolt, reducing bolt preload. This offers an explanation of why bolts with low flexural stiffness are prone to self-loosening.

Detail stresses within the bolts have an influence on their fatigue life. In-plane loads on the joint produce bending stresses in the bolts that have an effect on the fatigue life. Existing methods of calculating these bending stresses are not satisfactory. They are based on bolt bearing, which is an oversimplified, and unrealistic, model of how the bending moments on the bolts are generated. The work presented here proposes a more realistic model with improved accuracy in the calculation of bolt bending stresses. This new model allows more representative values for the bolt shear stresses to be calculated.

The work presented has shown that In-plane loads induce an additional tensile stress component in the bolt. These additional tensile stresses could be of significance bolts with a low flexural stiffness. The combined tensile and shear stresses could, in some cases, cause some bolts to exceed their limit of proportionality.

A further objective was to determine how well the bolt tightening procedure achieved the intended final preload condition. When assembling preloaded bolted joints, it is common practice to tighten bolts incrementally, following a tightening sequence starting with the bolt closest to the centroid of the bolt group. Incrementally tightening bolts helps to minimize variation in bolt preload. With incremental tightening and good friction control the bolt preloads could be within 95% to 101% of the target preload. With single pass tightening, still maintaining good friction control, the preload could be as low as

83% of the target load. Tightening sequences that started from the centroid resulted in the bolts that were preloaded to less than the target preload being located near the centroid of the bolt group, where the minimum shear loads would occur.

Torsional stiffness of the joint depends on the second polar moment of area of the flange cross-section. Similarly, the bending stiffness of the bolts, and their influence on the torsional stiffness of the joint, depends on the much smaller second moment of area of the bolt shanks. Hence, the torsional stiffness of the joint is dominated by friction at the faying surface, which arises from the bolt preload. The bolt shear and bending stresses have only a small influence on the torsional stiffness of the joint.

In-plane loads will be introduced into the flange across the interface between the flanges and the structural elements to which they are attached. This will result in a much higher, localised, shear stress at this interface. The 'intensity' of this shear stress will begin to be dispersed through the thickness of the flange, tending towards the value of the average shear stress.

The bolts closest to the interface of the flange and attached structural elements will experience flexural displacement of the bolt head greater than the displacement predicted by using the mean shear stress. This will result in greater additions tensile stresses than those predicted by the analysis. Similarly, it is possible to argue that the bolts furthest from the interface of the flange and structural elements will experience smaller bolt head flexural displacements than predicted.

It is known that for non-circular sections the 'torsional constant' is always less than the second polar moment of area and that the maximum shear stress is not necessarily at the maximum distance from the centroid. For example, for a rectangular cross-section the maximum shear stress is at the mid-positions of the longest sides.

If the maximum Von Mises stress exceeds the bolt material proof, or yield, stress the bolt material will no longer act elastically but instead will enter the plastic range and behave non-linearly and there will be some loss of the initial preload. The bolt displacement under plastic deformation will be controlled by the thickness of the flange pack.

There is a plane of symmetry at the mid-position of the flange pack laying parallel to the plane of the flange faces. This plane of symmetry will cause each of the flanges to behave as if it were attached to an infinitely solid structure.

5.1.3 Developments in Safe-Life Fatigue Analysis

It is not feasible to carry out visual inspection of the bolts within preloaded bolted joints. Removing the bolts for inspection purposes would introduce a large fatigue load cycle which would induce a significant amount of fatigue damage.

An original objective was to determine which of the existing methods of calculating a damage-equivalent stress was the more accurate and most applicable to preloaded bolts. However, the work showed that none of the methods considered were entirely suitable. The revised aim and objectives were to produce a Damage-Equivalent stress function suitable for use on preloaded bolted joints. A new damage-equivalent stress function has been presented. Earlier methods of calculating a damage-equivalent stress have their own limitations and are not accurate for high mean stresses combined with low alternating stresses, typical of preloaded bolts. The best of the other methods considered was the Smith-Watson-Topper function. However, it was found that this method can be up to 40% in error on stress. The new damage-equivalent stress function is particularly suited to high mean stress situations. It is also suitable for a wide range of elastic stress concentrations and tensile strengths, typical of those found in preloaded bolts. This new damage-equivalent function has an accuracy to within 16% with a root mean square error of 8%, a significant improvement on existing methods. It can be applied to the fatigue analysis of almost any carbon steel structure or component.

A further objective was to develop a series of S-N curve specific to high strength bolts and screws, property-class 8.8 to 12.9. S-N curves have been produced and presented for a range of stress concentrations applicable to various thread sizes. These should be of significant benefit to anyone undertaking safe-life fatigue analysis of bolts and screws.

The work presented has been produced with commercially produced screws and bolts in mind. Commercial screws and bolts, manufactured by the thread rolling process, have residual stresses at the thread roots which have a positive effect on the fatigue performance of the bolt.

- The residual stress in Property-class 12.9 bolts can be taken to be -460MPa.

- The residual stress in Property-class 10.9 bolts can be taken to be -660MPa.
- The residual stresses in Property-class 8.8 and Property-class 9.8 can be taken to be -680MPa.

The methods of analysis presented are still valid for machine cut threads. In this case there would be minimal residual stress in the thread root, only that due to the machining process.

5.2 Recommendations

The analysis methods presented in this thesis could be used as the basis for a design guide for preloaded bolted joints. Such a guide would need to include the engineering data required to allow the application of quality assurance of the design. For example, appropriate factors of safety, friction coefficients, bolt installation procedures and bolt make-up torque would need to be specified.

When preloaded bolts are tightened using a calibrated torque wrench, friction within the bolt assembly results in a wide tolerance on the bolt preload. For analysis purposes, BS 7608: 1993, BSI (1993a), recommends that a design preload of two third the target preload should be used. This would allow for the tolerances resulting from friction and potential preload relaxation in service due to embedding of the mating surfaces.

Dowels act by 'pegging' the joint to prevent slip. Dowels can be analysed by treating them as if they have the same stiffness as the area of the flange surrounding the bolts. This overestimates the stiffness of the dowels results in over estimating the load the dowels support. However, this type of analysis will demonstrate the dowels have sufficient 'engineering integrity'. The actual shear stress within a dowel would be equivalent to the shear stress at the faying surface local to the dowel's position.

In general, long bolts with a grip length of four or more times the nominal bolt diameter should be avoided. If they cannot be avoided then some form of thread locking should be used. It is also recommended that a 20% relaxation of preload early in the bolt's life should be assumed. The design load should reflect the loss of preload.

For non-circular sections, the true shear stress is always greater than that predicted by using the second polar moment of area. Given this, it is recommended that, wherever possible, the calculation of the bolt head flexural displacement, the resulting bending moment and additional tensile stress in the bolt should be calculated using an appropriate torsional constant for the flange geometry. The previous conclusions on the way the shear stress is introduced into the flanges and the shear stress intensity is dispersed through the thickness of the flange will still hold true. The bolts closest to the attached structural elements will experience bolt head flexural displacement, in the plane of the faying surface, greater than the predicted displacement. Again, this will result in greater additions tensile stresses than those predicted by the analysis. Similarly, the bolts furthest from the attached structural elements will experience smaller bolt head flexural displacements than predicted.

It is recommended that, when classical methods are used in computer-based applications such as spreadsheets, MathCAD© or SMath© Studio then parametric geometry and loads are used. Any geometry data should only need to be entered into the calculation once, any related geometry should be automatically calculated within the application. Similarly, Load data should only need to be entered once and any load combinations calculated automatically. This will 'program' the calculations into a 'model'. All the definitions of geometry should kept together within one section of the application document. Similarly, all the load data should be kept within one section. This is not as easy as it sounds and will take practice for it to become second nature. The benefits are that it will be easier to implement changes to the model as the design progresses and will reduce the risk of errors, particularly from failing to make an update to geometry because of multiple entries. With this type of model it is relatively easy, and fast, to study the effect of design changes before they are implemented. This type of model can also be used to investigate the effects of incidents that could affect structural integrity. It can also be used to study the effect of any repairs made post manufacture.

It is also recommended that the 'right hand rule' is used when defining loads. This practice will reduce the possibility of error, particularly when combining results for load combinations.

5.3 Further Work

5.3.1 Validation of the bolt bending theory

The bolt bending theory, Welch (2018b), should be further validated using both Finite Element methods and experimental testing.

One of the objectives of this work should be to determine, whether or not, the predicted additional tensile loads resulting from in-plane external loads are generated.

5.3.2 Develop the Damage-Equivalent Stress Function

The damage-equivalent stress function should be tested to see if can also be applied to other materials, in particular stainless steels. Other material could include Aluminium and Titanium.

This may require the numerical constants, b_1 to b_9, to be defined for each of the additional materials being considered. This could then subsequently lead to further empirical curve fitting of these constants against other material properties.

The fatigue analysis of composite materials considers each constituent material individually. The damage-equivalent function could be tested for its application to various constituent materials. Again, this may require the redefinition of the numerical constants and further empirical curve fitting. Areas that should be investigated are the relevance of fatigue stress concentration factors and the application of analysis methods based on notch sensitivity.

5.3.3 Develop further S-N Curves

Develop further S-N curves for stainless steel bolts.

Methods based on notch sensitivity should be used to modify S-N curves for materials with chemical compositions similar to those used for stainless steel bolts. Ideally, these S-N curves should be expressed as functions, predicting fatigue life based on the equivalent stress.

5.3.4 Develop Statistical Methods

Develop statistical methods to perform probabilistic analysis of bolt fatigue.

- Bolt material properties are specified for Basis A. That is, at least 99% of bolts are expected to equal or exceed the material minimum mechanical properties, with a 95% confidence.
- The S-N curves are based on 50% of bolts being expected to equal or exceed any predicted life, with 50% confidence.

It is desirable to be able to carry out a fatigue analysis to any chosen confidence level.

5.3.5 Develop Rotscher's Pressure Cone

Development of Rotscher's Pressure cone.

- Possibly consider the through flange compressive stress at having a 'barrel' shape.
- Possibly use 'beams on elastic foundations' as a means of defining the cone/barrel diameter.
- Include edge effects on the shape of the pressure cone contact area.

5.3.6 Develop Analysis of Dowels

Try to answer the questions:

- What actually happens to dowels under in-plane loads.
- What load do they really carry.

The dowel shear loads may ultimately depend on a function of the difference between the static and dynamic friction coefficients at the faying surface, as well as the applied external in-plane loads.

References

American Institute of Steel Construction, (1989), "*Specification for structural steel buildings – Allowable Stress Design and Plastic Design*". AISC, June 1, 1989.

American Institute of Steel Construction, (2004a), "*Steel Design Guide 4: Extended End-Plate Moment Connections*". AISC, April, 2004.

American Institute of Steel Construction, (2004b), "*Specification for Structural Joints Using ASTM A325 or A490 Bolt"*, AISC, June 30, 2004

American Institute of Steel Construction, (2005), "*Steel Construction Manual"*. AISC, December 2005

American Society of Mechanical Engineers, (2010), ASME PCC-1-2010 "*Guidelines for Pressure Boundary Bolted Flange Joint Assembly*", American Society of Mechanical Engineers.

David Archer, (2010), "*Pressure Distribution and Calculation of Pressure Cone Angle*", Fastener Technology International, April 2010

Davidson, B. Owens, G.W. editors, (2012), "*Steel Designers' Manual*", The Steel Construction Institute, Wiley-Blackwell, 2012

Richard T. Barrett, (1990), "*Fastener Design Manual*", NASA Reference Publication 1228, 1990

C. Batho and E.H. Bateman, (1934), "*Investigations on Bolts and Bolted Joints, Second Report of the Steel Structures Research Committee,*" London, 1934.

British Standards Institution, (1969a), BS 4395-1:1969 "*High strength friction grip bolts and associated nuts and washers for structural engineering metric series – Part 1: General Grade*", British Standards Institution, London.

British Standards Institution, (1969b), BS 4395-2:1969 "*High strength friction grip bolts and associated nuts and washers for structural engineering metric series – Part 2: Higher grade bolts and nuts and general grade washers*", British Standards Institution, London.

British Standards Institution, (1970), BS 4604-1:1970 "*The use of high strength friction grip bolts in structural steelwork metric series – Part 1: General grade*", British Standards Institution, London.

British Standards Institution, (1992), BS EN 20898-1:1992, "*Mechanical properties of fasteners – Part 1: Bolts, Screws and Studs*", British Standards Institution, London.

British Standards Institution, (1993a), BS 7608: 1993, "*Code of practice for fatigue design and assessment of steel structures*", British Standards Institution, London.

British Standards Institution, (1993b), BS 7644-1:1993 "*Direct tension indicators Part 1: Specification for compressible washers*", British Standards Institution, London.

British Standards Institution, (1993c), BS 7644-2:1993 "*Direct tension indicators Part 2: Specification for nut face and bolt face washers*", British Standards Institution, London.

British Standards Institution, (1964), BS 3580:1964, "*Guide to the design considerations on: The strength of screw threads*", British Standards Institution, London.

British Standards Institution, (2001), BS 3692:2001, ISO *metric precision hexagon bolts, screws and nuts – specification*, British Standards Institution, London.

British Standards Institution, (2005), BS EN 1993-1-8:2005 "*Eurocode 3: Design of steel structures - Part 1-8: Design of joints*", British Standards Institution, London.

British Standards Institution, (2009a), BS EN ISO 898:2009, "*Mechanical properties of fasteners made of carbon steel and alloy steel Code*", British Standards Institution, London.

British Standards Institution, (2009b), BS EN ISO 3506-1:2009, "*Mechanical properties of corrosion-resistant stainless steel fasteners Part 1: Bolts, screws and studs*", British Standards Institution, London.

British Standards Institution, (2009c), BS EN ISO 3506-2:2009, "*Mechanical properties of corrosion-resistant stainless steel fasteners Part 2: Nuts*", British Standards Institution, London.

British Standards Institution, (2009d), BS EN ISO 3506-3:2009, "*Mechanical properties of corrosion-resistant stainless steel fasteners Part 3: Set screws and similar fasteners not under tensile stress*", British Standards Institution, London.

British Standards Institution, (2013), BS EN 13001-3-1:2013 "*Cranes - General Design - Part 3-1: Limit States and proof competence of steel structure*", British Standards Institution, London.

Budynas R, Nisbett J K, (2006), "*Shigley's Mechanical Engineering Design". 8th* edition. McGraw Hill, Primis Online, ISBN 0-390-76487-6

ESDU, (2005), "*Analysis of pretensioned bolted joints subject to tensile (separating) forces"*. ESDU 85021. The Royal Aeronautical Society.

ESDU, (2006), "*Fatigue damage and life under random loading"*. ESDU 06009. The Royal Aeronautical Society.

Federal Aviation Administration, (2006), "*Metallic Materials Properties Development and Standardization (MMPDS)"*, Battelle Memorial Institute, MMPDS-03, October 2006.

Furukawa A, Hagiwara M., (2015), "*Estimation of the residual stress on the thread root generated by thread rolling process"*. Mechanical Engineering Journal, *2*(4), pp.14-00293.

Krishnamurthy, N. and Graddy, D., (1976), "*Correlation Between 2- and 3-Dimensional Finite Element Analysis of Steel Bolted End Plate Connections*", Computers and Structures, Vol. 6 (4/5), 381-389, August/October.

Krishnamurthy, N. (1978). "*A Fresh Look at Bolted End- Plate Behavior and Design*" Engineering Journal, AISC, 15(2), 39-49.

Krishnamurthy N, (1999), "*The Road to a Code*", Mysore, India, 1999 https://www.semanticscholar.org/paper/THE-ROAD-TO-A-CODE-Krishnamurthy/286c7b6f8ad9cc64c4e5044453d76d0c0b28247c

Kulak, G.L., Fisher, J.W. and Struik, J.H., (2001), "*Guide to design criteria for bolted and riveted joints*" second edition.

Lehnhoff TF, Bradley A, Bunyard A., (2000), "*Bolt thread and head fillet stress concentration factors"*. Journal of Pressure Vessel Technology. May 2000, 122(2): Pages 180-185.

Leitner M, Stoschka M, Schanner R, Eichlseder W., (2012), *Influence of high frequency peening on fatigue of high-strength steels*. FME transactions. 2012;40(3):99-104.

Marcelo AL, Uehara AY, Utiyama RM, (2011), Ferreira I." *Fatigue properties of high strength bolts"*. Procedia Engineering. 2011 Jan 1;10:1297-302.

McMillan AJ, Jones R., (2020) "*Combined effect of both surface finish and sub-surface porosity on component strength under repeated load conditions"*. Engineering Reports. 2020 Sep;2(9):e12248.

Novoselac S, Kozak D, Ergić T, Damjanović D., (2014), "*Fatigue of shaft flange bolted joints under preload force and dynamic response"*. FME Transactions. 2014;42(4):269-76.

Pástor, M. et al. (2018), *The use of Optical Methods in the Analysis of Areas With Stress Concentration*. Journal of Mechanical Engineering – Strojnicky časopis, Volume 68, Issue 2, pages 61 to 76.

Walter D Pilkey, (1997), "*Peterson's Stress Concentration Factors".* 2nd edition, 1997. John Wiley and Sons Limited, 2017, ISBN 0-471-53849-3

Research Council on Riveted and Bolted Structural Joints, (1951), "*Specifications for Assembly of Structural Joints Using High Tensile Steel Bolts*", American Institute of Steel Construction, January 1951

Rotscher, F. (1927) *Die Maschinenelements*. Julius Springer, Berlin, Germany.

de Souza MF, Serrão LF, Pardal JM, Tavares SS, Fonseca MC. (2022), :*Tempering influence on residual stresses and mechanical properties of AISI 4340 steel"*. The International Journal of Advanced Manufacturing Technology. 2022 May;120(1):1123-34.

Akbar R. Tamboli, (2017), "*Handbook of Structural Steel Connection Design and Details*". 3rd edition. McGraw Hill, 2017, ISBN 978-1-25-958552-4

Verein Deutscher Ingenieure (Association of German Engineers), (2003), VDI 2230 Part 1. 2003, *"Systematic calculation of high duty bolted joints with one cylindrical bolt"*, Verein Deutscher Ingenieure, Dusseldorf.

Verein Deutscher Ingenieure (Association of German Engineers), (2014), VDI 2230 Part 2. 2014, *"Systematic calculation of highly stressed bolted joints Multi bolted joints"*, Verein Deutscher Ingenieure, Dusseldorf.

Michael Welch, (2018a), "*Classical Analysis of Preloaded Bolted Joint Load Distributions*". International Journal of Structural Integrity. Vol. 9 (2018), No. 4, pages 455 – 456.
https://www.emeraldinsight.com/doi/abs/10.1108/IJSI-07-2017-0045

Michael Welch, (2018b), "*Analysis of Bolt Bending in Preloaded Bolted Joints*". Journal of Mechanical Engineering – Strojnicky časopis. Vol. 68 (2018), Issue 3, pages 183-194.
https://doi.org/10.2478/scjme-2018-0034

Michael Welch, (2019), *"A Paradigm for the Analysis of Preloaded Bolted Joints"*. Journal of Mechanical Engineering – Strojnicky časopis, Volume 69 (2019), Issue 1, pages 143 to 152.
https://doi.org/10.2478/scjme-2019-0012

Michael Welch, (2021), "*Bolted Joint Preload Distribution From Torque Tightening*". Journal of Mechanical Engineering – Strojnicky časopis, Volume 71 (2021), Issue 2, pages 329 to 342.
https://doi.org/10.2478/scjme-2021-0039

Michael Welch, (2022a), "*An Analytical Study of Asymmetrical Preloaded Bolted Joints*". International Journal of Modern Research in Engineering and Technology, Volume 7 (2022), Issue 3, March 2022, Pages 6 to 11.
https://www.ijmret.org/paper/V7I3/8954175862.pdf

Michael Welch, (2022b), "*An Empirical Approach to a Comprehensive Damage-Equivalent Stress for Fatigue*". FME Transactions. 2022;50(3):535-457.
https://www.mas.bg.ac.rs/_media/istrazivanje/fme/vol50/3/14_m._welch.pdf
DOI: 10.5937/fme2203535W

Michael Welch, (2022c), "*Fatigue Analysis of Preloaded Bolted Joints*". FME Transactions. 2022;50(4):607-614.
https://scindeks-clanci.ceon.rs/data/pdf/1451-2092/2022/1451-20922204607W.pdf
DOI: 10.5937/fme2204607W

Welch M, (2023), "*Supplementary Material to: An Empirical Approach to a Comprehensive Damage-Equivalent Stress for Fatigue*". ResearchGate publication 366352671.
https://www.researchgate.net/publication/366352671_Supplementary_Material_to_An_empirical_approach_to_a_universal_damage-equivalent_stress_function_for_fatigue
DOI: 10.13140/RG.2.2.31800.01283

Appendix A: Analysis of Bending Induced Bolt Tension

Introduction

This appendix contains the detailed analysis which was the basis for the analysis presented in section "*3.1 Bending Induced Bolt Tension*" of the paper "*Analysis of Bolt bending in Preloaded Bolted Joints*", Welch (2018b).

A1 – Bolt Extension

Assume that the bolt is installed into a clearance hole and that the transvers load $F_{s.b_{(n)}}$ is transmitted from the flanges to the bolt head and nut by friction. The free body diagram for the bolt is illustrated in figure A1.

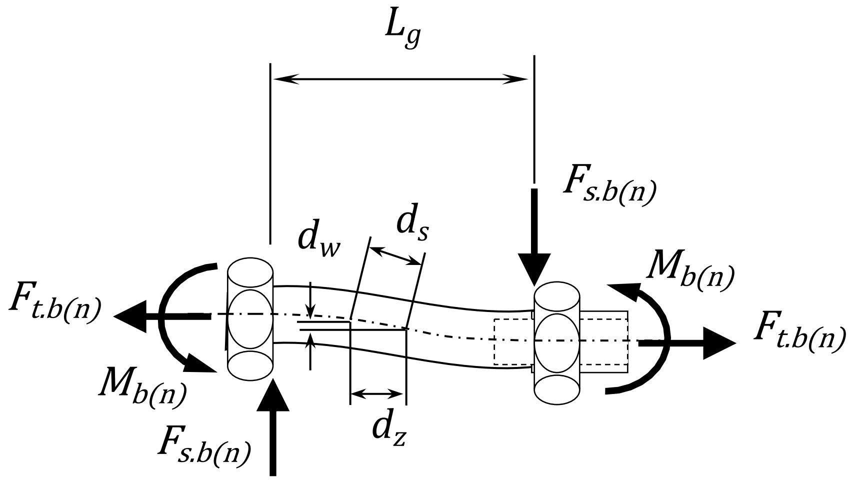

Figure A1. Bolt Freebody Diagram

Referring to Figure A1, the extended length of an element is:

$$ds = \sqrt{dz^2 + dw^2}$$

Where: ds and dz are incremental lengths along the centreline of the bolt and dw is an incremental deflection at the bolt centreline.

Then:

$$ds = dz \cdot \sqrt{1 + \left(\frac{dw}{dz}\right)^2}$$

which can be approximated as:

$$ds = dz \cdot \left(1 + \frac{1}{2} \cdot \left(\frac{dw}{dz}\right)^2\right) \tag{A1}$$

The extended length of the bolt can be given by:

$$Extended\ length = L + \delta_z = \int_0^L ds$$

Using the term for ds given in equation (A1):

$$L + \delta_z = \int_0^L \left(1 + \frac{1}{2} \cdot \left(\frac{dw}{dz}\right)^2\right) dz$$

Hence:

$$\delta_z = \frac{1}{2} \cdot \int_0^L \left(\frac{dw}{dz}\right)^2 dz \tag{A2}$$

Treating the bolt as a beam, for moment equilibrium about the bolt head:

$$E_b \cdot I_b \cdot \frac{d^2w}{dz^2} = F_{s.b(n)} \cdot (L_g - z) - M_{s.b(n)} \tag{A3}$$

Where: E_b is Young's Modulus of Elasticity for the bolt material, I_b is the effective second moment of area for the bolt shank, $F_{s.b(n)}$

Integrating equation (A3):

$$E_b \cdot I_b \cdot \frac{dw}{dz} = F_{s.b(n)} \cdot \left(L_g \cdot z - \frac{z^2}{2}\right) - M_{s.b(n)} \cdot z + C_1 \tag{A4}$$

At: $z = 0$ $\quad \frac{dw}{dz} = 0$ $\qquad$ hence $\; C_1 = 0$

Also, at: $z = L_g$ $\quad \frac{dw}{dz} = 0$

Hence:

$$M_{s.b(n)} = \frac{F_{s.b(n)} \cdot L_g}{2}$$

Then equation (A4) can be written as:

$$E_b \cdot I_b \cdot \frac{dw}{dz} = F_{s.b\,(n)} \cdot \left(L_g \cdot z - \frac{z^2}{2}\right) - \frac{F_{s.b\,(n)} \cdot L_g}{2} \cdot z$$

Simplifying:

$$\frac{dw}{dz} = \frac{F_{s.b\,(n)}}{2 \cdot E_b \cdot I_b} \cdot \left(L_g \cdot z - z^2\right) \qquad \text{(A5)}$$

Using equation (A5) in equation (A2):

$$\delta_{z\,(n)} = \frac{1}{2} \cdot \int_0^L \left(\frac{F_{s.b\,(n)}}{2 \cdot E_b \cdot I_b} \cdot \left(L_g \cdot z - z^2\right)\right)^2 dz$$

Expanding:

$$\delta_{z\,(n)} = \frac{1}{8} \cdot \left(\frac{F_{s.b\,(n)}}{E_b \cdot I_b}\right)^2 \cdot \int_0^L \left({L_g}^2 \cdot z^2 - 2 \cdot L_g \cdot z^3 + z^4\right) dz$$

Integrating:

$$\delta_{z\,(n)} = \frac{1}{8} \cdot \left(\frac{F_{s.b\,(n)}}{E_b \cdot I_b}\right)^2 \cdot \left(\frac{{L_g}^2 \cdot L^3}{3} - \frac{L_g \cdot L^4}{2} + \frac{L^5}{5}\right) \qquad \text{(A6)}$$

For an infinite through flange stiffness, $L = L_g$, hence, from equation A6:

$$\delta_{z\,(n)} = \frac{1}{8} \cdot \left(\frac{F_{s.b\,(n)}}{E_b \cdot I_b}\right)^2 \cdot \left(\frac{{L_g}^5}{3} - \frac{{L_g}^5}{2} + \frac{{L_g}^5}{5}\right) \qquad \text{(A7)}$$

Simplifying:

$$\delta_{z\,(n)} = \frac{{F_{s.b}}^2_{(n)} \cdot {L_g}^5}{240 \cdot (E_b \cdot I_b)^2} \qquad \text{(A8)}$$

N.B. Equation (A8) is the same as equation (12) of the paper by Welch (2018b).

The axial extension given by equation (A8) results in an axial load in addition to the bolt preload. This additional tensile bolt load component is given by:

$$F_{t.b\,(n)} = \frac{{F_{s.b}}^2_{(n)} \cdot {L_g}^4 \cdot A_b}{240 \cdot E_b \cdot {I_b}^2} \qquad \text{(A9)}$$

Similarly, equation (A9) is the same as equation (13a) of the paper by Welch (2018b).

A2 – Flange Thickness Reduction

The axial extension given by equation (A8) is based on an infinite through flange stiffness. Hence, $F_{t.b_{(n)}}$ given by equation (A9) the additional tensile bolt load component that would be produced by the shear load $F_{s.b_{(n)}}$ if the through flange stiffness were infinite.

When the bolt extends/stretches there is an increase in bolt tension. The increase in bolt tension will be reacted into the flanges hence, there will also be a reduction in the thickness of the flange pack.

If the flange stiffness k_{jp} is considered then the final bolt length would be $L = L_g - \delta_f$ where δ_f is the reduction in flange thickness. Using this term in equation (A6) gives:

$$\delta_{z_{(n)}} = \frac{1}{8} \cdot \left(\frac{F_{s.b_{(n)}}}{E_b \cdot I_b} \right)^2 \cdot \left(\frac{{L_g}^2 \cdot \left(L_g - \delta_f\right)^3}{3} - \frac{L_g \cdot \left(L_g - \delta_f\right)^4}{2} + \frac{\left(L_g - \delta_f\right)^5}{5} \right) \tag{A10}$$

The magnitude of the flange thickness reduction δ_f is small compared to the magnitude of the bolt grip length L_g. Hence, expanding equation (A11) and considering terms of ${\delta_f}^n$ where n > 1 as negligible gives:

$$\delta_{z_{(n)}} = \frac{1}{8} \cdot \left(\frac{F_{s.b_{(n)}}}{E_b \cdot I_b} \right)^2 \cdot \left(\frac{{L_g}^5}{3} - {L_g}^4 \cdot \delta_f - \left(\frac{{L_g}^5}{2} - 2 \cdot {L_g}^4 \cdot \delta_f \right) + \frac{{L_g}^5}{5} - {L_g}^4 \cdot \delta_f \right)$$

Which reduces to:

$$\delta_{z_{(n)}} = \frac{1}{8} \cdot \left(\frac{F_{s.b_{(n)}}}{E_b \cdot I_b} \right)^2 \cdot \left(\frac{{L_g}^5}{3} - \frac{{L_g}^5}{2} + \frac{{L_g}^5}{5} \right)$$

This is identical to equation (A7).

Then:

$$\delta_{z_{(n)}} = \frac{F_{t.b_{(n)}} \cdot L_g}{E_b \cdot A_b} + \frac{F_{t.b_{(n)}}}{k_{jp}}$$

Rearranging:

$$F_{t.b_{(n)}} = \frac{\delta_{z_{(n)}}}{\dfrac{L_g}{E_b \cdot A_b} + \dfrac{1}{k_{jp}}} \tag{A11}$$

Using equation (A8) in equation (A11)

$$F_{t.b_{(n)}} = \frac{F_{s.b_{(n)}}^{\;2} \cdot L_g^{\;5}}{240 \cdot (E_b \cdot I_b)^2 \cdot \left(\dfrac{L_g}{E_b \cdot A_b} + \dfrac{1}{k_{jp}}\right)}$$

Simplifying:

$$F_{t.b_{(n)}} = \frac{F_{s.b_{(n)}}^{\;2} \cdot L_g^{\;4} \cdot A_b}{240 \cdot E_b \cdot I_b^{\;2} \cdot \left(1 + \dfrac{A_b \cdot E_b}{k_{jp} \cdot L_g}\right)} \tag{A12}$$

Equation (A12) is the same as equation (13b) of the paper by Welch (2018b).

Appendix B: Supplementary Material

Supplementary Material to: An Empirical Approach to a Comprehensive Damage-Equivalent Stress for Fatigue

Michael Welch

Michael A Welch (Consulting Engineers) Limited, UK

This supplementary material to the paper "*An Empirical Approach to a Comprehensive Damage-Equivalent Stress for Fatigue*" presents plots of all the results data from the research work, including results not presented in the paper.

1 INTRODUCTION

The paper "*An Empirical Approach to a Comprehensive Damage-Equivalent Stress for Fatigue*" by Welch (2022), reference [1], uses twenty S-N curves, taken from MMPDS-03 (2006) reference [2], to derive a damage-equivalent stress function for fatigue. The damage-equivalent stress is the alternating stress under fully reversal load conditions that would produce an amount of damage equivalent to that caused by the combination of both an alternating and a non-zero mean stress. A further eighteen S-N curves, also taken from MMPDS-03 (2006) [2], were used in validating this damage-equivalent stress function.

The validation process compared the damage-equivalent stress function for fatigue with existing methods of calculating damage-equivalent stresses, reference ESDU 06009 (2006) [3]. The other methods used for comparison were the modified Goodman diagram or Haig diagram and other methods proposed by Gerber, Soderberg and Smith-Watson-Topper.

The paper by Welch (2022) [1] presents plots of calculated results using the damage-equivalent stress function plus the four other methods used for comparison relating to just six of the available S-N curves. These six curves represented the bounding cases for each of the methods used.

Supplementary Material

The supplementary material being presented here comprises plots for all thirty-eight S-N curves used for the analysis and validation. Each figure includes the S-N curve being considered.

2. SUPPLEMENTARY PLOTS

Figures S1 to S20 are respectively related to data-sets 1 to 20 referred to within reference [1]. Figures 21 to 38 are for the additional S-N curves that were used in the validation. Plots that were included within reference [1] are identified.

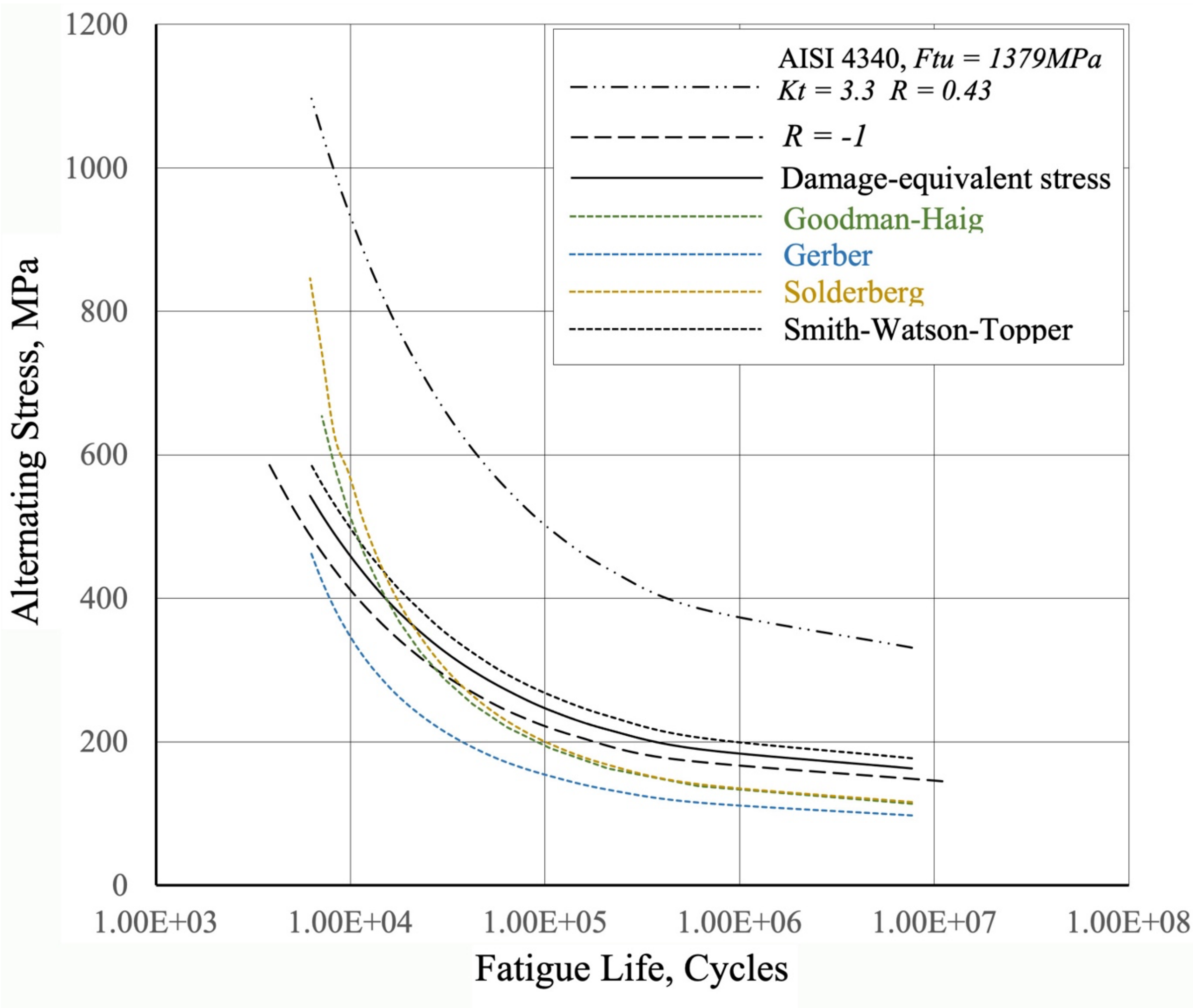

Figure S1. AISI 4340, *Ftu = 1379MPa(200ksi)*, $K_t = 3.3$ $R = 0.43$

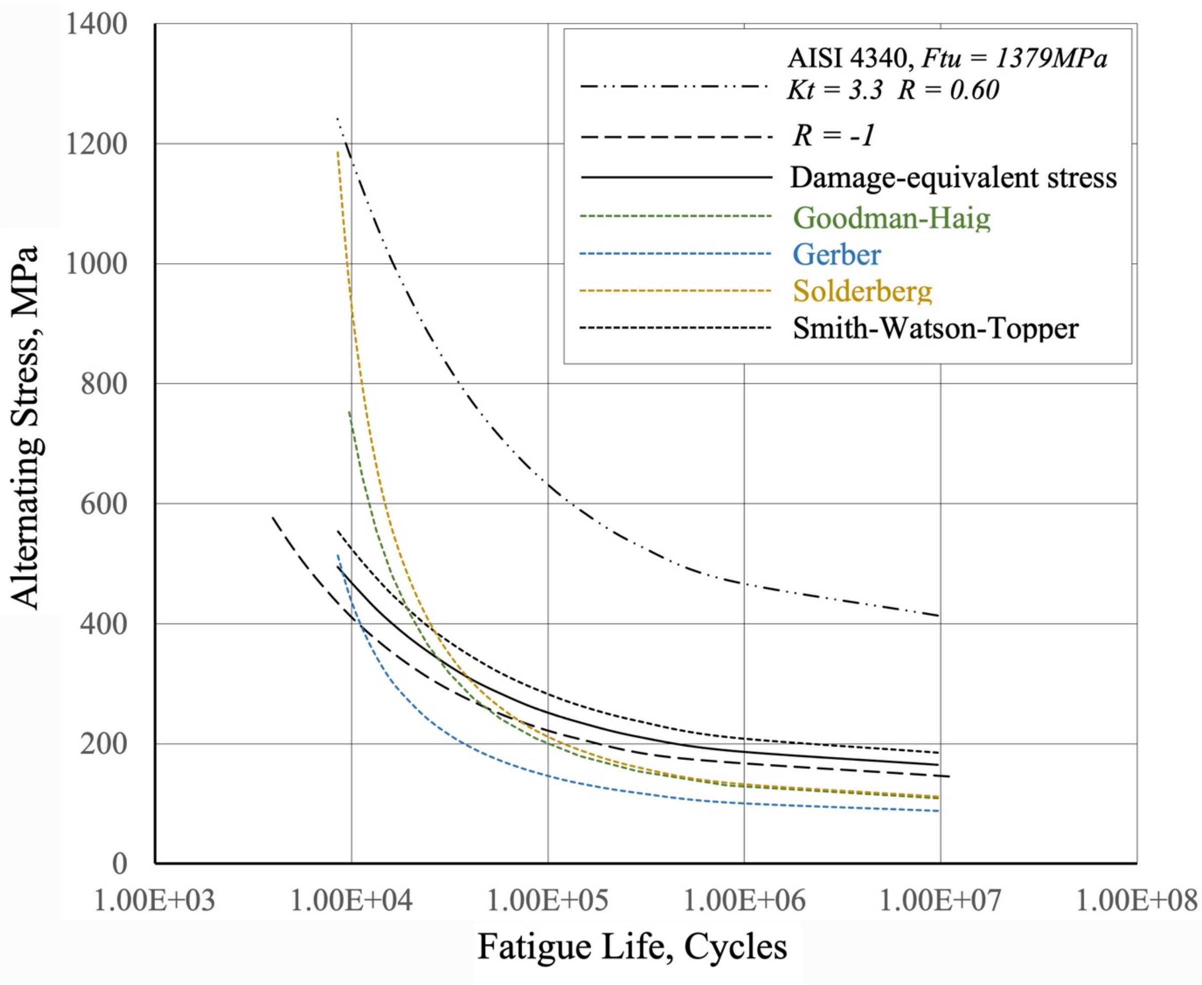

Figure S2. AISI 4340, *Ftu = 1379MPa(200ksi)*, $K_t = 3.3$ $R = 0.60$

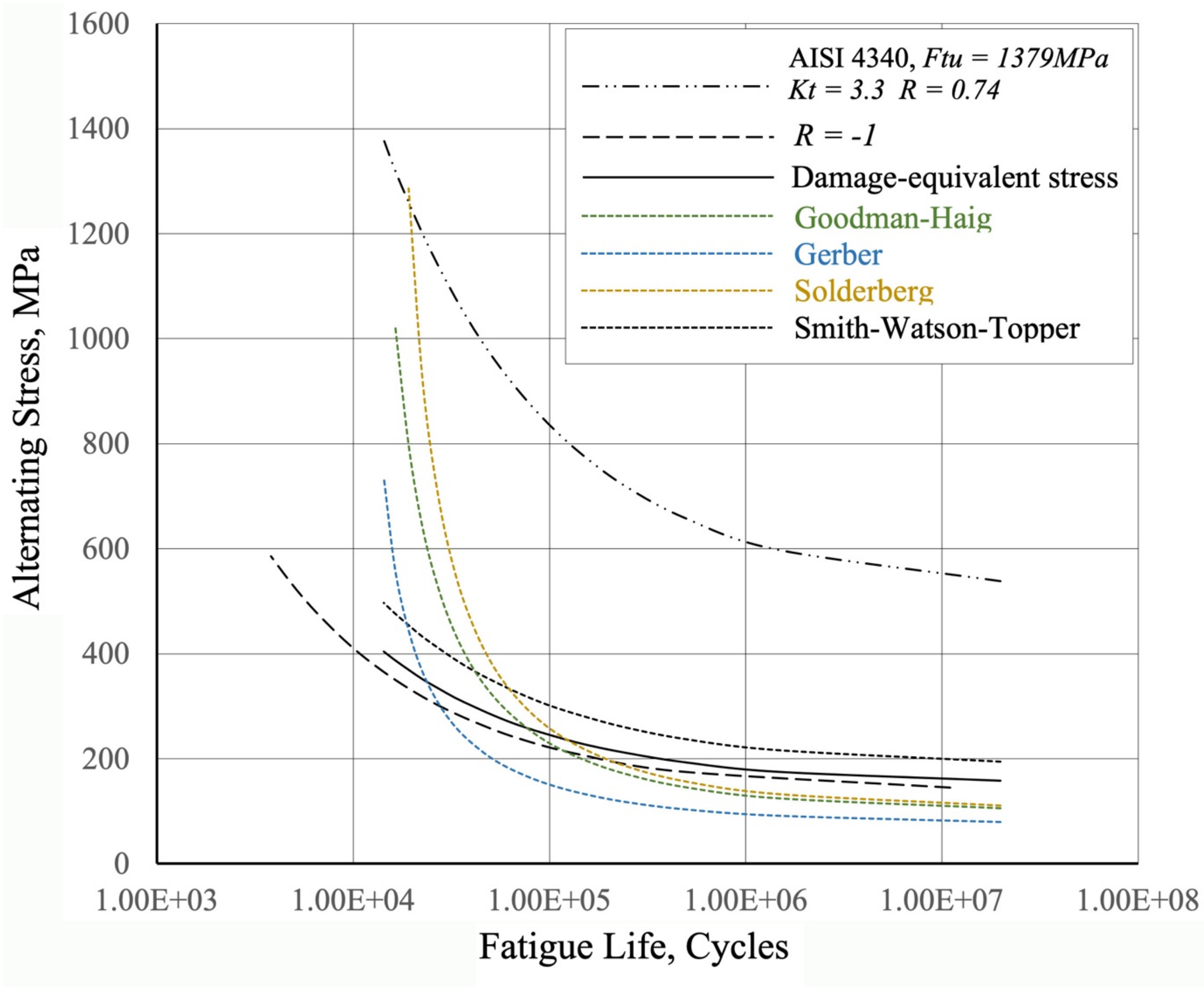

Figure S3. AISI 4340, *Ftu = 1379MPa(200ksi)*, $K_t = 3.3$ $R = 0.74$

Figure S3 is equivalent to Figure 16 of reference [1].

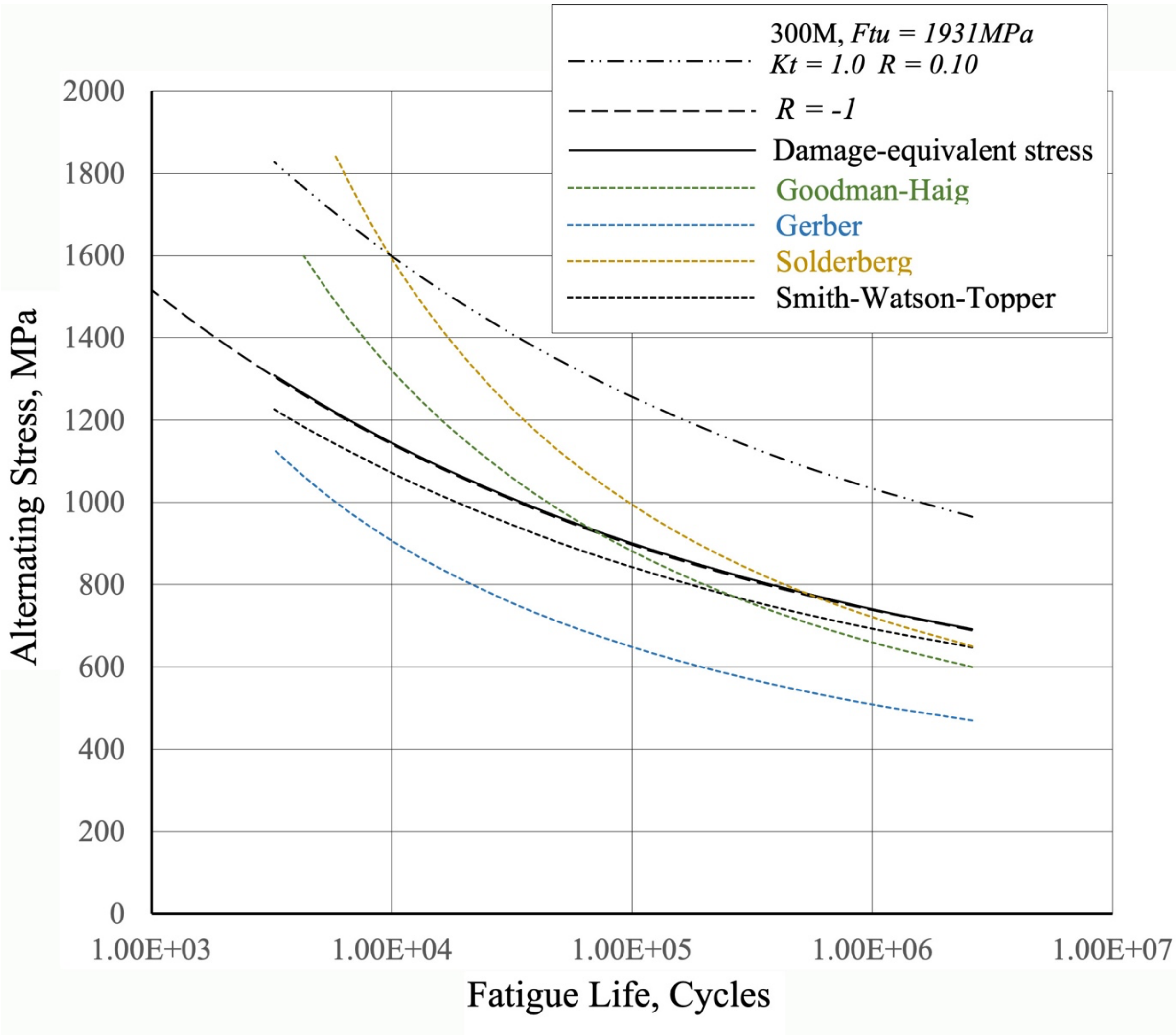

Figure S4. 300M, *Ftu = 1931MPa(280ksi)*, K_t = *1.0 R = 0.10*

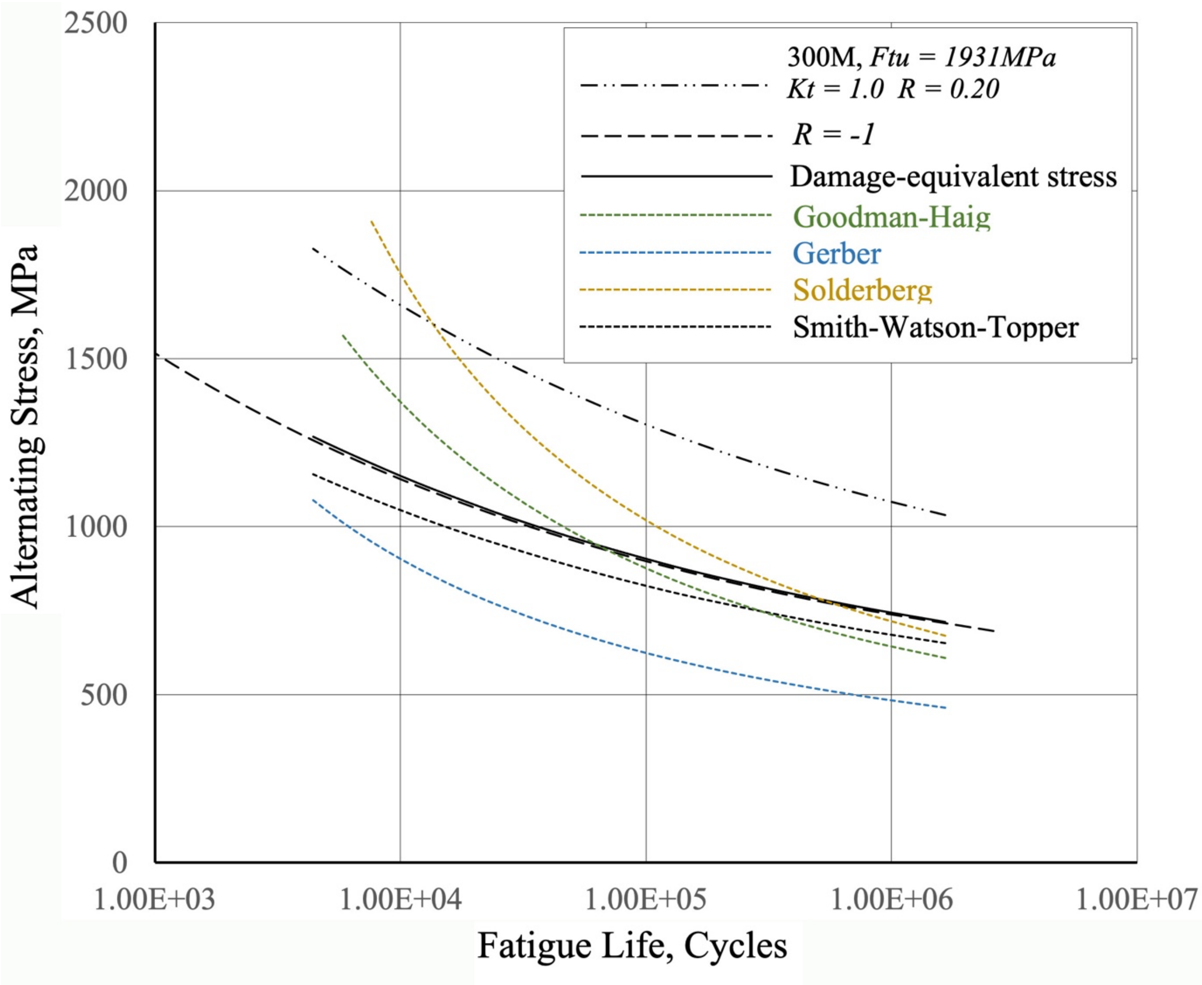

Figure S5. 300M, *Ftu = 1931MPa(280ksi)*, $K_t = 1.0$ $R = 0.20$

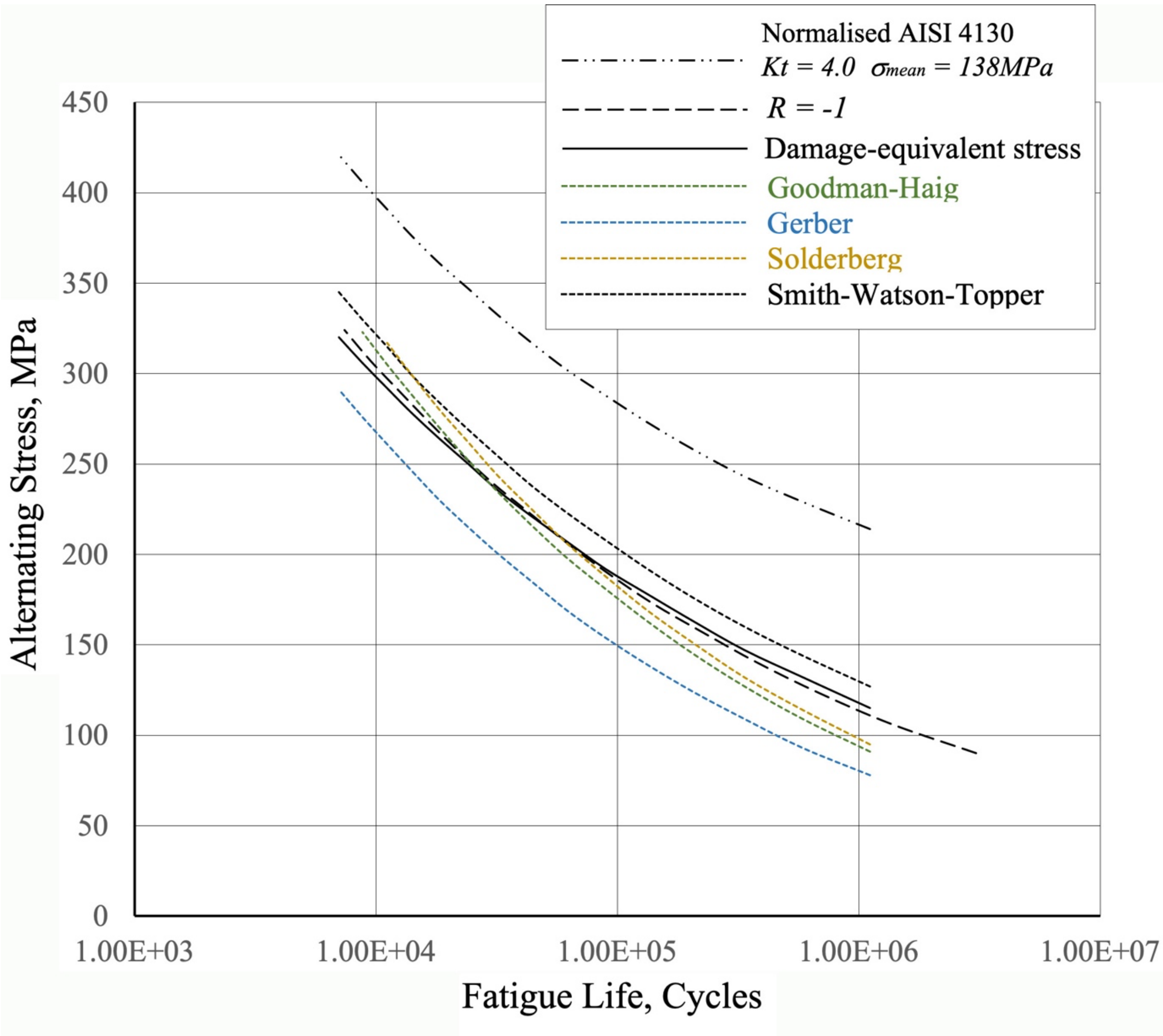

Figure S6. Normalised AISI 4130, K_t *= 4.0* s_{mean} *= 138MPa(20ksi)*

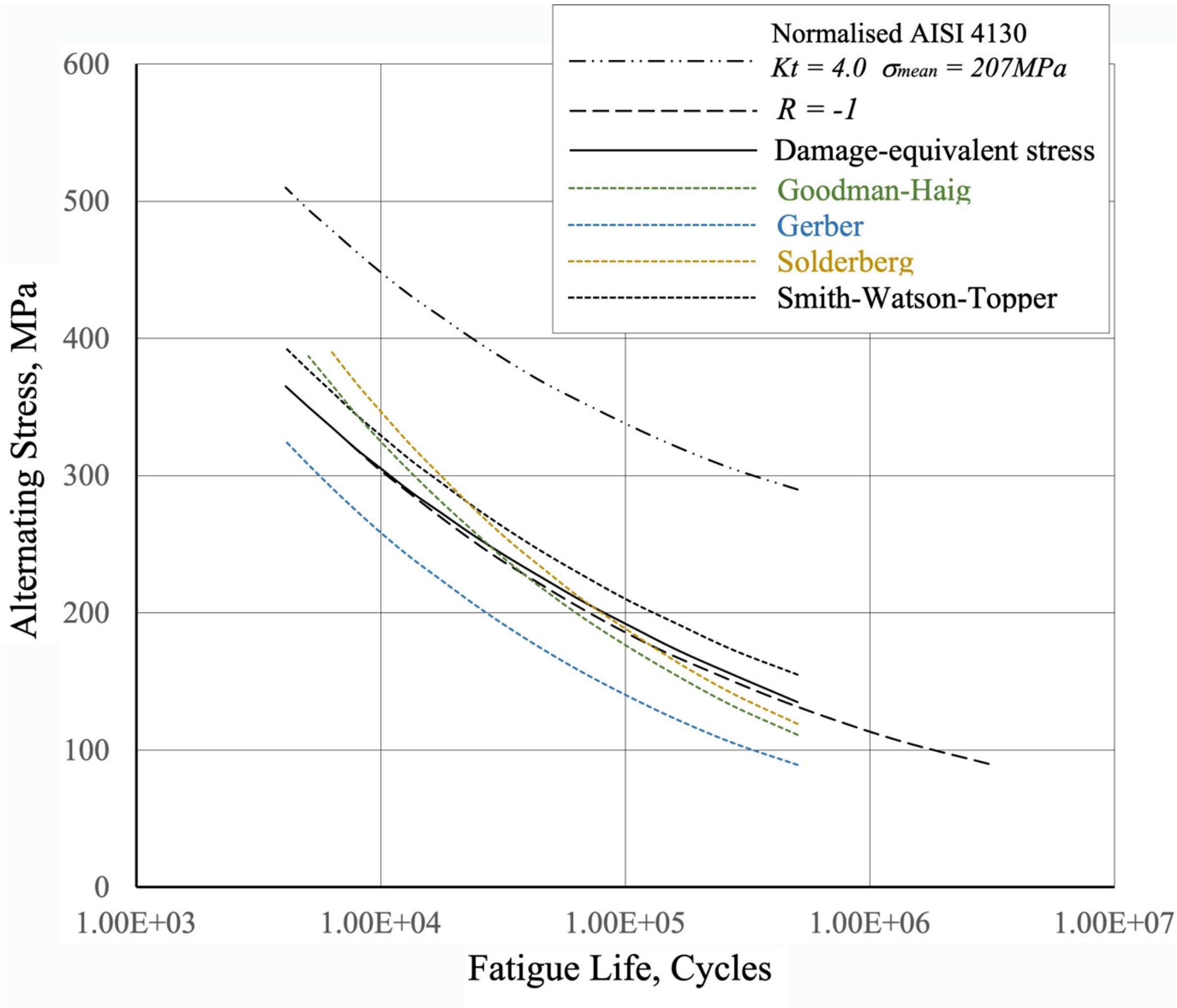

Figure S7. Normalised AISI 4130, K_t = *4.0* s_{mean} *= 207MPa(30ksi)*

Figure S7 is equivalent to Figure 13 of reference [1].

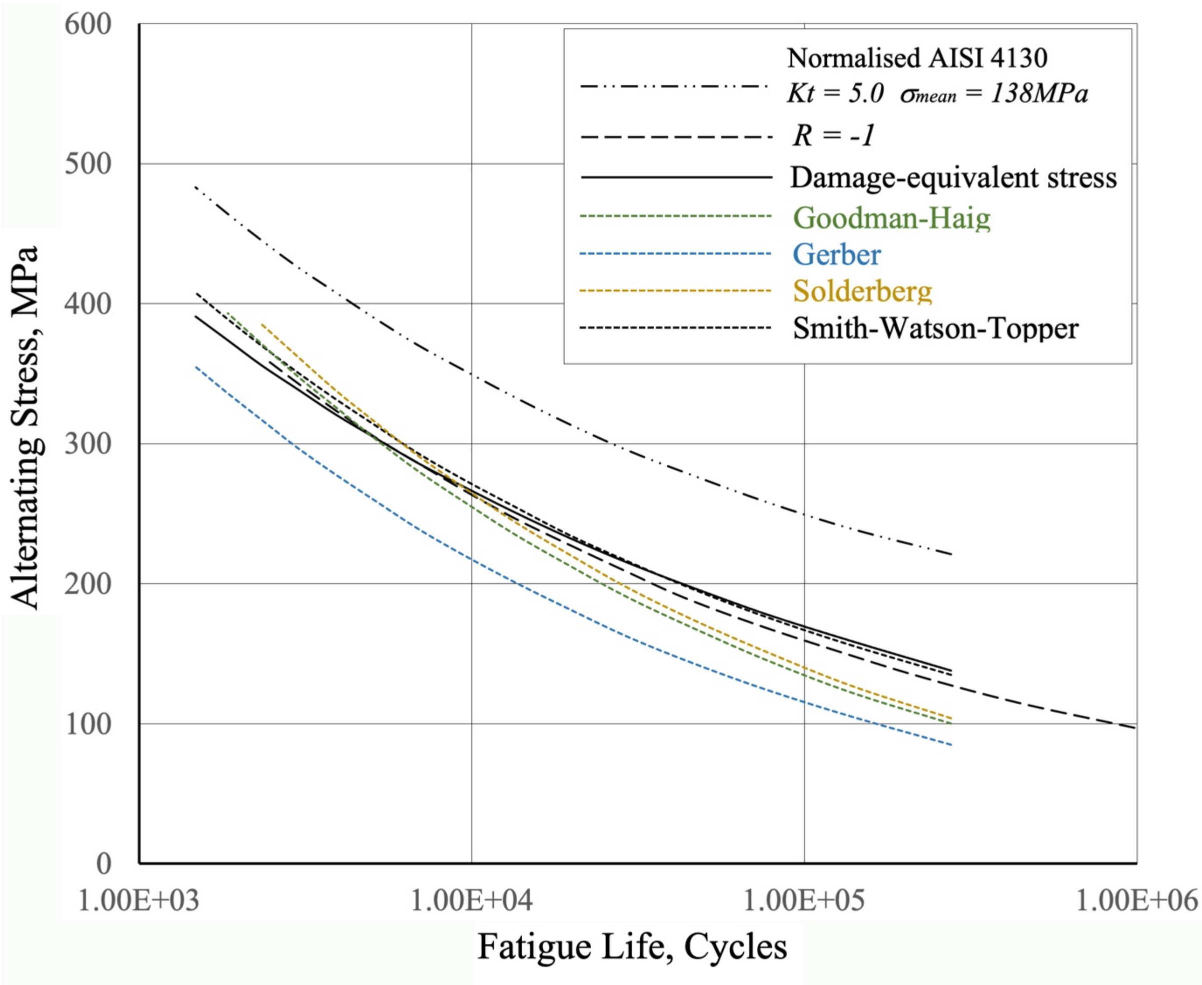

Figure S8. Normalised AISI 4130, K_t = *5.0* s_{mean} = *138MPa(20ksi)*

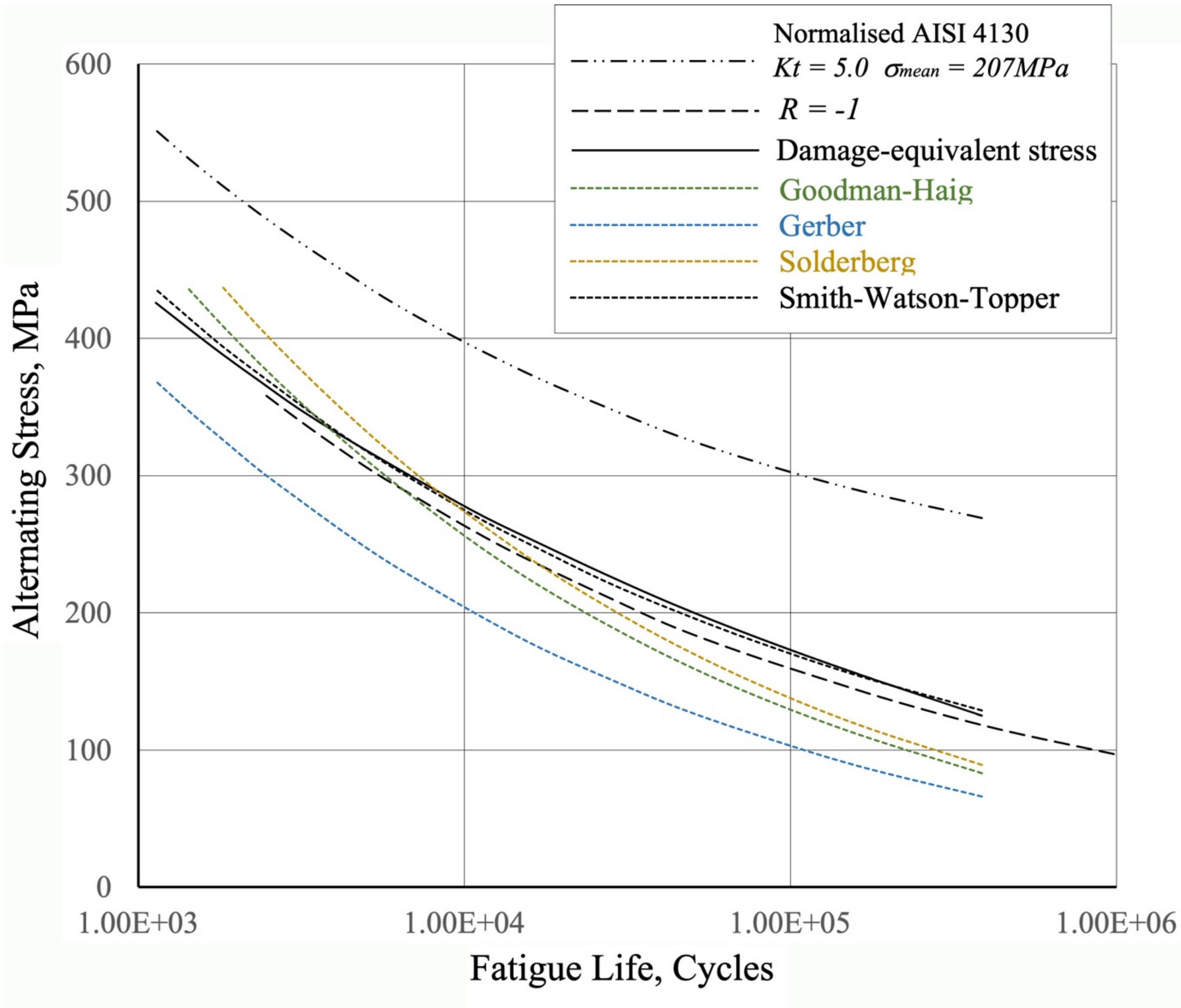

Figure S9. Normalised AISI 4130, K_t *= 5.0* s_{mean} *= 207MPa(30ksi)*

Figure S9 is equivalent to Figure 14 of reference [1].

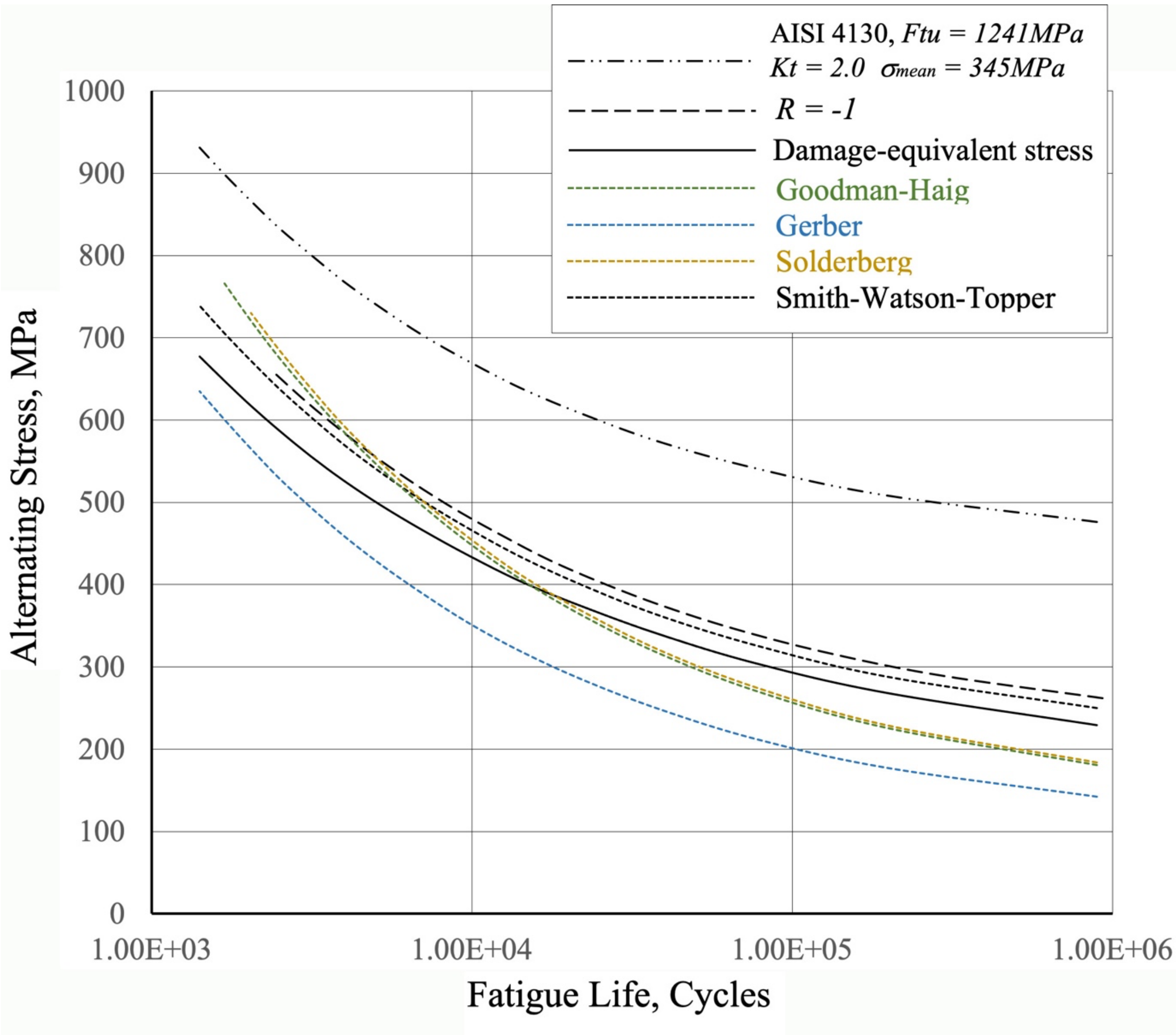

Figure S10. AISI 4130, *Ftu = 1241MPa(180ksi)*, $K_t = 2.0$ $s_{mean} = 345MPa(50ksi)$

Figure S10 is equivalent to Figure 12 of reference [1].

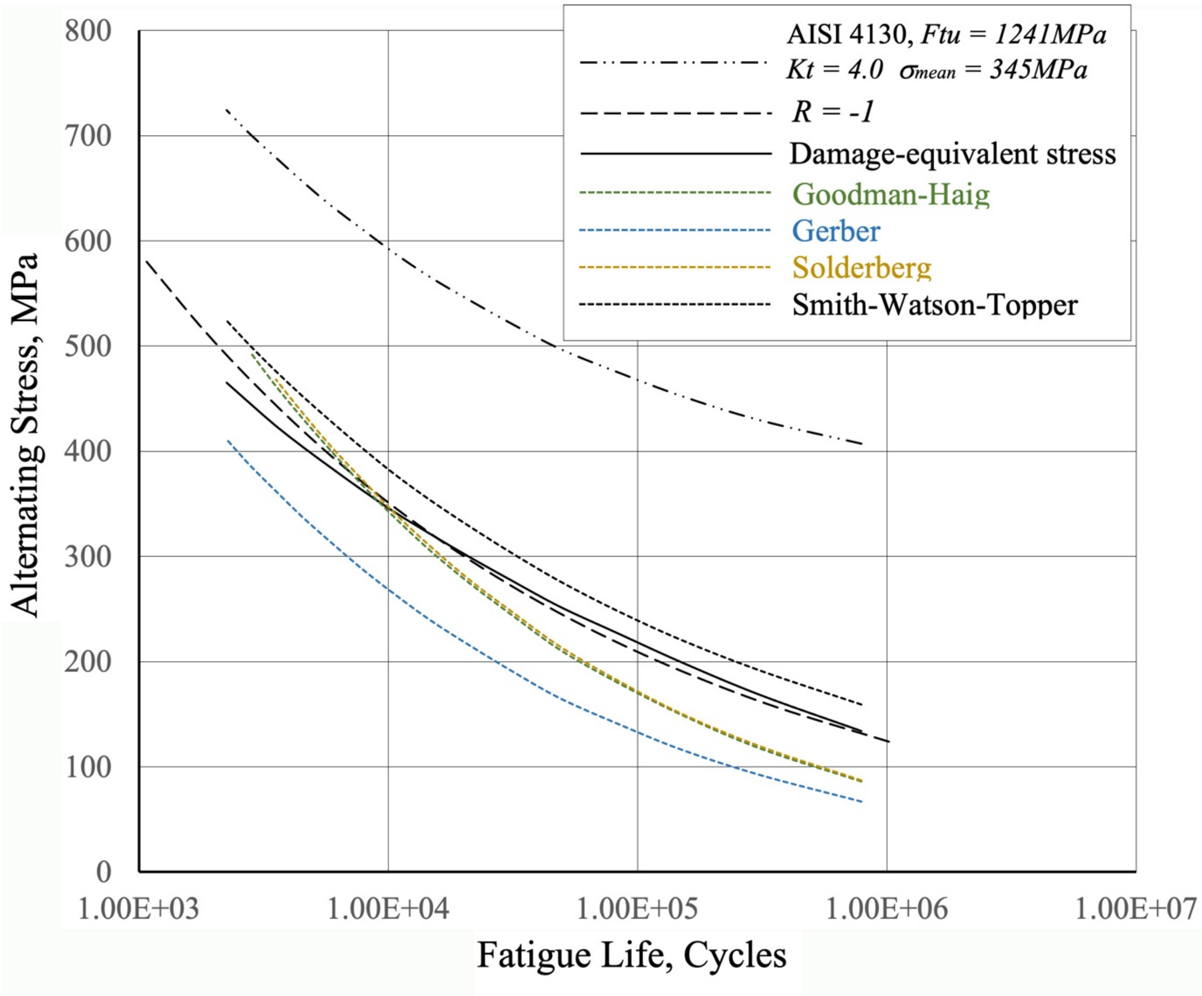

Figure S11. AISI 4130, *Ftu = 1241MPa(180ksi)*, K_t = *4.0* s_{mean} = *345MPa(50ksi)*

Figure S11 is equivalent to Figure 15 of reference [1].

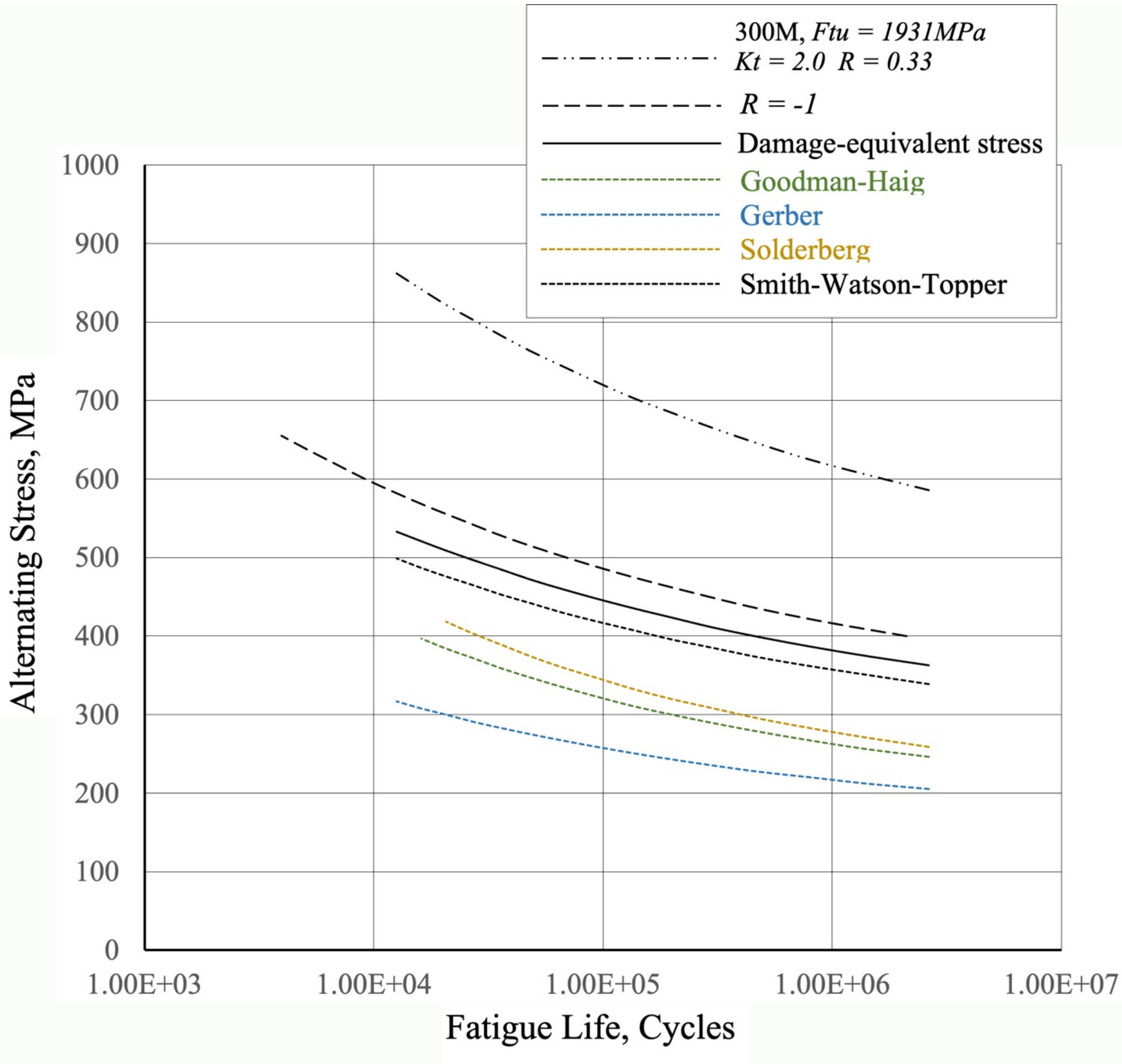

Figure S12. 300M, *Ftu = 1931MPa(280ksi)*, $K_t = 2.0$ $R = 0.33$

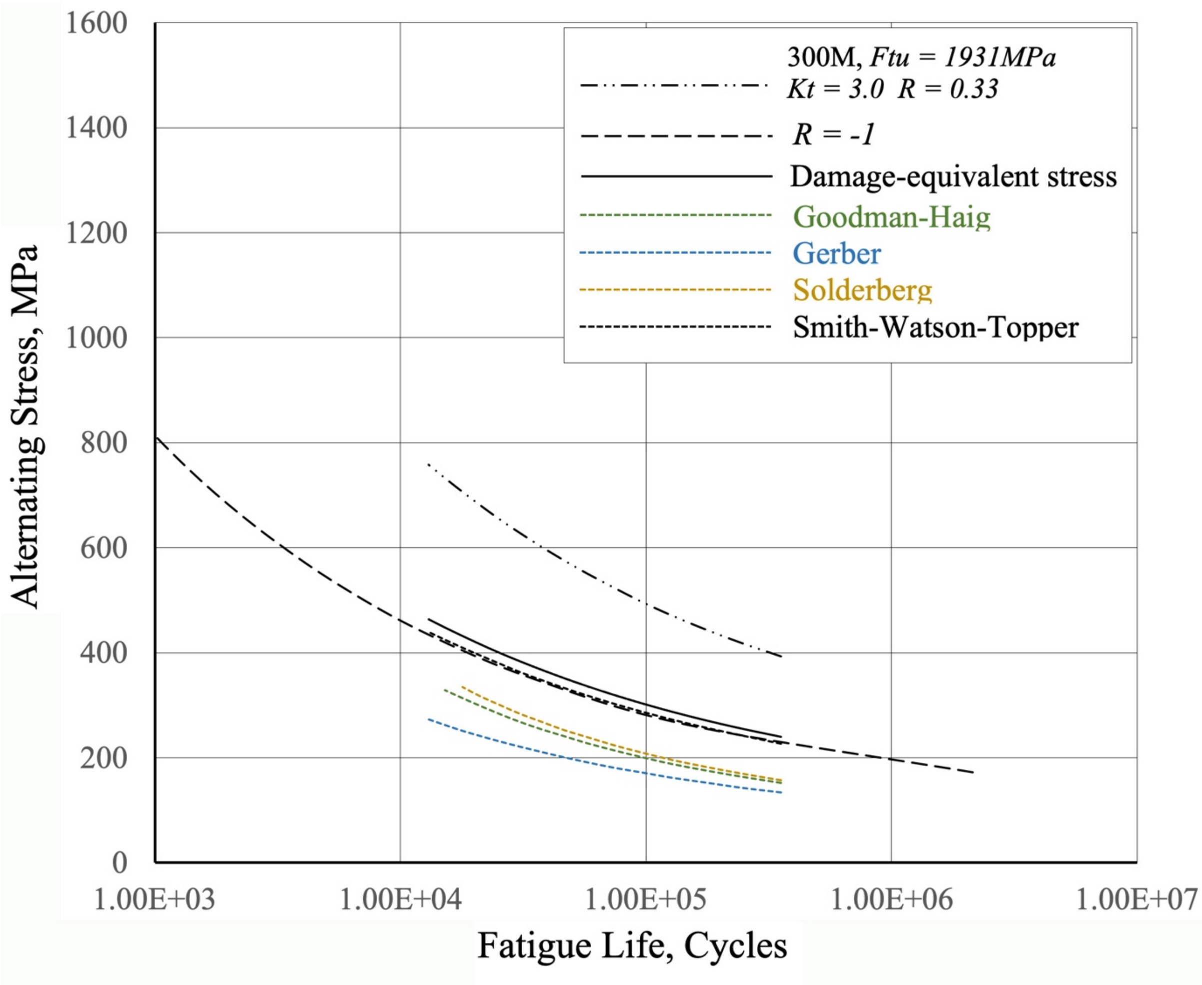

Figure S13. 300M, *Ftu = 1931MPa(280ksi)*, $K_t = 3.0$ $R = 0.33$

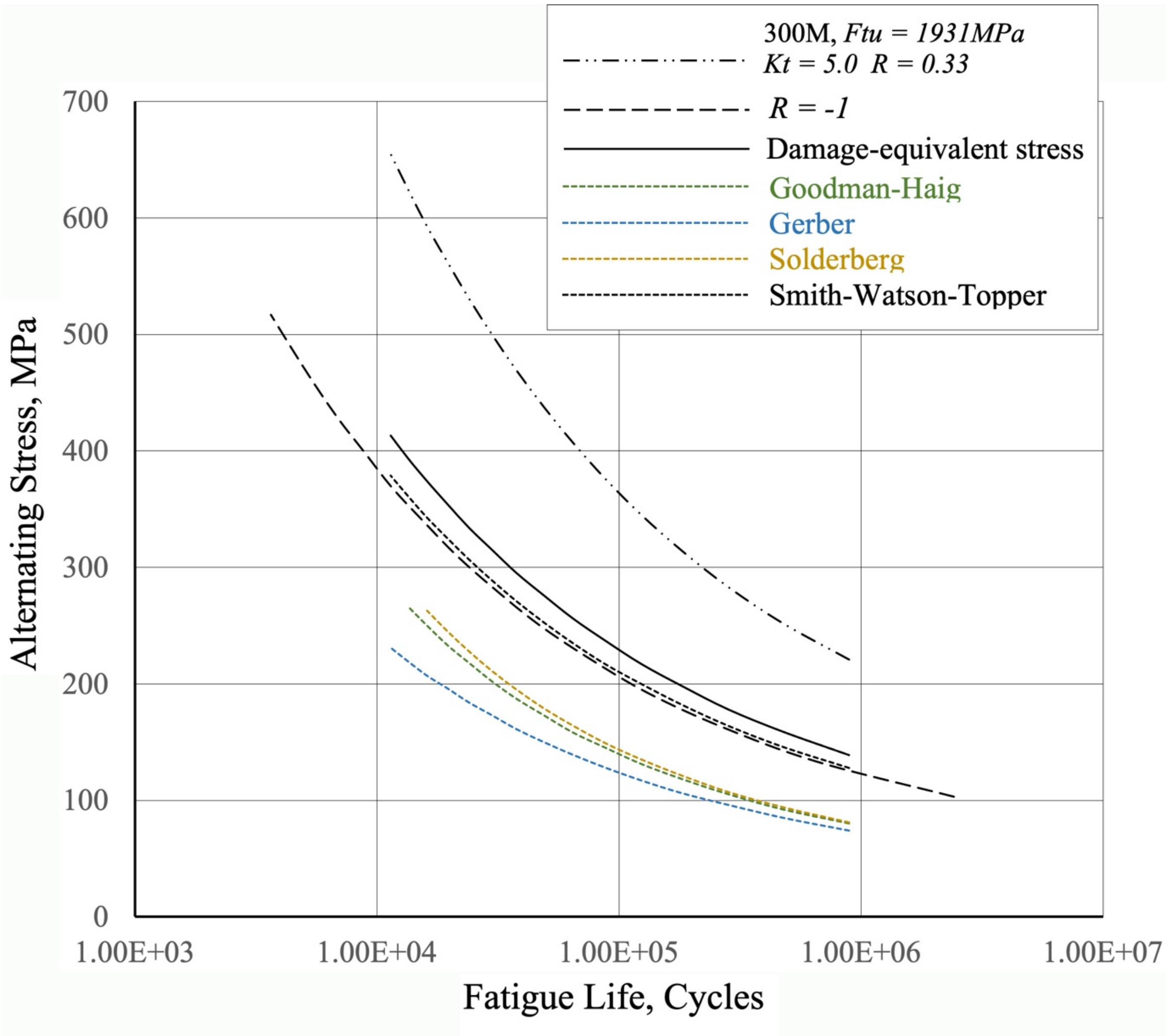

Figure S14. 300M, *Ftu = 1931MPa(280ksi)*, $K_t = 5.0$ $R = 0.33$

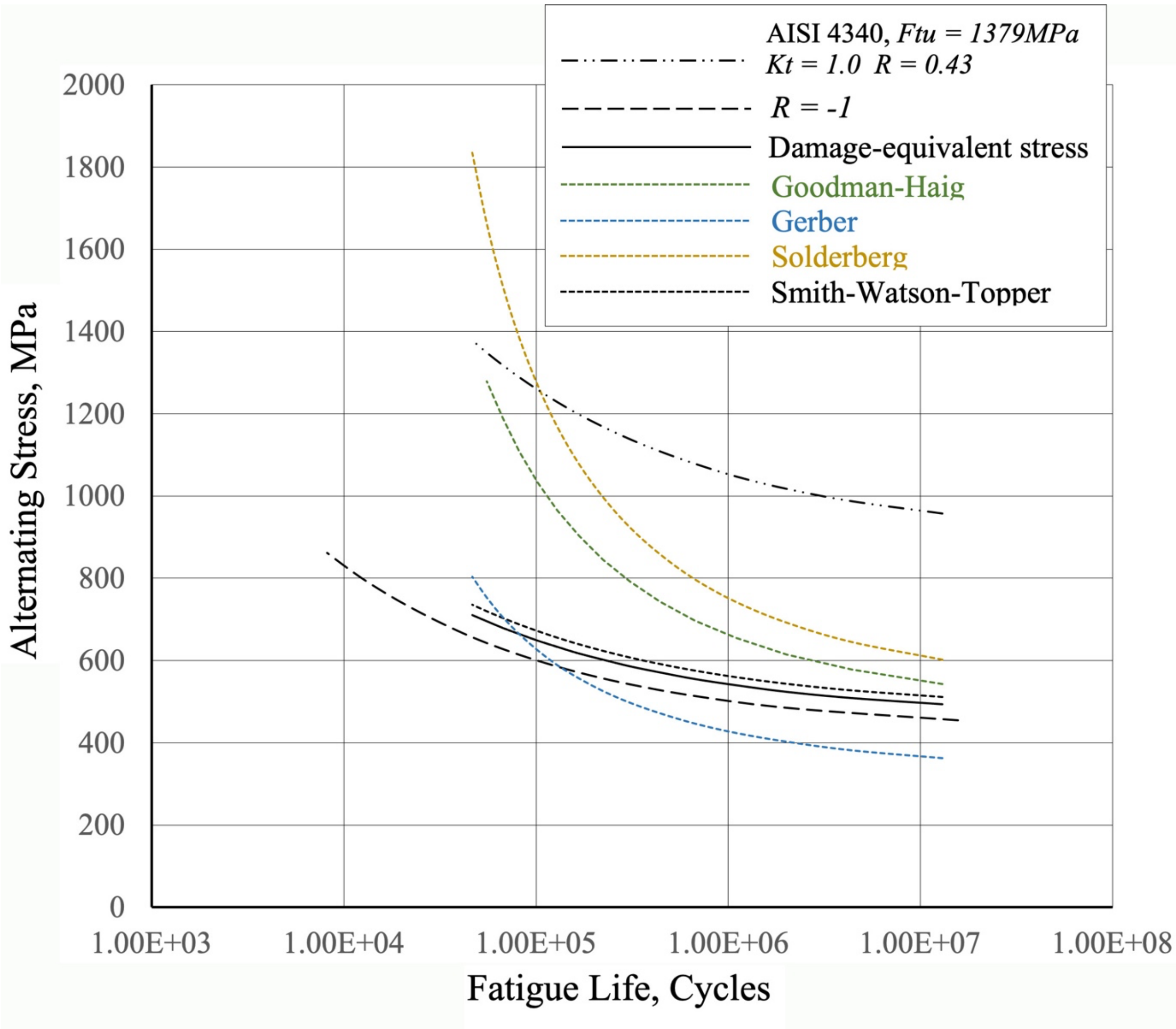

Figure S15. AISI 4340, *Ftu = 1379MPa(200ksi)*, $K_t = 1.0$ $R = 0.43$

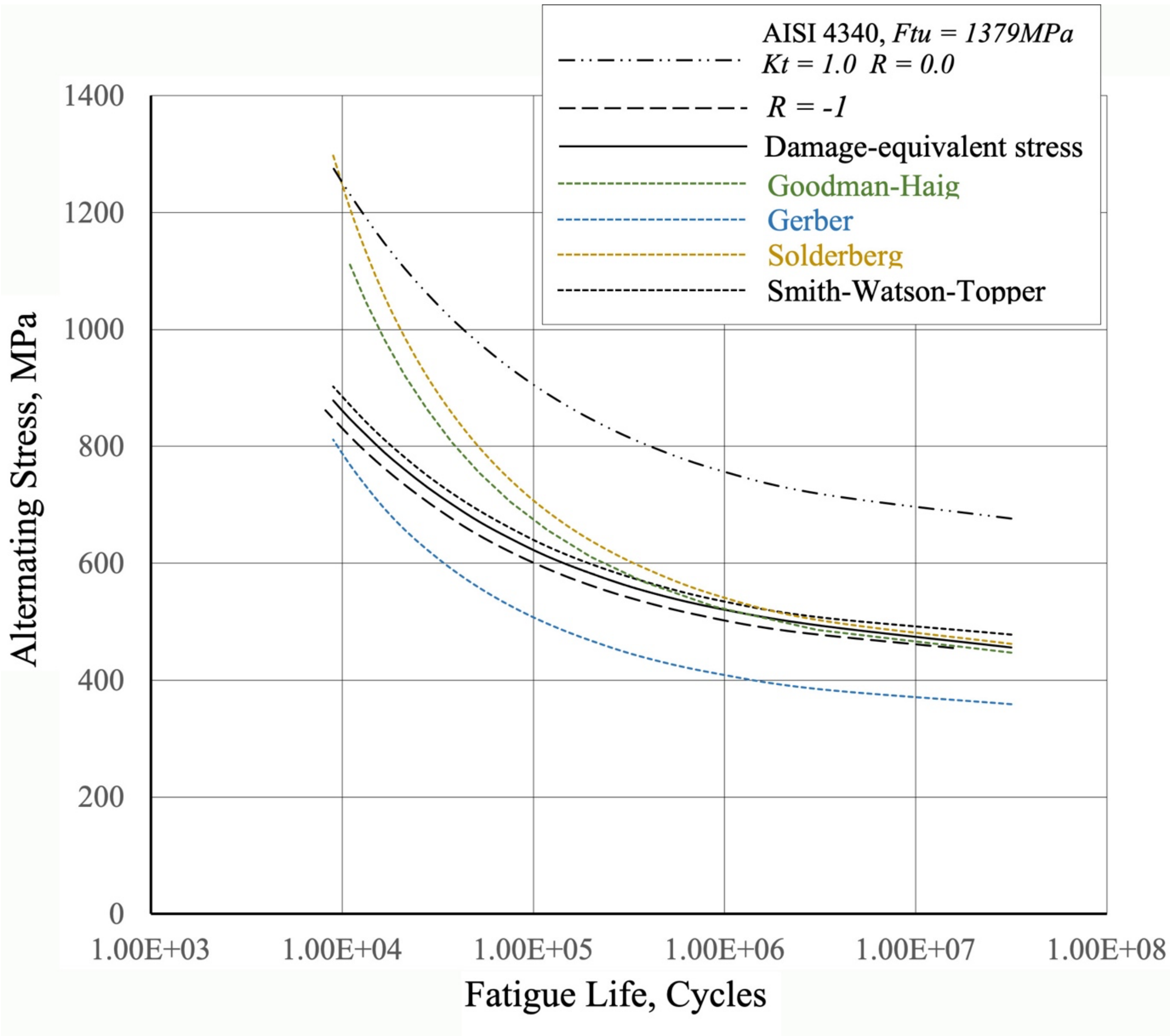

Figure S16. AISI 4340, *Ftu = 1379MPa(200ksi)*, $K_t = 1.0\ \ R = 0.0$

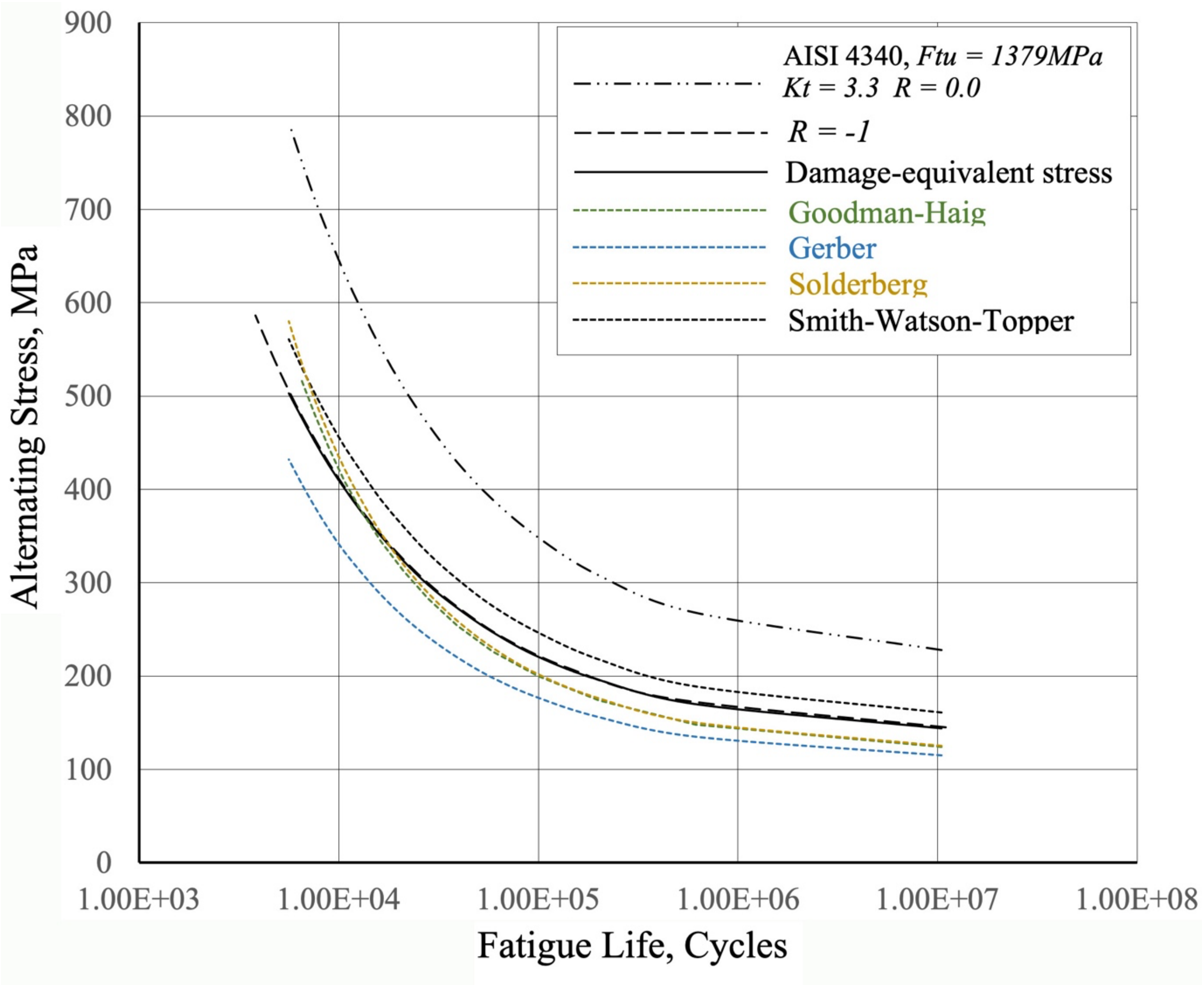

Figure S17. AISI 4340, *Ftu = 1379MPa(200ksi)*, $K_t = 3.3$ $R = 0.0$

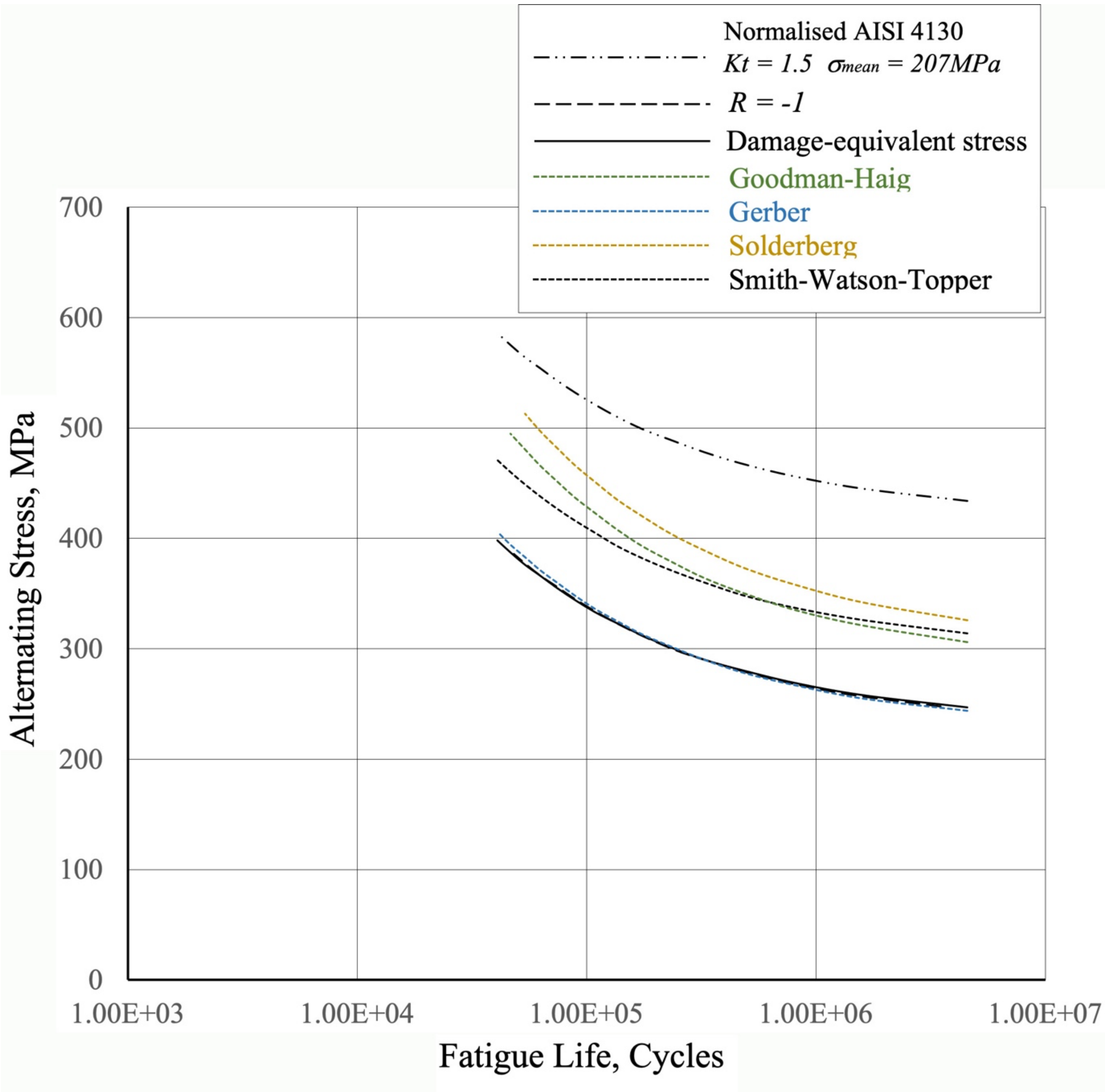

Figure S18. Normalised AISI 4130, $K_t = 1.5$ $s_{mean} = 207MPa(30ksi)$

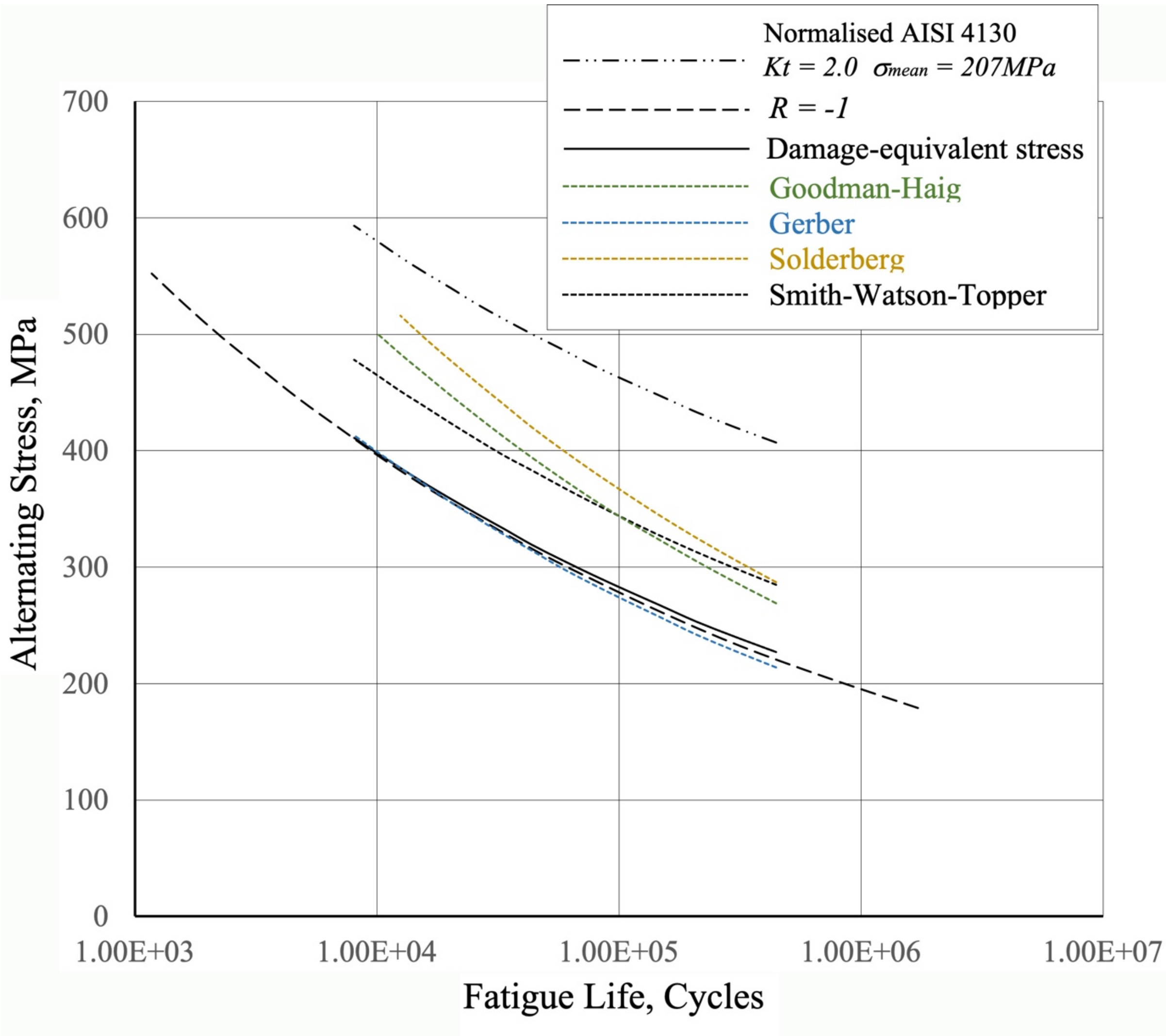

Figure S19. Normalised AISI 4130, $K_t = 2.0$ $s_{mean} = 207MPa(30ksi)$

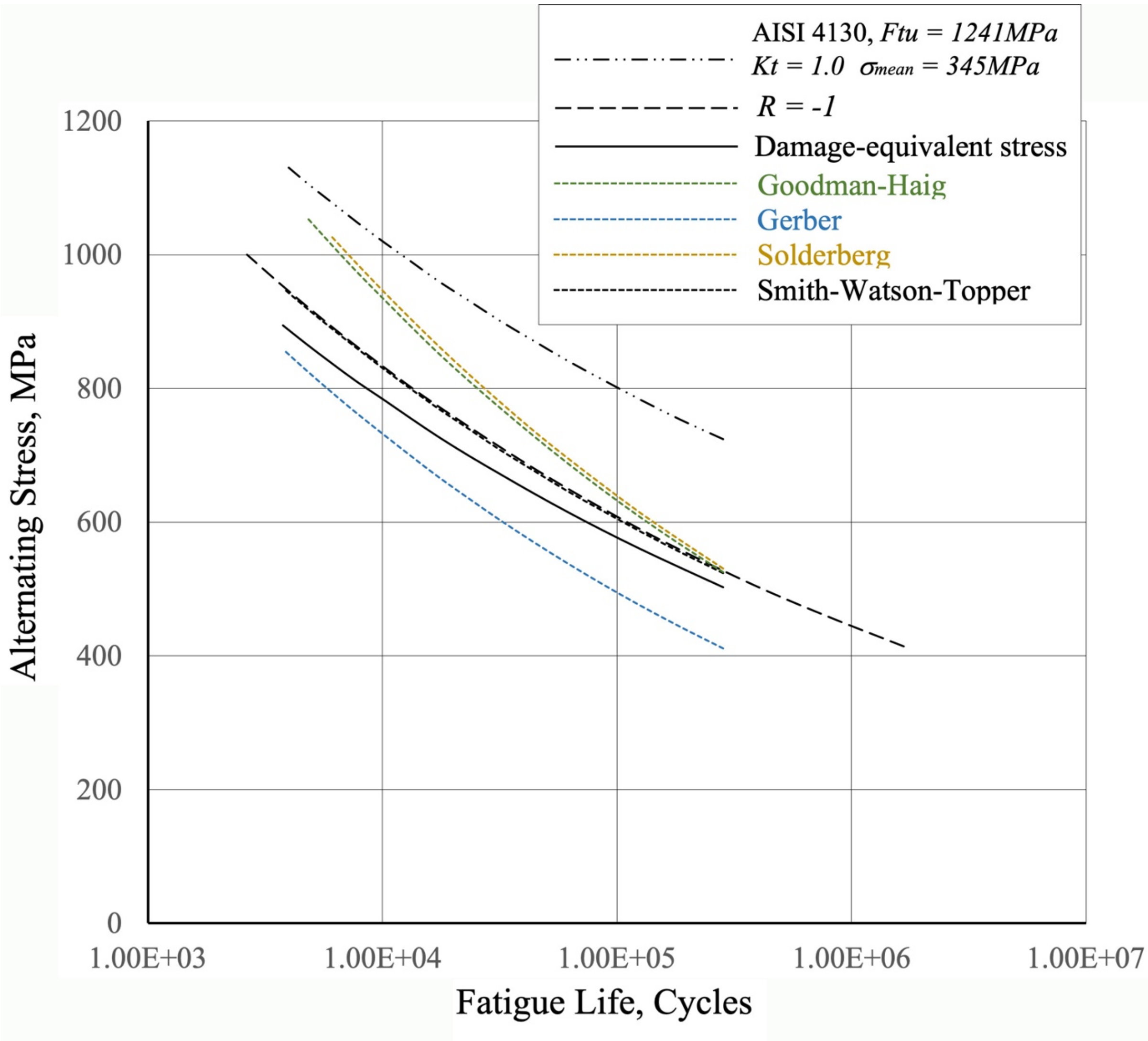

Figure S20. AISI 4130, *Ftu = 1241MPa(180ksi)*, $K_t = 1.0$ $s_{mean} = 345MPa(50ksi)$

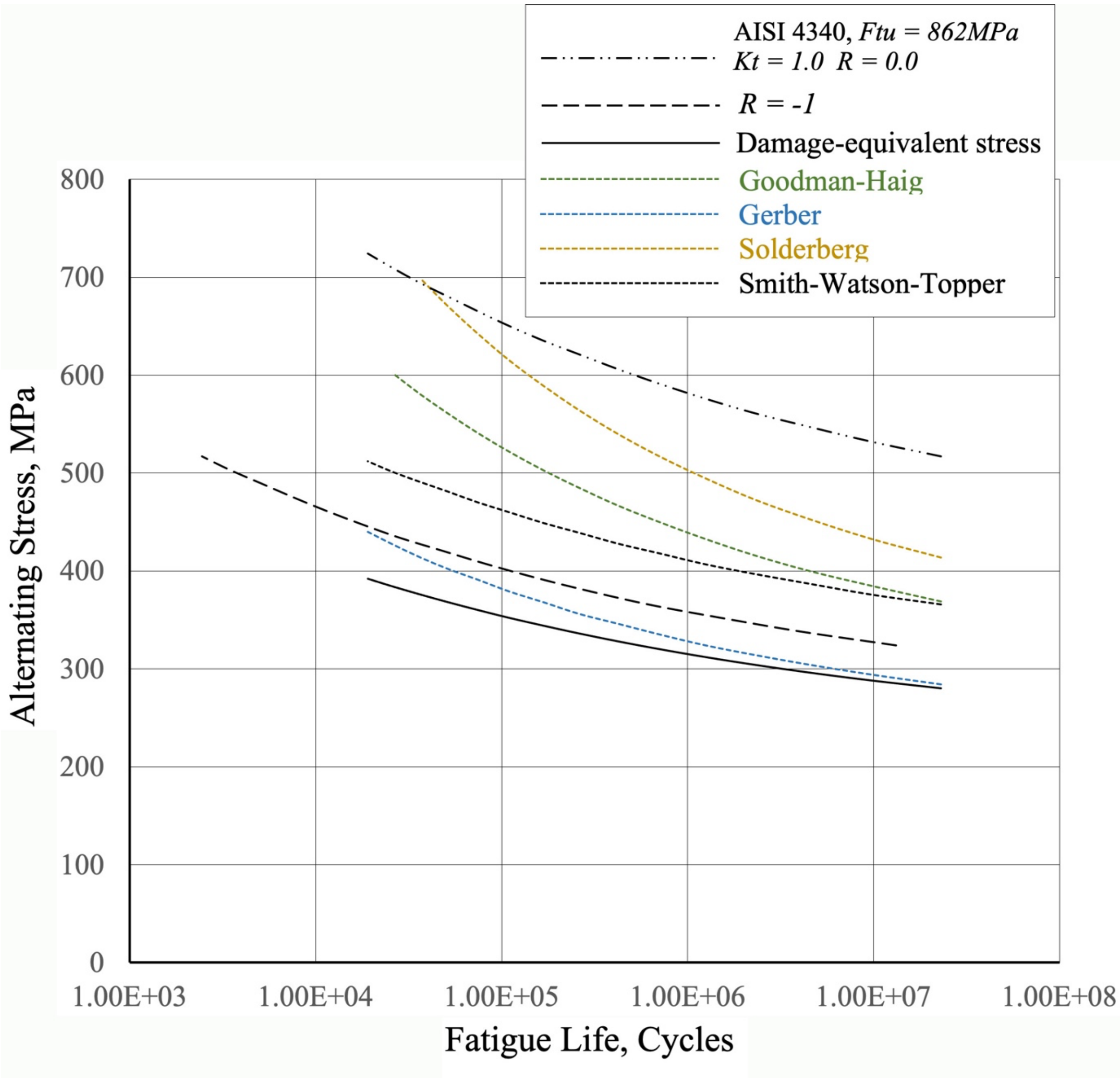

Figure S21. AISI 4340, *Ftu = 862MPa(125ksi)*, $K_t = 1.0$ $R = 0.0$

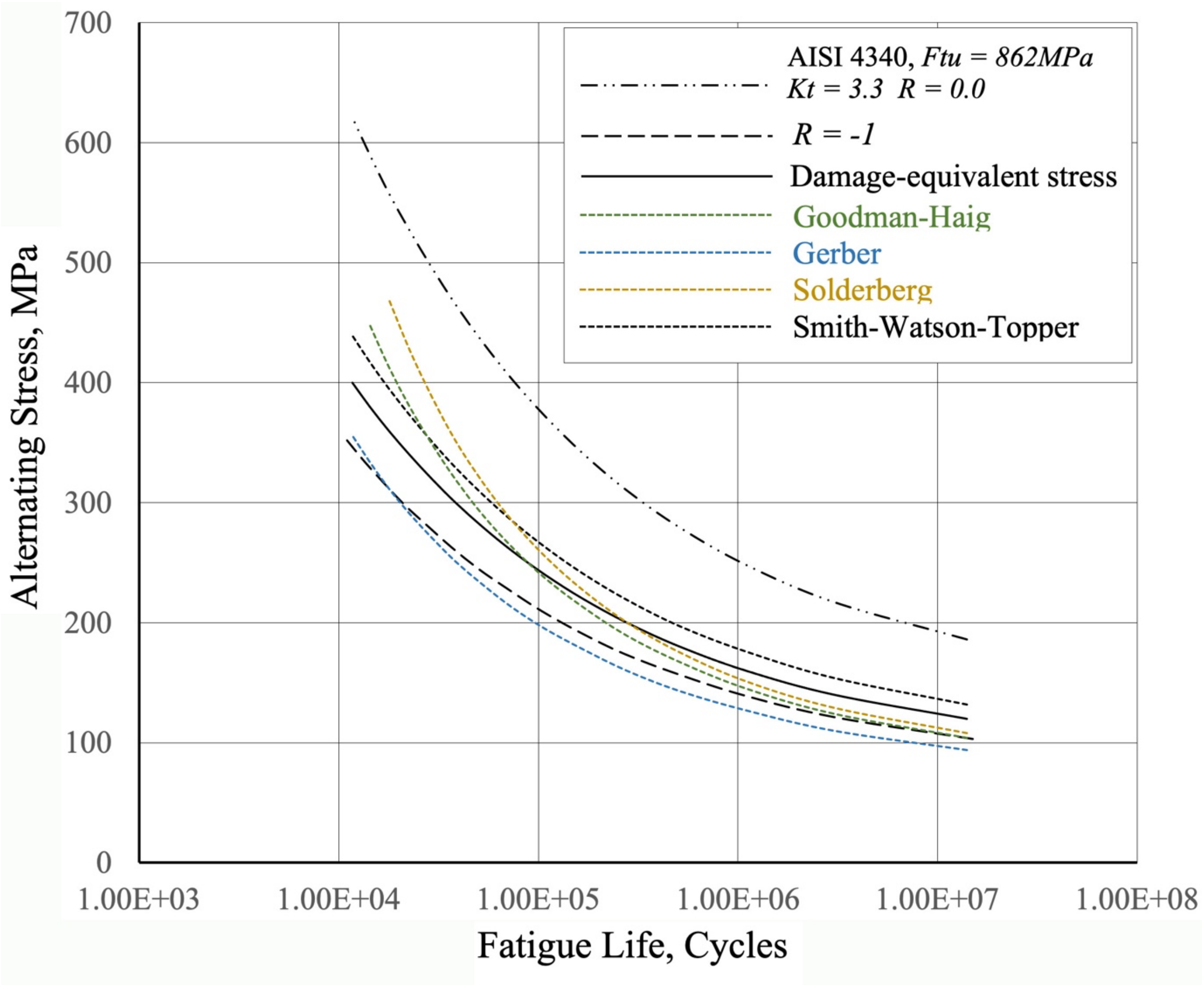

Figure S22. AISI 4340, *Ftu = 862MPa(125ksi)*, $K_t = 3.3$ $R = 0.0$

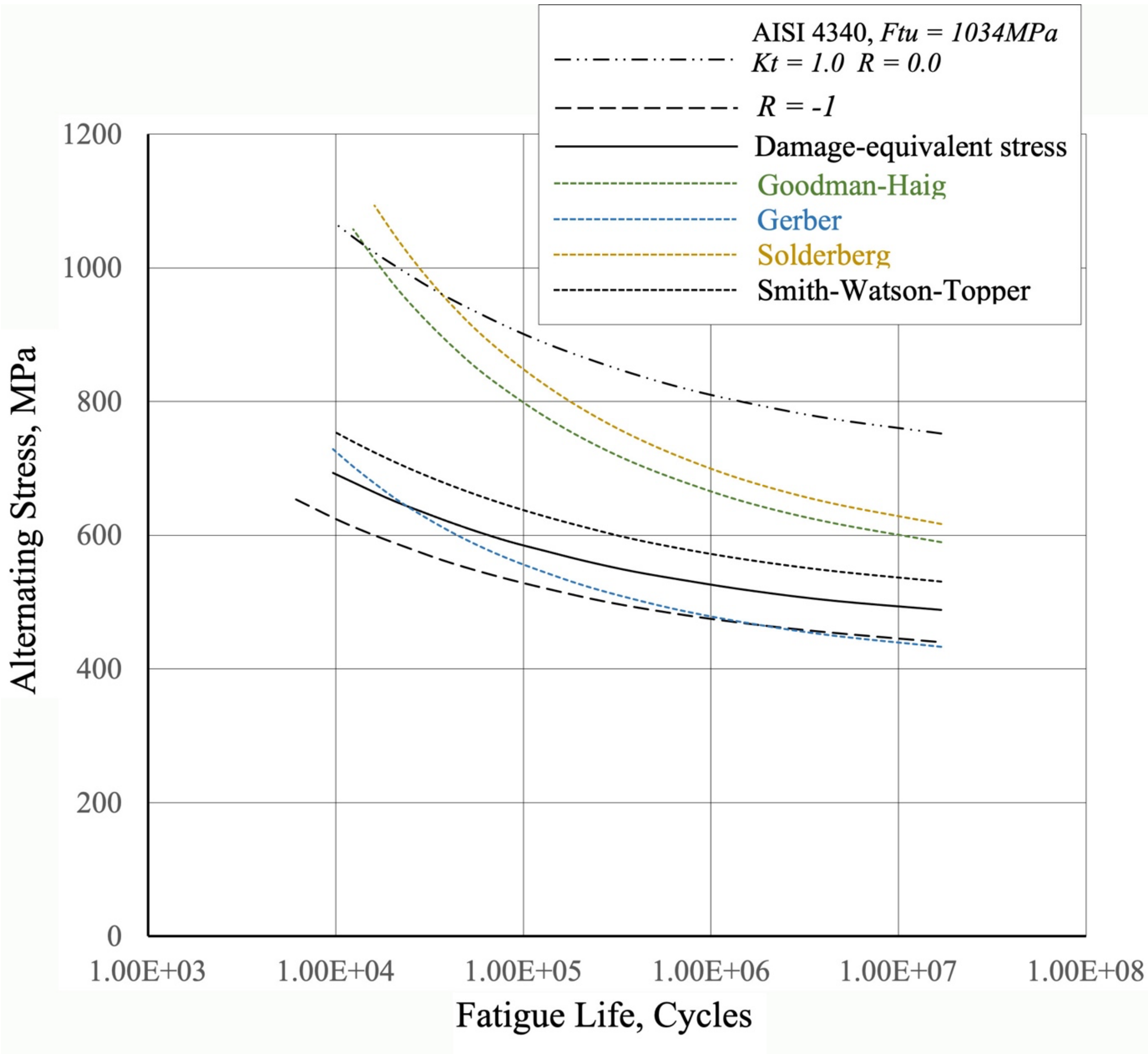

Figure S23. AISI 4340, *Ftu = 1034MPa(150ksi)*, $K_t = 1.0$ $R = 0.0$

Figure S23 is equivalent to Figure 11 of reference [1].

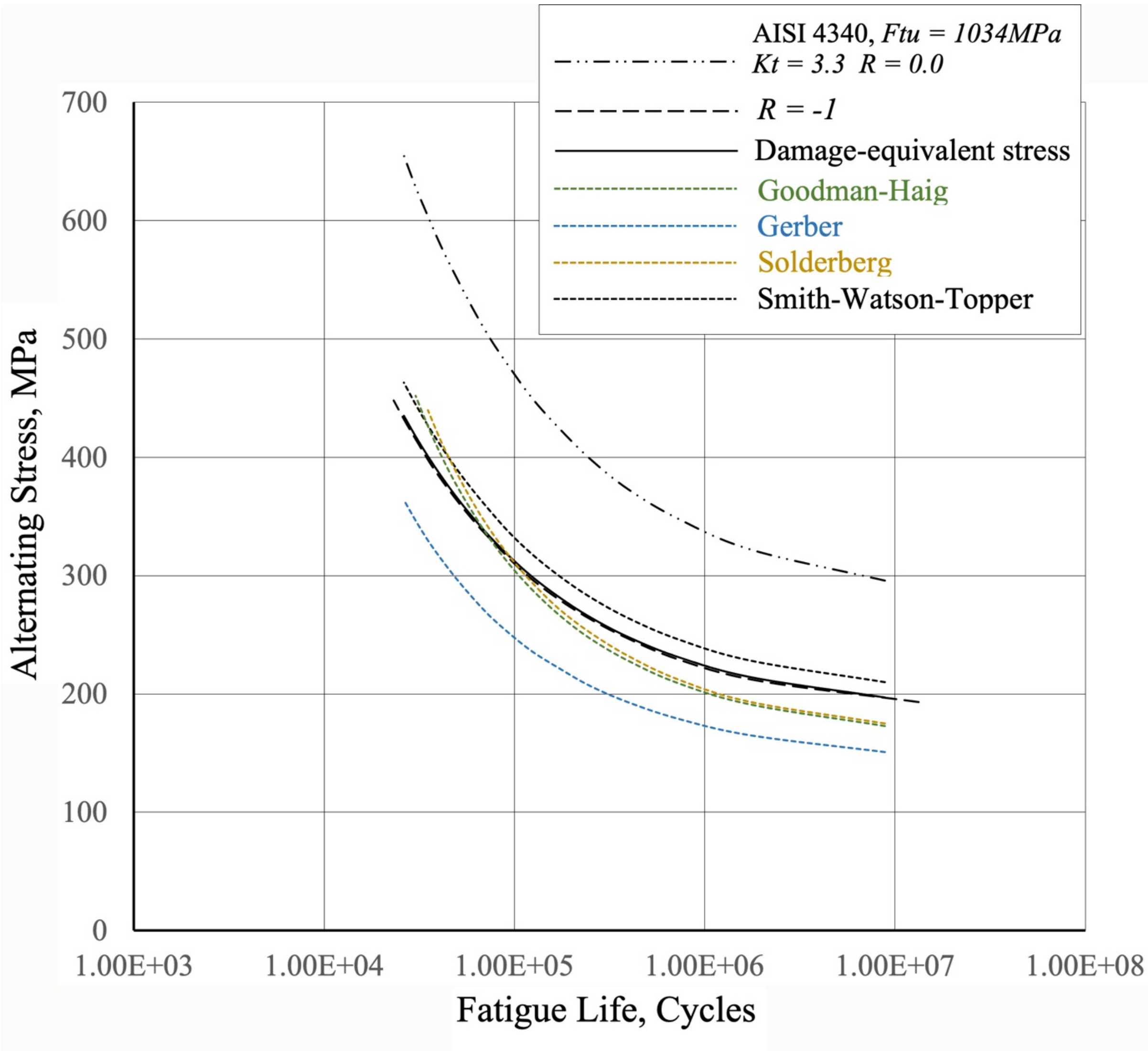

Figure S24. AISI 4340, *Ftu = 1034MPa(150ksi)*, $K_t = 3.3 \;\; R = 0.0$

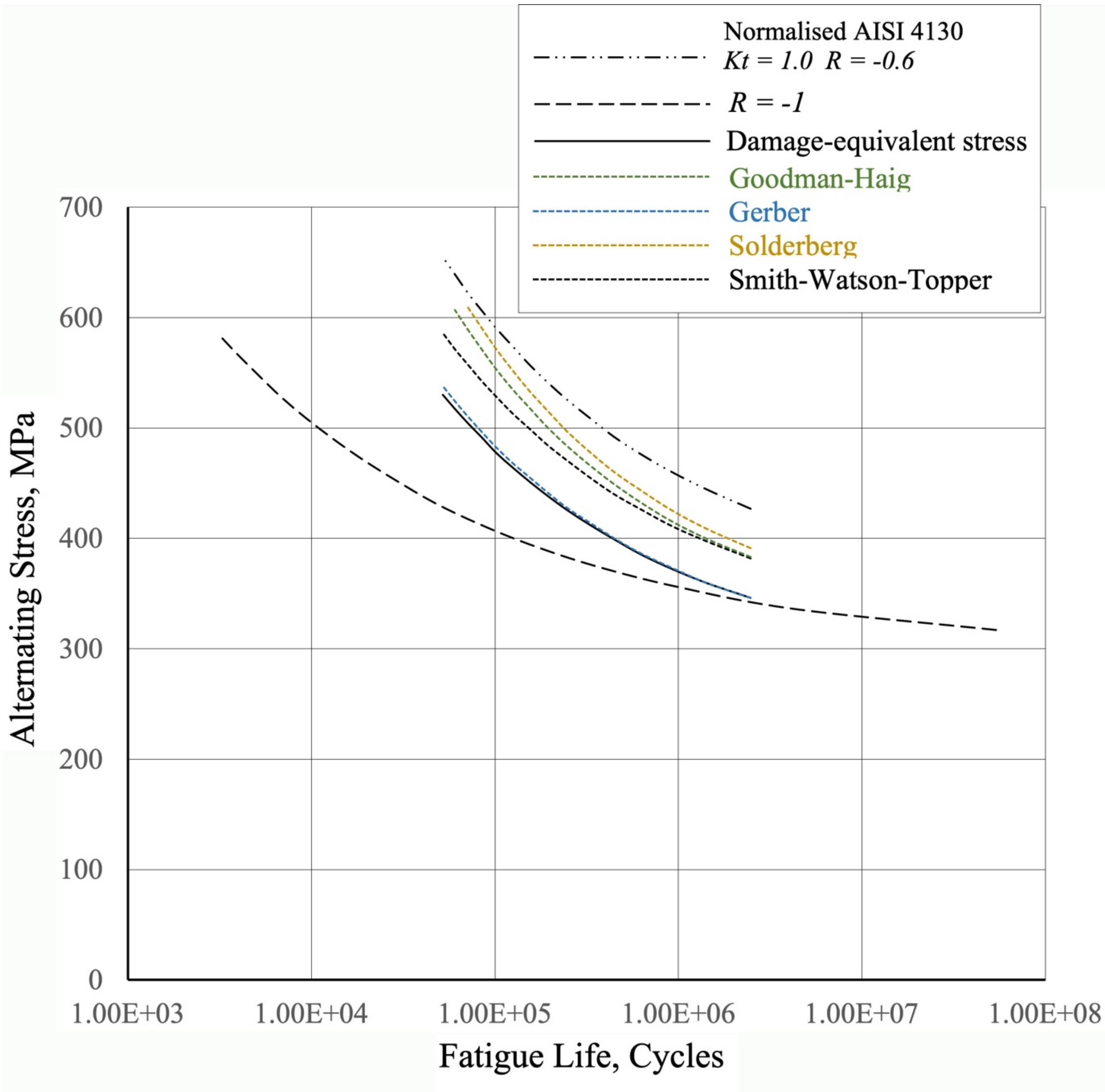

Figure S25. Normalised AISI 4130, $K_t = 1.0$ $R = -0.60$

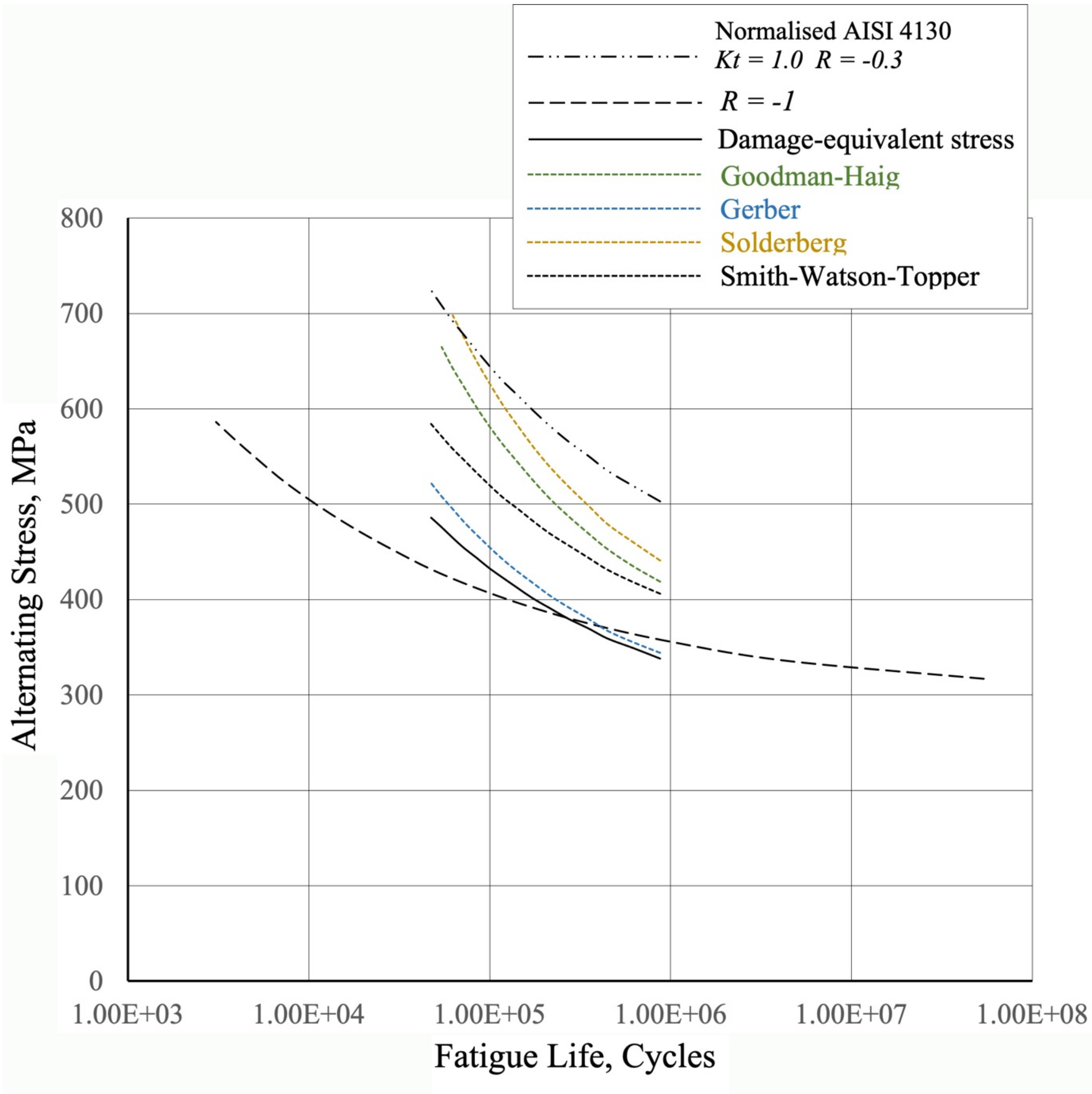

Figure S26. Normalised AISI 4130, $K_t = 1.0$ $R = -0.30$

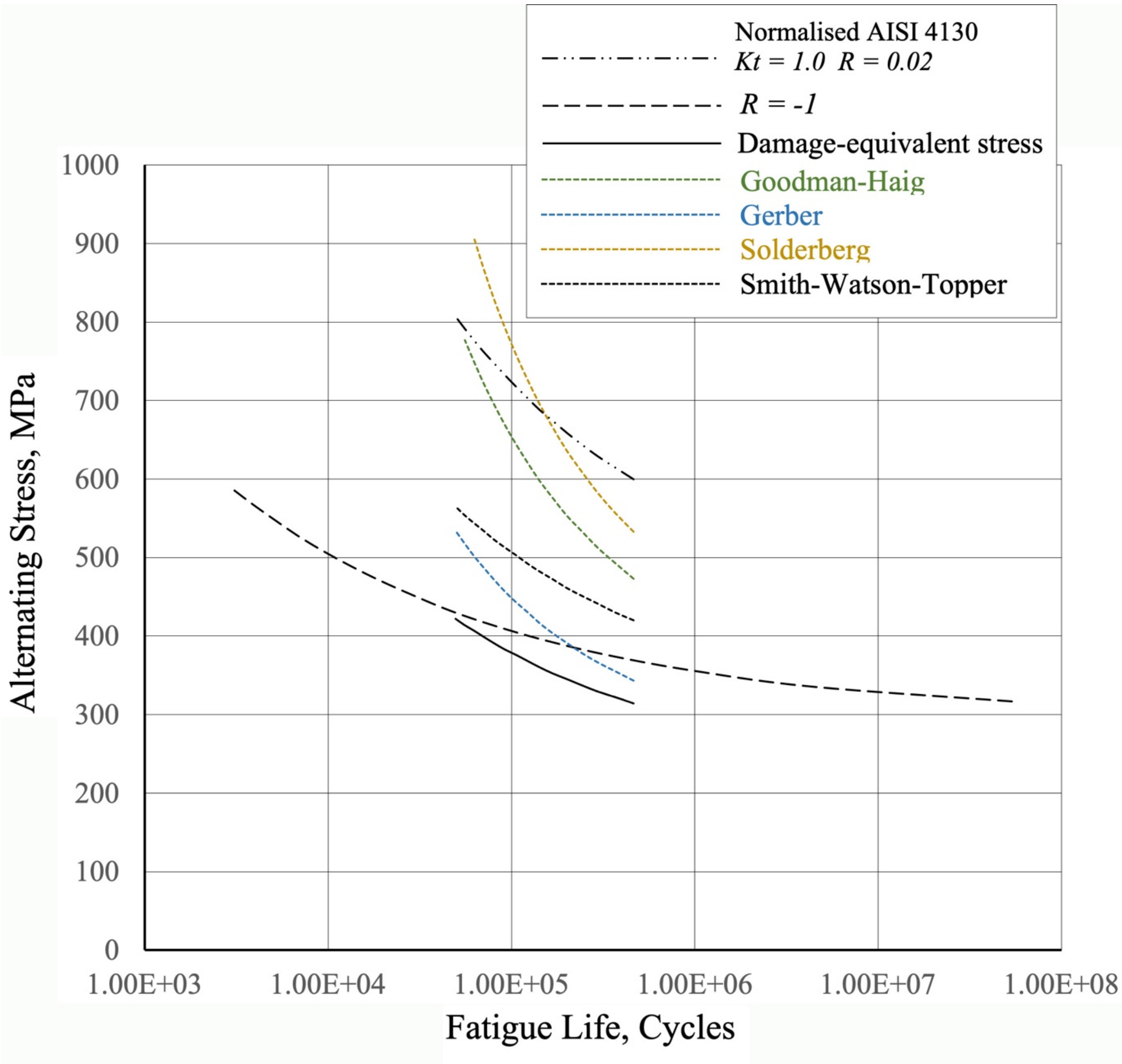

Figure S27. Normalised AISI 4130, $K_t = 1.0$ $R = 0.20$

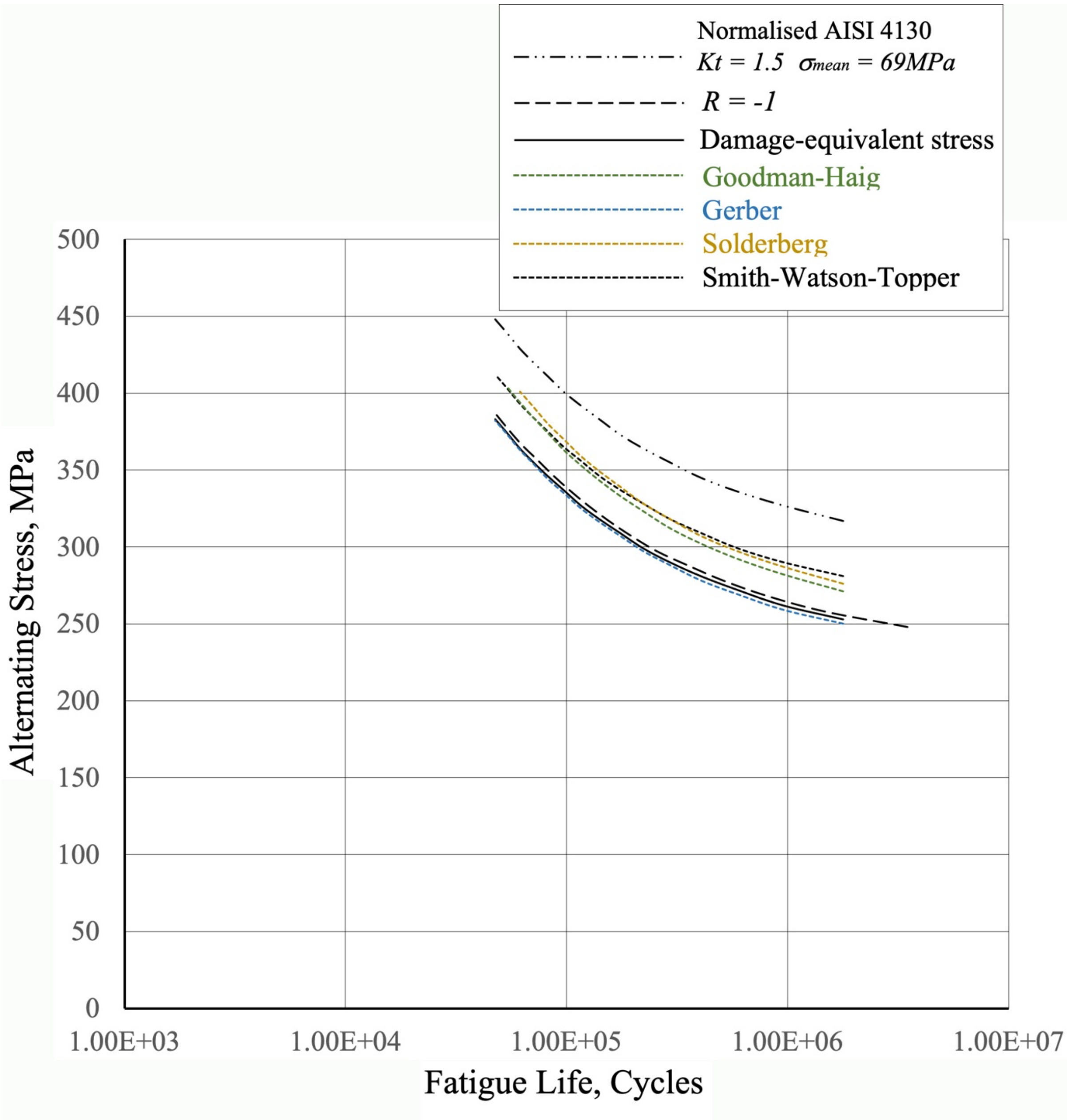

Figure S28. Normalised AISI 4130, K_t = *1.5* s_{mean} *= 69MPa(10ksi)*

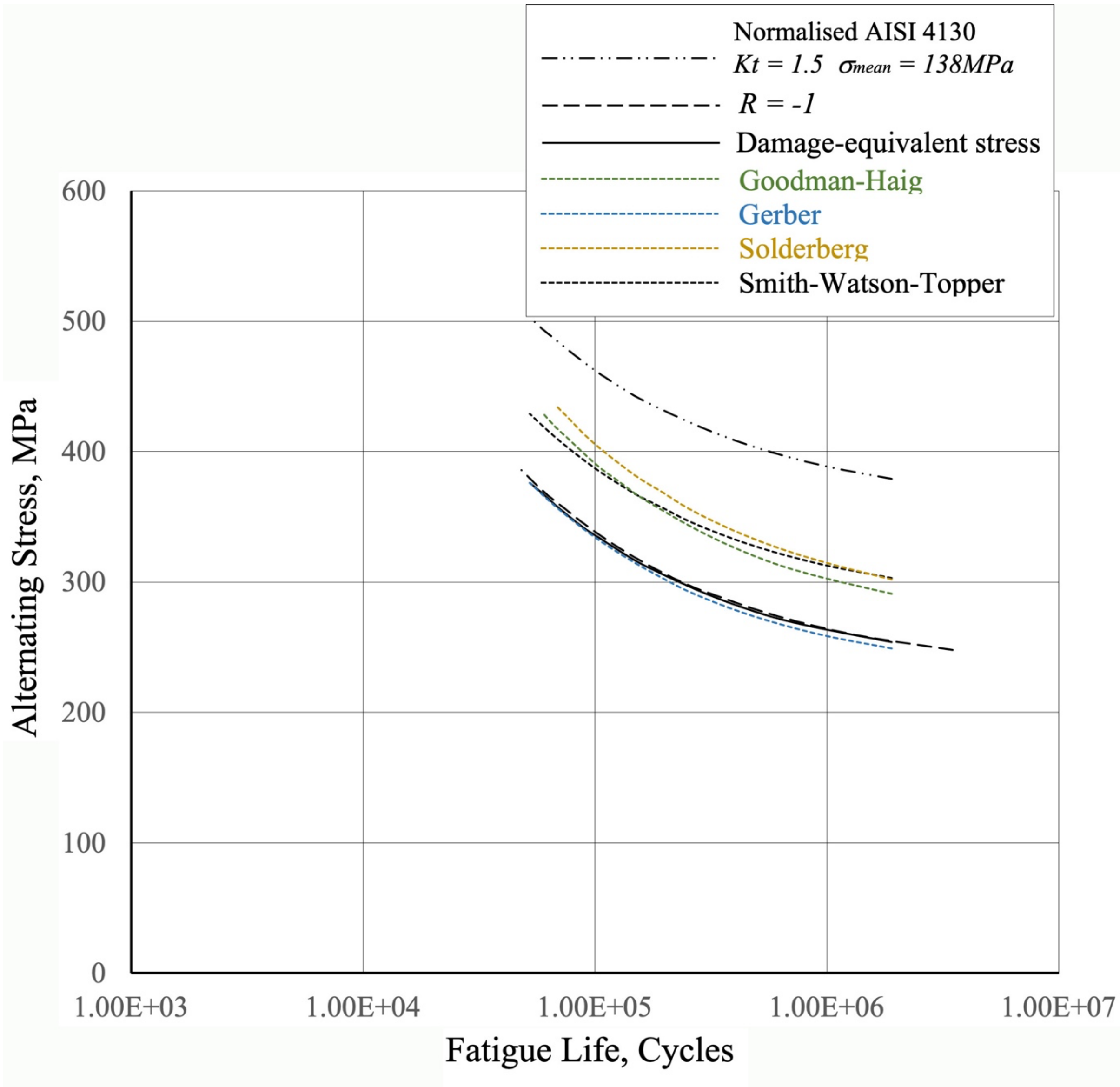

Figure S29. Normalised AISI 4130, $K_t = 1.5$ $s_{mean} = 138MPa(20ksi)$

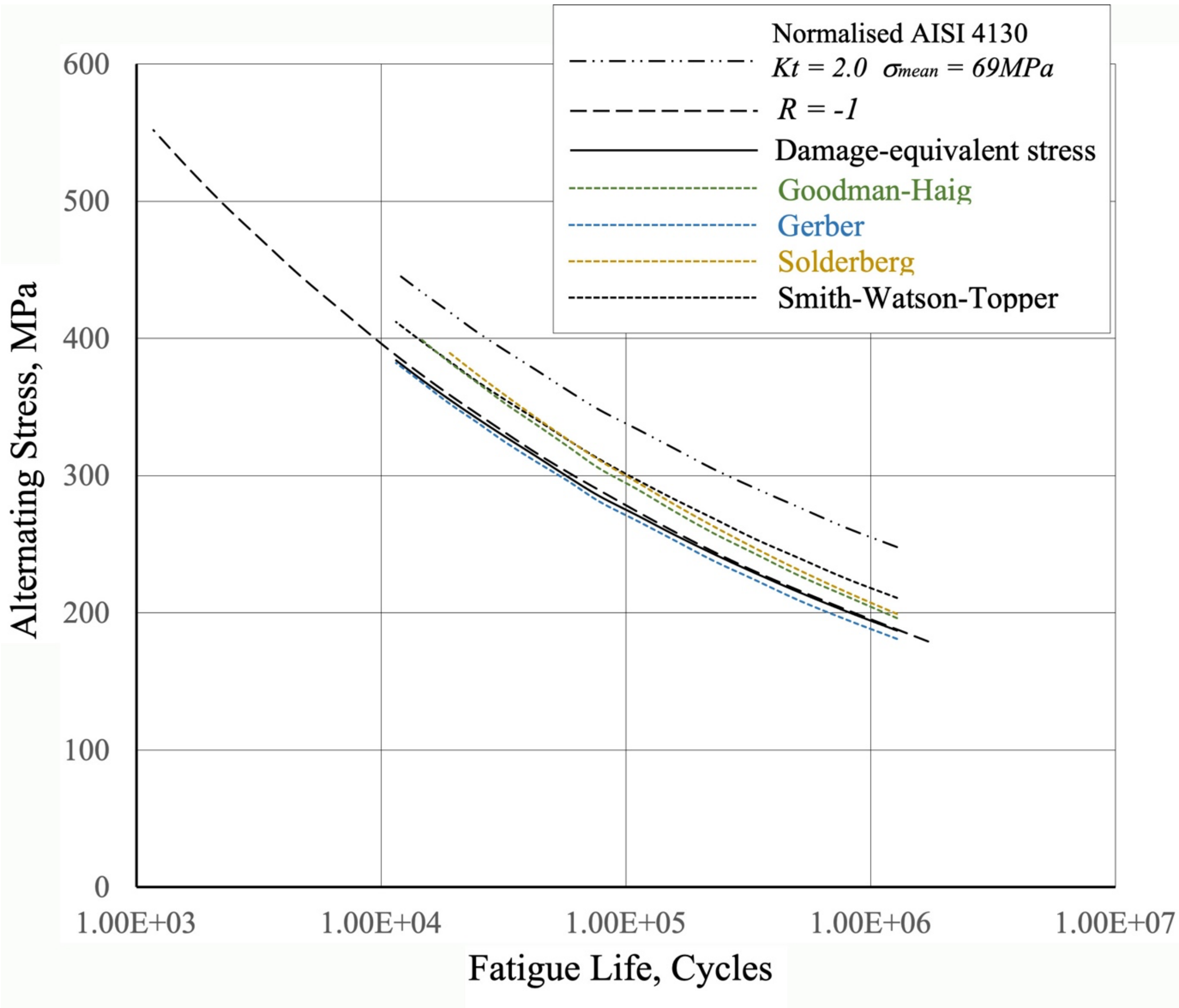

Figure S30. Normalised AISI 4130, $K_t = 2.0$ $s_{mean} = 69MPa(10ksi)$

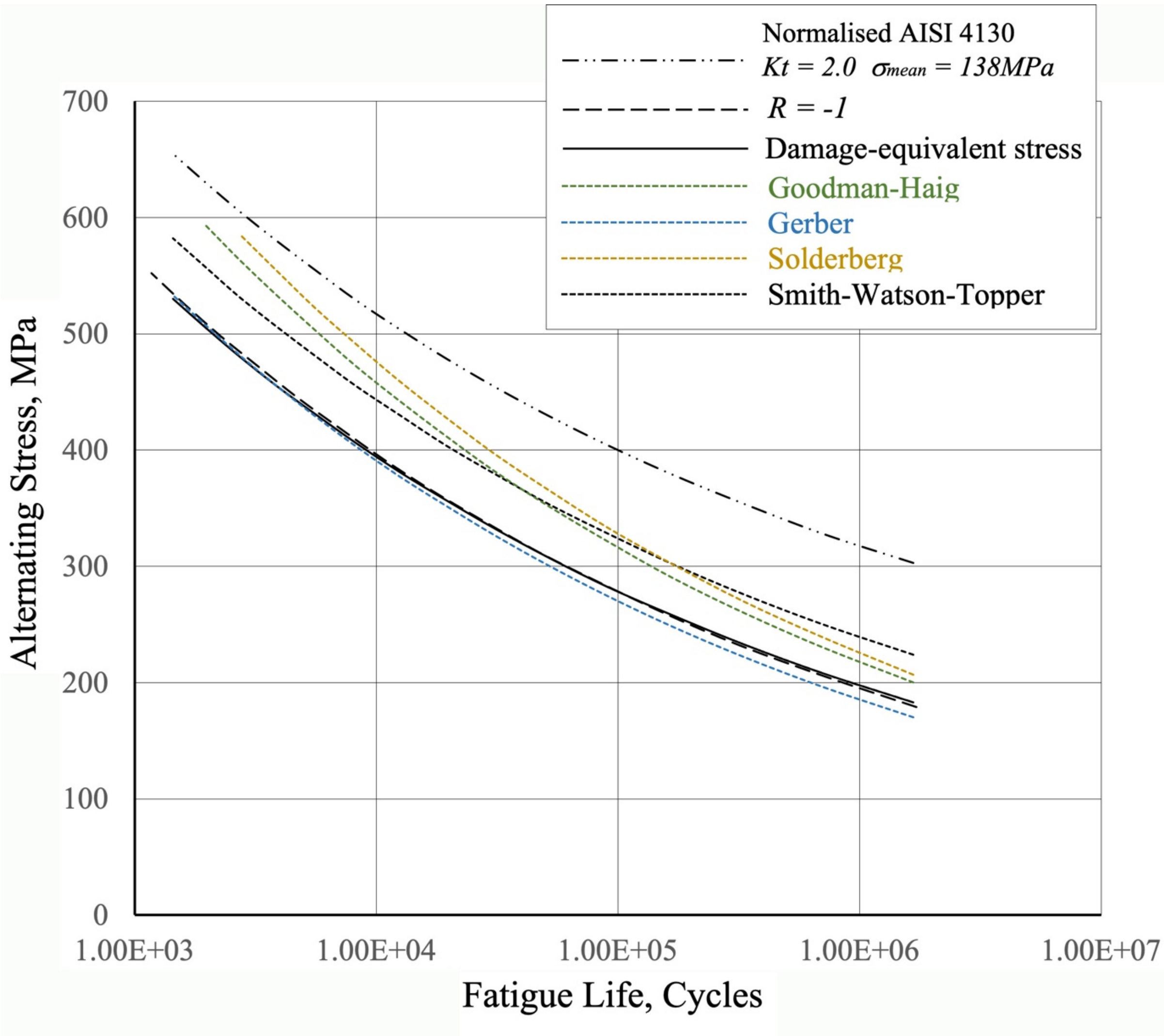

Figure S31. Normalised AISI 4130, K_t = 2.0 s_{mean} = 138MPa(20ksi)

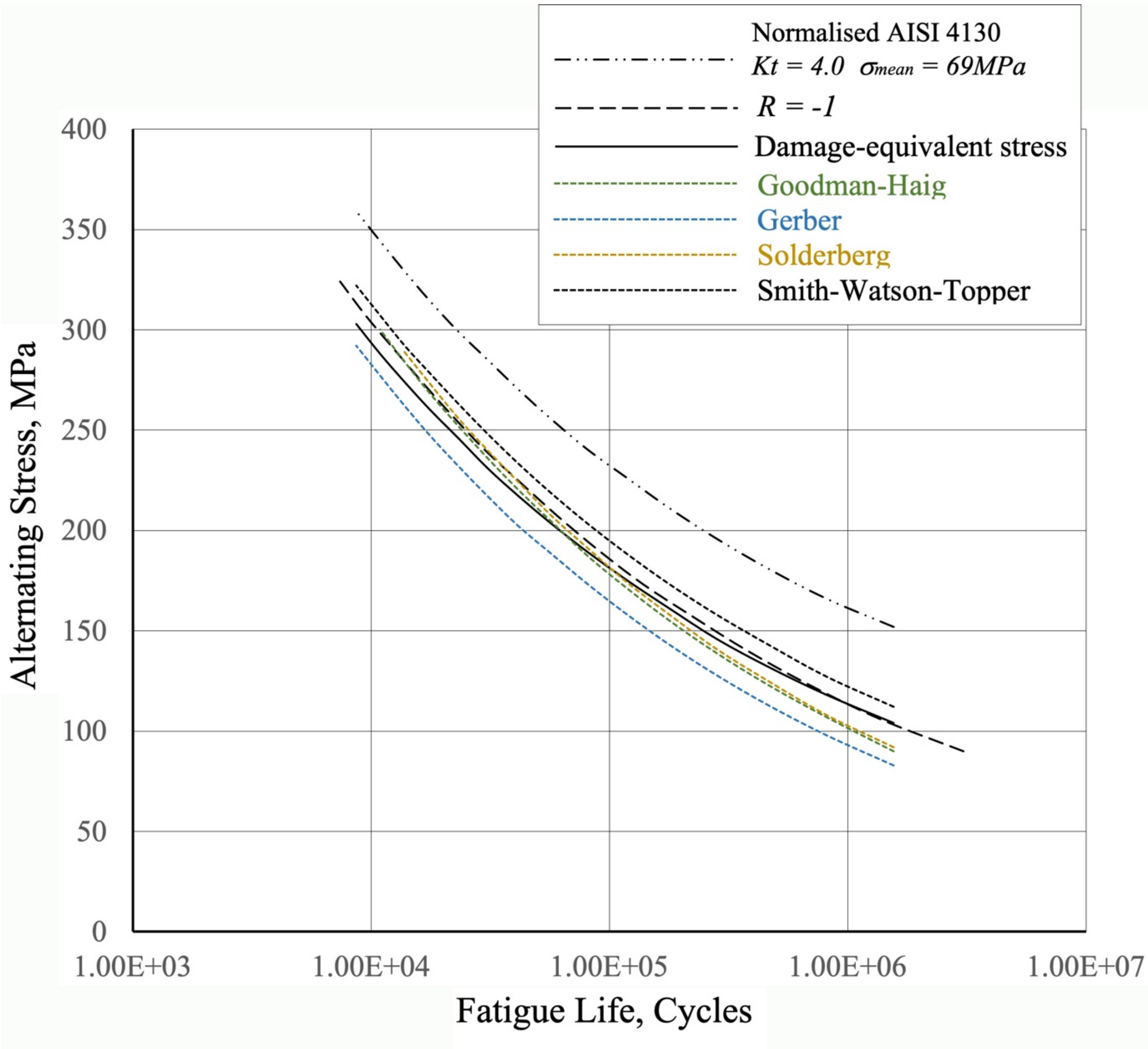

Figure S32. Normalised AISI 4130, K_t = *4.0* s_{mean} = *69MPa(10ksi)*

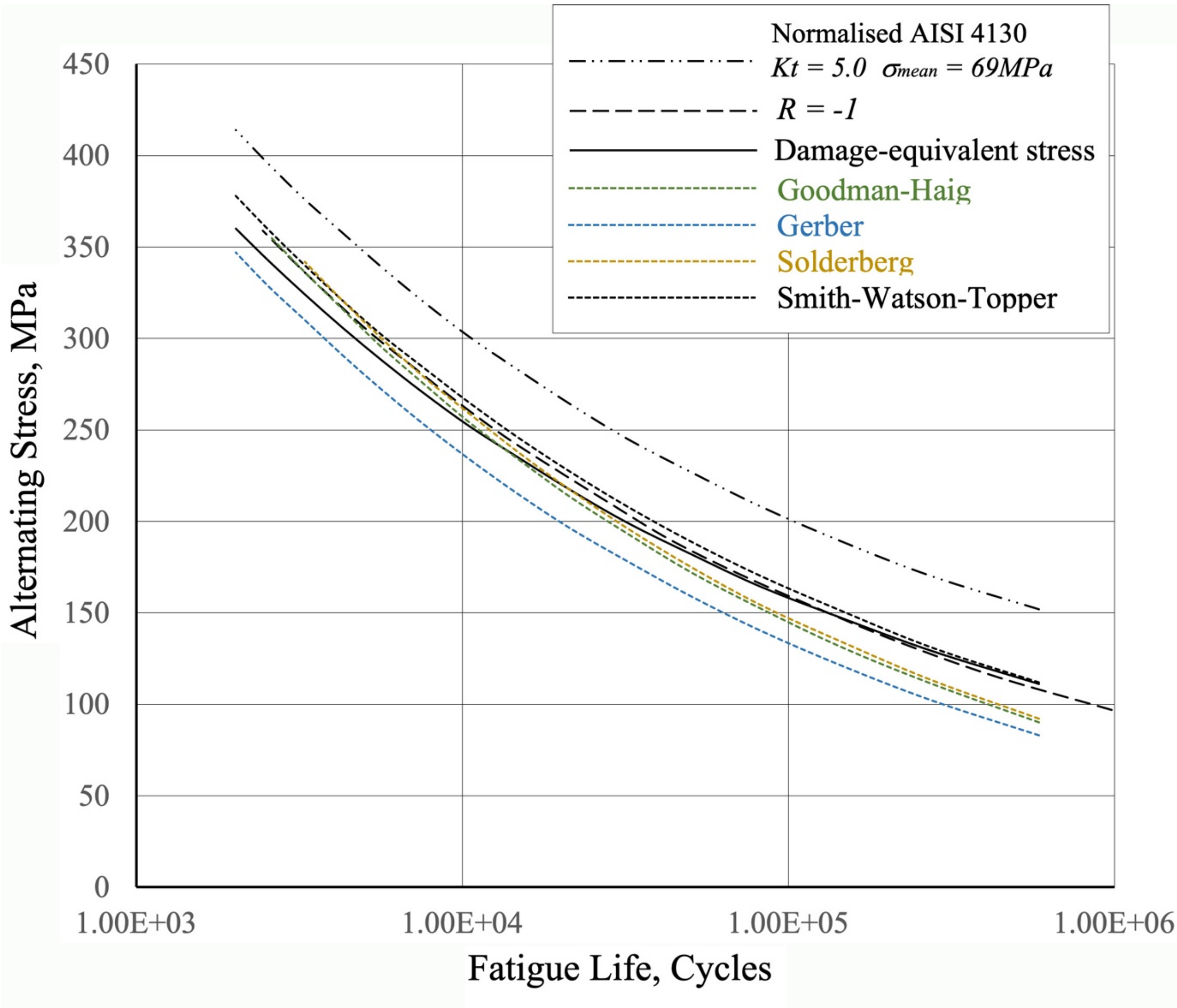

Figure S33. Normalised AISI 4130, $K_t = 5.0$ $s_{mean} = 69MPa(10ksi)$

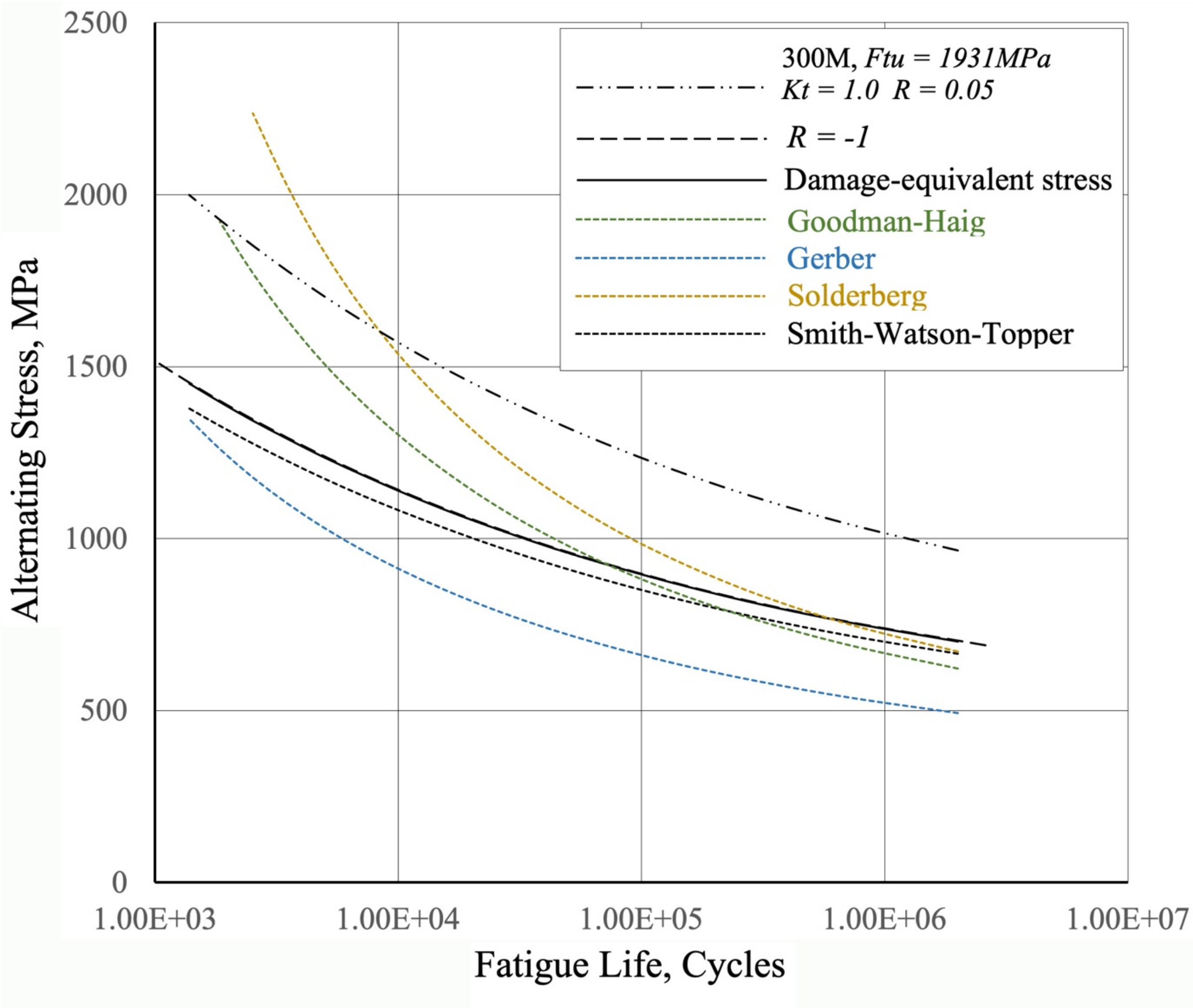

Figure S34. 300M, *Ftu = 1931MPa(280ksi)*, $K_t = 1.0$ $R = 0.05$

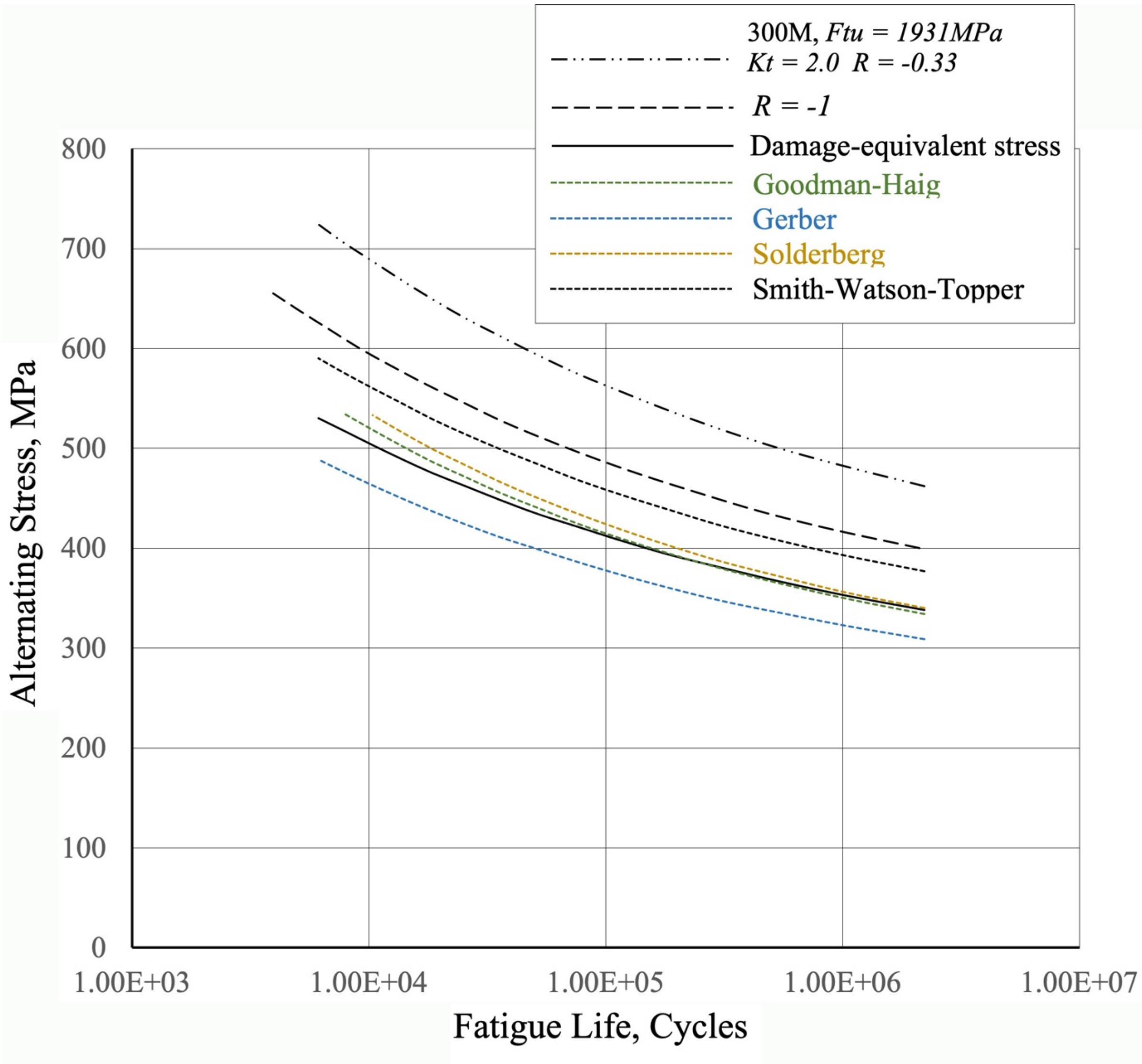

Figure S35. 300M, *Ftu = 1931MPa(280ksi)*, $K_t = 2.0$ $R = -0.33$

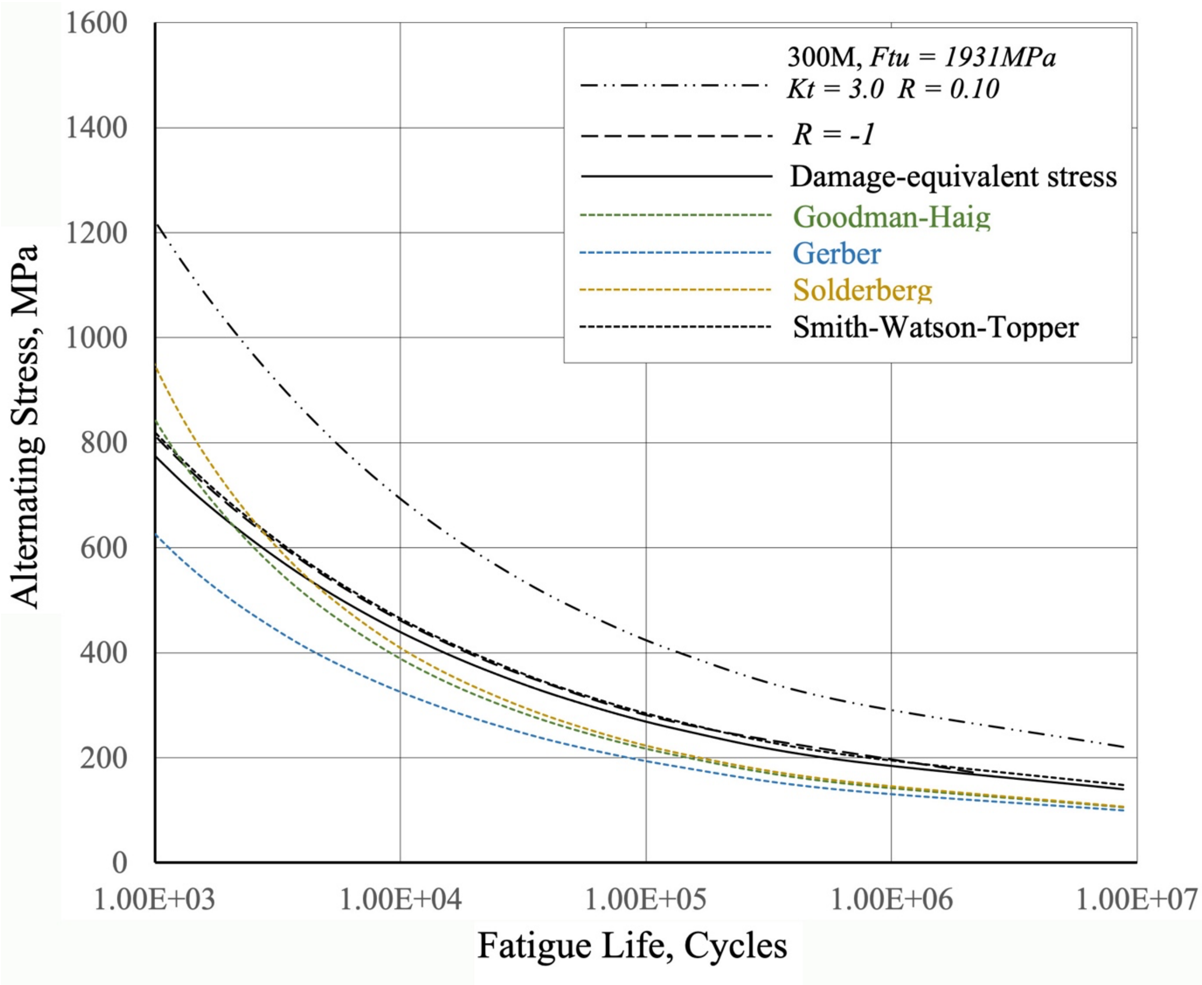

Figure S36. 300M, *Ftu = 1931MPa(280ksi)*, K_t = *3.0 R = 0.10*

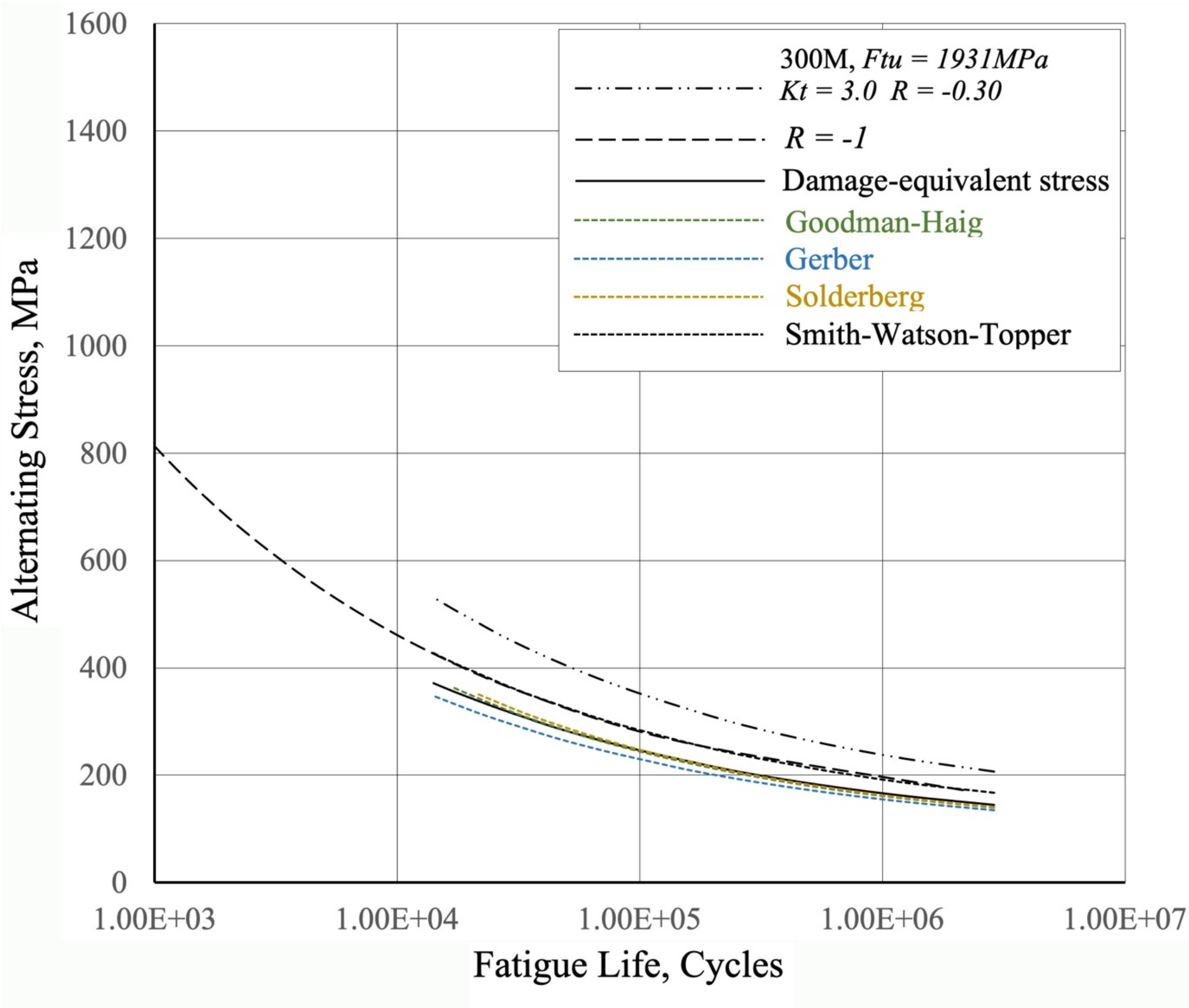

Figure S37. 300M, *Ftu = 1931MPa(280ksi)*, $K_t = 3.0$ $R = -0.30$

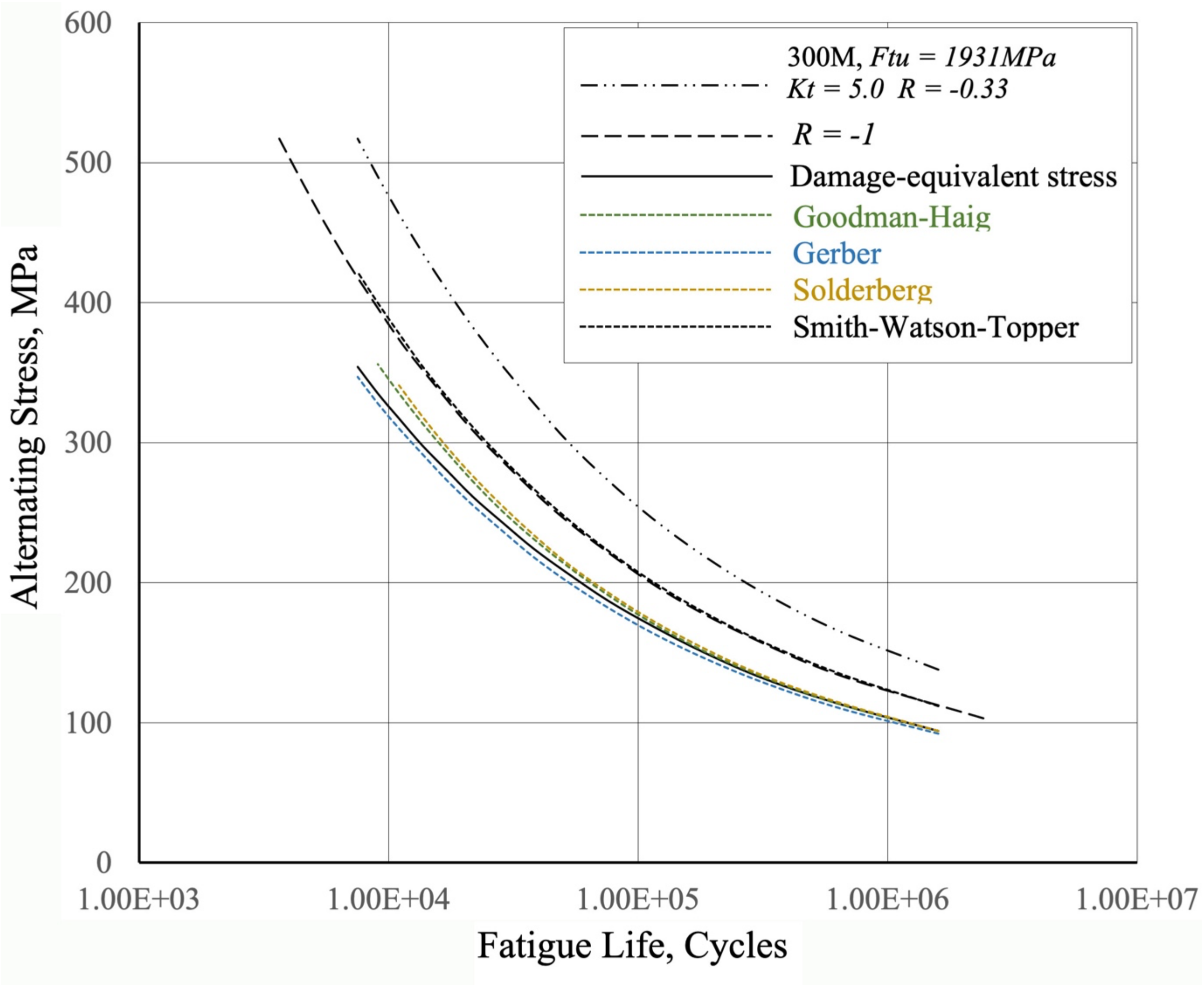

Figure S38. 300M, *Ftu = 1931MPa(280ksi)*, $K_t = 5.0$ $R = -0.33$

REFERENCES

[1] Welch M. *An Empirical Approach to a Comprehensive Damage-Equivalent Stress for Fatigue*. FME Transactions. 2022;50(3):535-457. https://www.mas.bg.ac.rs/_media/istrazivanje/fme/vol50/3/14_m._welch.pdf DOI: 10.5937/fme2203535W

[2] Federal Aviation Administration. *Metallic Materials Properties Development and Standardization (MMPDS)*, Battelle Memorial Institute, MMPDS-03, October 2006

[3] ESDU, 2006. *Fatigue damage and life under random loading*. ESDU 06009. The Royal Aeronautical Society.